12-4-2014

Tensile Behavior of Ultra-High Performance Fiber Reinforced Concrete and Reinforcement Bar

Corey P. Hollmann
Structural Engineering, corey.hollmann@gmail.com

Tensile Behavior of Ultra-High Performance Fiber Reinforced Concrete and Reinforcement Bar

Corey P. Hollmann

B.S. in Civil Engineering, University of Connecticut, 2012

A Thesis
Submitted in Partial Fulfillment of the
Requirement for the Degree of
Master of Science
at the
University of Connecticut 2014

APPROVAL PAGE

Master of Science Thesis

Tensile Behavior of Ultra-High Performance Fiber Reinforced Concrete and Reinforcement Bar

Presented by
Corey P. Hollmann, B.S. Civil Engineering

Major Advisor_____
Dr. Kay Wille

Associate Advisor_____
Dr. Arash Zaghi

Associate Advisor_____
Dr. Michael Accorsi

University of Connecticut
2014

ACKNOWLEDGEMENTS

I would like to thank my major advisor, Dr. Kay Wille, for providing me with the resources and guidance to accomplish my experimental tests. I would also like to thank the entire advisory committee and the UConn CEE staff and faculty for their assistance. I would like to thank Peter, Jim, and Serge of the UConn Engineering Machine Shop for their extensive help.

I would like to thank fellow graduate students: Kevin, Richard, Rui, Mandy, Manish, and Chris for donating time and expertise. Additionally I would like to thank my undergraduate assistants as well as all of the material suppliers that have contributed time, material, and product information.

I would like to thank my father for lending time and expertise in carpentry and construction. I would like to thank my mother, sister, family, girlfriend, and other friends for their love and continued support which made my education possible.

THIS RESEARCH IS SUPPORTED BY:

University of Connecticut
Department of Homeland Security (DHS)
Lafarge North America

TABLE OF CONTENTS

LIST OF FIGURES

LIST OF TABLES

1 CHAPTER ONE - INTRODUCTION

1.1 Background

Ultra high performance concrete (UHPC) is categorized as being a hydraulic cement-based concrete with compressive strength of at least 150MPa (21.7ksi) [1]. UHPC generally consists of cement, silica fume, sand, fibers, water, and high range water reducer, also known as superplasticizer. Typical water-to-binder (cement) ratios are 0.18 to 0.26 with 20% to 30% silica fume [2, 3].Ultra-high strength and excellent durability properties result from the material's enhancement of homogeneity and optimized particle packing density. However, UHPC on its own is very brittle and weak in tension. Steel fibers are incorporated to create ultra-high performance fiber reinforced concrete (UHPFRC) to improve ductility and allow for strain hardening [3, 4]. Typical fiber volume fraction around 2% but 1% has been proven to trigger strain hardening behavior [5]. UHPFRC has improved tensile strength, toughness, energy absorption, durability, freeze-thaw and corrosion resistance, tightness, appearance, stability, constructability, and lower lifetime costs in comparison to conventional concrete [2, 6].

Although UHPFRC has great benefits, its implementation into the US construction industry is hindered due, in part, to a lack of common test methods, production standards, or design guides for current concrete fabricators and designers to feel comfortable to use UHPFRCC [7, 8]. One large knowledge gap is a lack of information pertaining to combining steel reinforcement bars (rebar) with UHPFRC. This information is important because rebar is a commonly used material in current US construction industry. Similar to conventional reinforced concrete structures, rebar has the potential to increase

drastically the tensile strength of UHPFRC while still having the same serviceability advantages that UHPFRC offers on its own [5]. Additionally, rebar reinforced UHPFRC may have a positive economic impact by reducing the amount of expensive micro steel fibers needed in a structure. The effect of fiber volume fraction and fiber orientation play a large role in UHPFRC behavior [9] and therefore it is expected that the same variables will be of high importance in determining the behavior or rebar reinforced UHPFRC.

1.2 Purpose

The purpose of this research is to examine and characterize the behavior of rebar reinforced UHPFRC by completing three phases of experimental tests. The phases are designed to break down the complicated composite behavior of rebar reinforced UHPFRC into smaller components: Phase I) Uniaxial tensile behavior of UHPFRC and rebar. Phase II) Bond behavior of rebar embedded in UHPFRC. III) Uniaxial tension behavior of rebar reinforced UHPFRC. A basic illustration of the three phases is shown in Figure 1-1 and a picture of typical specimens used in the actual experiment are shown in Figure 1-2.

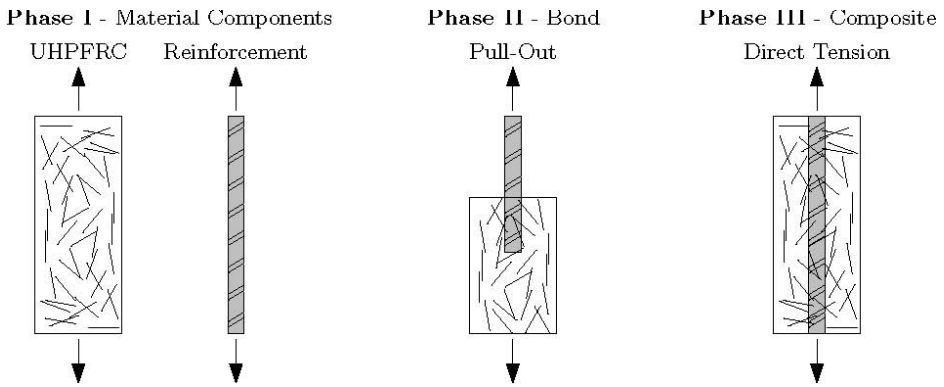

Figure 1-1: Basic Illustration of Phase I through Phase III

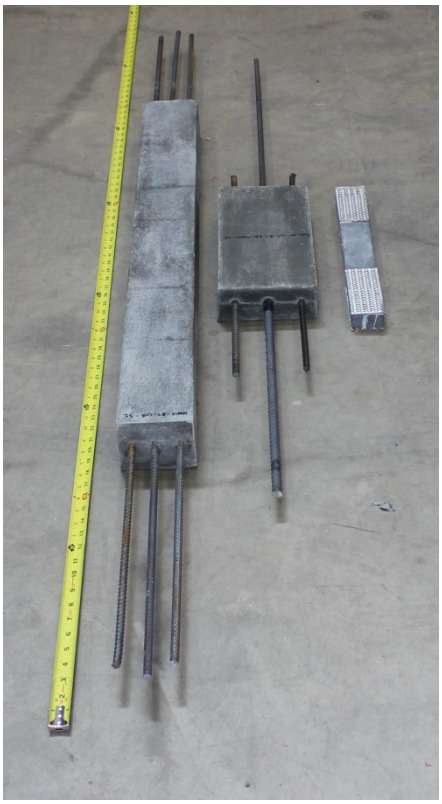

Figure 1-2: Typical Specimens for Phase I through Phase III (right to left respectively)

1.3 Variables

The key focus throughout the experiment is on the influence of fiber volume fraction and fiber orientation. Fiber volume fractions range from 0% to 3% and

orientations consist of perpendicular, parallel, and random alignment with respect to the applied load. Basic Illustrations of these variables are shown in Figure 1-3, Figure 1-4, and Figure 1-5. A third variable is the reinforcement bar type which is varied between ASTM A615 and ASTM A1035 bar.

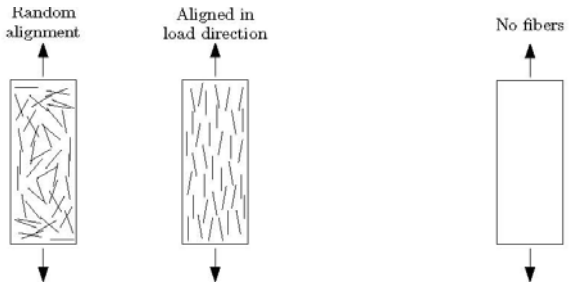

Figure 1-3: Basic Illustration of Fiber Orientation Cases in Phase I

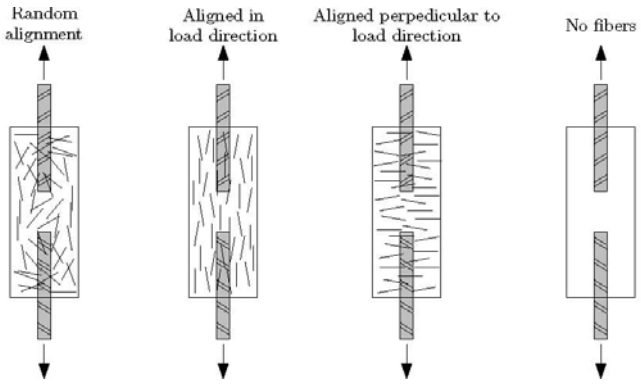

Figure 1-4: Basic Illustration of Fiber Orientation Cases in Phase II

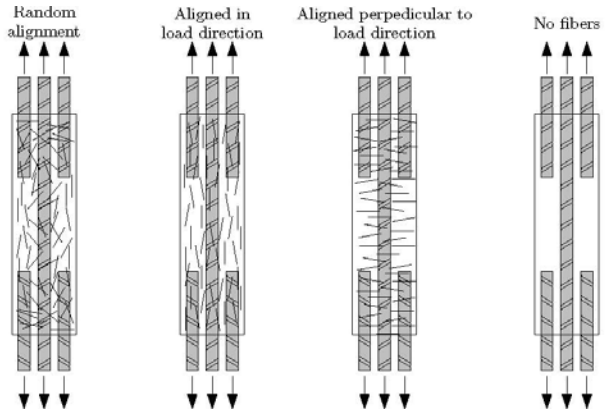

Figure 1-5: Basic Illustration of Fiber Cases in Phase III

1.4 Report Structure

Chapter Two contains extensive literature review of existing experiments and data pertaining to Phase I, II, III. Each of the phases has its own section within the chapter. Chapter Three, Four, and Five contain, respectively, the experimental study, experimental results, and conclusions. Similar to in Chapter Two, Phase I, II, and III each have their own section within each chapter.

2 CHAPTER TWO - LITERATURE REVIEW

2.1 Phase I: Uniaxial Tensile Behavior of UHPFRC and rebar

2.1.1 Tensile Behavior of UHPFRC

While conventional fiber reinforced concrete (FRC) is generally characterized by a tensile softening behavior after matrix cracking, UIHPFRC can be designed to exhibit

strain hardening beyond matrix cracking. Strain hardening behavior allows the material to increase in tensile strength in excess of matrix cracking accompanied by multiple cracking [10]. An illustration of the differing behavior is shown in Figure 2-1. Phase I is the linear elastic phase in which the elastic modulus is characterized by the stiffness of the material. Conventional FRC (top) goes directly from phase I to phase III because the matrix at the crack is not strong enough to open up another crack. UHPFRC (bottom) has a phase II where multiple cracking occurs after cracking and before softening [3, 10, 11]. In Figure 2-2, Graybeal and Baby [11, 12] add an additional phase in which the strain hardening is divided into multiple cracking followed by crack straining at crack saturation.

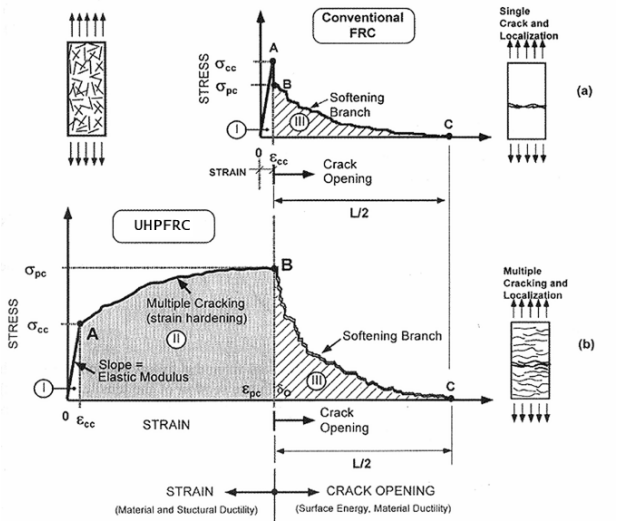

Figure 2-1: Comparison of the typical stress-strain response of conventional FRC vs. strain hardening UHPFRC ([3] made after Naaman [10])

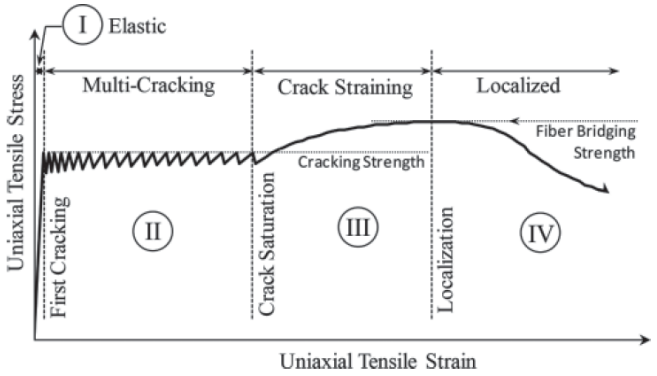

Figure 2-2: Idealized uniaxial tensile mechanical response of UHPFRC according to Graybeal and Baby [11].

2.1.2 Categorization of UHPFRC

The main categorizing feature of UHPC is its compressive strength of at least 150MPa (21.7ksi). The categorization of UHPFRC based on tensile performance is more complicated to quantify. Although no tensile performance requirement is standardized it is suggested that categorization be based on whether the UHPFRC is strain-softening or strain-hardening in tension or whether it is deflection-softening or deflection-hardening in bending [13]. Additional categories might be based minimum ductility, toughness, or fracture energy [2].

Naaman and Reinhardt [14] and Wille, El-Tawil, and Naaman [15] propose four levels of classification based on flexural performance and uniaxial tensile performance (Figure 2-3). The performance for tension and bending respectively are: Level 1) strain softening, deflection softening. Level 2) strain softening, deflection hardening. Level 3) strain hardening, deflection hardening with high energy absorption. Level 4) strain

hardening with high energy absorption, deflection hardening with high energy absorption. Level 0 was added to illustrate the behavior of non-fiber reinforced concrete. Important parameters are cracking stress σ_{cc}, associated strain ε_{cc}, elastic modulus E_{cc}, composite tensile strength or post cracking strength σ_{pc}, modulus of rupture σ_{f1}, equivalent bending strength σ_{f2}.

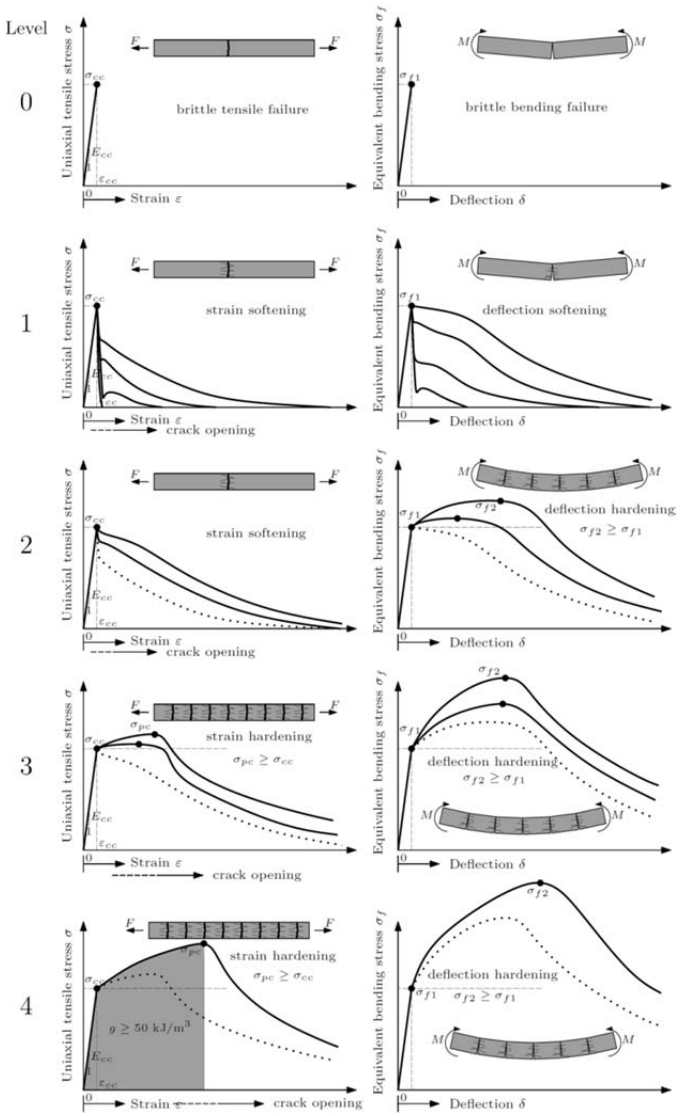

Figure 2-3: Depiction and description of proposed classification levels for fiber reinforced concretes [15] based off of [14]

2.1.3 Variables which Influence Tensile Behavior of UHPFRC

A large variety of factors affect UHPFRC tensile behavior including, but not limited to: matrix properties, fiber volume fraction, fiber geometry, fiber length, fiber stiffness, fiber orientation, curing conditions, size of specimen [8, 16, 13]. Tailoring matrix and fiber properties as well as the bond between them have allowed for record performance results in tensile stress and strain for UHPFRC (up to 27 MPa with 1.1% strain, and energy absorption of 304 KJ/m^3) (Figure 2-5) [2]. It is important to note that economics for each individual application of UHPFRC is important and that strain hardening has been observed for fiber volume fractions of as low as 1% [2].

- Fiber geometry and type influence many properties such as peak strength and strain. For instance, twisted fibers have been shown to have higher stress and strain than hooked fibers or straight fibers [5, 17-21].
- Increasing fiber volume can result in higher stresses and strains (Figure 2-4) and can also lead to difference in cracking behavior, spacing, and width (Figure 2-6) [5, 18, 22].
- Increasing strain rate of loading can result in an increase in strength and energy absorption capacity [23, 24].

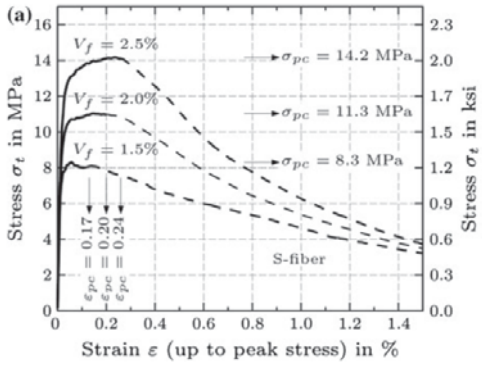

Figure 2-4: Effect of fiber volume fraction on tension [18]

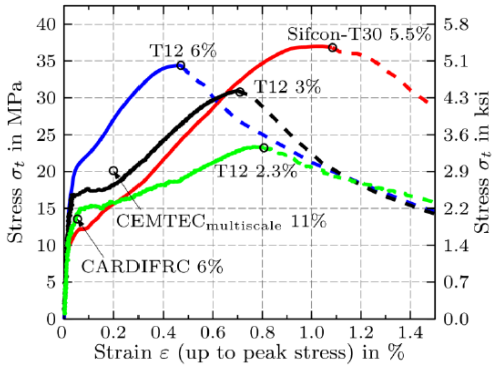

Figure 2-5: Tensile response curves of highest strengths recorded to date [2]

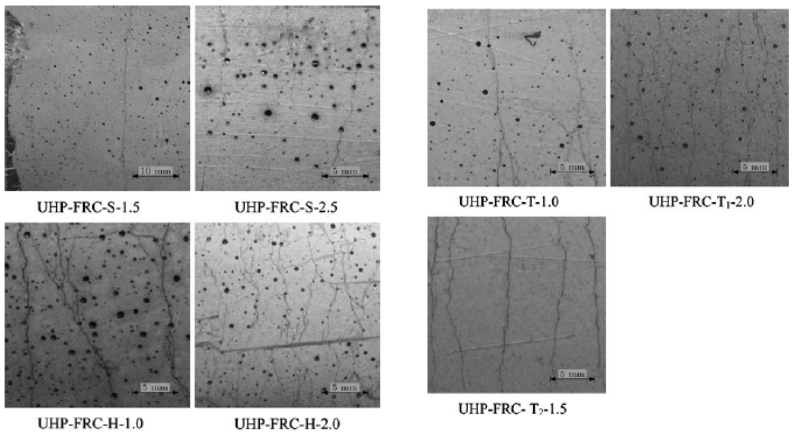

Figure 2-6: Effect of fiber volume and type on cracking behavior [5]

2.1.3.1 Fiber Orientation

- Fiber orientation aligned in the direction of loading leads to an increase in strength capacity over those aligned perpendicular to the direction of loading. [25-40]. Table 2-1 is a compilation of data from various authors with varying fiber

volume fractions and orientations. An attempt is made to only include data with similar fiber length and shape in order to reduce error in the comparison. Figure 2-7 is a graphical interpretation of the data in Table 2-1.

Table 2-1: Comparison of uniaxial tensile responses from various UHPFRC existing literature

Ref.	Fiber %	Fiber Length mm	f't (unknown) MPa	f't (unknown) ksi	f't (parallel) MPa	f't (parallel) ksi	f't (perp) MPa	f't (perp) ksi	perp% %	εmax in/in
[31]	3	varying			15.5	2.2				0.034
	3	varying					2.8	0.4	18.1	-
[39]	2.5	13			16.05	2.3				-
	2.5	13					11.8	1.7	73.5	-
[37]	3	12			16.5	2.4				-
	3	12					4.7	0.7	28.5	-
[16]	-	-			14.2	2.1				-
	-	-					7.9	1.1	55.6	-
[5]	1.5	13			8.3	1.2				0.17
	2	13			11.3	1.6				0.2
	2.5	13			14.2	2.1				0.24
[11]	2	13	11.2	1.6						0.00472
	2	13	9.18	1.3						0.00341
	2.5	13	11.56	1.7						0.005842
[11]	2	13			15	2.2				0.00472
	2.5	13			16.5	2.4				0.00341
	3	13			17.8	2.6				0.005842
[41]	2.5	9	13	1.9						-
	0.9	9	7	1.0						-
[8]	0	-	6.2	0.9						-
[1]	0	-	7.5	1.1						-
perp% = f't(perp)/f't(par)*100									Avg = 44%	

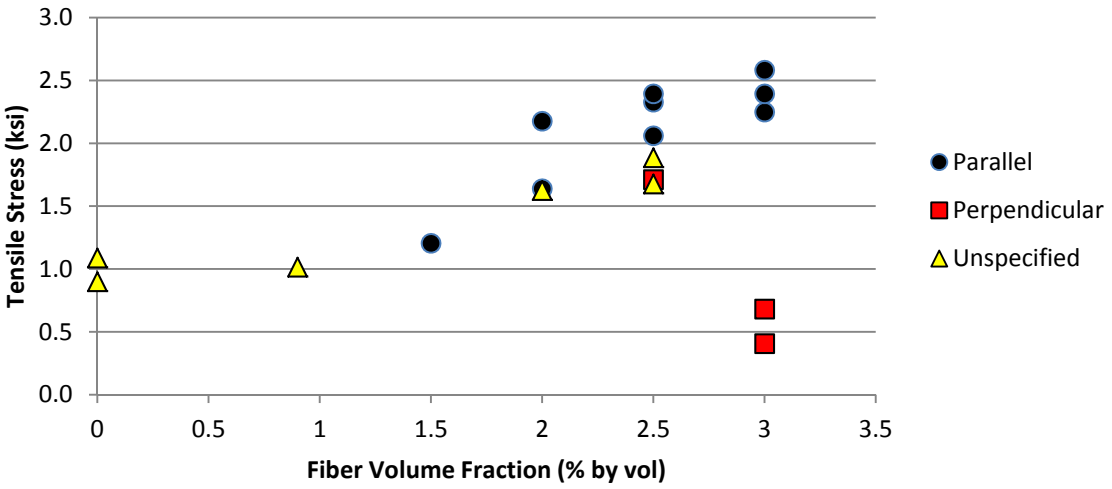

Figure 2-7: Comparison of uniaxial tensile responses from various UHPFRC existing literature (taken from Table 2-1)

2.1.4 Casting Method vs. Fiber Orientation

The casting method of UHPFRC into the formwork is largely responsible for the final fiber orientation in a specimen. The casting method dictates the flow of UHPFRC and the resulting fiber dispersion behavior. However, formwork size [29, 37, 41], mix workability [29, 42], fiber size and fiber volume fraction [43, 44] also influence fiber orientation. For example, Figure 2-8 shows various dispersions that can occur due to flow. Figure 14 illustrates the "wall effect" in which fibers align parallel to the flow along the walls, which confine the flow and align perpendicular to the flow at a distance away from the confining walls. This is due to the difference in flow gradient, which is faster at a distance away from the confining wall than it is near the wall [37]. Figure 2-10 shows how longer fibers incorporated with smaller fibers can help align the smaller fibers [38]. Lastly, it is important to note that incorrect plasticity and workability may result in undesirable fiber settling and segregation. Settling leads to inhomogeneous fiber

distribution and thus can lead to artificial deviation in material performance, such as bending, uniaxial tension and crack spacing, in comparison to homogeneous fiber distribution. (Figure 2-11) [44].

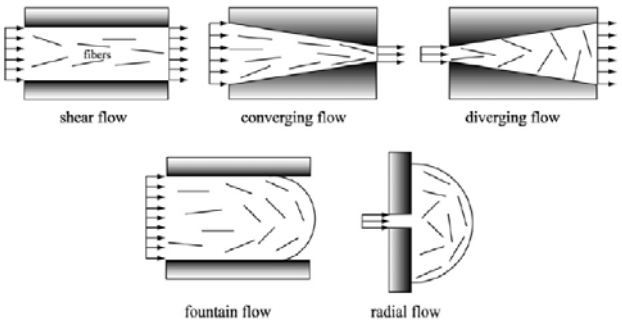

Figure 2-8: Various fiber dispersions based on different flow fields that can occur [42]

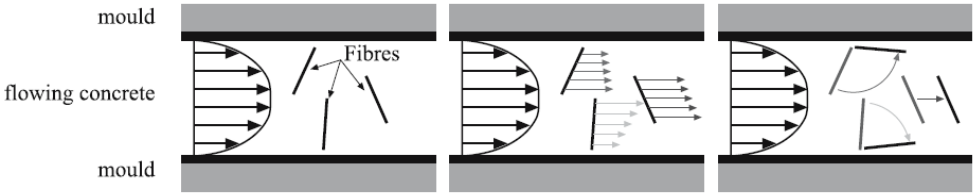

Figure 2-9: Explanation for fiber flow and the "wall effect" [37]

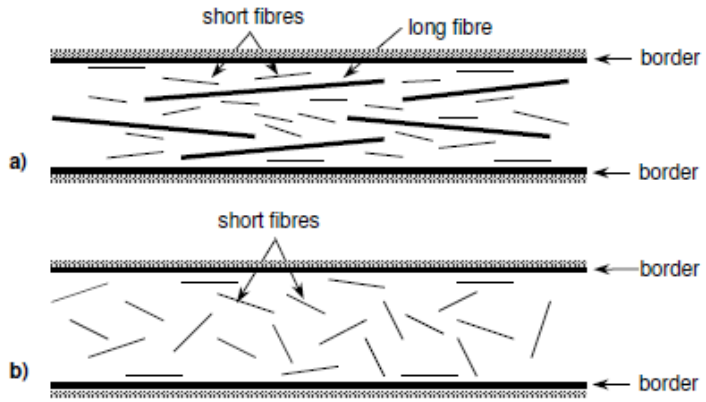

Figure 2-10: Fiber orientation of short fibers between border walls a) in combination with long fibers b) on their own [43].

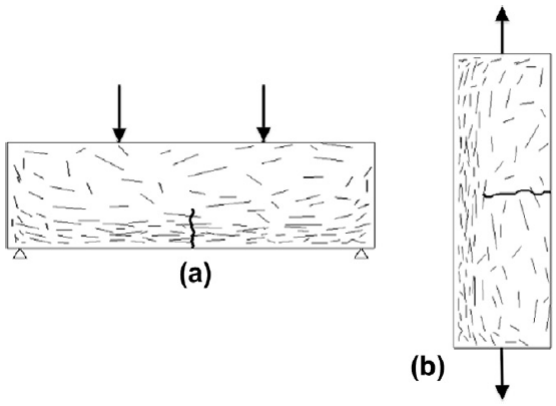

Figure 2-11: Uneven fiber distribution leading to a) artificially increased bending strength in the displayed example b) crack localization in the area of decreased fiber reinforcement in uniaxial tension [44]

Uchida and Zhou [30] used a transparent and viscous fluid with similar flow properties to that UHPFRC to cast beam specimens using two methods: "flow-filling" (dumping at one, allowing material to flow along to the opposite end) and "move-filling" (moving the pouring position continuously in the longitudinal direction to level the concrete depth along the longitudinal axis of the mold). They also poured UHPFRC specimens and observed similar fiber distribution and orientation after cutting open the

cured specimens. The process of flow filling (Figure 2-12) shows that at the bottom of the mold the fibers are parallel to the longitudinal direction but moving progressively upward the fibers orient more perpendicular to the longitudinal direction. Radial flow is shown in Figure 2-14. The move filled specimen (Figure 2-13) results in a more random fiber orientation.

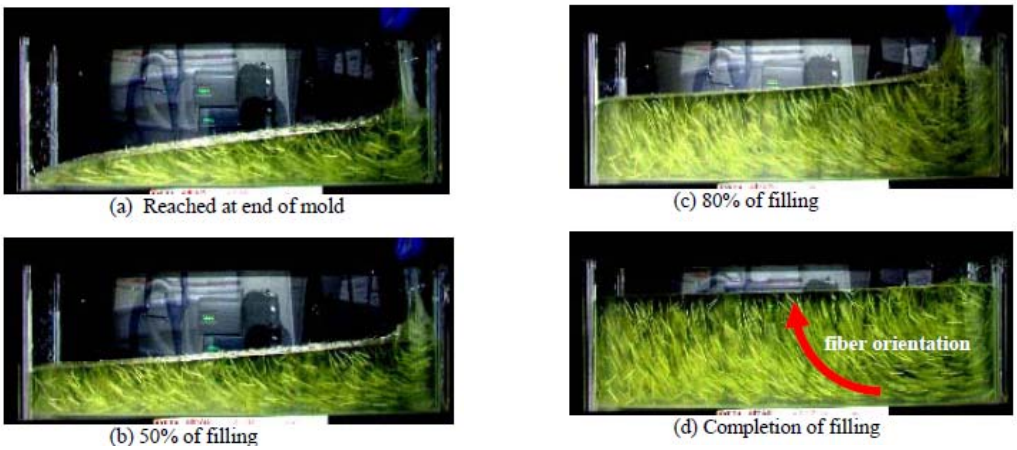

Figure 2-12: Visualization of the progressive stages of flow filling [30]

Figure 2-13: Final stage of move filled specimen [30]

Figure 2-14: Visualization of radial flow [30]

2.1.5 Fiber Orientation vs. Mechanical Behavior

Fiber orientation influences the mechanical behavior of UHPFRC specimens loaded in uniaxial tension as well as in flexure. Several literature sources exist on the

influence of fiber orientation on: flexure of FRC [25-28], flexure of UHPFRC [29-35], uniaxial tension of FRC [36-38], and uniaxial tension of UHPFRC [31, 37, 39]. van Mier, Nooru-Mohamed, and Timmers [38], and Behloul [35] are the only research that give a variety of orientations in terms of degrees with respect to loading direction [43]. The results are shown in Figure 2-15 and it is important to note that the tensile tests used SIFCON (slurry infiltrated concrete (not UPPFRC)). RPC (reactive powder concrete – one type of UHPFRC) was used for the flexural tests. All of the literature will be discussed more in detail in proceeding sections.

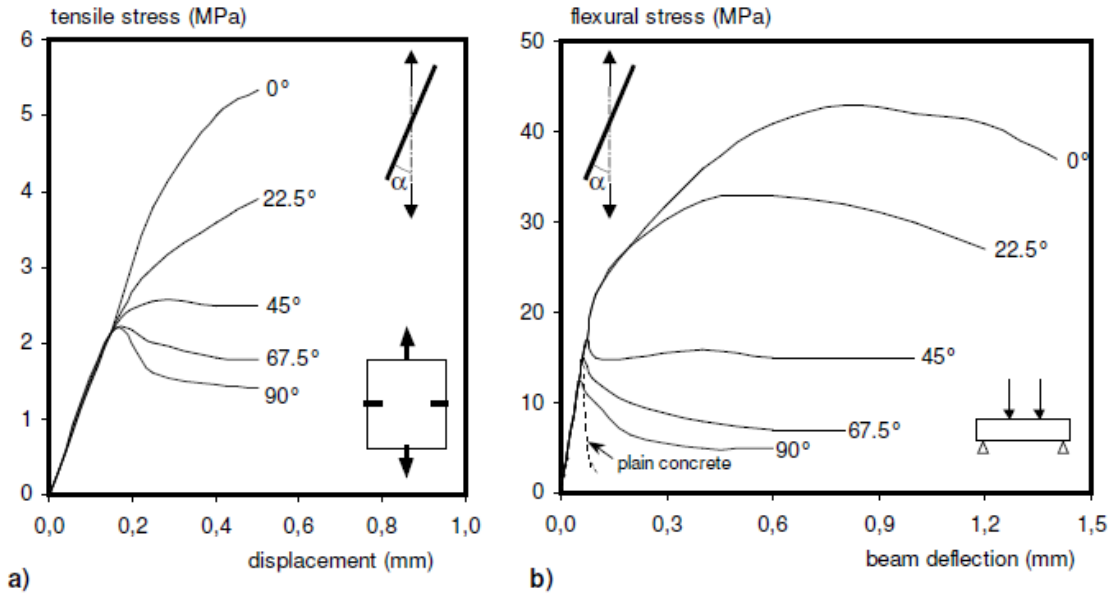

Figure 2-15: The influence of the orientation angle of fibers on: a) uniaxial tensile behavior of SIFCON after [38]; b) flexural behavior of RPC after [35], [43]

2.1.5.1 Flexural Behavior

- Uchida and Zhou [30] found that UHPFRC specimens cast in "move filled" (Figure 2-13) have 20% higher maximum flexural stress capacity over the flow filled specimens (Figure 2-12) because the move filled specimens had more quantities of fibers bridging the crack plain.

- Yazici, Aydin, Yigiter, Yardimci, and Alptuna [28] found that FRC beams using random casting had higher capacities than beams cast with fibers oriented along the length of the beam. Four different compressive strength concretes were used [30MPa (4.4ksi), 65Mpa (9.4ksi), 71 MPa (10.3ksi), and 127MPa (18.4ksi) without fibers] The increase in flexural strength from randomly cast to oriented cast is 17%, 16%, 17%, and 57% for the lowest to highest compressive strength respectively. This shows that higher compressive strength concretes may be more sensitive to fiber orientation [28].

- Stiel, Fehling, and Karihaloo [29] found that UHPFRC beams cast on end can only reach roughly 1/3 to 1/4 of the maximum stress of beams cast lying on their side [29]

- Kwon, Kang, Lee, and Kim [32] dumped UHPFRC in the center of large plate and allowed it to flow radially outward. Specimens were cut out of the plate and tested in flexure. The specimens cast farthest from the center of the flow had the highest flexural stress capacity

- Kang, Lee, Kim, and Kim [33] found that beams cast in the direction parallel to the applied load exhibited a cracking strength that was 5.5% larger and a flexural strength that was 61% larger than the beams cast in a direction perpendicular to the applied load.

- Barnett, Lataste, Parry, Millard, and Soutsos [34] cast a circular UHPFRC plate by three methods: dumping in the center and allowing radial flow out, casting at the edge and allowing flow inward, and random casting. The circular plates were subjected to flexure in which three symmetrical pivots supported the specimen at the perimeter and a load was applied in the center. The specimen cast in the center performed best, the random cast performed second best, and the edge cast performed the worst. There was some variation to the trend depending on the fiber volume and fiber geometry.

- Wille and Parra-Montesinos [41] cast UHPFRC beams by using a long chute to pour in the middle of the mold and allowing it to flow outward, as well as layer casting along the length of the mold with 3 different shoot speeds: slow (0.13m/s [5 in/s]), medium (0.25m/s [10 in/s]), and fast (0.5m/s [20in/s]). For 1.5% twisted fibers the strengths decreased by 22% from fast to medium and decreased 46% from fast to middle cast. For 1.5% straight fibers the strength decreased by 31% from fast to medium, 54% from fast to slow, and 27% from fast to middle cast. The reason for this is that at slow speeds the UHPFRC makes a snake like pattern and leads to orientation perpendicular to the length of the beam. At higher speeds

orientation is best if the layers become thinner while not going too fast as to cause a break in flow.

2.1.5.2 Steel Fiber Pullout

- Lee, Kang, Kim [45] completed multiple fiber pullout tests on straight steel fibers embedded in UHPC at angles of 0, 15, 30,45, and 60 with respect to applied direct tensile load. It was observed that fibers embedded at 30 and 45 degrees have the highest pullout strength whereas the peak slip increases with increasing angle so that 60 degrees has the greatest slip at peak stress
- Krasnikovs and Kononova [46] completed single fiber pullout tests on Dramix hooked fibers embedded at 0, 10, 20, 30, 45, and 60 degrees with respect to applied direct tensile load. It was observed that 60 degrees has the highest fiber pullout load.

2.1.5.3 Uniaxial Tensile Behavior

2.1.5.3.1 Kang and Kim [39]

Specimens with 2% fibers that were cast both parallel (Figure 2-16a) and perpendicular (Figure 22b) to the applied load. The dog bone specimens were notched in the middle and a clip gauge was used to measure the behavior at the notch (Figure 2-17). The average cracking stress for the parallel and perpendicular specimen respectively is 10.93MPa (1.59ksi) and 9.96MPa (1.44ksi) while the average maximum tensile stress for the parallel and perpendicular specimen respectively is 11.8MPa (1.7ksi) and 16.05MPa

(2.33ksi). For the perpendicular cast specimen the cracking stress and maximum stress is approximately 10% and 40% respectively. The orientation of the fibers can be seen in Figure 2-18. The limiting factor in this experiment is that the strain hardening of the entire element cannot be captured with a clip gauge.

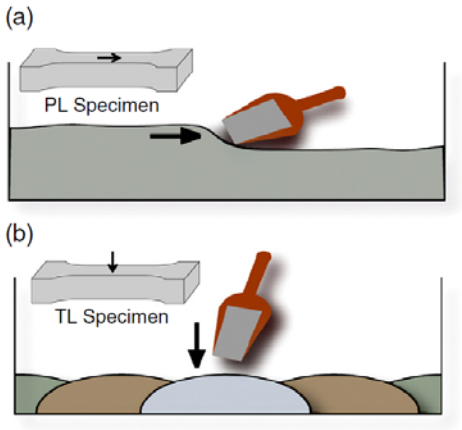

Figure 2-16: Tensile specimen casting direction [39]

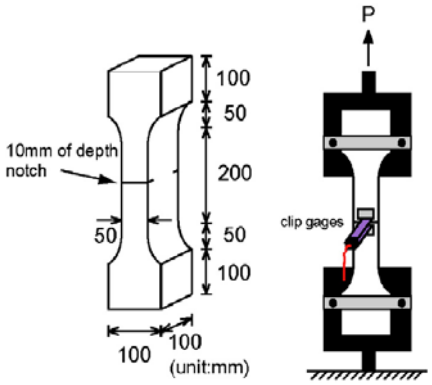

Figure 2-17: Notched specimen with clip gauge measure the behavior at notch [39]

Figure 2-18: Cuts taken across crack plane for perpendicular specimen (left) and parallel specimen (right) [39]

2.1.5.3.2 Pansuk, Sato, Sato, and Shionaga [36]

Specimens that were cut out parallel and perpendicular from a beam that was cast by dumping at one end and allowing the concrete to flow to the other end (Figure 2-19). The concrete strength is 62MPa (8.99ksi) but it is self-consolidating. Due the results being given in terms of crack opening it is assumed that the material is not strain hardening. “Series A” uses 6mm fiber and “Series B” uses 13mm fiber (Table 2-2). From Figure 2-20 specimen C-2 it can be assumed that fibers are relatively well oriented along the flow in the center zone where series A and B are taken from. Taking results from the graph (Figure 2-20) it seems that specimens with near parallel orientation have approximately 20% and 90% higher maximum stresses than perpendicular orientation for 13mm and 6mm fiber respectively.

Table 2-2: Summary of cut direction, location and fiber length [36]

Specimens	Fiber length	Direction to flow direction	Selected zone
Series A			
A-1	6 mm	Parallel	Center
A-2			
A-3		Perpendicular	
Series B			
B-1	13 mm	Parallel	Center
B-2		Perpendicular	
Series C			
C-1	6 mm	Parallel	Filling
C-2			Center
C-3			End

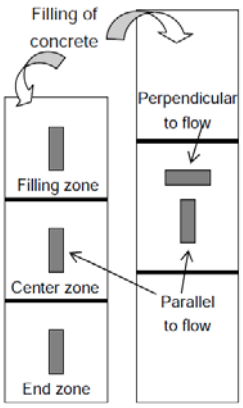

Figure 2-19: Flow direction and cut direction [36]

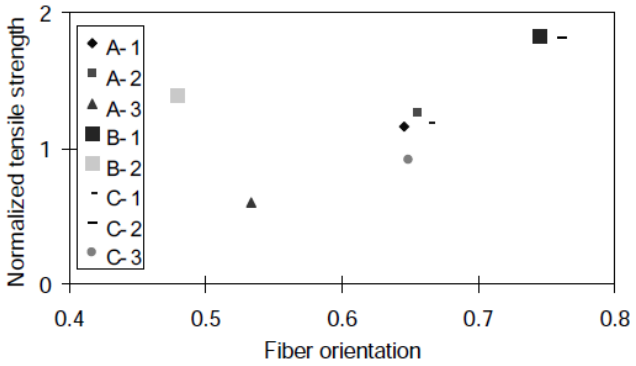

Figure 2-20: Tensile strength vs series [36]

2.1.5.3.3 Osterlee, Denarie, and Bruehwiler [31]

UHPFRC with 3% straight steel fibers was cast into a 150cm x 300cm x 4.2cm width (60in x 120in x 1.65in) panel that was standing on its width. Tensile test specimens 100cm x 20xm (40in x 8in) were sawn out of the panel at various locations. The saw cuts and the fiber orientation as determined by fiber orientation coefficients from cross section cuts for each region are shown in Figure 2-21 and the maximum tensile stress of the three tests from each zone are shown in Figure 2-22. The areas where the orientation is relatively perpendicular to the load (zone I, coefficient of orientation = 0.19) are very

weak, in fact, significantly weaker than the matrix on its own. The reason is that the fibers act as defects in the matrix and actually decrease the cross section area of the matrix. The areas where the fibers are relatively parallel to the load are strong (zone V, coefficient of orientation = 0.74) are the strongest.

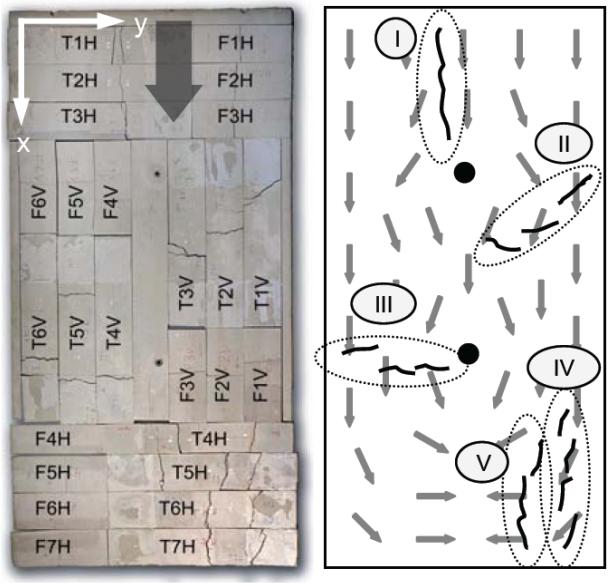

Figure 2-21: Saw cuts, fiber orientation, and the zone number [31]

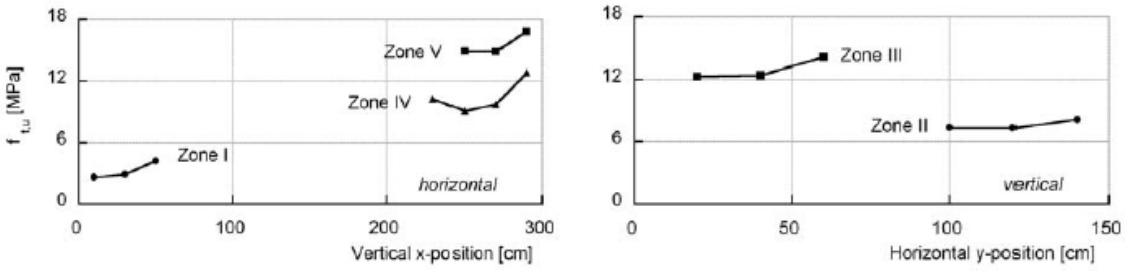

Figure 2-22: The maximum tensile stress of three tests from each zone [31]

2.1.5.3.4 Stahli and van Mier [37]

A High Performance Fiber Reinforced Concrete of unspecified compression strength was used, although the material components appear to be representative of UHPC components and percentages. Three different filling methods were used to fill tensile dog bone specimens (Figure 2-23). The 'conventional' method is when the concrete is filled from the top and is not allowed to flow but just plops into the mold; the 'fill' method is when the concrete is filled from the top but is allow to flow as it is poured in; the climb method in where the material is filled/pumped from the bottom to the top of the mold using pressure. For fiber length of 12mm and 3% fiber volume the maximum achieved tensile stress was 16.52MPa (2.49ksi), 14.05MPa (2.04ksi), and 4.66Mpa (0.68ksi) for climb, fill, and conventional casting methods respectively.

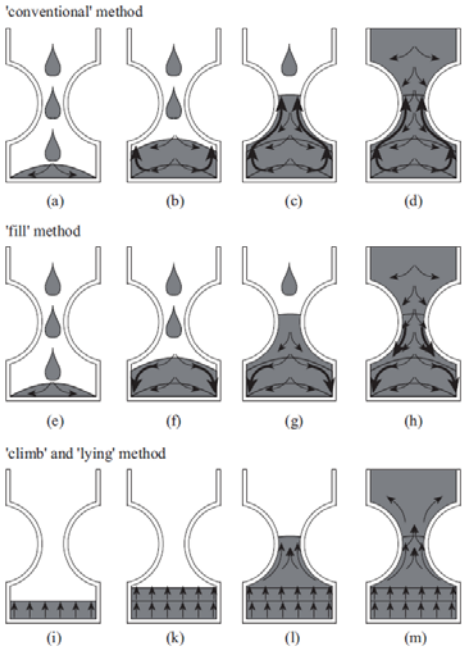

Figure 2-23: Schemes of different filling methods: 'conventional' (a-d), 'fill' (e-f), and 'climb' (i-m). The arrows show the direction of flow [47]

2.1.6 Uniaxial Tensile Test Methods

For fiber reinforced concretes, direct tension test methods [48, 49] and indirect tension testing methods have been standardized [50, 51]. However every type of test has shortcomings [11]. Indirect test methods have issues with restraint of the heavily loaded tensile face, there are complex computations necessary to back calculate the uniaxial behavior, and notched specimens do not allow investigation of the multiple cracking behavior of strain-hardening [11, 15, 41, 52, 53].

Wille, El-Tawil, and Naaman [15] distinguish tension test shapes into dogbone shapes, unnotched and notched prisms or cylinders, in addition to fixed or rotating boundary conditions. Specimens glued to the loading device lead to an increase in duration of test setup [11] and potentially lead to bond failure [11, 15]. Notched specimens impart stress concentrations, make a predetermined failure location, and do not capture strain hardening [11, 15]. Specimens that allow for relative rotation of the specimen ends reduces initial bending but it invalidates post-cracking response because it does not allow for even crack openings throughout the cross section compared to a fixed boundary.

2.1.6.1 Wille, El-Tawil, and Naaman [15]

The test setup used is shown in Figure 2-24 was chosen for the following reasons:

- Accommodates small specimens so it can reduce material usage
- Employs specimens that are easy to cast, prepare, install, and align
- Uses specimens with a region of constant area to employ multiple cracking
- Does not require additional reinforcement at a haunch or head

- Easy, quick, removable, lightweight, reusable, highly accurate system
- High probability of achieving uniaxial stress due to translation in two axis
- Facilitates stable and even crack growth throughout the cross section

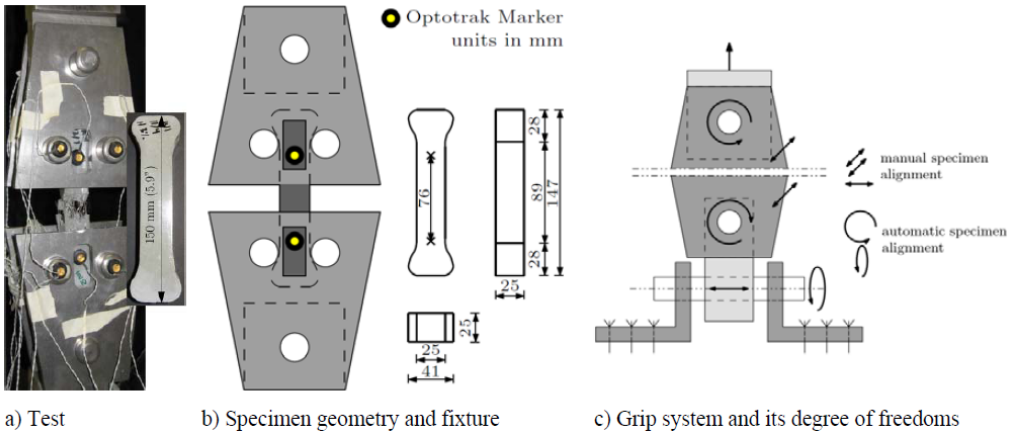

Figure 2-24: Tensile test setup used by Wille, El-Tawil and Naaman [15]

2.1.6.2 Graybeal and Baby [11]

The test setup used is shown in Figure 2-25 was designed based off the following criteria:

- Must be able to be completed with commercially available testing equipment
- Must be applicable to both cast and extracted specimens without requiring the use of milling or machining of specimens
- Must strive to limit magnitude of flexural strain
- Must be able to be completed in a sufficiently short time frame (6 tests in 4 hours)
- Must accurately capture the uniaxial tensile mechanical response of UHPFRC from elastic behavior through strain localization

- Must forestall the relative motion of the specimen ends so as to limit the non-uniform localization of strain within individual cracks
- Must have high likelihood any individual test being completed successfully

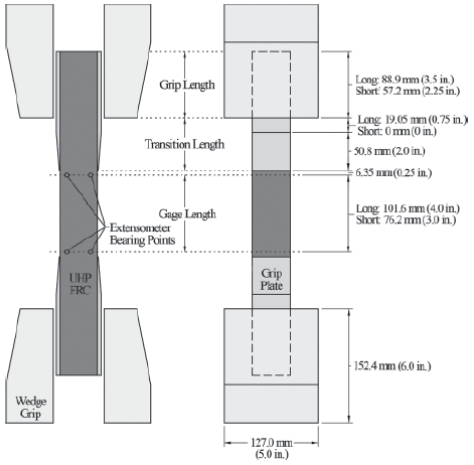

Figure 2-25: Tensile test setup used by Graybeal and Baby [11]

2.1.7 Phase I Literature Review Summary

- The effect of various fiber orientation on UHPFRC behavior under flexural loading has been shown in UHPFRC under flexure [28-30, 32-34, 41]. However, under direct tensile loading there exists few sources: Parallel versus perpendicular cast [39], cutting open cross section and examining orientation [31], and examining 3 filling methods [37].

- Based on the data in Table 2-1 and Figure 2-7 we can expect to see as much as an 82% decrease in strength of fibers oriented perpendicular to applied load as compared to parallel with an average decrease of 56%.

- Based on UHPFRC flow properties and wall effects of formwork and casting devices it is possible to align fibers in one direction with modest error by casting fast (0.5m/s) back and forth along the axis of alignment in thin layers without breaking the flow [41].

- A relatively simple direct tension test method for small UHPFRC specimens has been proposed by Graybeal and Baby [11] that works for prismatic specimens cut from panels. A similar method was used by Osterlee, Denarie, and Bruehwiler [31].

2.2 Phase II: Bond Behavior of Rebar Embedded in UHPFRC

2.2.1 Bond Mechanics in Conventional Concrete

Reinforcement bar (rebar) allows transferring of tensile stresses across cracks and into the concrete through bond. The bond consists of chemical adhesion, frictional resistance (Figure 2-26a), and bearing of the ribs on the concrete (Figure 2-26b). When a small tensile load is applied to the steel the adhesion between the concrete and the steel is the first resistance to be overcome a range of 0.5 to 1.0MPa (70-150psi) in normal concrete [54]. Friction is due to micro-irregularities along the surface of the steel, wedging of granular material between the bar and the concrete, and bearing force components that act parallel to the ribs to the rib face. Typical friction resistance values range from 0.4 to 10.0MPa (60 to 1250psi) in normal concrete [54].

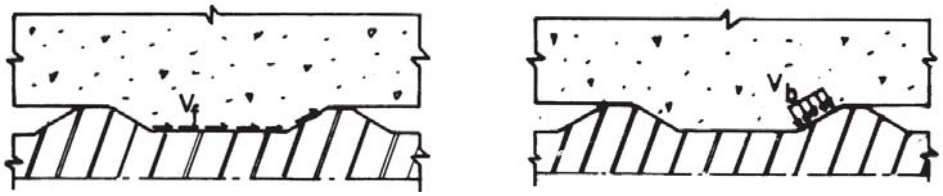

(a) Friction (b) Bearing

Figure 2-26: Idealized force transfer mechanisms [54]

Friction and Adhesion play a very small role in bond strength compared to the third mechanism, bearing of the ribs. After breaking free of adhesion, the bar slips slightly and the bearing forces are activated as the ribs come in contact with concrete between the ribs known as the concrete keys. The ribs contact the concrete at an angle which means the concrete must provide resistance to forces that act both parallel to the length of the bar and perpendicular outward from the bar in order to counteract the resultant force from the ribs (Figure 2-27) [55]. The effect of forces parallel to the bar can cause concrete keys to crush and shear between the ribs (Figure 2-29). It can also cause transverse cracks, also known as Gote cracks [56] and can be seen on Figure 2-27 "internal crack" and from Figure 2-30 "transverse cracks". The forces perpendicular outward to the bar put stresses outward all along the perimeter of the bar and forms a tensile ring (Figure 2-28) of radial stresses [57]. The tensile ring is caused by wedging action of the ribs onto the concrete keys and leads to radial cracks, also known as longitudinal cracks and splitting cracks (Figure 2-30).

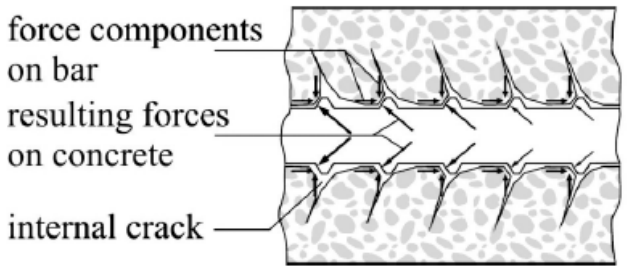

Figure 2-27: Components of bearing [55]

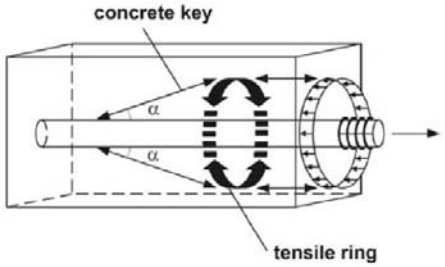

Figure 2-28: Strut and tie model of concrete key and tensile ring [57]

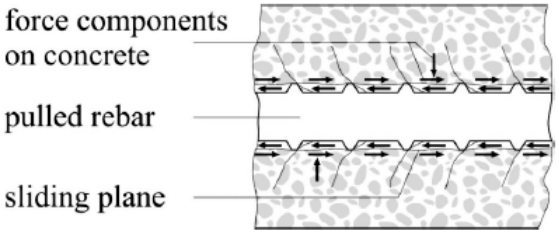

Figure 2-29: Formation of a sliding plane in pullout failure [55]

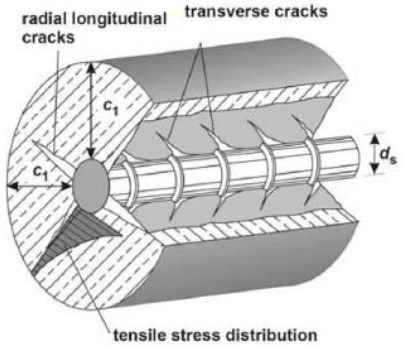

Figure 2-30: Formation of radial and transverse concrete cracking [57]

2.2.2 Bond Failure Modes in Conventional Concrete

Splitting and pullout failure are the two types of bond failure. Pullout failure happens when the ribs crush the concrete keys and the concrete keys completely shear off at the point of maximum bond stress. This leads to the formation of a sliding plane (Figure 2-29) in which friction allows for a slow reduction in stress and a ductile failure

[3, 55, 58]. The ductile failure is shown as step IV with a dark line in Figure 2-31. However, if the concrete cover or confinement is reduced, the resistance against radial decreases and can lead to a failure that is somewhere between the dotted line and the solid line in Figure 2-31. Sometimes the concrete or confinement is so insufficient that the splitting cracks shown in Figure 2-30 penetrate the entire concrete (Figure 2-33, Figure 2-34 left) in what is known as splitting failure. Typically the bond stresses reached are less than that of pullout failure because the splitting cracks happen before the concrete crushing and shearing occurs and therefore it is not uncommon to see undamaged concrete keys in splitting failure (Figure 2-33) [59]. The failure mode is very brittle and results in a sudden loss of bond strength [54, 56]. In practice, where large concrete covers are not feasible, it may be necessary to provide transverse reinforcement such as confining steel (Figure 2-32) [59] to reinforce splitting cracks and prevent brittle failure [59, 60].

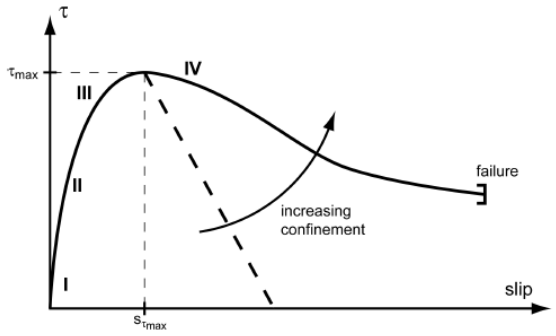

Figure 2-31: Conceptual bond stress-slip behavior at various levels concrete confinement [3]

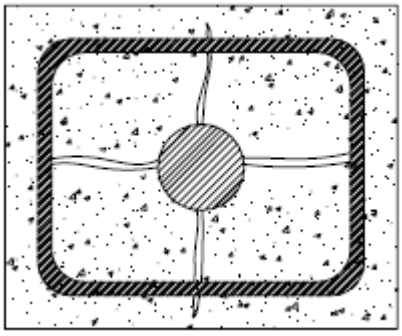

Figure 2-32: Confining steel containing radial cracks [59]

Figure 2-33: Cross section of a pullout specimen with splitting crack resulting in otherwise undamaged concrete between the ribs [59]

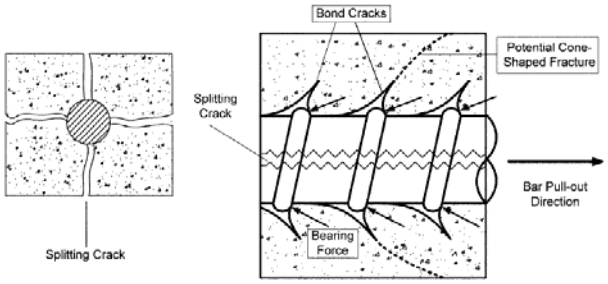

Figure 2-34: Crack formations in conventional concrete [61]

2.2.3 Variables which Influence Bond

Bond is affected by a very numerous amount of variables that are not all necessarily mentioned in this section. Holschemacher, Weibe, and Klotz [62] came up with the general parameters that influence bond and divided them into 4 groups (presented in Table 2-3). It is important to note that in different scenarios (cyclic loading, splitting failure vs pullout failure, etc.) different variables may play a lesser or greater role in deciding bond behavior [54].

Table 2-3: Parameters that influence bond according to Holschemacher et al [63]

Concrete • Concrete composition (grading curve of aggregate, binder content) • Fresh concrete properties (flow, slump, compactability) • Hardened concrete properties (compressive and tensile strength, modulus of elasticity, fracture characteristic (brittleness))

Properties of Reinforcement • Rebar diameter • Rib geometry and arrangement (high or deep ribbed, orientation, number of rows of ribs) • Relative Rib Area
Loading Regime • Short or long term monotonic (static) loading (loading rate) • Dynamic loading (frequency, amplitude)
System Parameter • Concrete cover, confinement (due to transverse reinforcement, fibers) • Position of the rebar during casting • Orientation of the rebar relative to the direction the concrete is placed

2.2.4 Definition of Bond Stress

A typical measure of bond strength is called average bond stress (τ_b) [61, 64] .

$$\tau_b = \frac{F}{\emptyset_b \pi l_b} \qquad \textbf{Equation 1}$$

Where F is the applied force, $\emptyset_b$ is the nominal bar diameter, l_b is the embedment length. Typically the average maximum bond stress is the desired parameter because at the point of maximum load it can be assumed that bond stress is evenly distributed (Figure 2-35c) throughout the length of the bar embedment and can therefore be averaged using the above equation. At other stages in the loading or in cases where splitting failure happens or the bar ruptures, the bond stress may yield artificially low results. The reason for this is the uneven distribution of shear stresses along the embedded (Figure 2-35a). As the load increases the concrete keys crush which allows further ribs to be activated (Figure 2-35b). The process repeats until all of the ribs on the embedded length are

activated through concrete crushing and the distribution is assumed to be uniform (Figure 2-35c). In splitting failure and rebar rupture the bond stress distribution would be more like Figure 2-35b or c depending on the severity because all of the ribs have not had a chance to be activated. (Figure 2-35c) [65].

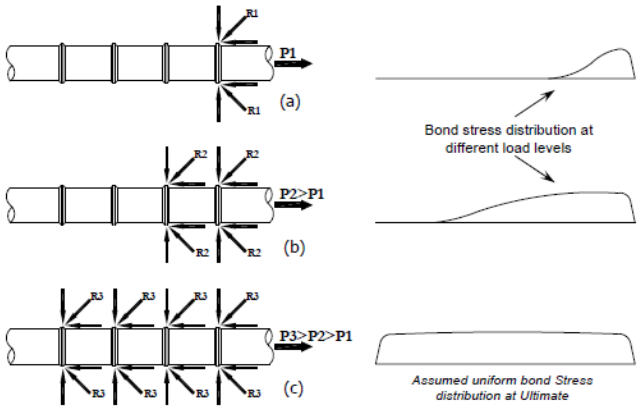

Figure 2-35: Idealized stress behavior of rebar embedded in concrete and subjected to tension [65]

2.2.5 Bond Forces in Fiber Reinforced Concrete

It is important to note that fibers have the ability to provide confinement to the rebar by bridging cracks, controlling crack openings and propagation, and therefore increase bond strength. Chao, Naaman, and Parra-Montesinos [61] describe the bond mechanics of FRC as the following: After initial cracking the tensile ring is redistributed around the whole matrix due to the presence of fibers. At this stage the strain hardening characteristics of the FRC is the deciding factor in whether multiple splitting cracks form in addition to the typical three or four (Figure 2-36 left). Multiple radial cracks due to strain hardening allows for higher bond stresses to be reached because the bearing stress is redistributed among multiple cracks instead of building up in one location. (Figure 2-37). Bond cracks, also known as transverse cracks, are also bridged by fibers which

reduces slip and thereby may increases stiffness. Upon further slippage, following the pullout of the fibers, longitudinal cracks develop along the bar axis and this corresponds with the approximate maximum bond strength. At this point, if the fibers can effectively bridge the longitudinal cracks without excessive opening the failure will be a relatively ductile pullout failure (Figure 2-38d). Otherwise the longitudinal cracks will open and the failure is more of a sudden splitting failure (Figure 2-38e) [61].

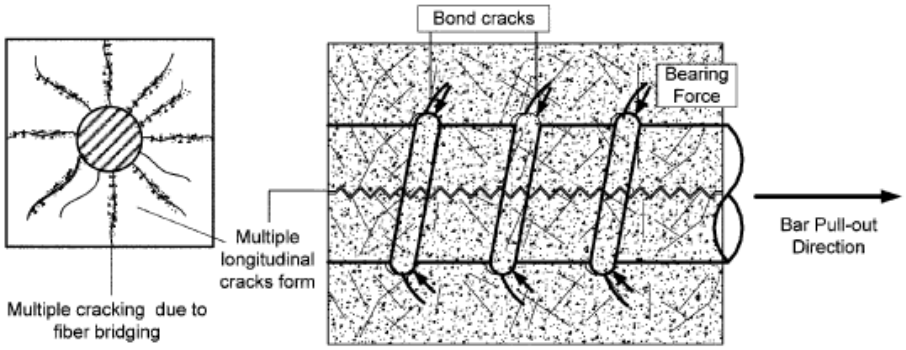

Figure 2-36: Multiple cracking of strain hardening HPFRC [61]

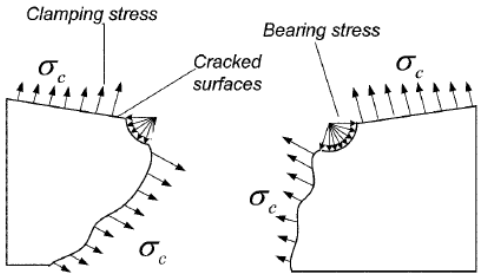

Figure 2-37: Bearing stresses redistributed as clamping stresses [61]

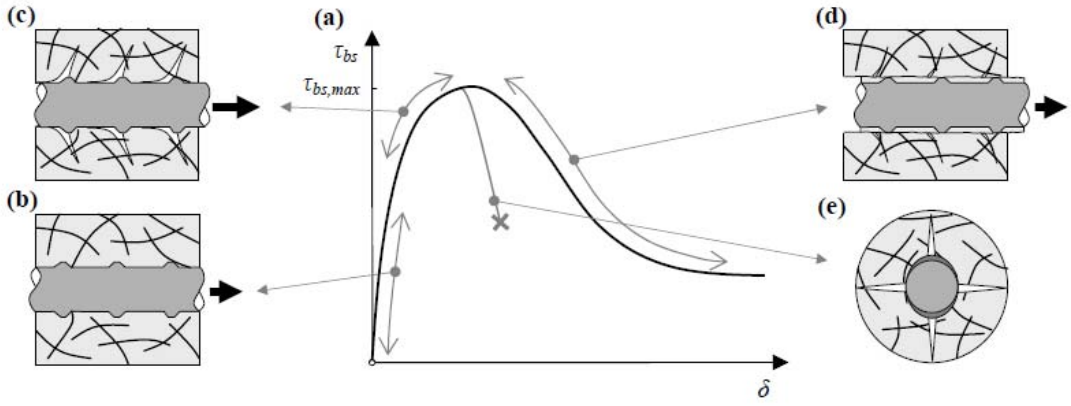

Figure 2-38: Splitting failure versus pullout failure [58]

2.2.6 Rebar Pullout Test Standards

Rebar bond strength in conventional concrete typically follows the RILEM pullout guidelines [66]. Rebar is inserted into a square mold but a portion of the bar near the top of the mold is covered in a plastic sleeve so that when concrete is poured it does not bond to the rebar in that location. A schematic of this is shown in Figure 2-39. ACI 408R-03, however, concludes that in this type of pullout specimen the stress state is significantly different from typical reinforced members in the real world in which both the bar and ribs are subject to compressive force [56]. ACI 408R-03 concludes that Figure 2-40a, which is comparable to the RILEM procedure, is less comparable to real life than a bond test in flexure shown in Figure 2-40c.

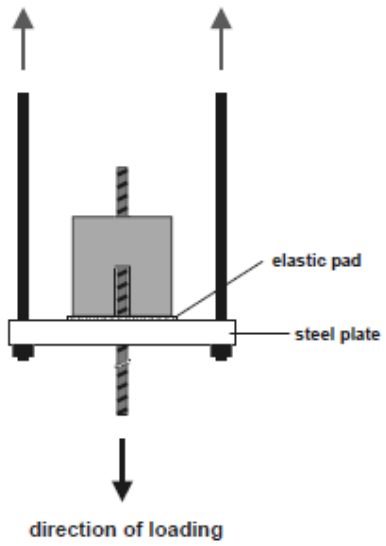

Figure 2-39: Schematic of RILEM pullout test [63]

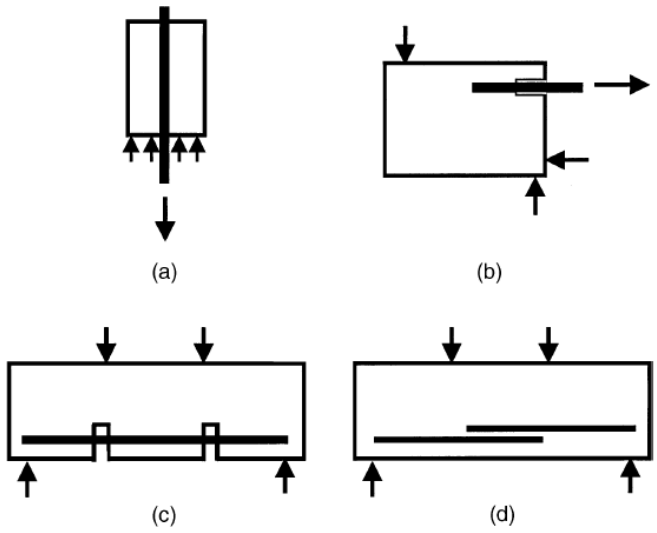

Figure 2-40: Basic Schematic of: (1) pullout specimen; (b) beam-end specimen; (c) beam anchorage specimen; (d) splice specimen [56]

2.2.7 Influence of Concrete Strength on Bond (UHPC vs NSC)

UHPC has recorded much higher bond stresses than NSC as long as necessary cover is available to prevent splitting. Reference data for "modified" RILEM tests with varying concrete strengths have been compiled in tabular form in and graphically in

Figure 2-41. The "modified" RILEM test has 4.5db cover and the embedment length is modified or varied to prevent rebar rupture. There are either no fibers, fibers with an unknown orientation, or fibers with parallel or perpendicular orientation. Looking in

Figure 2-41 strictly at the "No Fiber" specimens (black hollow circles in the key) the bond stress increases with increasing compressive strength. However after 100MPa the increase in bond stress is not as great. From the data if we assume that NSC bond stress is 15MPa and UHPC bond stress is 60MPa then the bond for UHPC is 4 times stronger for

UHPC than for NSC. Table 2-4 shows that the slip at maximum stress is also smaller for UHPC than NSC and this is because the stiffness is greater in higher strength concrete because they have a higher modulus of elasticity. Holschemacher, Weibe, Klotz [63] in Figure 2-42 show that for 62MPa, 135 MPa, and 147 MPa the slips were about 0.7mm, 0.4mm and 0.4mm respectively [67].

Table 2-4: Compilation of Modified RILEM tests on varying concrete strength

Ref.	Compressive Strength		Maximum Average Bond Stress		Slip at Max	Fibers	Orientation
	MPa	ksi	MPa	ksi	mm	%	
[67]	29	4.2	13.5	2	0.7	-	-
	29	4.2	14.5	2.1	-	yes	par
	29	4.2	17.4	2.5	-	yes	perp
[60]	52	7.5	21	3	0.8	-	-
	52	7.5	23	3.3	-	yes	-
[68]	62	9	23	3.3	0.7	-	-
[67]	95	13.7	45	6.5	0.9	-	-
	95	13.7	49	7.1	-	yes	par
	95	13.7	54	7.8	-	yes	perp
[68]	135	19.6	58	8.4	0.4	-	-
[68]	147	21.3	67	9	0.4	-	-
[69]	190	27.6	57	8.3	0.2	-	-
	190	27.6	55	8	0.15	1	-
	190	27.6	59	8.6	-	2	-
[64]	197	28.6	68	9.9	0.3	1	-
	207	30	72	10	0.36	3	-
[70]	180	26.1	50	7.3	0.2	2	-

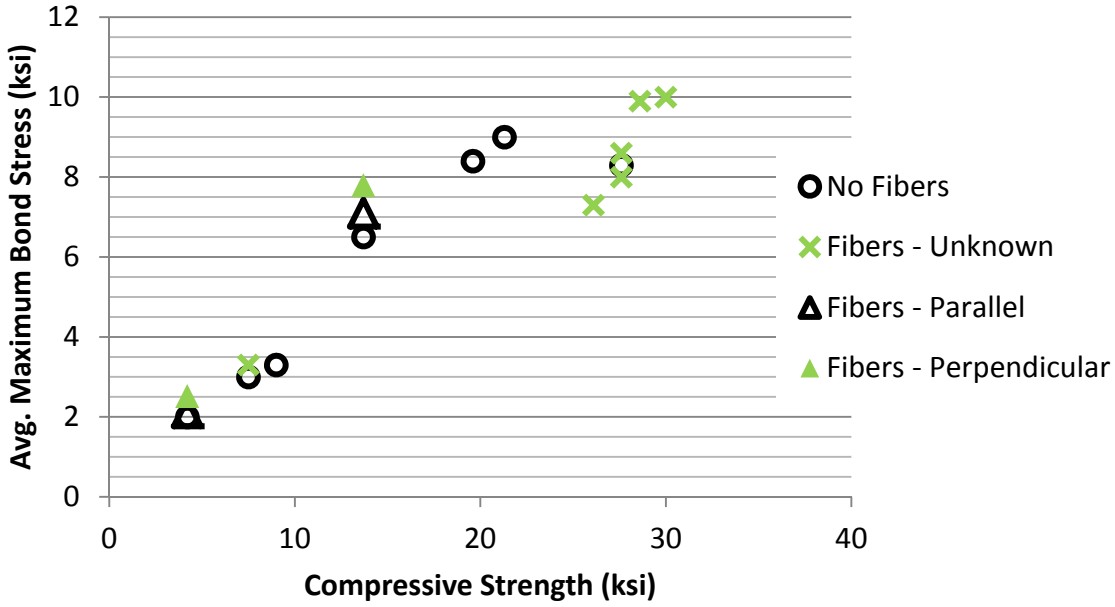

Figure 2-41: Compilation of Modified RILEM tests on varying concrete strength based on Table 2-4

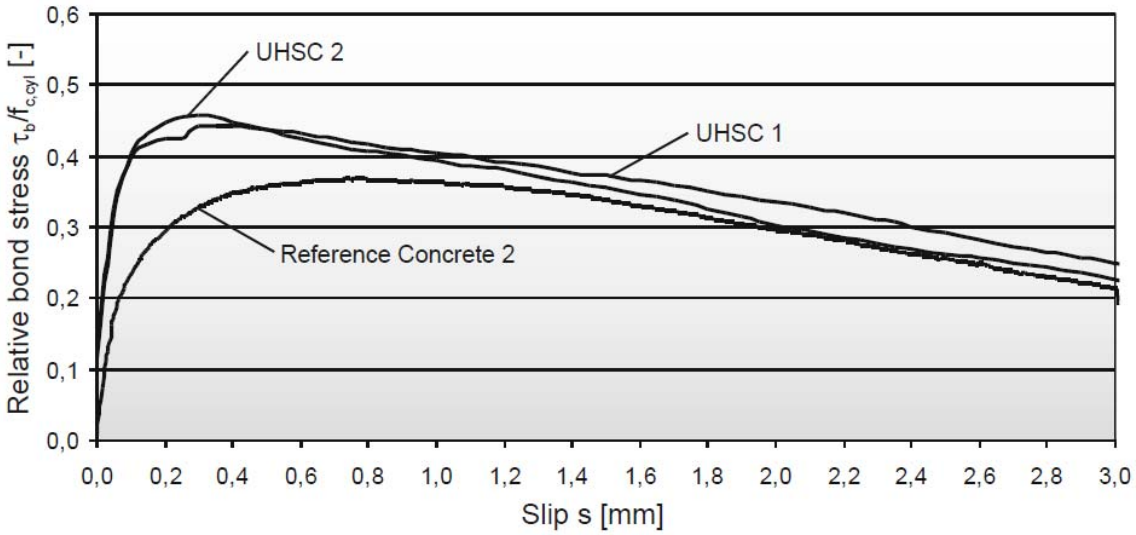

Figure 2-42: Relative Bond Stress slip relationship for reference concrete 2 (62MPa), UHSC1 (135 MPa), and UHSC 2 (147 MPa) [63]

2.2.8 Influence of Fibers on Bond (UHPC vs UHPFRC)

2.2.8.1 Influence of Fiber Orientation on Bond

Holschemacher and Weibe [67] provide results pertaining to fiber orientation, however, the concrete strength only varies from NSC (29MPa [4.2ksi]) to HSC (95MPa [13.7ksi]) and would not be considered UHPC. The important variables in the experiment are fiber volume fraction, bar size, concrete strength, and fiber orientation. Fiber volume fraction varies from 0% to an unspecified amount of fibers, bar size changes from M10 (US #3) vs M16(US #5). Fiber orientation is casted perpendicular and parallel to the rebar. Further information on the casting technique is limited. The test is a modified RILEM test (4.5db cover, varied embedment of 5db for NSC and 2.5db for HSC [to prevent rupture].

According to Figure 2-43 the specimens with fibers casted vertically (parallel to rebar length) do not play a significant role in behavior or bond stress compared to the specimens with no fiber. This is not surprising because the concrete cover is large enough to provide sufficient confinement on its own

What is interesting with the Holschemacher and Weibe [67] results is that according to Figure 2-44 the specimens with fibers casted horizontally (perpendicular to rebar) do not play a significant role in the behavior or maximum stress slip values for NSC either unless there is a splitting failure. When the horizontally cast fiber specimen (Figure 2-44: “wire fibre VB 1 - rebar…”) failed in pullout it is nearly identical to the specimen with fibers cast vertically (Figure 2-44: “wire fibre - rebar…”). However when the horizontally cast fiber specimens failed in splitting failure (Figure 2-44: “wire fibre VB 2+3 - rebar…”) there is roughly a 20% increase in maximum bond stress and a

somewhat brittle drop in strength to roughly 55% of its peak stress. Little explanation has been given as to why splitting failure was caused with horizontal orientation and why bond stress is significantly higher. It is explained that the fibers offer confinement after splits open so that the failure is not as brittle, but still not as ductile as a pullout failure.

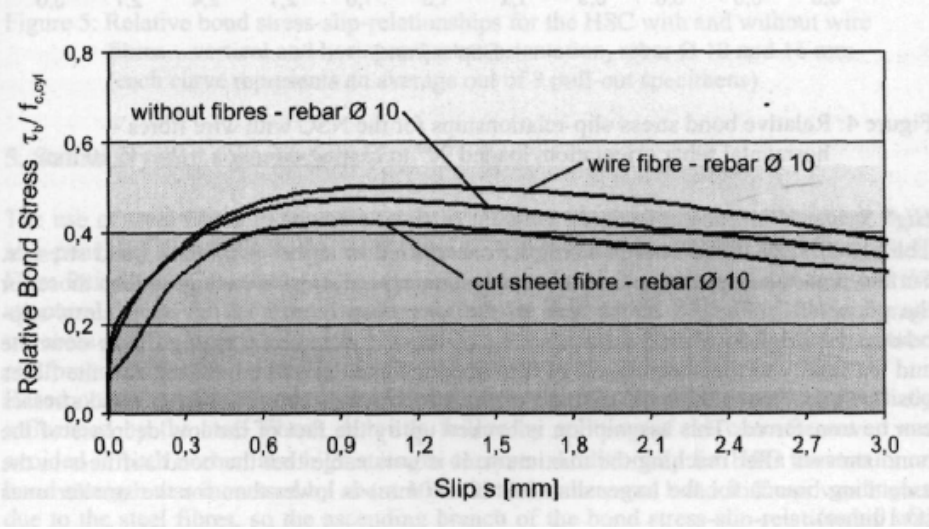

Figure 2-43: Relative bond stress-slip relationships for NSC with and without fibers, all cast parallel to rebar [67]

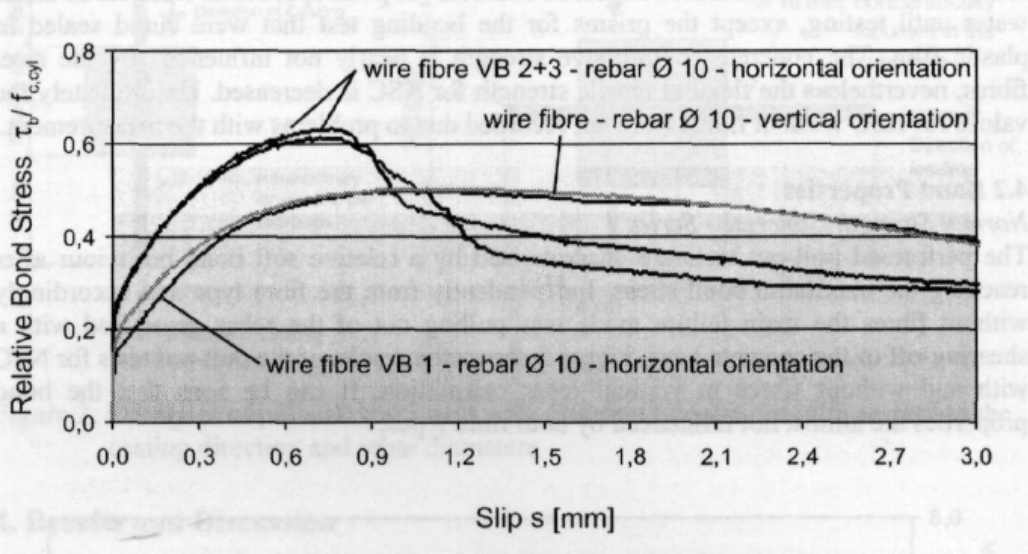

Figure 2-44: Relative bond stress-slip relationship for NSC with varying casting direction, all with fiber [67]

For HSC, the presence of fibers in addition to their orientation with regard to the rebar play a larger role (Figure 2-45). For M10 bars the bond stresses are roughly 54MPa (7.8ksi), 49MPa (7.1ksi), 45MPa(6.5ksi) for perpendicular to rebar (horizontal), parallel to rebar (vertical), and no fibers respectively. Stiffness is relatively similar for all of the No 10 bar series. For No16 bars the maximum stress (49MPa [7.1ksi]) are similar for both parallel and perpendicularly cast. However the stiffness is much greater for the parallel specimens. The only explanation given is that this might be linked to the fiber redistribution.

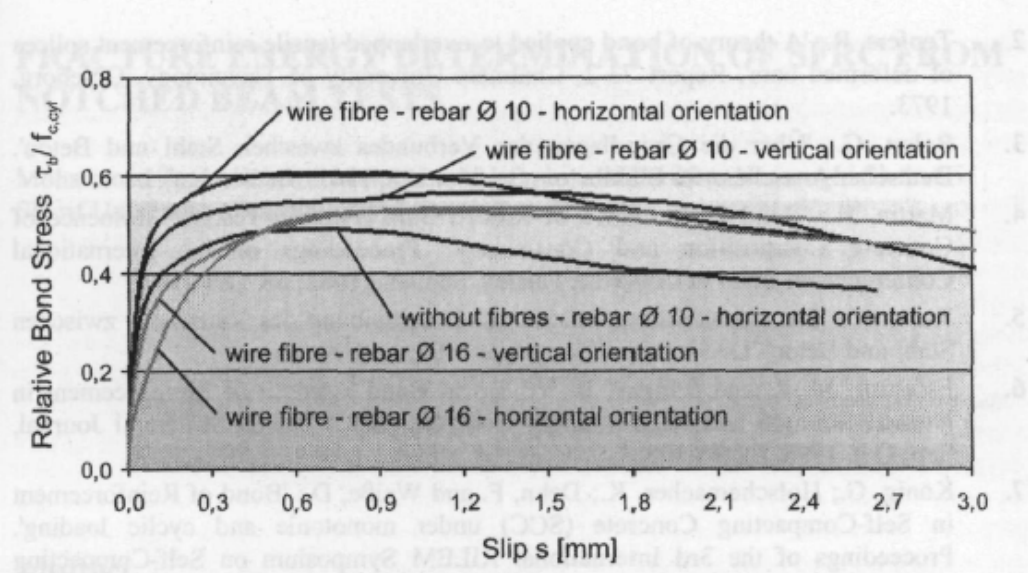

Figure 2-45: Relative bond stress-slip relationships for the HSC with and without fibers, vertical and horizontal fiber orientation, No10 and No16 rebar size [67]

The significance of this experiment is that it explores casting method (and hence fiber orientation) versus bond behavior. It also explores various concrete strengths, rebar sizes, and failure modes. The limit of the experiment is that the casting method is not explicit, the maximum strength concrete used is 95MPa (13.7ksi) < UHPC, the fiber strain hardening properties are not given, fiber volume is not given, and definitive conclusions are lacking.

2.2.8.2 Influence of Fibers in Conjunction with Large Concrete Covers

Different fiber volume fractions and orientations of UHPFRC show relatively small change in the bond behavior as long as cover is substantial enough to prevent splitting. Looking in

Figure 2-41 at the “No Fiber” specimens in addition to the other 3 types of specimens with fibers there is not a very distinct difference between specimens with fibers and specimens without fibers for the same concrete strength. It is important to note that this data is with 4.5db concrete cover. Schumacher [60] found that for 52MPa (7.5ksi) concrete the average maximum bond stress only increases from roughly 22.5MPa (3.3ksi) to 21MPa (3ksi) and the ductility increases ever so slightly when fibers are added (Figure 2-46). The average range of the fiber reinforced specimens were in the upper range of the specimens with no fiber. The reasoning given for this is that the concrete cover is large enough and provides enough confinement that the radial tensile strains (radial cracks) do not exceed the strains (crack widths) at which the fibers become activated. Another possible reason, only for the slight increase in ductility, is that the steel bars can be blocked by neighboring fibers with which result in a dowel action of the fibers obstructing the movement of the rebar when it is pulled out of the concrete (Figure 2-47).

Leutbecher [69] found that for 195MPa (28.3ksi) concrete and 10mm diameter 500MPa (72ksi) rebar the maximum average stress and the corresponding slips are 56.7MPa(8.22ksi) / 0.2mm and 54.8MPa(7.94ksi) / 0.15mm for 1% fiber volume and no fibers respectively. It appears that in this case the addition of fibers may have increased the stiffness, perhaps due to decreased bond crack width due to fiber bridging, but decreased the maximum average bond stress. Jungwirth and Muttoni [64] used threaded 12mm and 20mm diameter bars embedded in a UHPFRC mix with 190MPa (27.6ksi) and 2% fiber volume fraction. Various embedment lengths were explored. The bond stress for the bar rupture was artificially low at 38MPa (5.5ksi) while for all other embedment lengths the maximum bond stress were all similar at an average of 59MPa (8.6ksi).

Greiner and Reineck [71] found that UHPFRC with 180MPa (26.1ksi), 2% steel fiber volume fraction, 4mm diameter bar allows for developing yield stress in the bar (500MPa) with 2 bar diameters instead of 5 [66]. Maximum bond strengths ranging from 40MPa-50MPa (5.8ksi – 7.3ksi) were achieved. Interpolating from a graph in their report, the slip at maximum bond stress is approximately 0.2mm. Yoo, Shin, Yang, and Yoon [72] found that with bars of ultimate capacity of 607MPa (88ksi) and 766MPa (111ksi) that the maximum bond stress are very close to each other. They also found that varying the fiber volume fraction from 1%, 2%, 3% allowed for a slight increase in bond stress due to the increase in compressive strength with addition of fibers. However, at 4% the compressive strength decreased and so did the maximum bond stress. Holschemacher and Weisse [67] have explored the effect of fiber volume fraction and orientation on bond for HSC (95MPa [13.7ksi]) and NSC (29MPa [4.2ksi]). There is varying results that need more in depth analysis that are given (see 2.2.8.1 Influence of Fiber Orientation).

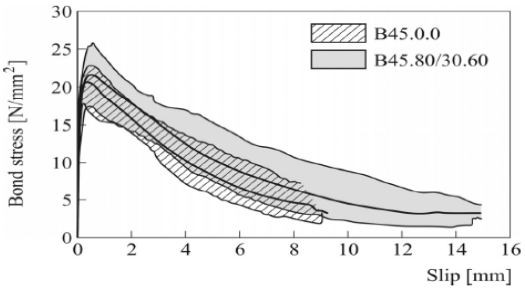

Figure 2-46: Comparison of pullout between specimens with fibers (grey) and without fibers (hashed) [60]

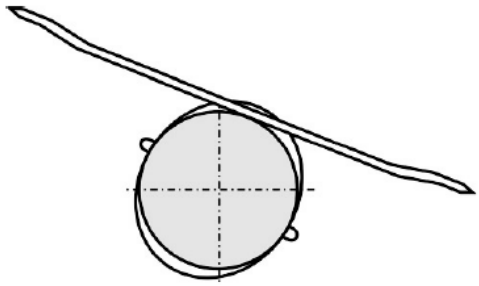

Figure 2-47: Dowel action of the fibers blocking the ribs of the rebar [60]

2.2.8.3 Influence of Fibers in Conjunction with Small Concrete Covers

UHPFRC bond stress is significantly affected by fiber volume fraction when covers are small enough to induce splitting type failure. Bigaj-van Vliet [73] did a literature review in 2002 on twelve different sources that had various experimental pullout tests results arrived at using a wide variety of test setups, concrete strengths (including UHPC), and varying fiber presence. The conclusion was that in terms of pullout failure (i.e. when concrete cover is large) there is no conclusive evidence of fibers contributing anything significant. However the majority of the researchers agreed that bond strength increases with increased fiber presence in the case of splitting failure (i.e. when concrete cover is small). There is nothing conclusive for bond stiffness (pre-peak behavior) increase or decrease. Most agree that bond ductility (post-peak behavior) for splitting failure is affected by fibers but the behavior for pullout failure has differing opinions. Arup et al [70] examined the behavior or Compact Reinforced Concrete with a 28day compressive strength of 165MPa (23.9ksi) and fiber volume fraction varying between 3% and 6%. The bar used was 16mm and the cover was 1.8db in order to be more realistic for what might be used on site. The embedment length was changed from 8.75db which caused rebar rupture and a bond stress of 19.4MPa(2.81ksi) to 6.25db embedment length which allowed for pullout failure type and bond stress of 23.6MPa (3.4ksi). The author notes that in general, smaller embedment lengths allow for higher bond stresses and noted that tests done at the Institute of Concrete Technology, Shimizu, Japan used 3 bar diameter bar embedment and was able to obtain a maximum of up to 85MPa (12.3ksi) bond stress.

Chao, Naaman, and Parra-Montesinos used strain hardening FRC with a compressive strength of 76MPa (11ksi). US No.5 and US No.8 bars were used which correspond to 4.18db and 2.6db cover. Various fiber types and percentages were used. They found that at 2% fiber volume fraction there is very little behavior difference between different fiber shapes and that the bond behavior and crack behavior is better. Any fiber volume fraction greater than 0% greatly helped specimens of both 2.6db and 4.18db cover.

Cheung & Leung [74] used 150MPa (21.7ksi) concrete with both 2% and 0% fibers with both 5db and 8db embedment lengths and a constant cover of 3.25db. The failure mode in all cases was a splitting failure, however the average pullout strength increased with 2% fibers. For 5db it increased by 144% and for 8db it increased by 154%.

In the next section the experiments, test setups, and data of several authors will be explored in detail because they have very large importance to the variables and test setups chosen in this thesis: Leutbecher [69] and Fehling, Leutbecher, and Lorenz [75] look at bond on UHPC and UHPFRC with varying fiber volume fractions and covers. Chao & Naaman [61] look at bond on 76MPA (11ksi) compressive strength strain hardening concrete with varying fiber volume fraction and fiber geometry/type. Saleem, Mirmiran, Xia, and Mackie [76] look at bond on UHPFRC with High Strength MMFX bars with very small concrete cover and varying embedment lengths.

2.2.8.3.1 Leutbecher [69]

Leutbecher [69] used two different strength bars (500MPa [72ksi]) and (1420MPa [206ksi]) embedded in both UHPC and UHPFRC that has 48hr 90ºC steam cured

strength of 190MPa (27.5ksi). The data is presented in Figure 2-48 and the key to interpreting the data is as follows: 1st designation is bar strength (BSt = 500MPa bar, St = 1420MPa bar, 2nd designation is bar diameter (10 mm), 3rd designation is concrete cover (c10 = 1db, c25 = 2.5db, c45 = 4.5db), 4th designation is whether or not there is fiber reinforcement (F = 1% fiber by volume, blank = 0% fibers). St10c45 compared to BSt10c45 shows that the much lower yield strength bar has lower bond stress (56.7MPa [8.2ksi]) than the high strength bar (51.4MPa [7.5ksi]), with a slip at maximum stress of 0.2mm and 1.5mm for BSt and St respectively. BSt is very stiff whereas the St exhibits very pronounced softening. The difference in stress slip behavior can be attributed to the relative rib area.

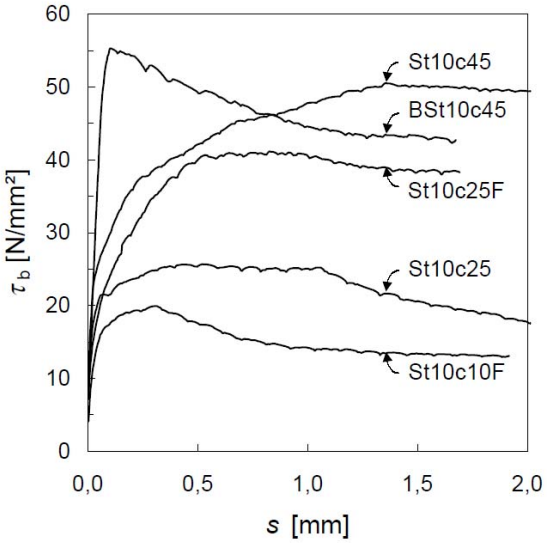

Figure 2-48: Graph from Leutbecher [69]

Another set of data from Leutbecher is shown in Table 2-5. Leutbecher [69] used 10mm diameter 500MPa (72ksi) rebar embedded in both UHPC and UHPFRC with a 28 day room temperature cured compressive strength of 150MPa (21.8ksi). The UHPFRC has 1% fiber by volume. The test setup is not a Modified RILEM test but it does have

4.5db concrete cover as RILEM suggests. The maximum average stress and the corresponding slip are 56.7Mpa(8.22ksi) / 0.2mm and 54.8MPa(7.94ksi) / 0.15mm. This shows that at large covers (4.5db) the fibers are not so influential. It appears that in this case the addition of fibers may have increased the stiffness, perhaps due to decreased bond crack width due to fiber bridging, but decreased the maximum average bond stress.

Table 2-5: Summarized results taken from Leutbecher [69]

Leutbecher (2007)									
series #	1	2	3	4	5	6	7	8	9
comp strength (MPa)	195								
fiber volume (%)	0	1	0		1		0	0	0
bar fy (MPa)	500		1420					1470	
bar fu (MPa)	550		1570					1620	
bar diam (mm)	8.00							10.00	12.00
bar area (mm²)	50.27							78.54	113.10
rel rib area	0.072		0.019			0.019		0.026	0.022
embedment length/db	1.5								
cover/db	4.5			2.5		1	2.5		
max pullout strength (N)	340.2	328.8	308.4	144.6	246.0	120.0	220.8	176.4	204.0
max bond stress (MPa)	56.7	54.8	51.4	24.1	41.0	20.0	36.8	29.4	34.0
slip at max bond (mm)	0.20	0.15	1.52	0.96	0.72	0.34	0.63	0.35	0.65
failure Mode	x								
casting direction	par						perp	par	

2.2.8.3.2 Saleem, Mimiran, Xia, and Mackie [76]

The experiment used MMFX rebar embedded into 175MPa (25.5ksi) UHPC with very small cover to simulate what might be seen in a very thin bridge deck slab . US #3 and #7 rebar were used which resulted in having a cover of 2.2db and 0.65db respectively. A summary of the data is shown in Table 2-6 and typical load-slip responses are shown in Figure 2-49 (for #3 rebar) and Figure 2-50 (for #7 rebar). The variation in

slip behavior between different embedment lengths is not consistent and no conclusions can be drawn from this. The #7 rebar embedded 18db has a lower peak load than with 12db embedment (Figure 2-50). This concludes that for such a small cover an increase in embedment length helps to a threshold after which behavior worsens. In this instance the threshold is somewhere between 12db and 18db. The failure modes for typical specimens are shown in Figure 2-51.

Table 2-6: Summarized Data from Mackie et al [76]

Mackie et al (2012)							
Series #	1	2	3	4	5	6	7
comp strength (MPa)	175						
Fiber volume (%)	2						
bar fy (MPa)	689 (100ksi)						
bar fu (MPa)	1172 (170ksi)						
casting direction (to load dir.)	x						
bar diam (mm)	9.525			22.225			
rel rib area	x						
cover/db	2.2			0.65			
embedment length/db	8	10	12	8	10	12	18
ult rebar strain (avg from 3 tests)	0.0074	0.0098	0.0137	0.0017	0.0021	0.0023	0.0043
ult strain / yield strain	0.62	0.82	1.26	0.43	0.53	0.57	0.35
slip at ult	0.08	0.055	0.064	0.036	0.07	0.06	0.15
Failure Mode	split		split +crush	split	split +crush	crush	
rebar	no yield		yield	no yield			

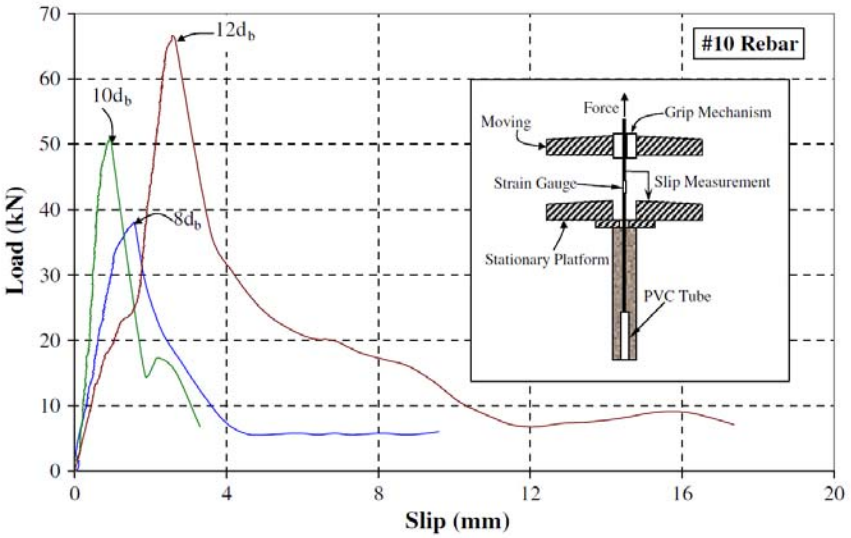

Figure 2-49: Typical load-slip responses for #3 rebar pullout specimens [76]

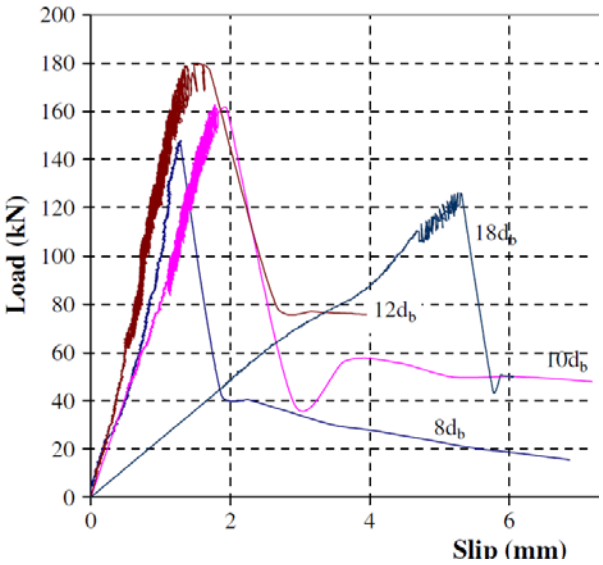

Figure 2-50: Typical load-slip responses for #7 rebar pullout specimens [76]

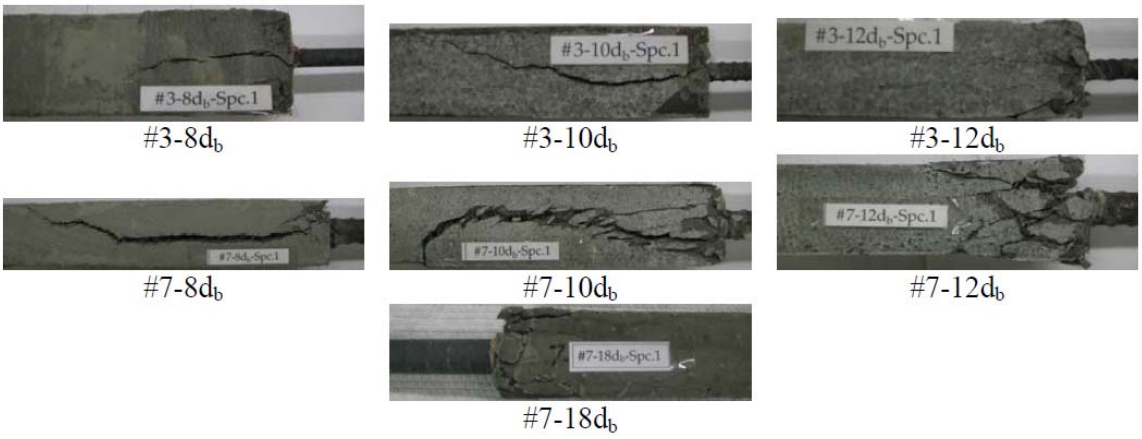

Figure 2-51: Modes of failure in typical pullout specimens [76]

2.2.8.3.3 Fehling, Lorenz, Leutbecher [75]

Fehling, Lorenz, and Leutbecher ran pullout tests with a specimen type shown in Figure 2-52. The shorter embedded bar which sometimes is smaller diameter, is expected to fail first, and it is referred to as the anchorage bar. The longer embedded bar which sometimes has a larger diameter is expected not to fail, and is referred to as the support bar. The other bars are referred to as longitudinal reinforcing and they prevent the UHPC in between the bars from failure. UHPFRC with 1.5% fibers was used with varying covers and embedment lengths. The exact specifications and results are shown in Table 2-7 as well as in Figure 2-55. Failure modes and conclusions are shown in Figure 2-53 and Figure 2-54. They conclude that a concrete cone failure has little or no residual stress at 7mm slips. This failure mode is rather brittle and should be avoided. Splitting failure and V splitting is more ductile because the fibers are activated and act as confinement.

Table 2-7: Summary of data extrapolated from the graphs of Fehling, Lorenz, and Leutbecher [75]

Fehling et al (2012)										
comp strength (MPa)	165									
Fiber volume (%)	1.5									
bar fy (MPa)	500 (72ksi)									
bar fu (MPa)	x									
bar diam (mm)	12									
rel rib area	x									
casting direction (to load dir.)	perpendicular									
Series #	1	2	3	4	5	6	7	8	9	10
cover/db	1					1.5				
embedment length/db	4	6	8	10	12	4	5	6	8	10
max bar stress (MPa)	280	365	510	510	510	395	480	510	650	670
slip at max bond (mm)	0.4	0.5	0.5	0.6	0.7	0.65	0.6	0.55	1.7	6.3
Failure Mode	V split		Split			V split			Split	
Steel state	no yield					no yield			yielding	
Series #	11	12	13	14	15	16	17	18	19	20
cover (db)	2					2.5				
embedment length (db)	3	4	5	6	8	2	3	4	5	7
max bar stress (MPa)	350	420	550	590	675	320	425	540	620	620
slip at max bond (mm)	0.25	0.75	0.9	0.5	4.6	0.3	0.4	0.4	0.65	x
Failure Mode	cone			V split	Split	Cone			V split	
Steel state	no yield			yield		no yield			yielding	

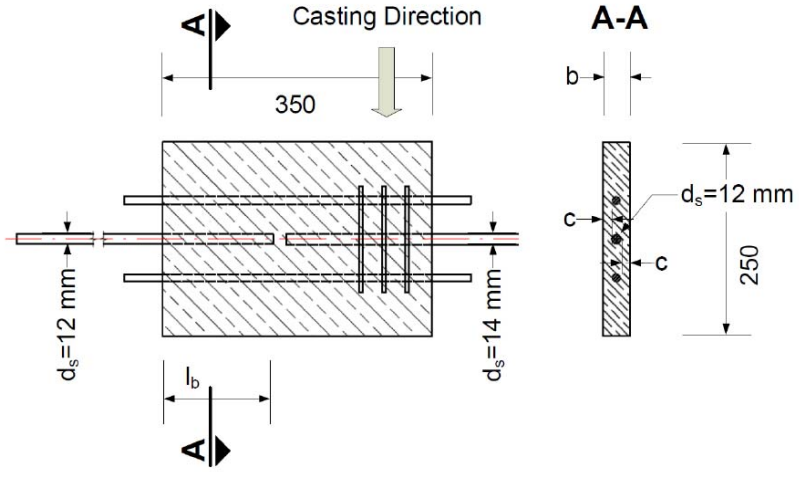

Figure 2-52: Specimen design [75]

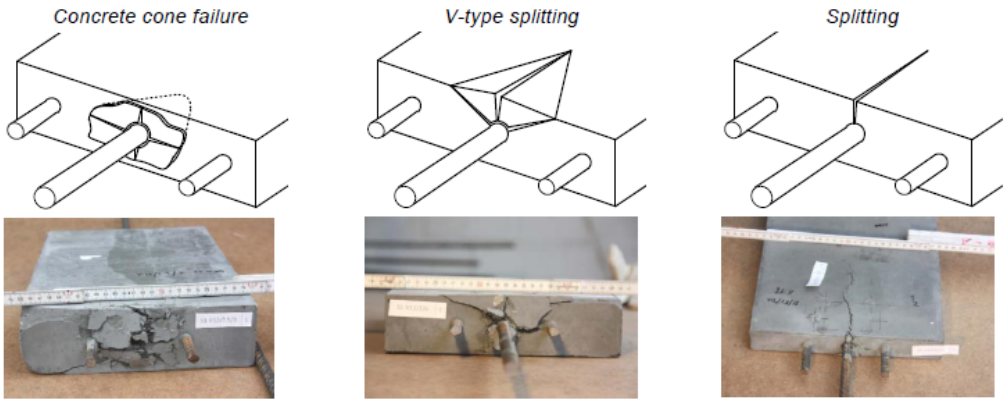

Figure 2-53: Specimen failure modes [75]

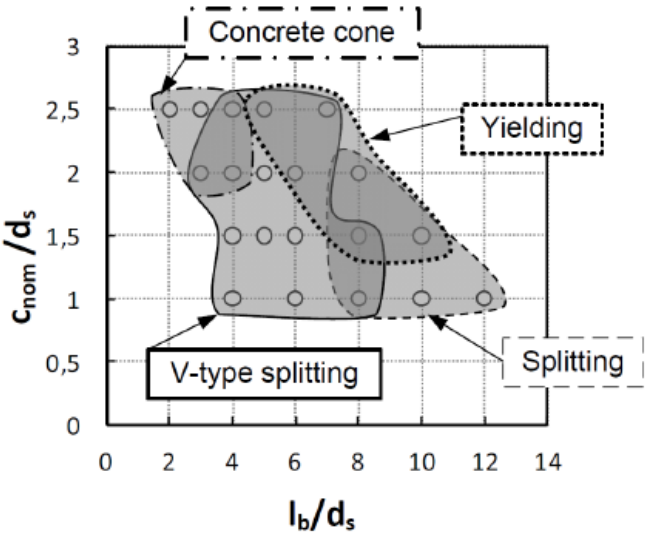

Figure 2-54: Failure modes of the test specimens compared based on cover and embedment [75]

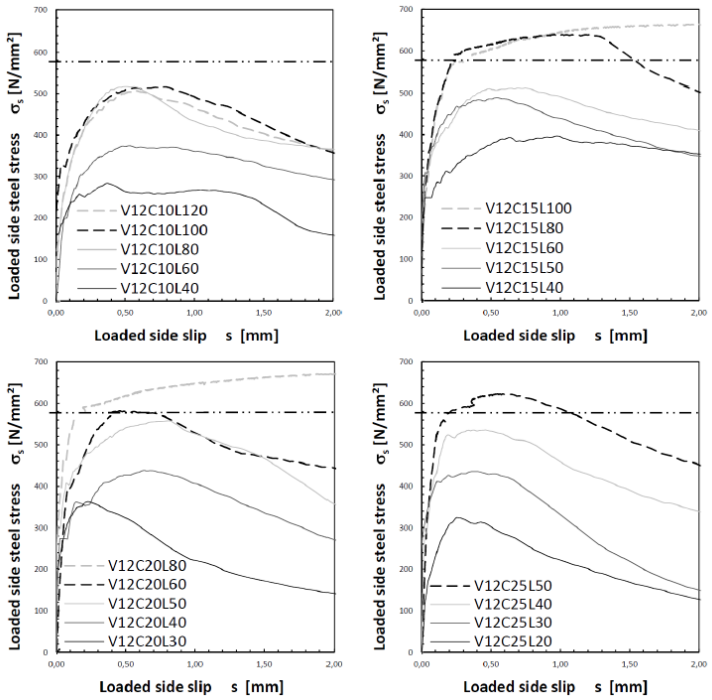

Figure 2-55: Stress-slip relationships for four different covers [75]

2.2.9 Phase II Literature Review Summary

- The effect of fiber orientation on bond stress has not been studied for UHPFRC, it has only been studied for HSC (95MPa [13.7ksi]) and NSC (29MPa [4.2ksi]). The effect of fiber orientation on bond stress in any strength FRC needs more data to make any conclusions [67].

- Bond strength of UHPFRC with regard to multiple fiber percentages beyond 0% is lacking. (in addition to 0%) with other parameters remaining the same have not been studied. [70] used 3% and 6% fibers, [75] used 1.5% fibers, [69] used 0% and 1% fibers. [61] used multiple fiber percentages in strain hardening FRC but

the concrete compression strength is 76MPa(11ksi), roughly half that of UHPC. Shin, Yang, and Yoon [72] explored 1,2,3, and 4% fibers but with larger covers.

- Only Saleem, Mimiran, Xia and Mackie [76] have done pullout tests with UHPFRC using MMFX rebar.

2.3 Phase III: Uniaxial Tensile Behavior of Rebar Reinforced UHPFRC

2.3.1 Mechanics of Reinforced UHPFRC

Reinforced UHPFRC is a composite made of UHPFRC and rebar. An idealized force-strain curve for the two components as well as their composite behavior is shown in Figure 2-56. Reinforced UHPFRC differs from conventional reinforced concrete (RC) in that RC behavior is almost completely controlled by the type and amount of reinforcement. The tensile strength of normal concrete is very small which means that in RC the cracks tend to open early and with well-defined spacing. Reinforced UHPFRC, in contrast, is controlled both by the type and amount of rebar reinforcement as well as the fiber reinforcement. The fibers allow tensile forces to be transferred across cracks (Figure 2-58b), resulting in tension stiffening that has a large impact on the reinforced UHPFRC behavior [77]. RC specimens without fibers tend to develop many, relatively even spaced macro cracks at failure (Figure 2-57 bottom). In comparison to this, UHPFRC with fibers tend to develop many small micro cracks and only one or very few macro cracks at failure (Figure 2-57 top) (micro cracks are not visible in this picture).

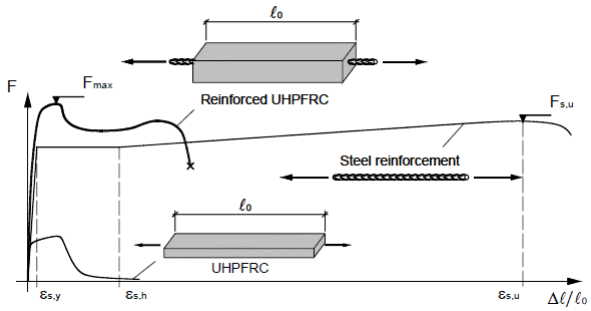

Figure 2-56: Typical force-strain curves for UHPFRC, rebar, and reinforced UHPFRC [78]

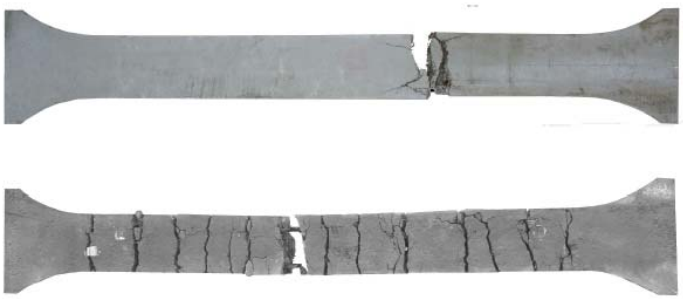

Figure 2-57: Reinforced UHPFRC (top), Reinforced UHPC (no fibers) bottom) [79]

In an uncracked state reinforced UHPFRC can be assumed to behave elastically with perfect bond (Figure 2-58a). Micro cracks develop after the matrix reaches its cracking strength (Figure 2-58b). The fibers in the cracks help transfer stresses through the cracks and lead to a stiffness greater than that of the rebar. In Figure 2-59 as soon as the "Ordinary reinforced concrete" is cracked the stiffness drops very close to that of the rebar because there are no fibers to bridge cracks. In contrast the "Reinforced UHPFRC" loses some stiffness after initial cracking but the fibers still leave a large linear stiffness. The fiber bridging results in multiple cracking of the matrix (Figure 2-58c). Eventually, a threshold of micro cracks is reached and a further increase in displacement results in softening of the matrix and development of a macro crack (Figure 2-58d). The rebar will

strain harden in the macro crack resulting in multiple macro cracks (Figure 2-58e) followed by rebar softening and rebar rupture (Figure 2-58d).

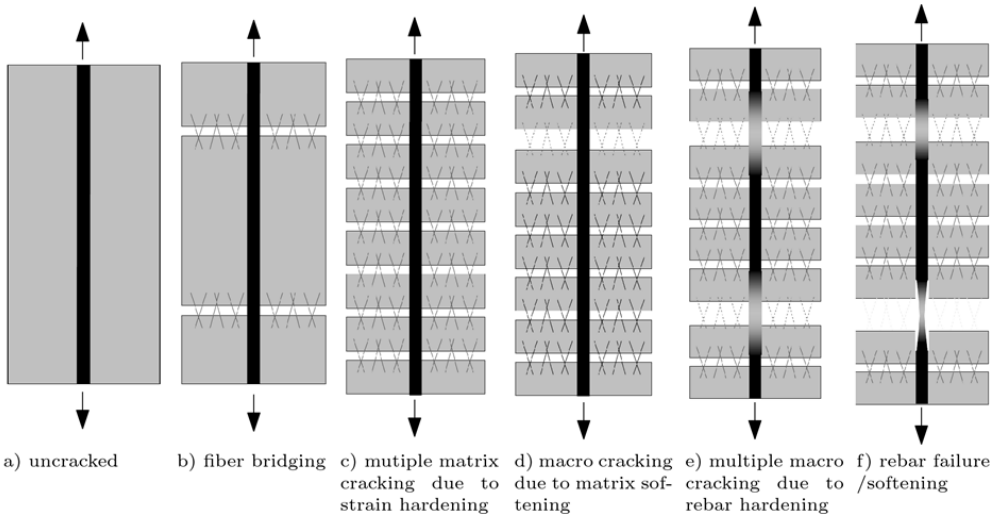

Figure 2-58: Mechanics of strain hardening reinforced UHPFRC under tension (modeled after [58])

2.3.2 Advantages of Reinforced UHPFRC

Reinforced UHPFRC has better serviceability that standard RC. Radaelli [78] found that there is an increase in stiffness of the composite as well as favorable multiple cracking with considerably smaller crack widths. Leutbecher and Fehling [80] also found that strain hardening behavior with very small crack spacing and crack widths can be achieved at fiber volumes as low as 0.9% when combined with the rebar, whereas a typical UHPFRC on its own may require roughly 2% fiber volume to achieve strain hardening and favorable crack width. This is of high importance because the high cost of UHPFRC is largely due to expensive steel fibers. A significant reduction in fiber volume fraction can result in a significant reduction in project cost.

Research has also been carried out on FRCs and the findings show positive results with crack widths and crack spacing: Kunieda et al [81] used 95MPa concrete with 1.5% PE fiber. Moreno et al [82] used a range of 30-53MPa concrete with varying fiber volume fraction as well as various confinements [83,84]. Larusson and Fischer [85] used 60MPa concrete with ECC in conjunction with rebar. Deluce et al [86] used 30-95MPa concrete. Yun et al examined the damage tolerance of SHCC tension ties under cyclic loading [87]. Leutbecher, and Fehling tested UHPFRC uniaxial specimens of various sizes [88] as well as panel type specimens with UHPFRC and rebar [80]

2.3.3 Stress vs Strain Behavior of Reinforced UHPFRC

Proper RC is designed so that the reinforcement bar has a larger stress capacity than the stress required to bridge a local crack in the concrete [78]. Oppositely, it is possible for the reinforcement bar used in reinforced UHPFRC to have a smaller stress capacity than the stress required to bridge a localized crack in the UHPFRC. An illustration of this difference in behavior is shown in Figure 2-59. In reinforced UHPFRC strain localization may happen at a stage when the steel reinforcement is yielding. In this case the fibers pullout during strain localization and the stress released by the fibers may surpass the capacity of the reinforcement. This can lead to a sudden failure [78]. Sturwald and Fehling [89], Schumacher et al [68], and Habel [3] found this same problem in beams where higher fiber volume fractions lead to less rotation capacity because of crack localization.

For ultimate limit state design the influence of the fibers has to be considered not only to achieve an adequate safety but also to attain a ductile behavior with an announcement of failure by excessive cracking [88]. Sturwald and Fehling propose that at higher fiber dosage more bar reinforcement in order to make bar hardening more pronounced then softening behavior of the fibers [89].

Predictive modeling with varying degrees of complexity exist in literature for reinforced FRCs [40, 68, 86, 89-91] and reinforced UHPFRCs [58, 77, 79, 81, 92-95]. The models will provide a good resource for comparison.

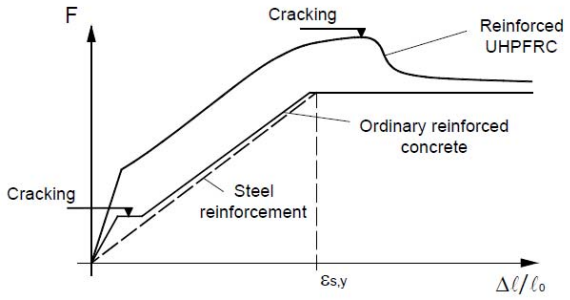

Figure 2-59: Ordinary RC versus Reinforced UHPFRC [78]

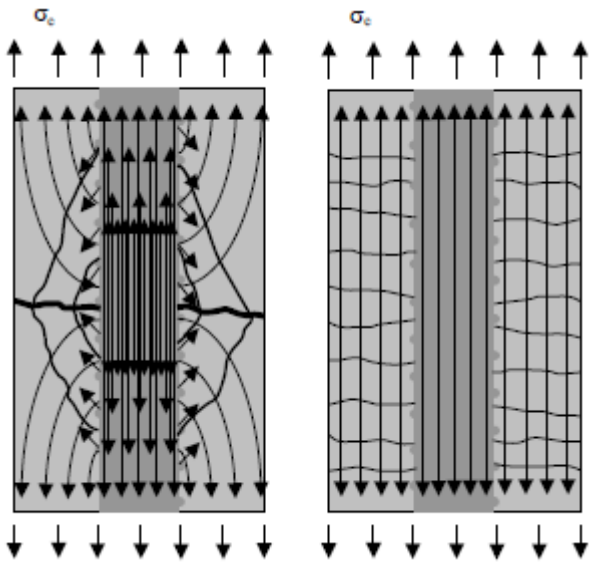

Figure 2-60: Crack formation and internal stresses in RC (left) vs FRC (right) [96]

2.3.4 Influence of Fiber Orientation on Tensile Behavior

Shionaga [97] casted HPFRC specimens with 0%, 0.8% and 1.6% fiber volume percentages along with a 12mm diameter rebar. They also changed the fiber orientation by varying flow direction. In Figure 2-61 some of the results are displayed. The "(x)" denotes fibers aligned parallel to the bar and the "(y)" denotes fiber aligned perpendicular to the bar. There is some difference between the behaviors based on orientation but they are very small. No analysis was carried out to prove that the fibers were oriented in the assumed direction.

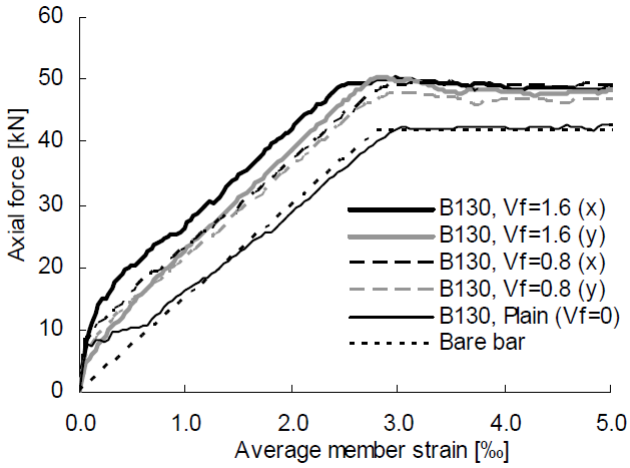

Figure 2-61: Axial strain of tensile specimens (x denotes fibers aligned along bar, y denotes fibers oriented perpendicular to the bar)

2.3.5 Uniaxial Tensile Test Methods

Test setups for reinforced UHPFRC are more complicated than a test setup for standard RC because the fibers allow the peak stress to reach a peak stress greater than the rebar itself. This means a single bar run through the axis of the specimen and grabbed on both ends would fail outside of the specimen because the exposed bar is the weakest point. In order to prevent failure outside of the specimen different researchers have used setups ranging from dog-bones [78, 82] to heavier reinforced ends [81, 97] or a combination of both [58, 64, 85].

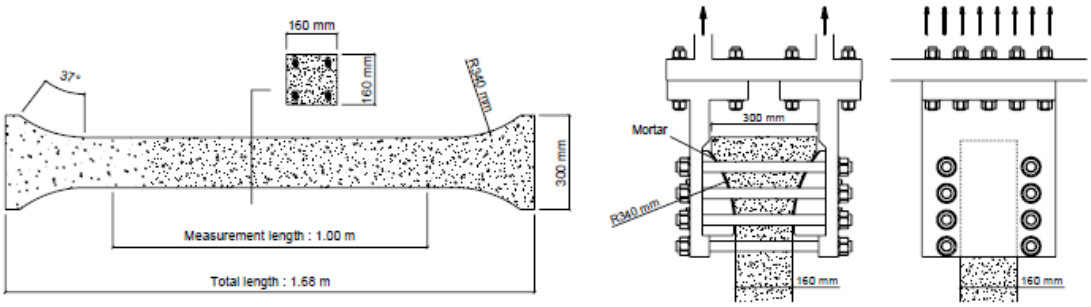

Figure 2-62: Dog-bone test setup for Redaelli [78]

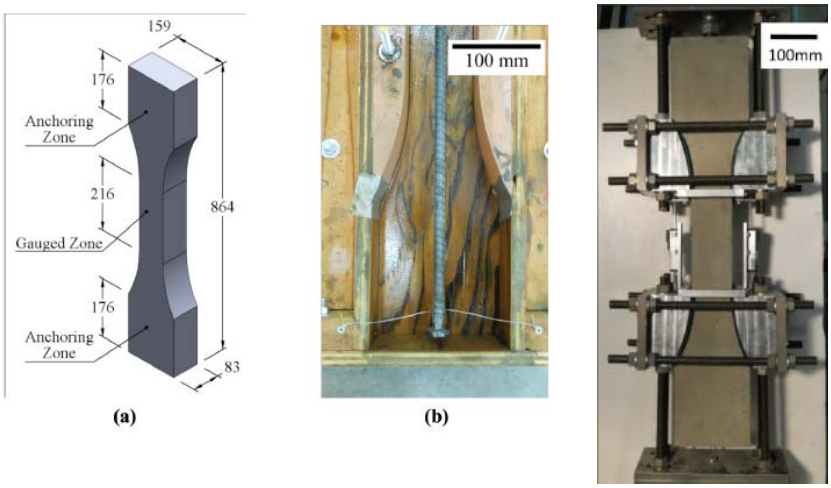

Figure 2-63: Dog-bone test setup for Moreno et al [82]

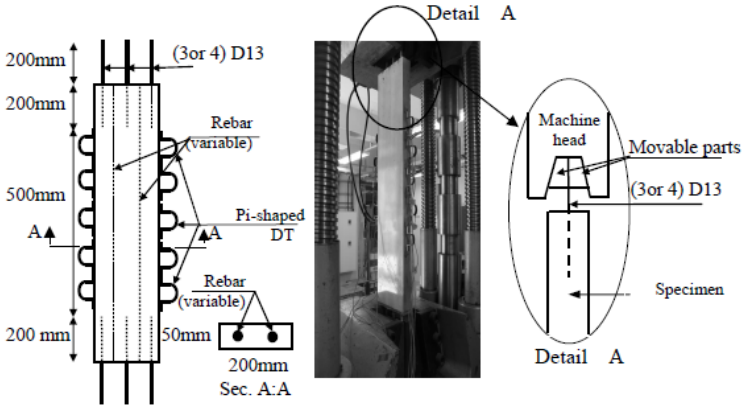

Figure 2-64: Heavily reinforced end test setup used by Kunieda et al [81]

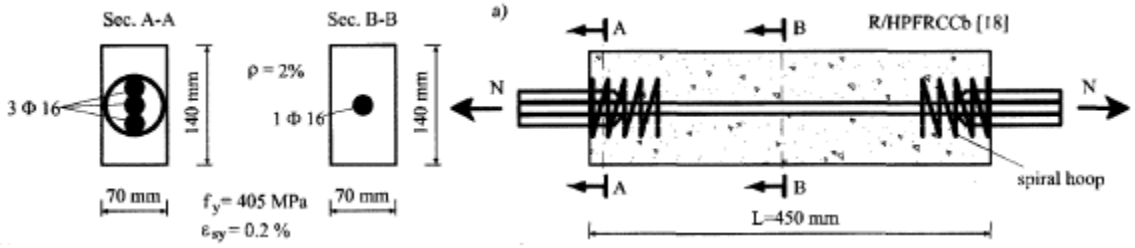

Figure 2-65: Heavily reinforced end test setup used by Fantili et al [91] and Otsuka [98]

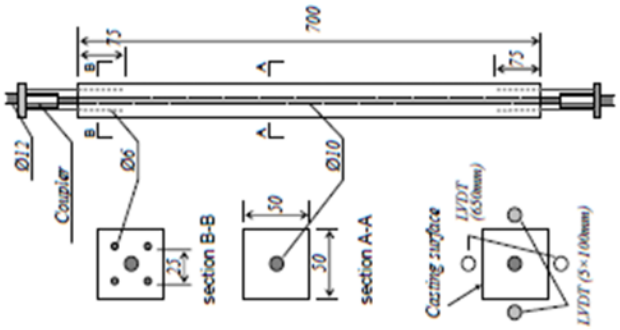

Figure 2-66: Heavily reinforced end test setup used by Shionaga [97]

3 CHAPTER THREE - EXPERIMENTAL STUDY

3.1 Materials

3.1.1 Rebar

Two different grades of uncoated deformed steel rebar are used in the experiment: normal strength Grade 60 rebar and high strength Grade 100 rebar. The Grade 60 meets the specifications of ASTM A615 [99] and will be referred to as A615. The Grade 100 rebar meets the specifications of ASTM A1035 [100] and will be referred to as A1035. The A1035 rebar used is manufactured by MMFX Technologies and has a different

composition than standard rebar that makes it virtually non-corrosive. It also has about twice the yield strength and twice the ultimate strength. Therefore less steel is needed, constructability is improved, and life cycle costs may be improved due to corrosion resistance. Comparison of the stress versus strain curves for each type of rebar are shown in Figure 3-1.

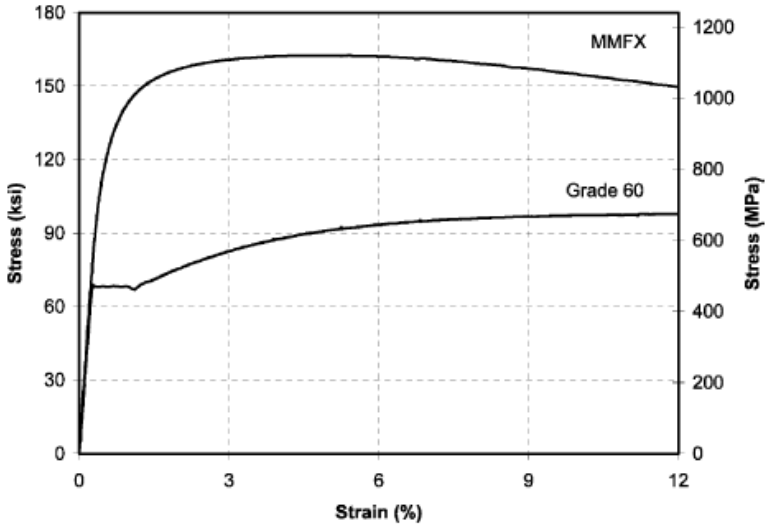

Figure 3-1: Stress-strain characteristics of ASTM A1035 and ASTM A615 rebar [101]

3.1.2 UHPFRC

Two types of UHPFRC are used in the experiment. The first (UHPC1) is a proprietary UHPC produced by Lafarge North America called Ductal JS1000. Ductal JS1000 is typically used as a field-cast joint fill solution for precast deck panel bridges due to its properties of durability, fluidity, and increased bond capacity. The mix proportions are shown in Table 3-1. The Premix consists of undisclosed amounts of silica fume, ground quartz, sand, and cement. The fibers are 0.2mm (0.008in) diameter x

13mm(0.55in) long. The fibers are slightly deformed in the mid-section (Figure 3-2a) and have a tensile yield strength of greater than 2000MPa (290ksi)

Table 3-1: UHPC1 (Ductal JS-1000) mix proportions

Material	Proportion (kg/m^3)
Premix	2195
Water	120
Superplasticizer	30
Steel Fibers (2%)	156

The second, (UHPC2), is a non-proprietary mix based on the mix developed at the University of Michigan Ann Arbor by Wille et al. [1]. It is important to note that due to the limitation of available materials the quality of material constituents is decreased, requiring an adjustment of the mix proportions. Therefore, UHPC2 is a modified version of the mix developed in Michigan resulting in different material properties. Small agglomerations of fine particles could not be broken up during mixing (Figure 3-7) leading to sub-optimal material properties. The mix proportions are shown in Table 3-2. The fibers are 20mm (0.0071in) diameter x 13mm(0.51in) long. They are straight, high strength steel fibers with a ultimate tensile strength of approximately 2600MPa (377ksi) (Figure 3-2b).

Table 3-2: UHPC2 (non-proprietary) mix proportions

Material	Proportion (kg/m^3)
Portland Type I Cement	888.0
Silica Fume	222.0
Silica Powder	222.0
Fine Sand	235.1
Coarse Sand	548.6
Water	173.0
Superplasticizer	32.0
Steel Fibers (2%)	157.0

Figure 3-2: UHPC fibers (a) UHPC-1 (Ductal JS-1000) (b) UHPC-2 (non-proprietary) [102]

3.1.2.1 Mixing Procedure

The mixer used for all phases of the experiments is a ¾ horsepower floor mounted rotary mixer capable of mixing a maximum of about 9 Liters (0.317cu.ft.) of UHPFRC. The mixing procedures for both UHPC1 and UHPC2 are based off a combination of suggestions in [1] [103].

The mixing procedure UHPC1 is to mix the premix at a low speed for 5 minutes. The water and superplasticizer are combined into a large glass, swirled for 5 seconds, and added to the mixer, medium speed, over the course of 1 minute. Once turned over, the speed is turned to high, and is allowed to mix for 1 minute before the mix is put back at medium speed and fibers are added over the course of 30 seconds. Finally the mix is allowed to mix for another 2 minutes on medium speed before casting.

UHPC2 mixing procedure is similar except for the beginning portion involving adding the dry materials. The first step is to mix the silica fume and the sand together at low speed for 8 minutes. The cement and silica powder are added to the bowl and mixed for an additional 8 minutes at low speed. Then the remaining procedure is identical to that of UHPC1.

Figure 3-3: Rotary floor mixer used in this research

Figure 3-4: Mixing of UHPC-1 (a) Water and high range water reducer (b) dry UHPC mix (c) adding water and superplasticizer (d-f) various stages of turning over (g) fiber agglomerations (h) fibers well distributed

3.2 Phase I: Uniaxial Tensile Behavior of UHPFRC and Rebar

3.2.1 Uniaxial Tensile Test of Rebar

A quantity of 3 No.3 bars each for A615 and A1035 rebar were tested in accordance to ASTM A370 [104] as shown in Figure 3-5 .

Figure 3-5: Extensometer attached to A615 rebar

3.2.2 Compression Test of UHPFRC

3.2.2.1 Test Specimen Design

The compressive portion of phase one consists of casting and testing 3 compression test cylinders for each of the variable combinations shown in Table 3-3. The specimens were casted into 3" x 6" (76mm x 152mm) greased steel cylinder molds. The material was casted in a circular motion using a small scoop. Neither the fiber specimens nor the non-fiber specimens were vibrated. The specimens were covered with plastic and left at room temperature. After four days the specimens were de-molded and the top eighth inch of each specimen was cut off with a masonry saw. After this 4 specimens at a time were ground in a cylinder end grinder, produced by Dam-END, to a planeness of ±5µm (0.000197") (Figure 3-6 and Figure 3-7).The planeness is checked by placing the cylinder on a rotating platen which has a dilatometer attached to it. A spray bottle is used

to cover the specimens with water. Afterwards they are wrapped with plastic wrap (Figure 3-8) and remain at room temperature until the day they are tested. The curing procedure has been chosen to imitate that which is used in Phase II and Phase III to accommodate the much larger pullout and rebar reinforced specimens.

Table 3-3: Compression cylinder series to be tested

UHPC1 0%fv	UHPC1 2%fv	UHPC2 0%fv	UHPC2 2%fv
7day	7day	7day	7day
14day	14day	14day	14day
28day	28day	28day	28day

Figure 3-6: Cylinder End Grinder (a) full view of machine (b) close up view of specimen

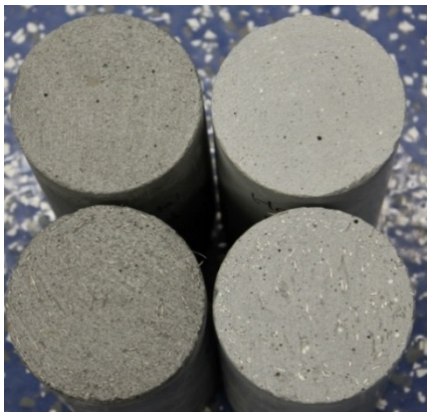

Figure 3-7: Ground and plane specimens with fibers (top) and without fibers (bottom). Dark grey is Ductal, light grey is non-proprietary

Figure 3-8: Cylinders wrapped in plastic shrink-wrap to keep in moisture

3.2.2.2 Test Procedure

The compression tests were completed using a Sate 1780kN (400 kip) load frame (Figure 3-9) with an MTS controller. For all of the specimens the load applied was recorded. For only the specimens with fibers the load vs concrete displacement data was captured. The concrete displacement was captured with a set of three linear variable transformers (LVDTs) attached to a holster on the concrete (Figure 3-10). The concrete displacement was later used to find the elastic modulus of the concrete through the slope of the stress vs. strain curve. Specimens without fibers were not tested with LVDTs due to the tendency of an explosive rupture.

The compressive load was applied using an actuator displacement rate of 0.5mm/min. This speed was chosen so that the concrete would rupture within 5 minutes. Using ASTM C29 standard for compression tests would have resulted in tests that may take more than 15 minutes per specimen. [103]. Before loading the specimen, the LVDT holsters, if necessary, were attached to the specimen using thumb screws (Figure 3-10).

The length from top screw tip to bottom screw tip was measured as the initial length for the strain calculations. When the specimen alignment in the machine was complete the loading began and the data was recorded at a rate of 51.2 Hz.

Figure 3-9: Overall compressive test setup

Figure 3-10: LVDT holders for compressive test data acquisition [102]

3.2.3 Uniaxial Tensile Test of UHPFRC

3.2.3.1 Test Specimen Design and Casting Procedure

The direct tension of UHPFRC portion of phase one consists of casting and testing at least 3 specimens from each series shown in Table 3-4. Eventually, due to the occurrence of several invalid tests, some series do not have data for all 3 specimens. The specimens were casted into 16” (406mm) long x 1” (25mm) wide x 2” (50mm) tall PVC molds. The “Parallel” casting method consists of using a scoop to drag the UHPC along

the length of the mold in small layers at a pace fast enough to align the fibers such as the method used by Wille and Parra-Montesinos [41]. The "RandomA" middle method consisted of dumping the UHPC in the center of the length and allowing the material to flow to the ends. The "RandomB" method consisted of dumping the UHPC in the end of the length and allowing to flow to the opposite ends (Figure 3-12).

After 3 days the specimens were de-molded, sprayed with water, and wrapped in a sealed plastic bag. After 10 days the specimen edges were ground with rubbing stone, the surfaces were lightly sanded, and wiped down with rubbing alcohol. Epoxy is used to glue 5" (127mm) long x 2" (51mm) wide x 0.032" (8.1mm) thick aluminum alloy 3003 interweave sheets onto the ends of the specimen. The aluminum is used to strengthen the ends of the specimen so that failure happens in the middle of the specimen rather than in the tensile testing wedge grips. The interweave pattern is used because it is more malleable in the tension wedge grips and allows for the wedge teeth to sink into the specimen which helps prevent eccentric loading (Figure 3-11). After 24 hours the specimens are sprayed with water, and wrapped back up in plastic until the 14 day testing date.

Table 3-4: Uniaxial UHPFRC specimens to be tested

UHPC1				UHPC2
0%	1%	2%	3%	2%
Parallel	Parallel	Parallel	Parallel	Parallel
-	-	RandomA	-	-
-	RandomB	RandomB	-	RandomB

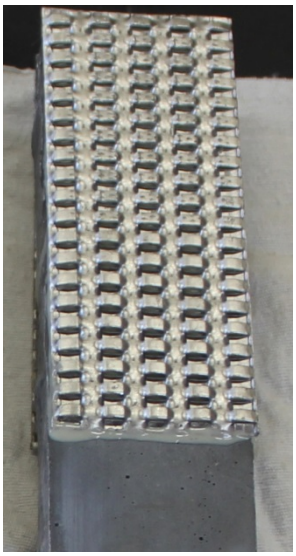

Figure 3-11: Interweave textured aluminum plate epoxied to the end of a tensile prism specimen

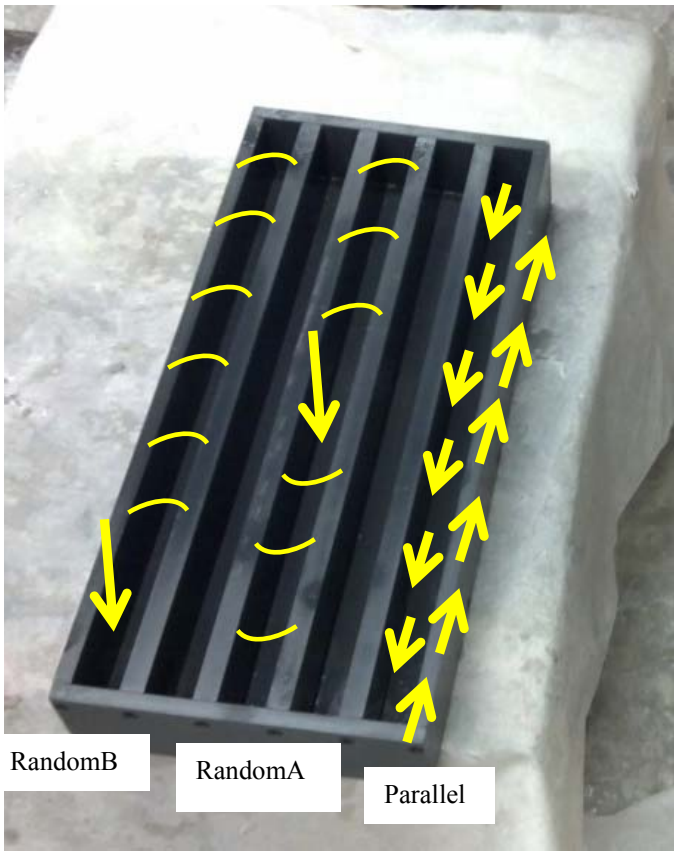

Figure 3-12: Direct Tension PVC molds and 3 different casting methods. Arrows represent casting location and the arcs represent flow direction.

3.2.3.2 Test Procedure

Like the compression tests, the UHPFRC tension tests were also completed using a Satec 1780kN (400 kip) load frame with an MTS controller. Serrated faced steel wedge grips were used to grab approximately 3" length at each end of the specimens on the aluminum plates. The whole aluminum plate was not grabbed because the wedge grips were slightly recessed into the load frame platens. Secondly, another small portion of the aluminum plates remained exposed in order to attach the LVDTs. The LVDTs were attached just inside the aluminum plate area as close to the edge of the aluminum as possible (Figure 3-13). It was anticipated that if the LVDTs were placed outside of the aluminum plates then they would be disturbed by failure cracks which may occur close to the aluminum plates where stress concentrations exist [12]. The downside of this setup is that the LVDTs may pick up strain in the area of the aluminum. The LVDT length is measured from bolt to bolt (Figure 3-13) and it is expected that the strain reduction in the aluminum plate is negligible.

The specimen was aligned in the machine using a square and a level. After alignment, the loading is applied displacement controlled at a rate of 0.5mm/min and data is recorded at a rate of 51.2 Hz. The test ended when the load decreased to 0.5kips (0.25ksi) which took about 15 minutes. The displacement rate is much higher than that of Graybeal and Baby [11] and that of Wille et al [15] however the gauge length is longer, displacement action is partly used in compressing the wedge grips, and the tests needed to be completed in a short period of time.

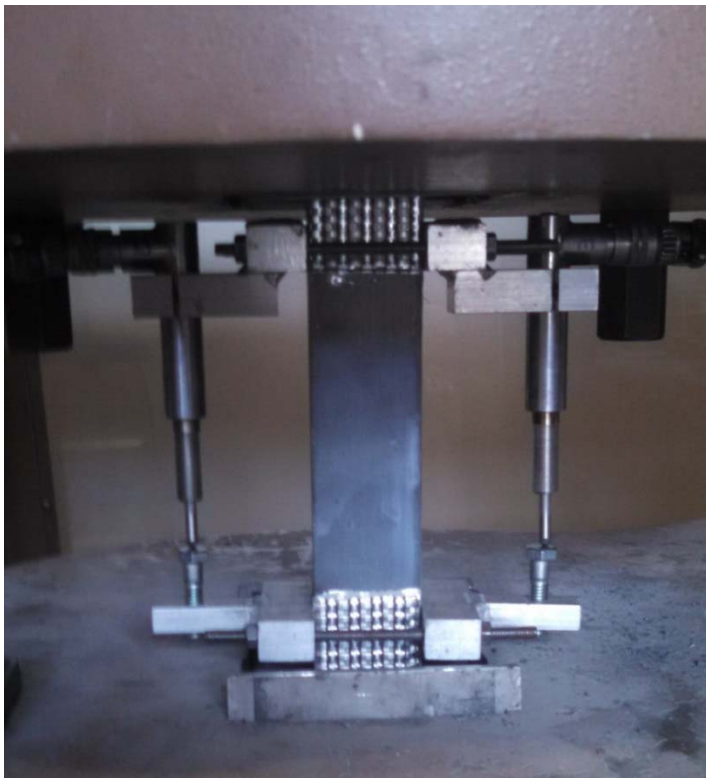

Figure 3-13: UHPFRC direct tension test setup with LVDTs

3.3 Phase II: Bond Behavior of Rebar Embedded in UHPFRC

3.3.1 Test Specimen Design

The first goal of the pullout test setup was to mimic tensile stresses as close as possible to those in the field. The second goal of the test setup was to pick something that was easy enough to cast and test 3 specimens per series and to test at least 10 series. A total of 21 series were tested and for the most part 3 specimens were tested per each series. In Table 3-5 the different series can be found by matching embedment lengths with fiber percentage / orientation (left column) and UHPC type / rebar type / rebar size / cover size (top row).

Figure 3-14 shows the formwork for the pullout specimens along with a typical rebar setup in the formwork. The specimen design is based very closely off of Fehling, Lorenz, and Leutbecher [75] and is also similar to that of Cheung and Leung [74] and Arup, Karlsen, and Lindstrom [70].

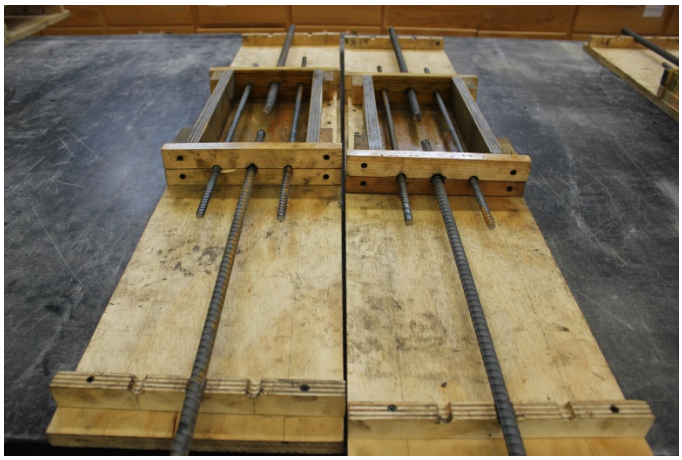

Figure 3-14: View of two fully assembled pullout molds

Table 3-5: Embedment lengths to be tested for specimens with various fiber volume fractions and orientations. Also, slightly varied are the UHPC mix type, rebar type, and rebar cover.

	UHPC Type: Rebar Type: Rebar Size / Cover:	UHPC1 A1035 #4 / 1.5db	UHPC1 A615 #4 / 1.5db	UHPC1 A1035 #3 / 2.17db	UHPC2 A1035 #3 / 2.17db
Fiber percentage and orientation	0	8db - -	- - -	8db 12db -	- - -
	1 (random)	8db 12db -	- - -	8db 12db 16db	- - -
	2 (random)	8db 12db -	8db - -	8db 12db -	8db - -
	2 (parallel)	- 12db -	- - -	- 12db -	- - -

	-	-	-	-
2 (perpendicular)	12db	-	12db	-
	-	-	-	-
	8db	-	8db	-
3 (random)	12db	-	-	-
	-	-	-	-

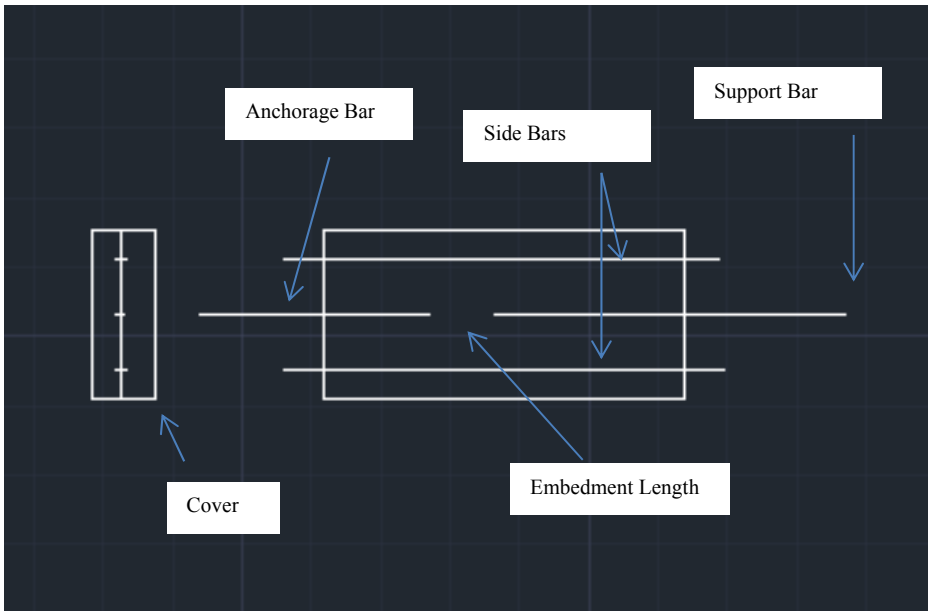

Figure 3-15: Pullout specimen dimensioning and naming

3.3.2 Procedure

3.3.2.1 Casting

Before concrete is poured the formwork is greased with light mineral oil and the rebar are set in place. Any gaps in the formwork were filled with putty. In order to align fibers in one direction a casting device was constructed which uses the wall effect and speed to its advantange. Wille and Parra-Montesinos [41] found that casting with a chute moving at speeds high enough to create thin layers while avoiding breakage in the stream

leads to the best results. The wall effect is responsible for having fibers aligned parallel to the flow near the walls and more perpendicular away from the walls. This is due to a flow gradient which is faster in the middle and slower at the walls.

Eighteen channels with 5’ length x 1.14” base x 1.65” leg height were glued next to each other a plywood ramp set 20 degrees with horizontal. UHPC is aligned into the channels using a scoop and then tilted into position. It is allowed to flow for 10-20 seconds to allow for a constant flow out the end of the channel. Then the formwork is pushed back and forth on wheels underneath the ramp at a speed of about 0.2ft/s or about as fast as possible without breaking the stream of UHPC. The casting device was used to cast both perpendicular and parallel to direction of applied load. Perpendicular is shown in Figure 3-19 while parallel is similar and is shown in Figure 3-18. In order to cast randomly the concrete was dumped at the support bar end and allowed to flow to the anchorage bar end (Figure 3-17)

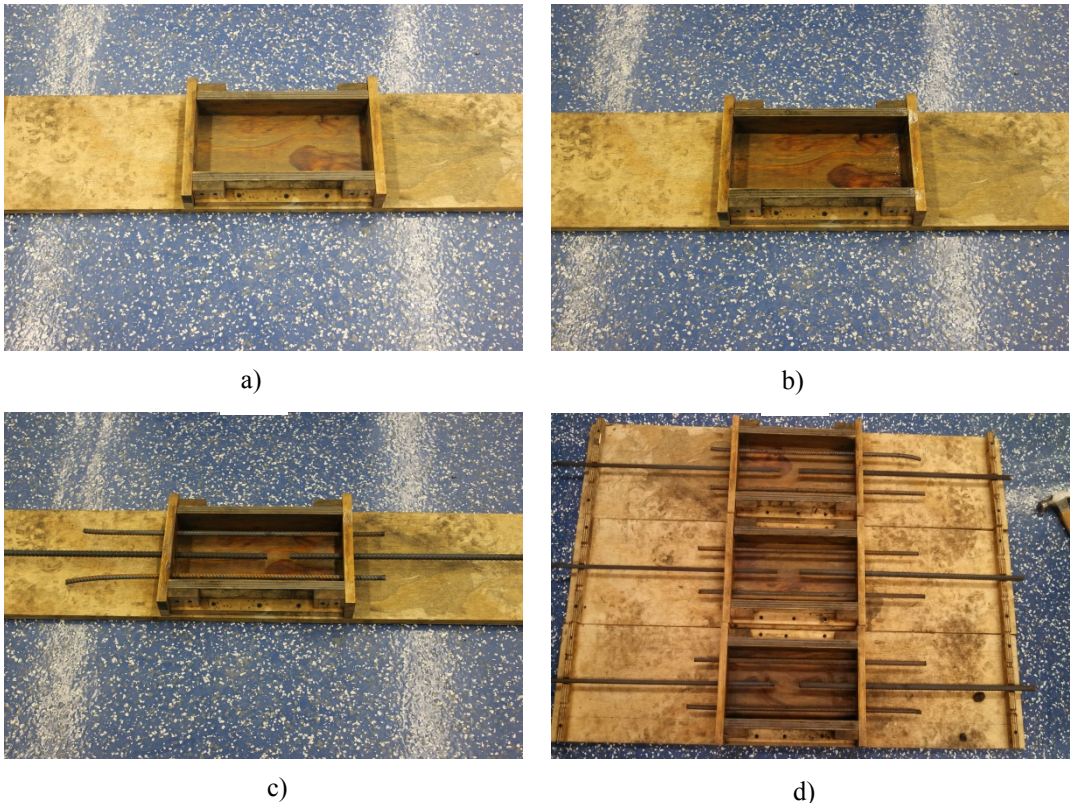

a) b)

c) d)

Figure 3-16: (a) mold is assembled (b) mold is greased (c) rebar is set in place (d) 3 molds next to each other

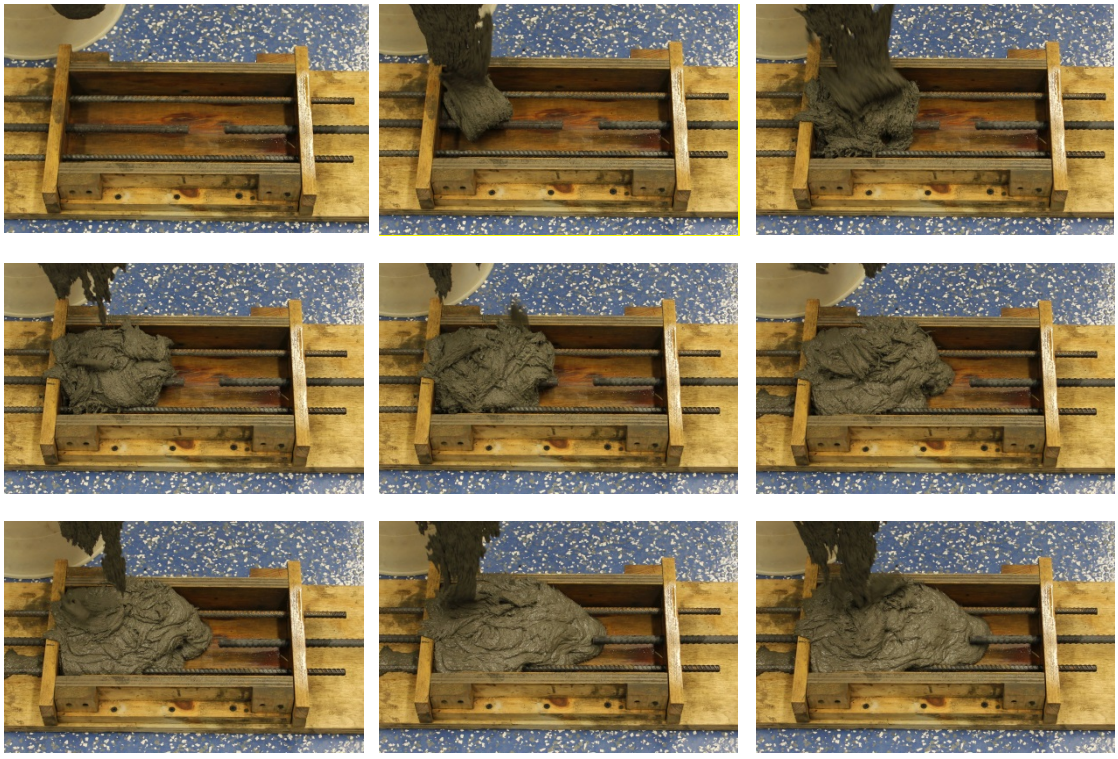

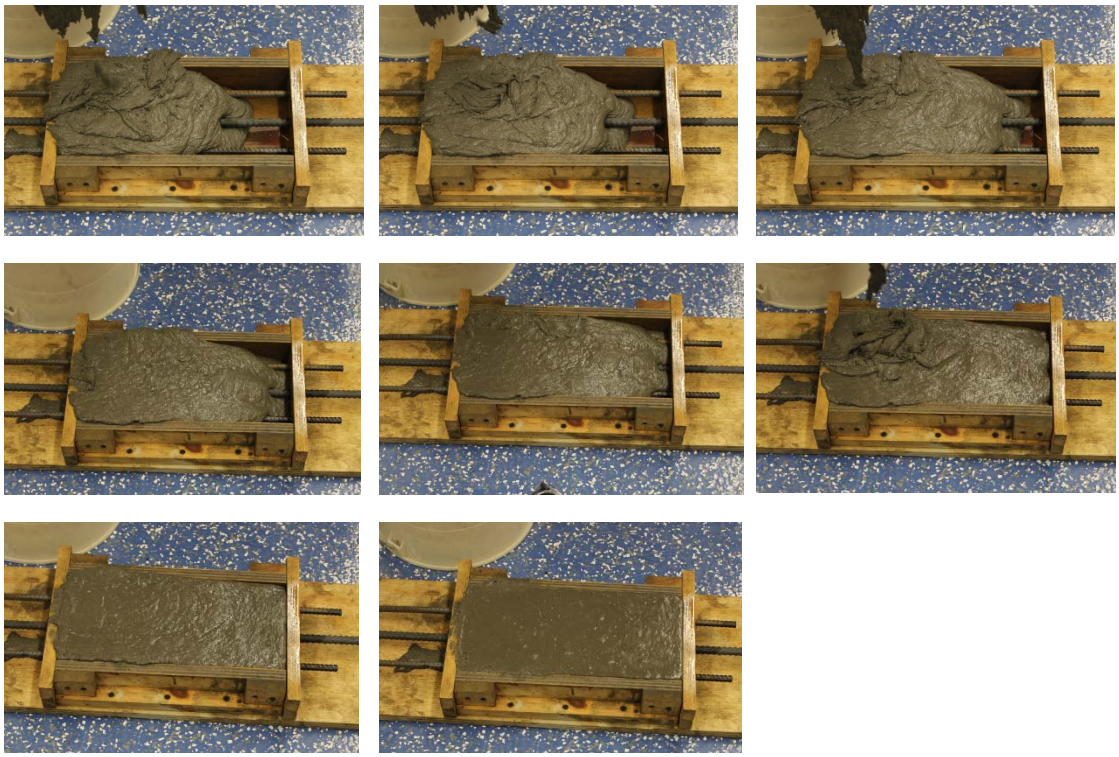

Figure 3-17: Casting pullout specimens with the random method (beginning to end, top left to bottom right respectively

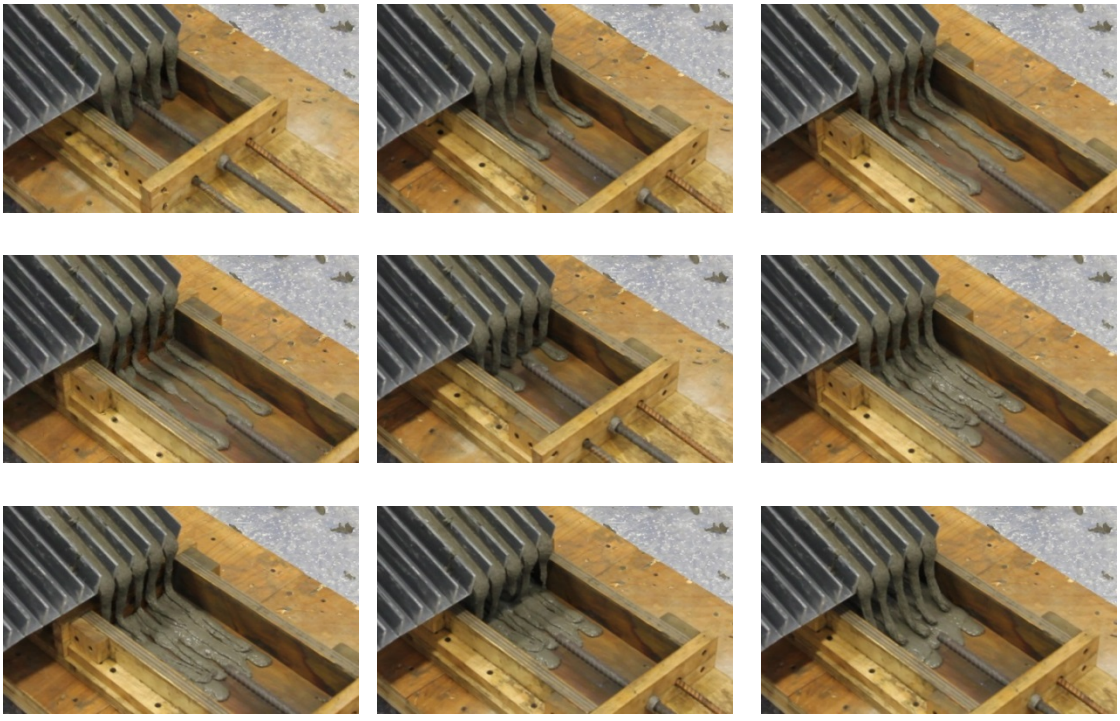

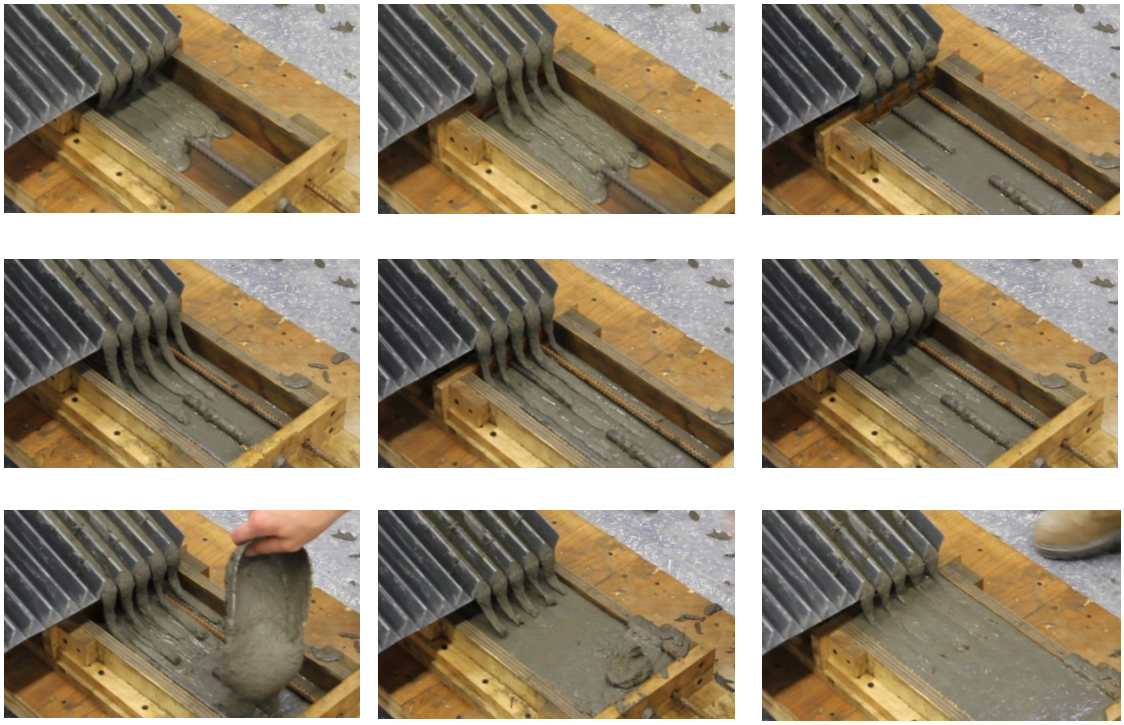

Figure 3-18: Casting pullout specimens parallel to the rebar (parallel to the applied load)

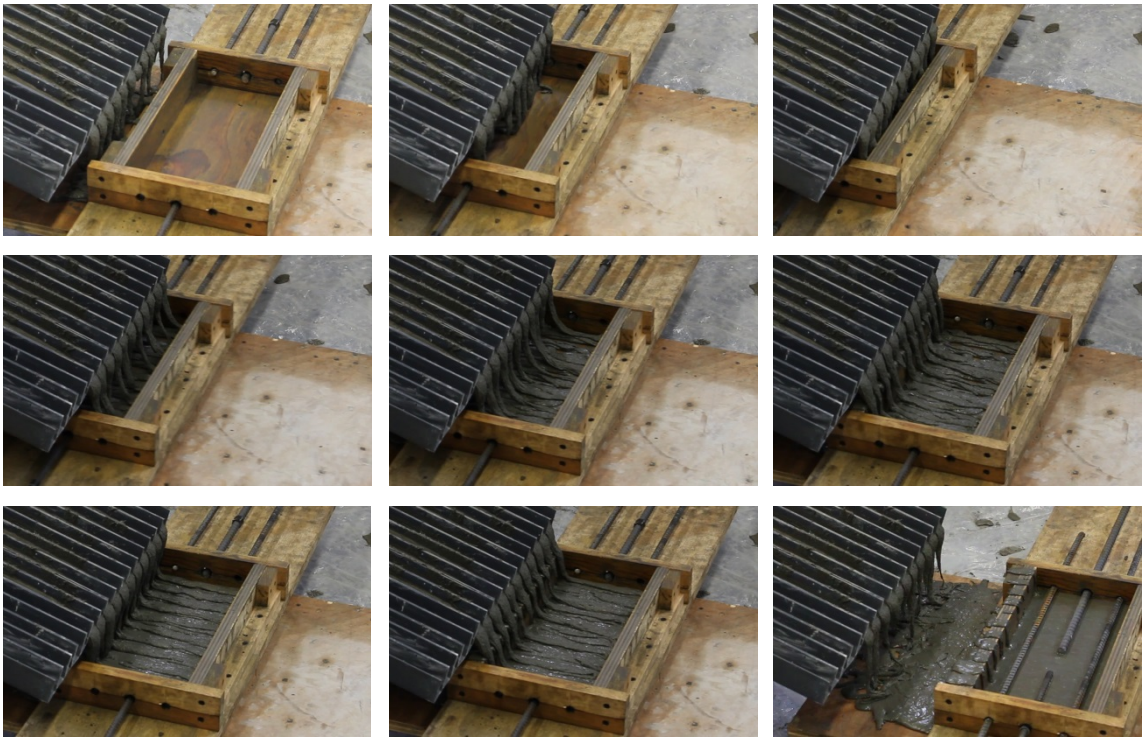

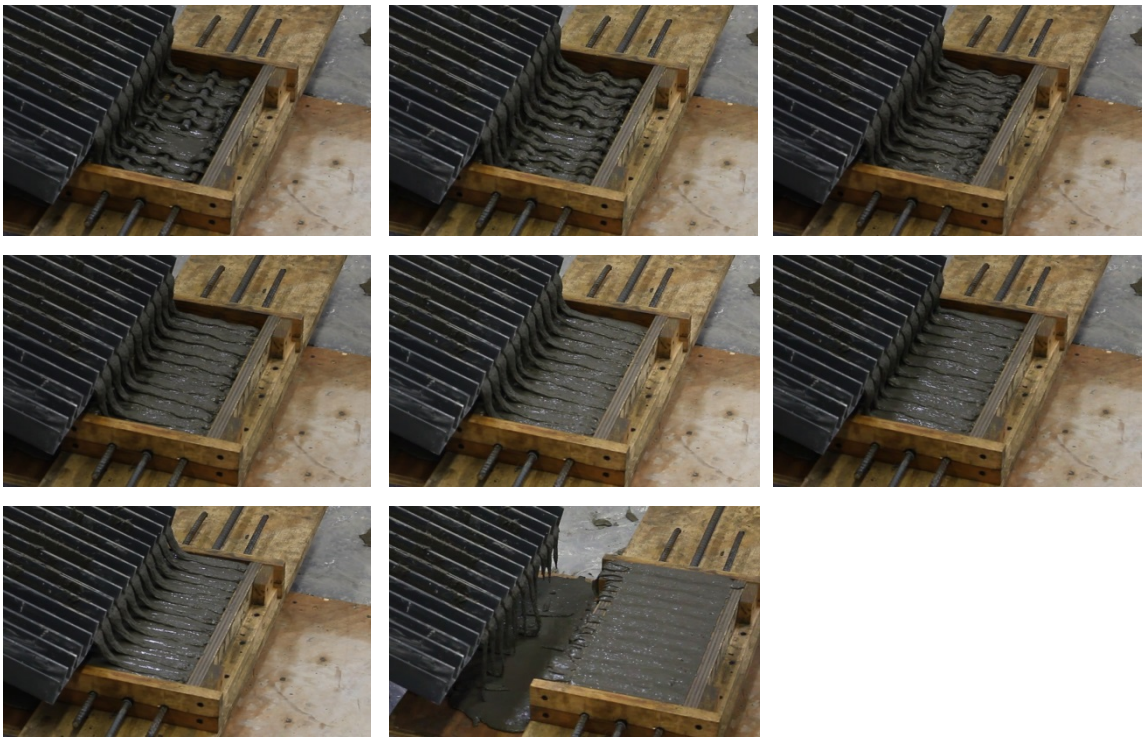

Figure 3-19: Casting pullout specimens perpendicular to the rebar (perpendicular to the applied load)

3.3.2.2 Preparing

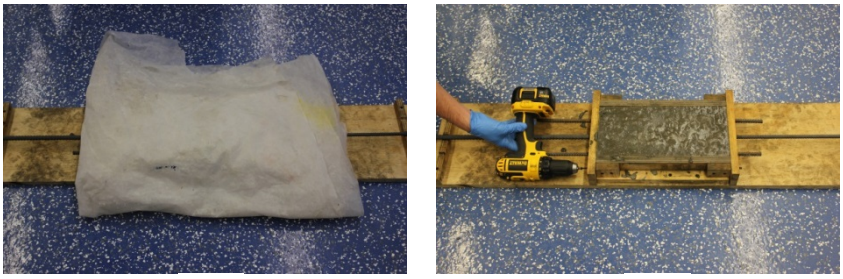

a b

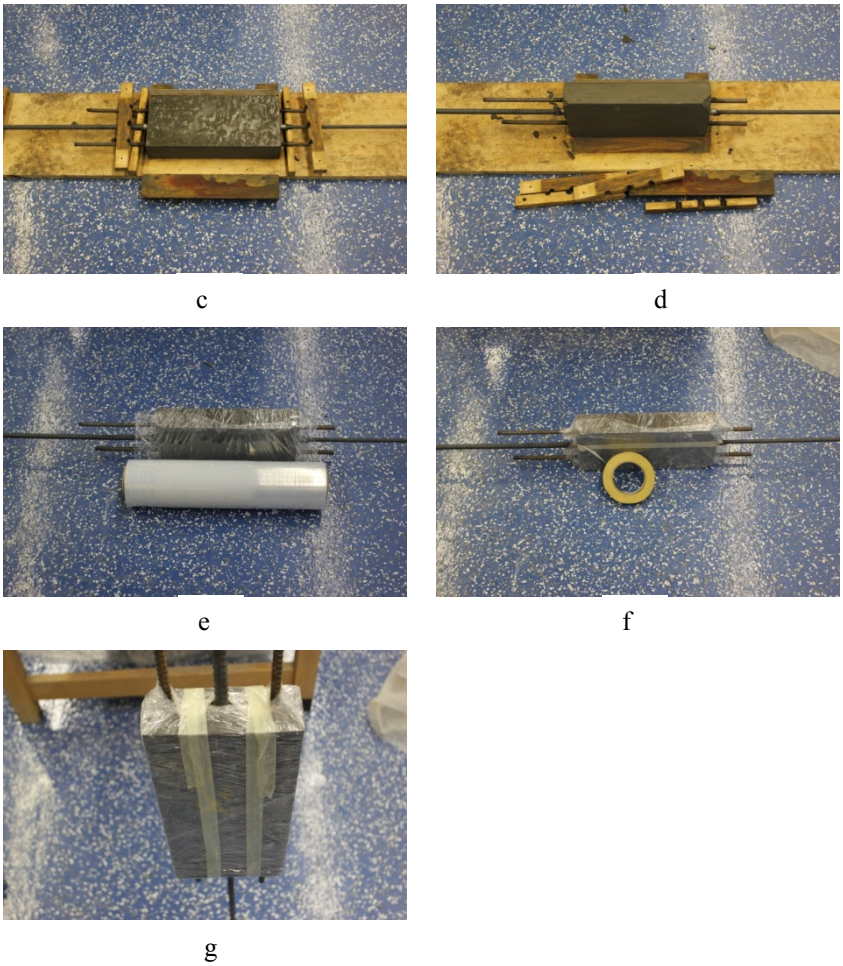

Figure 3-20: (a) temporary cover of specimen immediately after casting (b-d) de-molding of specimen (e-g) shrink-wrapping of specimen for moisture retention

3.3.2.3 Test Procedure

All specimens were demolded after 48 hours and wrapped in plastic at room temperature until the 14 day testing time. At first the specimen was set up into the non-hydraulic wedge grips of the 400kip load frame. Three LVDTs were attached to the anchorage bar and rest on an aluminum bar which was attached to the protruding side bars (Figure 3-21 a & b). The tests were displacement controlled at 5 mm/min and force vs the average displacement of the three LVDTs were recorded.

The slip is calculated by using both the force vs strain curve recorded and the pullout force vs displacement data. The strain*measurement length is subtracted from the pullout displacement at every force interval recorded in the pullout test. This calculation assumes that the conditions of strain in the measurement length of the pullout test are identical to the conditions of the force strain test. The calculation is also limited to force vs displacement data at which the force does not plateau. Pictures were taken of some specimens during testing. Water was rubbed onto the surface to aid in viewing cracks.

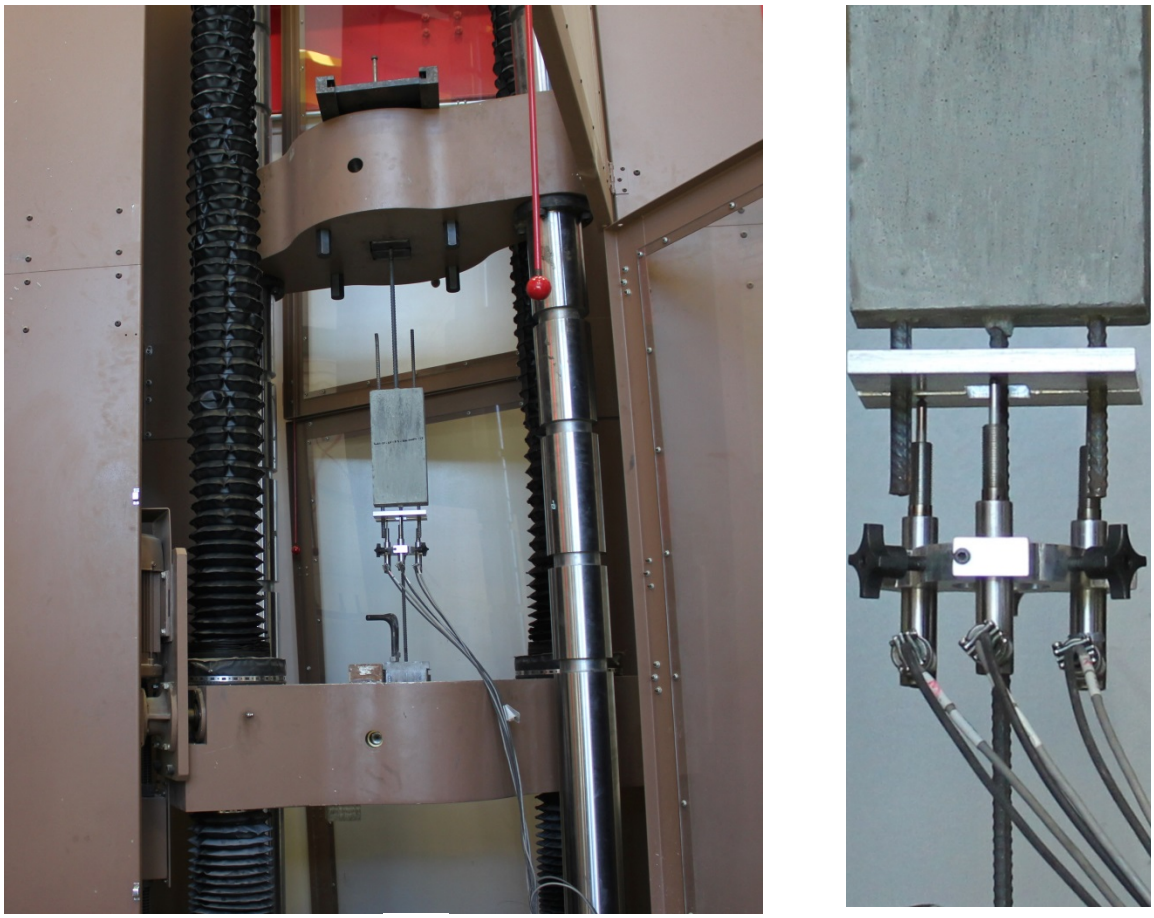

Figure 3-21: Pullout Test Setup (a) load frame (b) LVDT holder

3.4 Phase III: Uniaxial Tensile Behavior of Rebar Reinforced UHPFRC

3.4.1 Test Specimen Design

The test specimen was designed around the need to run tests using wedge grips and therefore dog bone specimens were ruled out. Instead, more reinforcement was added to the end of specimen similar to the design used by Fantili et al [91], Kunieda et al [81], and Otsuka [98]. Figures of the length-wise cross section in the formwork, complete specimen in the formwork, and width-wise cross section of the center of the specimen are shown in Figure 3-22. The specimen dimensions are 3in (7.6cm) x 4in (10.2cm) x 40in (102cm) long. The span in the middle of the specimen with a singular bar is 2ft (61cm) in length, and the bars extend out of the ends of the specimen by 16in (40.6cm). More detail is shown in proceeding subchapters.

A total of 19 series were tested with one specimen tested per series except for a select few series. The combinations of bar type, fiber volume fraction, orientation, and number of specimens tested are shown in Table 3-6.

Figure 3-22: Length-wise cross section in the formwork, complete specimen in the formwork, and width-wise cross section of the center of a ruptured specimen with perpendicular fiber orientation (left to right respectively).

Table 3-6 Test Specimen Parameters to be Tested for Rebar Reinforced UHPFRC

	UHPC Type Rebar Size Fiber Orientation	UHPC1 #3 Parallel		UHPC1 #3 Perpendicular		UHPC1 #3 Random	
	Rebar Type	A1035	A615	A1035	A615	A1035	A615
Fiber Percentage	0	-	-	-	-	x1	x1
	0.5	x1	x1	-	-	x1	-
	0.75	x1	x2	-	-	-	-
	1.0	x2	x2	x1	x1	x1	x1
	2.0	x1	x2	-	-	x1	-
	3.0	x1	x1	-	-	x1	-

3.4.2 Procedure

3.4.2.1 Casting

Before concrete is poured the formwork is greased with light mineral oil and the protruding end rebar are set in place. The middle rebar will be put in place after half of

the formwork is already cast. Due to a large volume of material required to cast the specimens the casting device from Phase II was not used. Instead a process shown in Figure 3-23 was used for parallel specimens. Four layers were cast, the middle bar was put in, and four more layers were cast on top. Perpendicular specimens were cast similarly but orthogonal. UHPFRC was dumped at random spots throughout the specimen and not given too much time to flow before another spot near it was dumped. This prevented fibers from aligning along a flow.

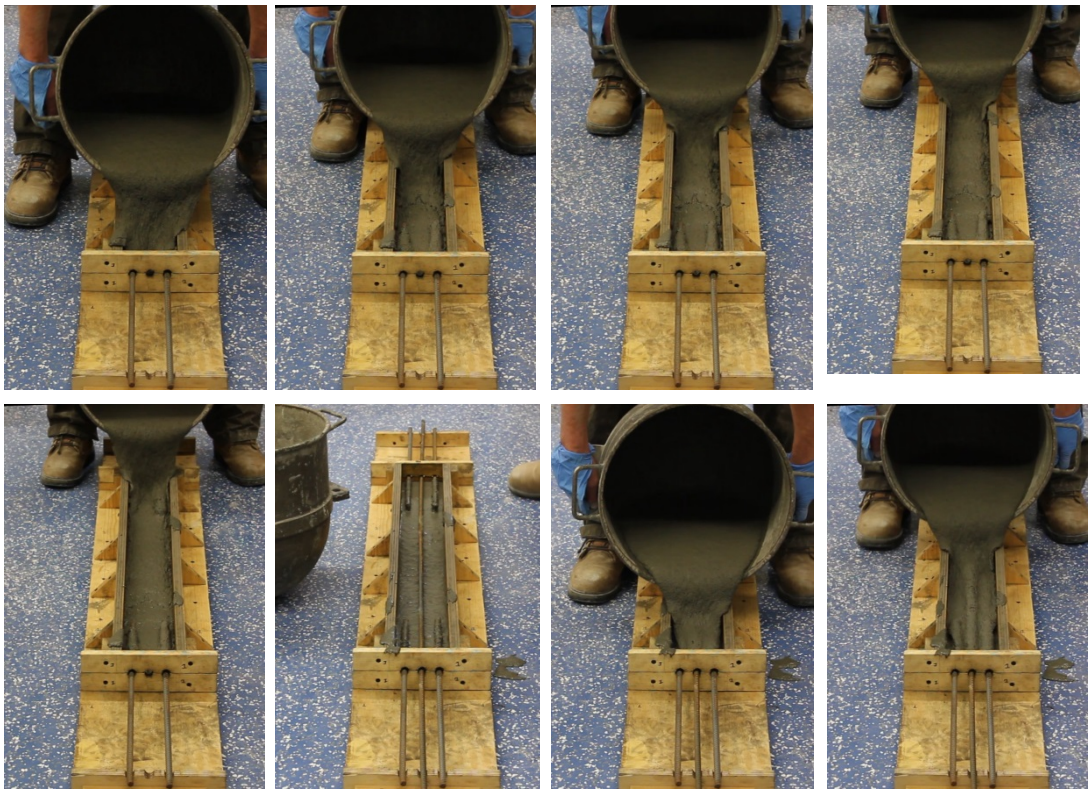

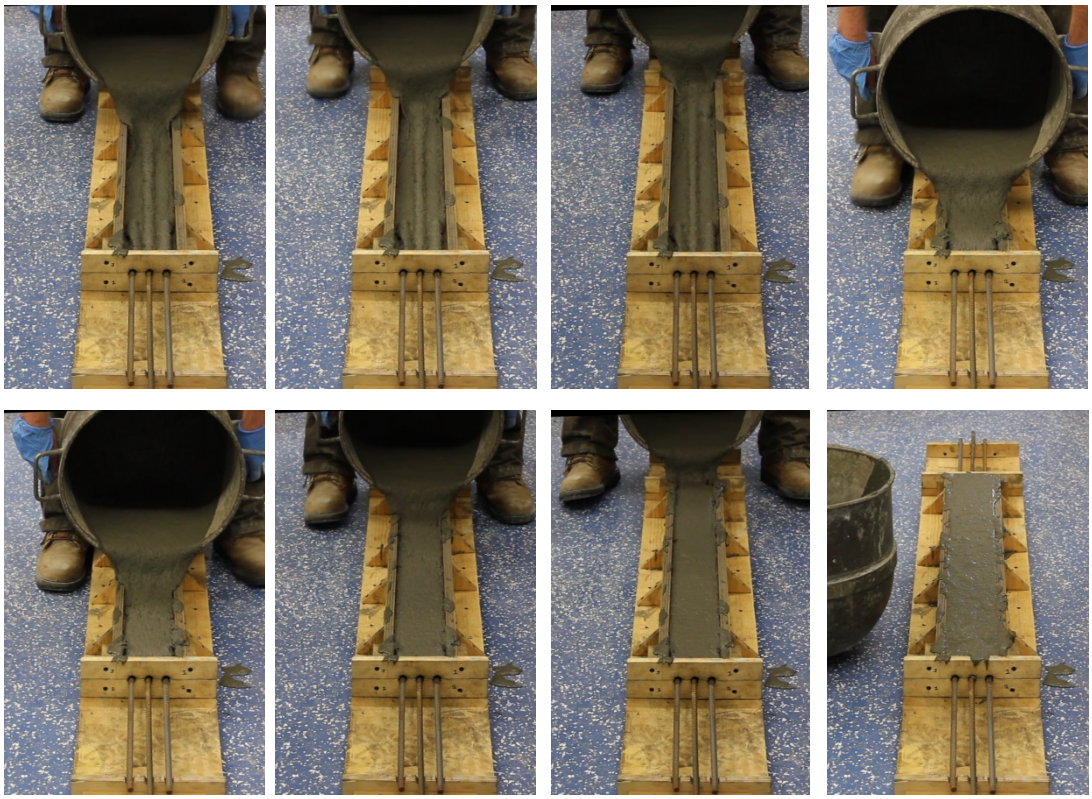

Figure 3-23: Casting method parallel to the direction of applied load.

3.4.2.2 Preparing

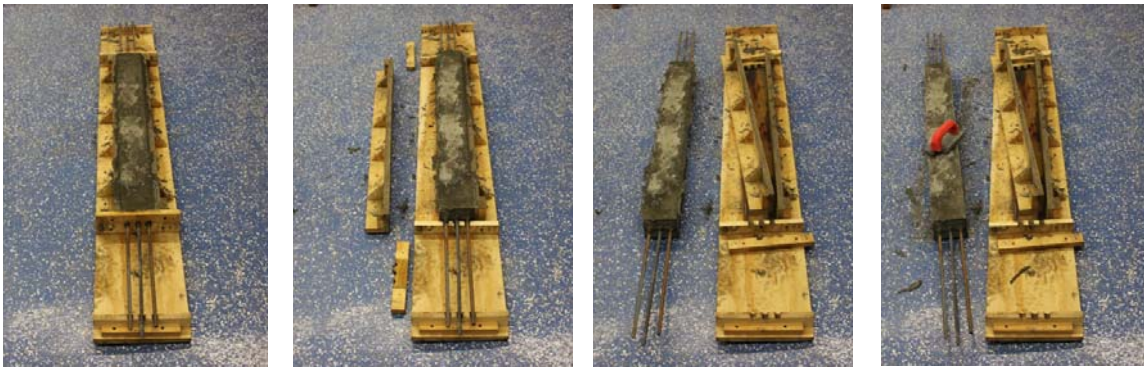

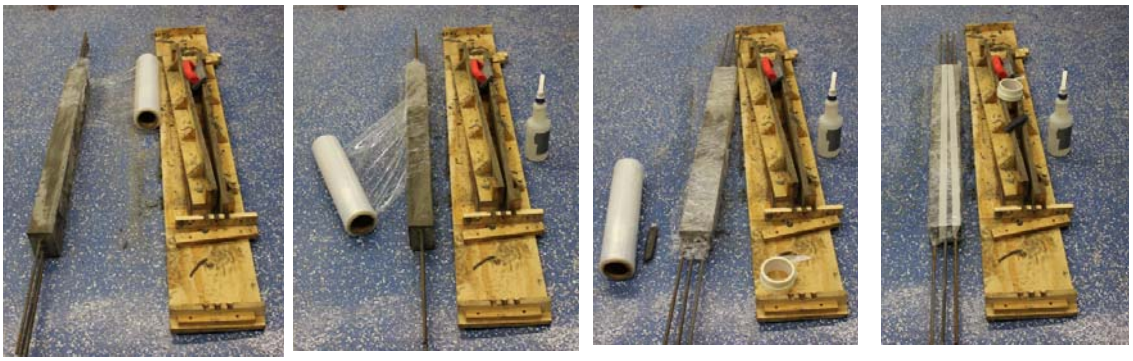

Figure 3-24: De-molding and plastic-wrapping of the composite specimens for moisture retention.

3.4.2.3 Test Procedure

All specimens were stripped of formwork after 48 hours and wrapped in plastic at room temperature until the 14 day testing time. The first step of testing was to set up the specimen into the non-hydraulic wedge grips of the 400kip load frame. A set up 2 LVDTs were attached to custom holders that were pin head screwed to the specimen at each end of the specimen where the protruding bars stopped, so as to have a 2ft long measurement length as shown in Figure 3-25. The tests were displacement controlled at 2 mm/min and force vs the average displacement of the 3 LVDTs were recorded. The stress vs strain data is derived from the force vs displacement data recorded during the test. Pictures were taken of some specimens during testing. Water was rubbed onto the surface to aid in viewing cracks.

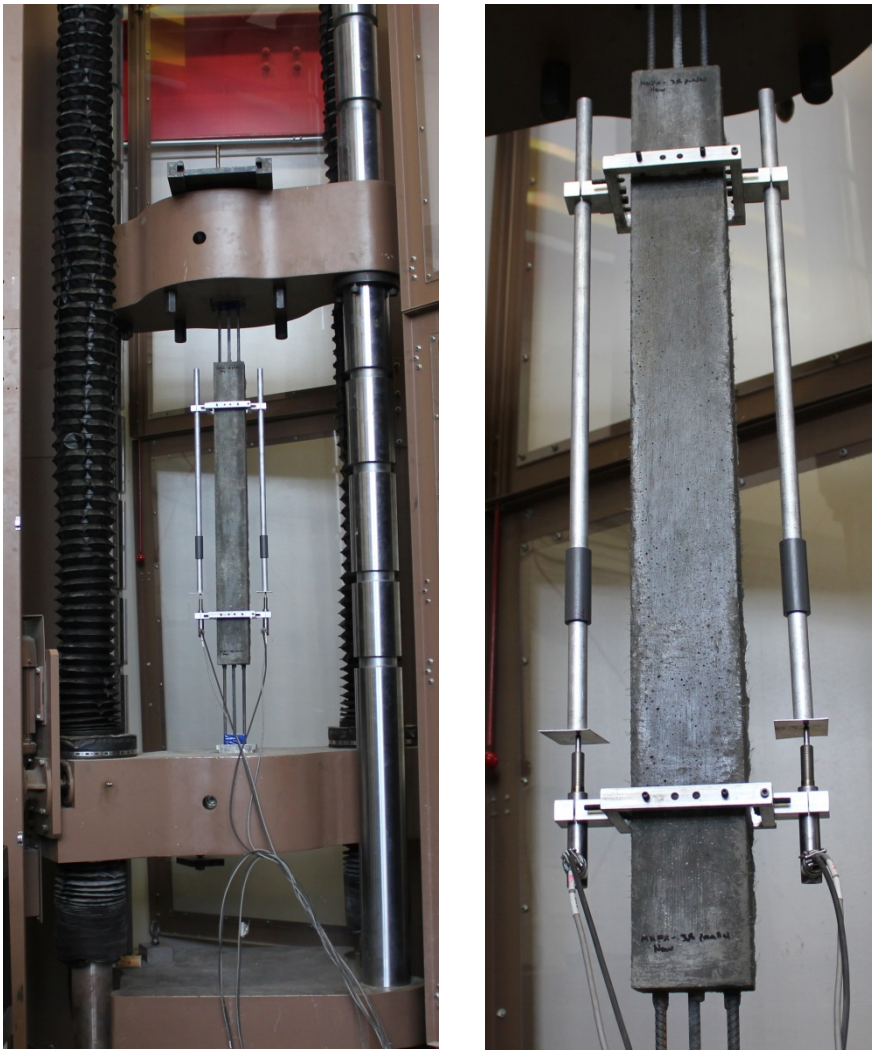

Figure 3-25: Test setup for uniaxial tension for rebar reinforced UHPFRC (a) load frame (b) LVDT holder

4 CHAPTER FOUR - RESULTS

4.1 Phase I: Uniaxial Tensile Behavior of UHPFRC and Rebar

4.1.1 Uniaxial Tensile Behavior of Rebar

Table 4-1: A615 and A1035 stress strain test results

		E x10^3 ksi	f_y ksi	ε_y %	f_{peak} ksi	ε_{peak} %	f_{rup} ksi	ε_{rup} %
A615	S1	30.8	64.4	0.185	102.0	9.53	94.4	14.40
	S2	30.3	68.6	0.240	106.1	8.79	88.8	14.29
	S3	29.5	66.1	0.220	105.0	10.09	98.1	13.71
	Avg	**30.2**	**66.4**	**0.215**	**104.4**	**9.47**	**93.8**	**14.13**
A1035	S1	31.8	98.1	0.300	159.8	3.89	100.3	9.45
	S2	30.8	105.0	0.350	160.2	4.35	98.9	9.93
	S3	34.0	101.6	0.290	160.1	3.63	100.4	8.90
	Avg	**32.2**	**101.6**	**0.313**	**160.0**	**3.95**	**99.9**	**9.42**

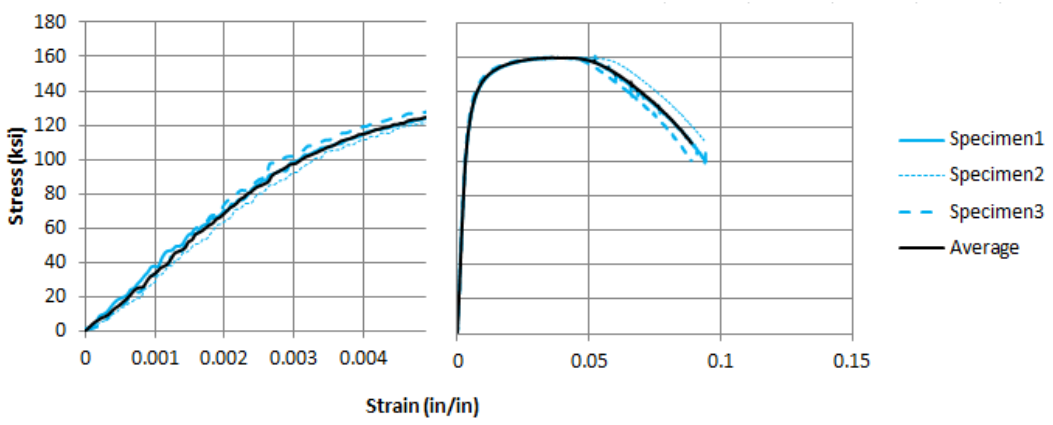

Figure 4-1: A1035 stress strain curves

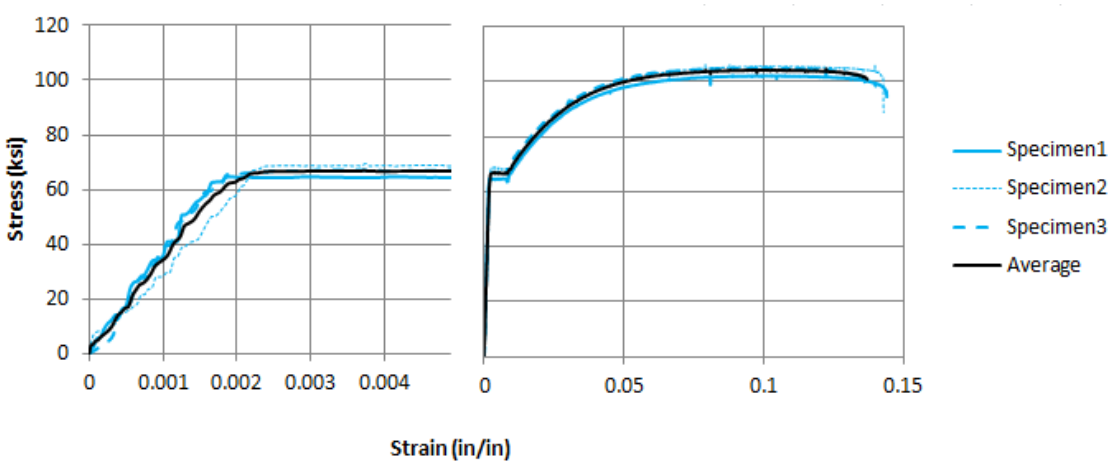

Figure 4-2: A615 stress strain curves

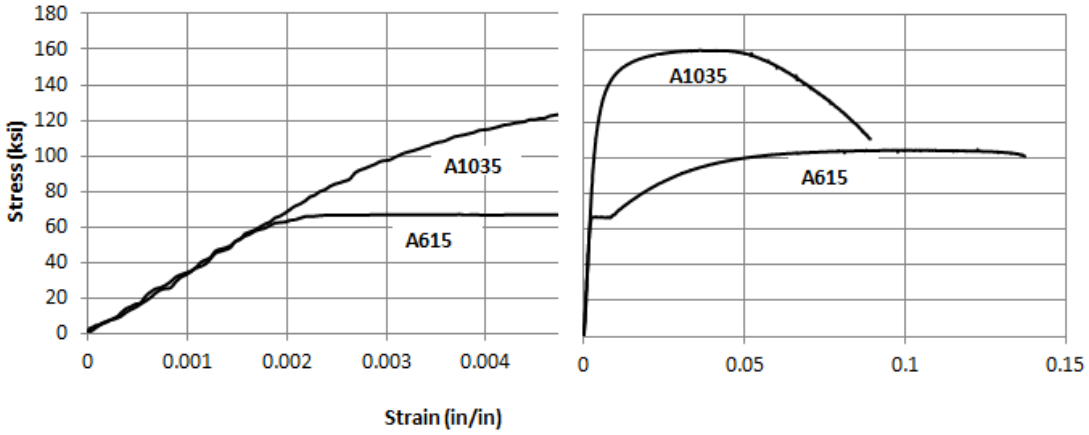

Figure 4-3: Average stress-strain curve of A1035 and A615 rebar

Figure 4-4: Typical rupture mode of A605 (left) and A1035 (right)

4.1.2 Compressive Behavior of UHPFRC

Table 4-2: UHPC1 and UHPC2 compressive test average results

UHPC Type:		UHPC-1				UHPC-2			
Fiber Volume:		0%		2%		0%		2%	
		ksi	MPa	ksi	MPa	ksi	MPa	ksi	MPa
7day	Θ_{max}	18.6	128.1	17.8	122.5	18.6	127.9	18.5	127.6
	ε (%)	-		0.446		-		0.542	
14day	Θ_{max}	23.3	161.0	23.5	162.0	21.0	144.5	22.3	153.8
	ε (%)	-		0.574		-		0.748	
28day	Θ_{max}	25.0	172.7	25.5	176.0	23.1	159.5	22.7	156.3
	ε (%)	-		0.569		-		0.638	

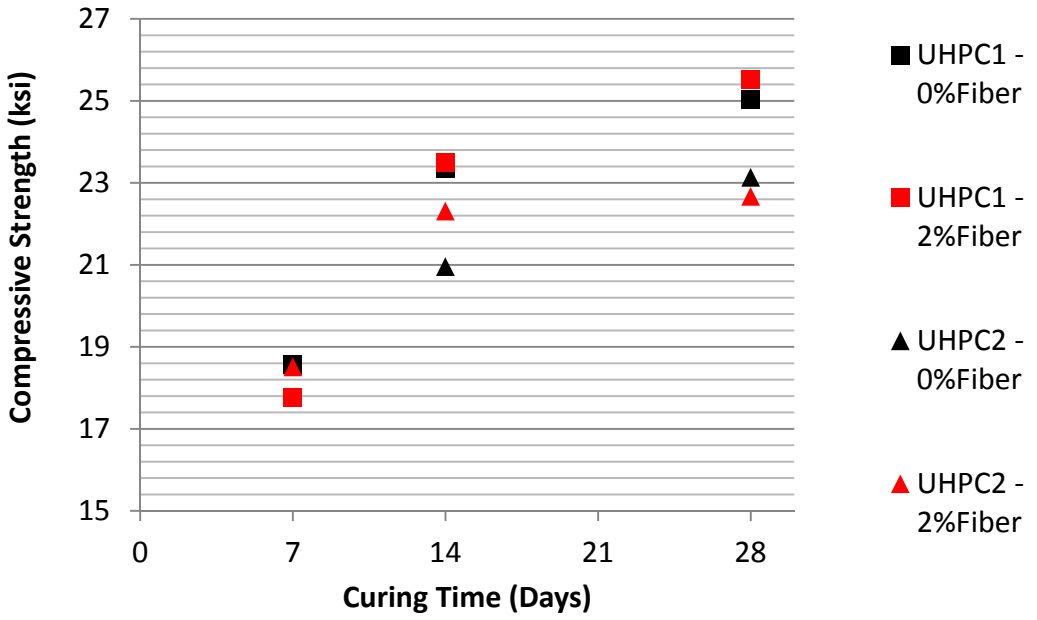

Figure 4-5: Average compressive strength vs curing time for UHPC1 and UHPC2 with 0% and 2% fiber volume fraction

4.1.3 Uniaxial Tensile Behavior of UHPFRC

Table 4-3: UHPC1 uniaxial tension results

		E	Θ_{pc}		ε_{pc}	Cr/in	Cr_{spac}
		ksi	ksi	Mpa	%		in
3%_Parallel_UHPC1	S1	-	2.61	17.97	0.331	8.00	0.13
	S2	-	2.95	20.34	0.428	9.23	0.11
	Avg	**0.00**	**2.78**	**19.16**	**0.379**	**8.62**	**0.12**
2%_Parallel_UHPC1	S1	-	2.05	14.11	0.349	6.00	0.17
	S2	-	2.04	14.05	0.312	4.32	0.23
	S3	-	1.76	12.13	0.164	3.64	0.23
	Avg	**0.00**	**1.95**	**13.43**	**0.275**	**4.65**	**0.21**
2%_RandomB_UHPC1	S1	-	1.95	13.42	0.362	4.00	0.25
	S2	-	1.58	10.91	0.201	4.44	0.23
	S3	-	1.81	12.50	0.220	5.33	0.19
	S4	-	1.71	11.78	0.231	4.80	0.21
	Avg	**0.00**	**1.76**	**12.15**	**0.254**	**4.64**	**0.22**
2%_RandomA_UHPC1	S1	-	1.58	10.90	0.223	3.00	0.33

	S2	-	1.60	11.06	0.119	2.40	0.42
	S3	-	1.68	11.58	0.136	3.00	0.33
	Avg	**0.00**	**1.62**	**11.18**	**0.159**	**2.80**	**0.36**
1%_Parallel_UHPC1	S1	-	1.60	11.02	0.258	3.00	0.33
	S2	-	1.34	9.22	0.426	2.22	0.45
	S3	-	1.09	7.53	0.144	1.25	0.80
	Avg	**0.00**	**1.34**	**9.25**	**0.276**	**2.16**	**0.53**
1%_RandomA_UHPC1	S1	-	1.12	7.71	0.776	1.50	0.67
	S2	-	1.33	9.20	0.263	0.80	1.25
	S3	-	1.50	10.34	1.010	1.40	0.71
	Avg	**0.00**	**1.32**	**9.08**	**0.683**	**1.23**	**0.88**

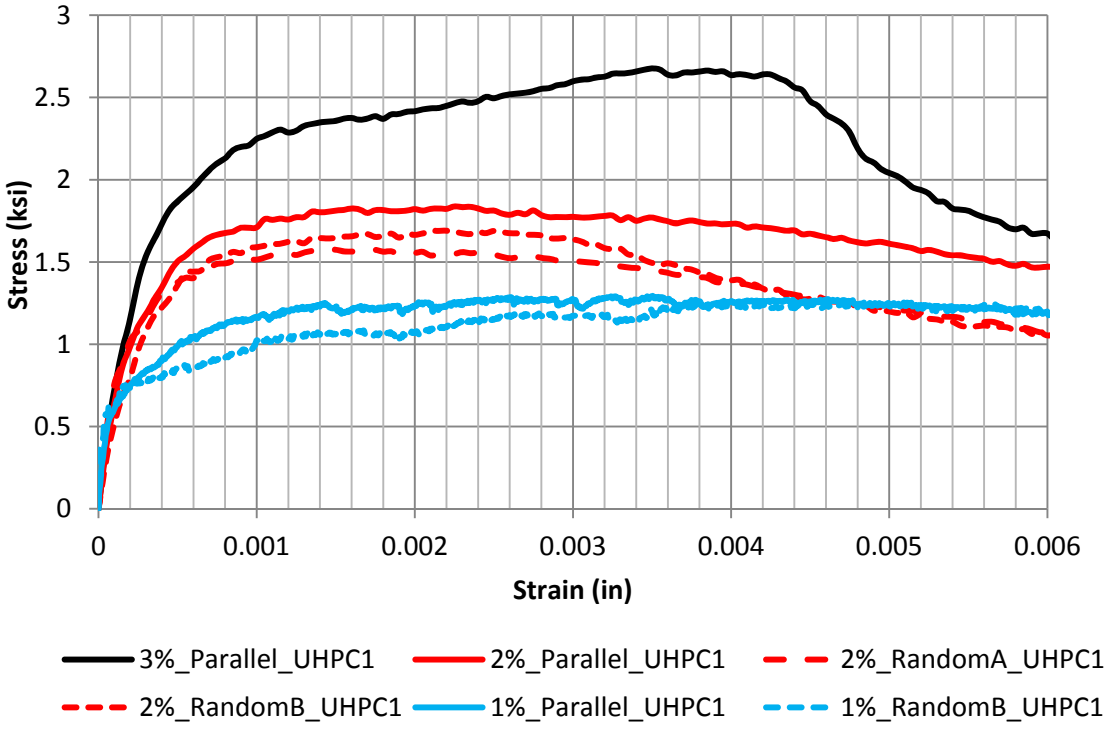

Figure 4-6:UHPFRC1 average stress vs strain curves for direct tension

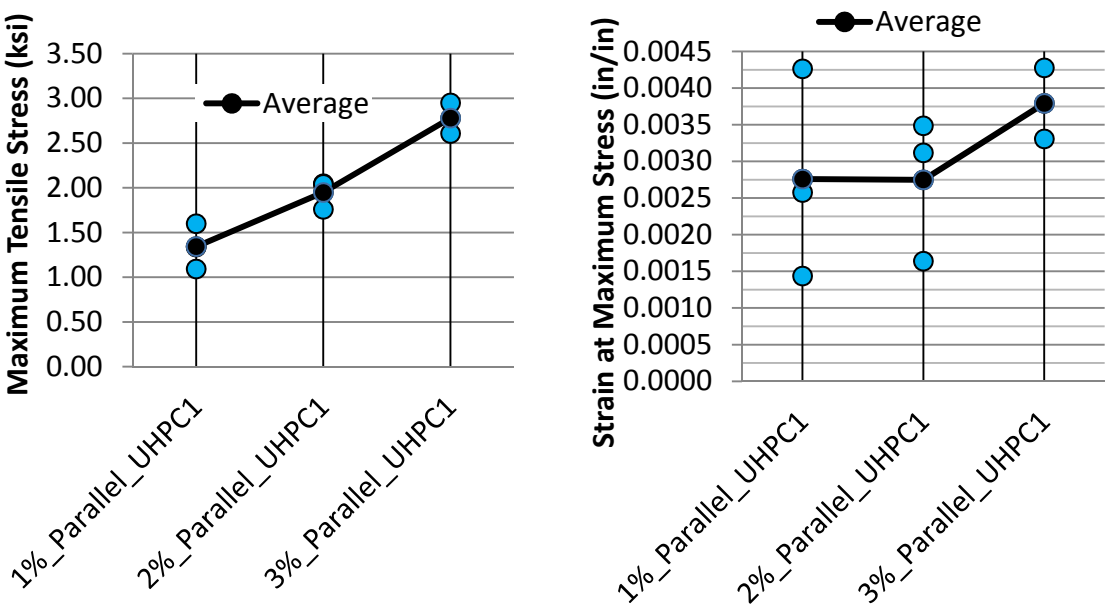

Figure 4-7: UHPC1 maximum tensile stress (left) and the associated strain (right) for parallel oriented direct tension specimens

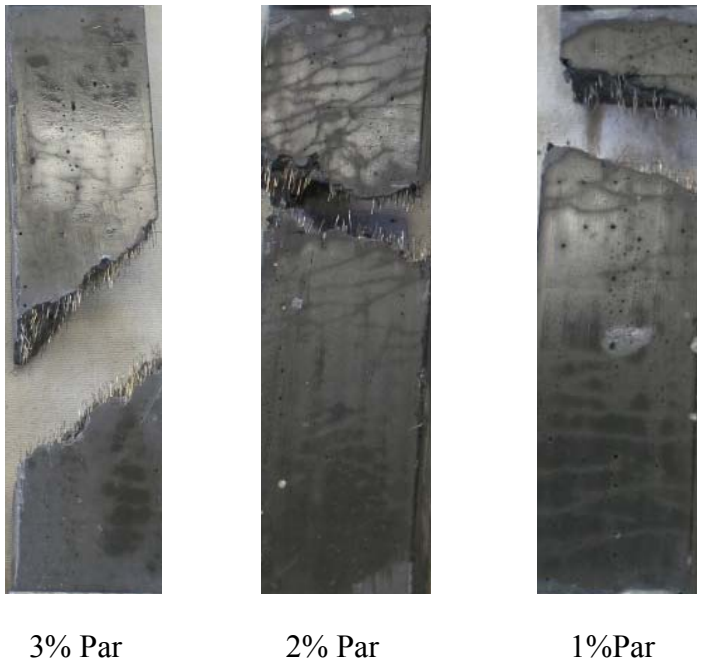

Figure 4-8: UHPFRC1 typical crack pattern of direct tension specimens for 3%_Parallel, 2%_Parallel, and 1% Parallel (left to right respectively)

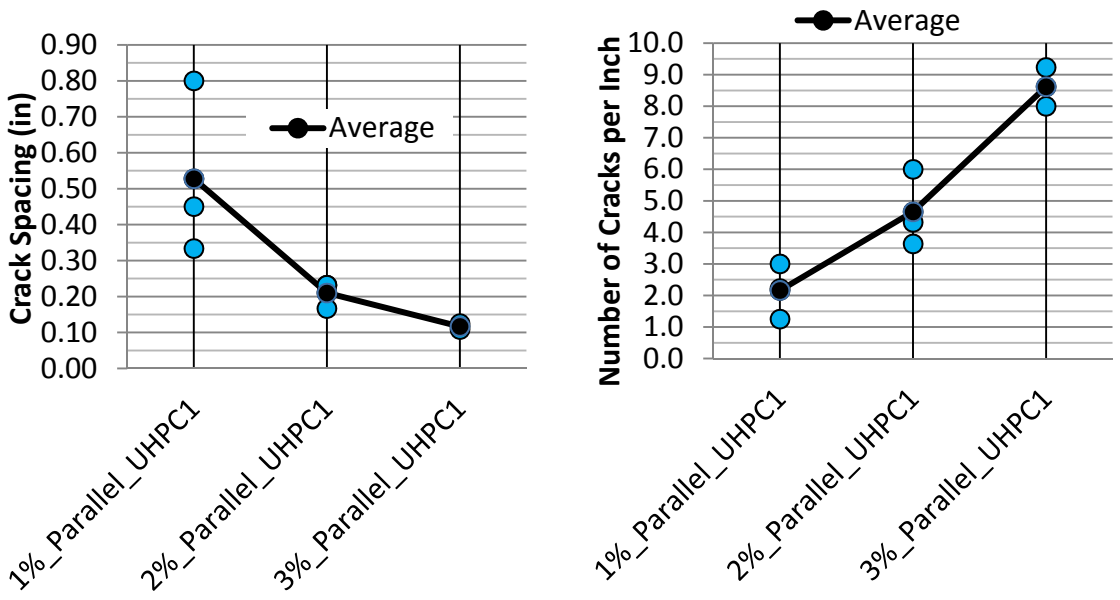

Figure 4-9: UHPC1 cracks spacing (left) and number of cracks per inch (right) for parallel oriented direct tension specimens

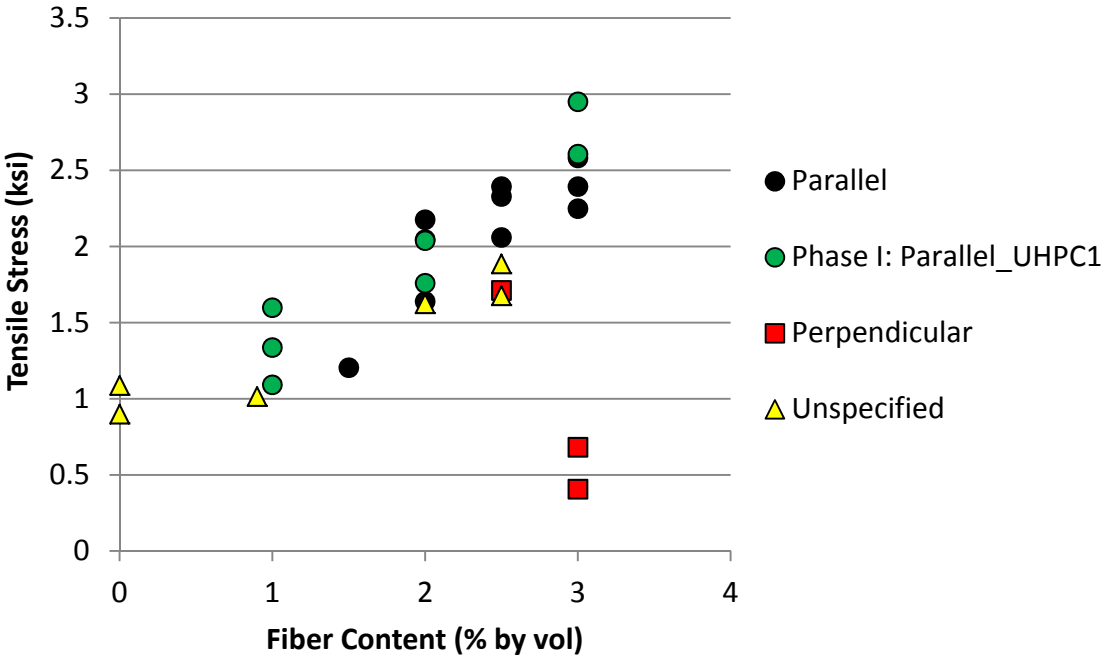

Figure 4-10: Comparison of Parallel_UHPC1 fiber volume fractions 1%-3% to the existing data from literature shown in Figure 2-7

Table 4-4: UHPC2 uniaxial Tension Results

		E	Θ_{pc}		ε_{pc}	Cr/in	Cr_{spac}
		ksi	ksi	Mpa	%		in
2%_Parallel_UHPC2	S1	-	1.75	12.09	0.146	6.00	1.50
	S2	-	1.68	11.56	0.163	4.00	0.27
	S3	-	1.38	9.55	0.162	4.00	0.40
	Avg	**0.00**	**1.61**	**11.07**	**0.157**	**4.67**	**0.72**
2%_RandomB_UHPC2	S1	-	1.48	10.20	0.288	5.50	0.31
	S2	-	1.47	10.15	0.365	5.00	0.25
	S3	-	1.32	9.12	0.316	4.00	0.20
	Avg	**0.00**	**1.42**	**9.82**	**0.323**	**4.83**	**0.25**

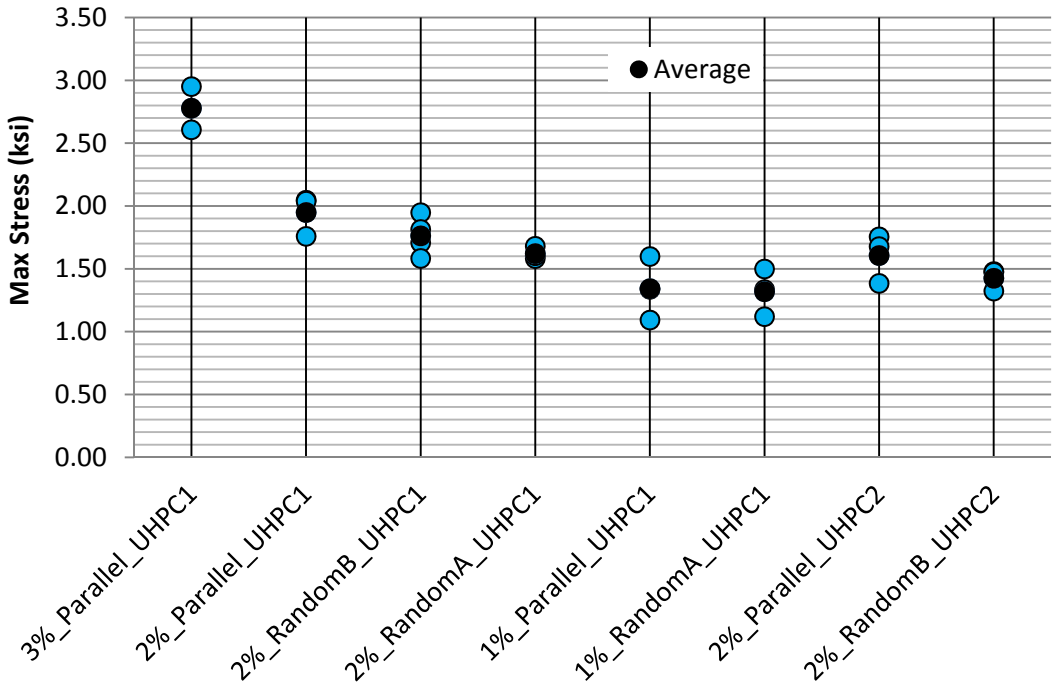

Figure 4-11: Maximum tensile stress for uniaxial tension specimens

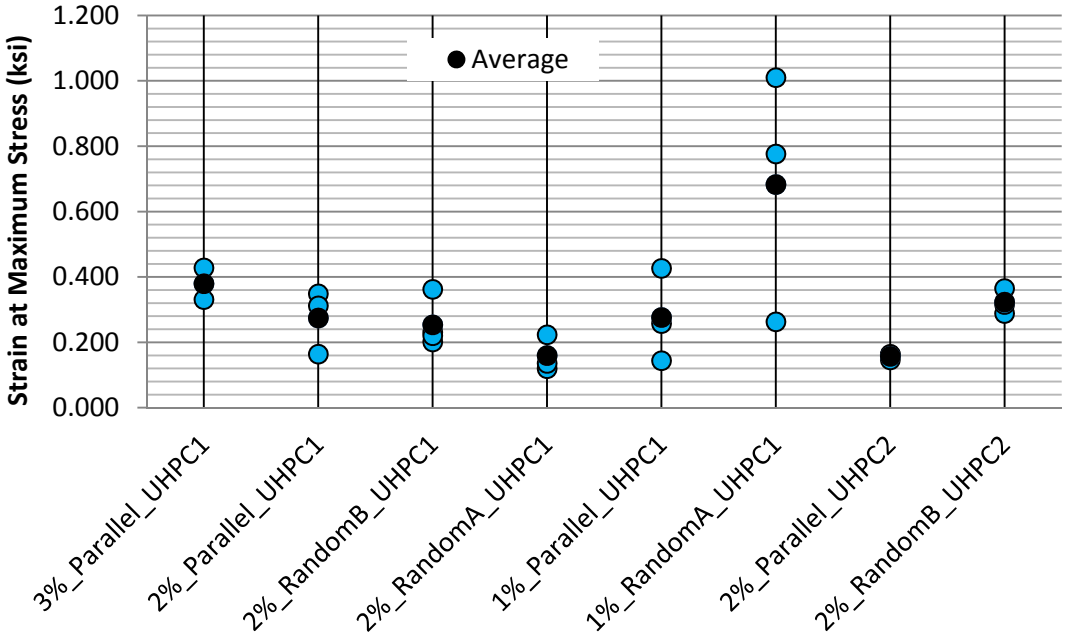

Figure 4-12: Strain at maximum stress for uniaxial tension specimens

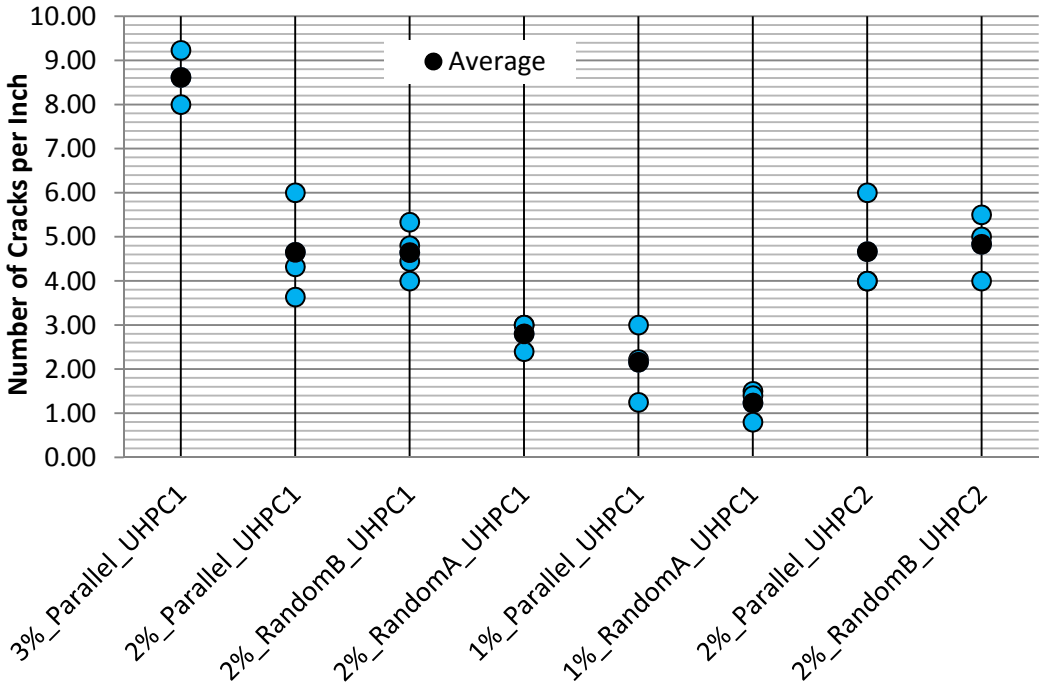

Figure 4-13: Number of cracks per inch uniaxial tension specimens

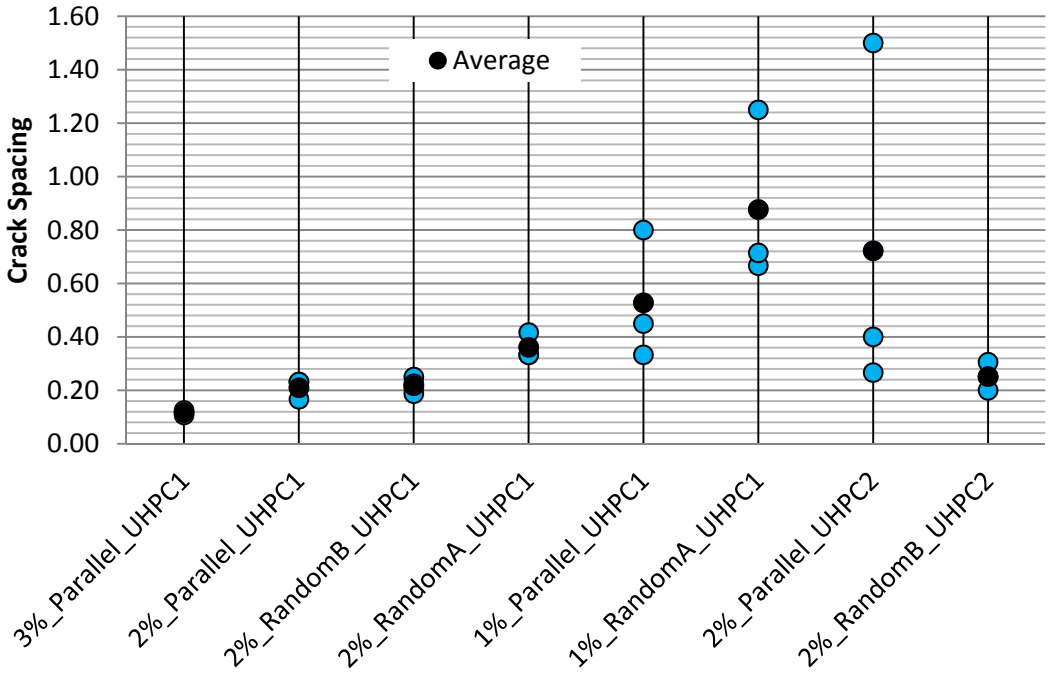

Figure 4-14: UHPC1 number of cracks per inch for direct tension specimens

4.2 Phase II: Bond Behavior of Rebar Embedded in UHPFRC

4.2.1 Pullout Behavior For Size #3 Bars

Table 4-5: Pullout Results for #3 bars embedded 8db

		Stiffness	F_{peak}	Θ_{peak}	S_{peak}		T_{bpeak}	
		ksi	kip	ksi	mm	x10^{3}in	MPa	ksi
#3_0%_8db_rand_1035_UHPC1	S1	4.45	2.87	25.94	0.15	6.07	5.6	0.811
	S2	4.16	4.42	40.05	0.28	10.86	8.6	1.252
	S3	4.61	4.29	38.83	0.26	10.17	8.4	1.213
	Avg	**4.41**	**3.86**	**34.94**	**0.23**	**9.03**	**7.5**	**1.092**
#3_1%_8db_rand_1035_UHPC1	S1	3.82	8.43	76.35	1.11	43.89	16.5	2.386
	S2	3.91	10.31	93.36	1.01	39.67	20.1	2.917
	S3	3.97	8.89	80.49	0.99	39.11	17.3	2.515
	Avg	**3.90**	**9.21**	**83.40**	**1.04**	**40.9**	**18.0**	**2.606**
#3_2%_8db_rand_1035_UHPC1	S1	4.24	13.93	126.13	1.84	72.52	27.2	3.942

	S2	3.89	10.22	92.49	0.98	38.51	19.9	2.890
	S3	4.27	11.01	99.72	1.07	42.13	21.5	3.116
	S4	4.38	14.09	127.59	1.44	56.71	27.5	3.987
	Avg	**4.19**	**12.31**	**111.48**	**1.33**	**52.5**	**24.0**	**3.484**
#3_2%_8db_rand_1035_UHPC2	S1	3.94	9.35	84.69	0.87	34.08	18.2	2.647
	S2	4.12	11.81	106.90	1.17	45.96	23.0	3.341
	S3	3.69	10.74	97.28	1.05	41.25	21.0	3.040
	Avg	**3.91**	**10.63**	**96.29**	**1.03**	**40.4**	**20.7**	**3.009**
#3_3%_8db_rand_1035_UHPC1	S1	4.40	16.01	144.97	1.91	75.09	31.2	4.530
	S2	4.72	16.84	152.49	2.72	106.99	32.9	4.765
	S3	3.91	16.76	151.70	2.65	104.40	32.7	4.741
	Avg	**4.34**	**16.54**	**149.72**	**2.43**	**95.5**	**32.3**	**4.679**

Table 4-6: Pullout Results for #3 bars embedded 12db and 16db

		Stiffness	F_{peak}	Θ_{peak}	S_{peak}		T_{bpeak}	
		ksi	kip	ksi	mm	$x10^3$in	MPa	ksi
#3_0%_12db_rand_1035_UHPC1	S1	4.31	4.11	37.23	0.31	12.32	5.3	0.776
	S2	4.31	2.84	25.74	0.18	7.09	3.7	0.536
	S3	4.80	3.37	30.50	0.21	8.13	4.4	0.635
	Avg	**4.48**	**3.44**	**31.16**	**0.23**	**9.18**	**4.5**	**0.649**
#3_1%_12db_rand_1035_UHPC1	S1	4.34	10.91	98.75	1.06	41.61	14.2	2.057
	S2	4.44	11.33	102.61	1.07	42.24	14.7	2.138
	S3	4.25	12.33	111.67	1.19	46.98	16.0	2.327
	Avg	**4.34**	**11.52**	**104.34**	**1.11**	**43.61**	**15.0**	**2.174**
#3_2%_12db_perp_1035_UHPC1	S1	4.37	17.48	158.24	3.25	127.79	22.7	3.297
	S2	4.02	18.86	170.73	5.70	224.37	24.5	3.557
	S3	3.82	17.09	154.70	3.38	133.09	22.2	3.223
	Avg	**4.07**	**17.81**	**161.22**	**4.11**	**161.75**	**23.2**	**3.359**
#3_2%_12db_rand_1035_UHPC1	S1	4.44	17.13	155.12	2.63	103.48	22.3	3.232
	S2	4.20	15.22	137.76	2.15	84.49	19.8	2.870
	S3	4.41	14.93	135.18	1.87	73.56	19.4	2.816
	Avg	**4.35**	**15.76**	**142.69**	**2.21**	**87.18**	**20.5**	**2.973**
#3_2%_12db_par_1035_UHPC1	S1	4.42	14.58	131.99	1.31	51.69	19.0	2.750
	S2	3.91	11.41	103.33	1.15	45.18	14.8	2.153
	S3	3.62	12.87	116.56	1.32	51.83	16.7	2.428
	Avg	**3.99**	**12.95**	**117.29**	**1.26**	**49.57**	**16.8**	**2.444**
#3_1%_16db_rand_1035_UHPC1	S1	3.67	15.84	143.45	2.32	91.47	15.5	2.241
	S2	3.61	15.67	141.87	2.26	88.92	15.3	2.217
	S3	3.76	15.07	136.47	2.06	80.95	14.7	2.132
	Avg	**3.68**	**15.53**	**140.60**	**2.21**	**87.12**	**15.1**	**2.197**

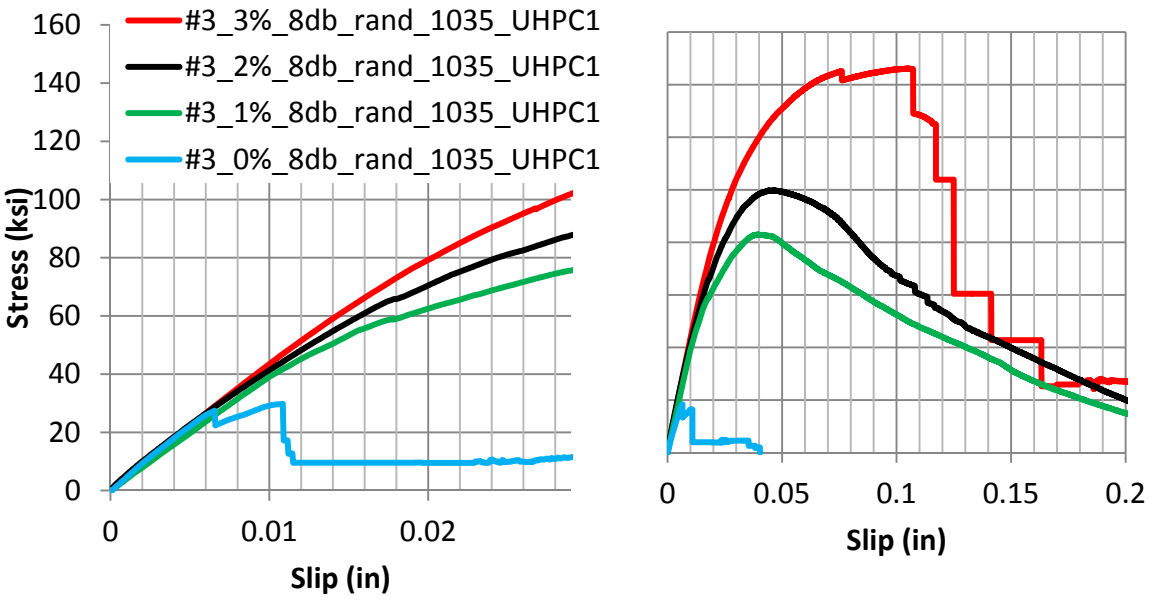

Figure 4-15: Average bar stress vs slip curves for #3 1035 bar embedded 8db into UHPC1

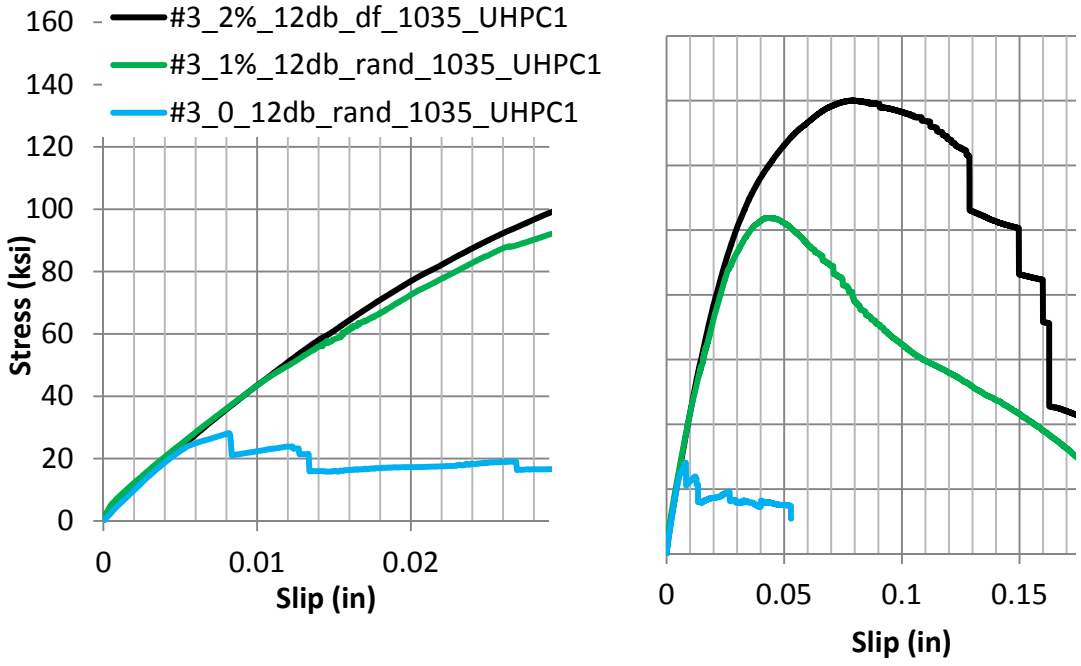

Figure 4-16: Average bar stress vs slip curves for #3 1035 bar embedded 12db in UHPC1

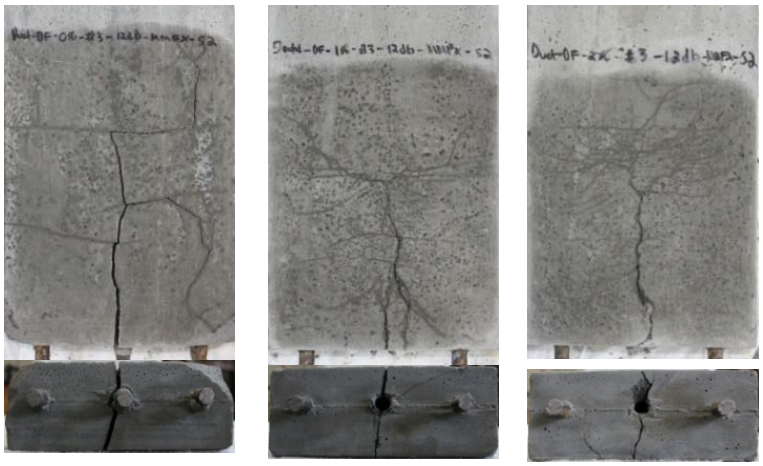

Figure 4-17: Photographs of typical #3_12db_rand_1035_UHPC1 specimens after failure, fiber volume fraction varies.

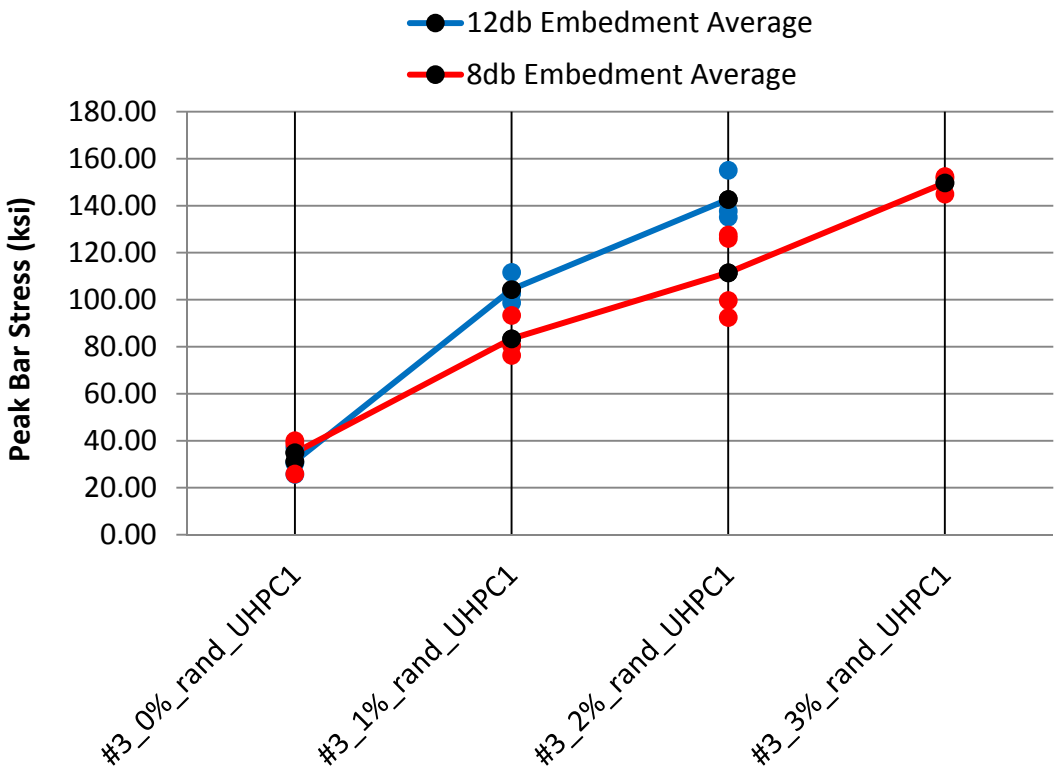

Figure 4-18: Peak bar stress for #3_rand_UHPC1 specimens with varying embedment length and fiber volume fraction

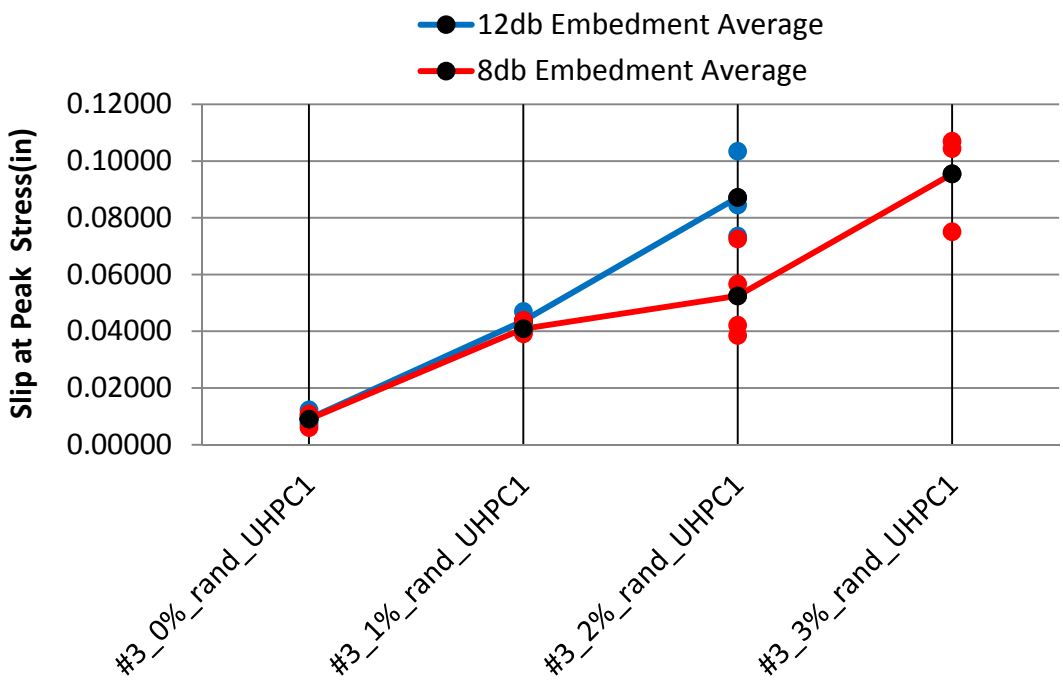

Figure 4-19:Slip at peak bar stress and for #3_rand_UHPC1 specimens with varying embedment length and fiber volume fraction

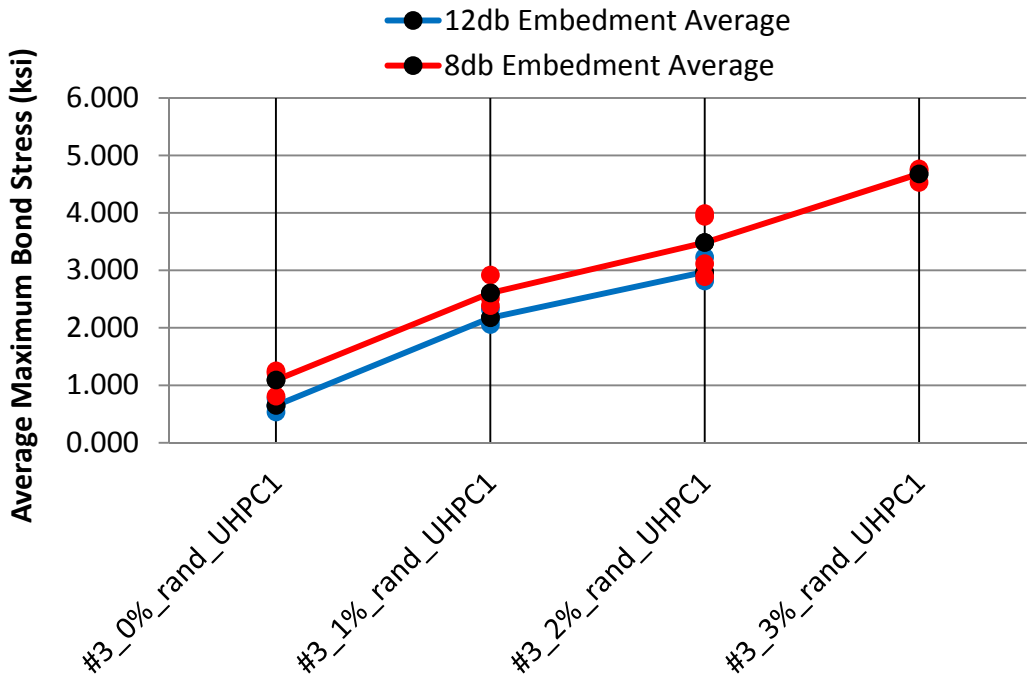

Figure 4-20: Average maximum bond stress for #3_rand_UHPC1 specimens with varying embedment length and fiber volume fraction

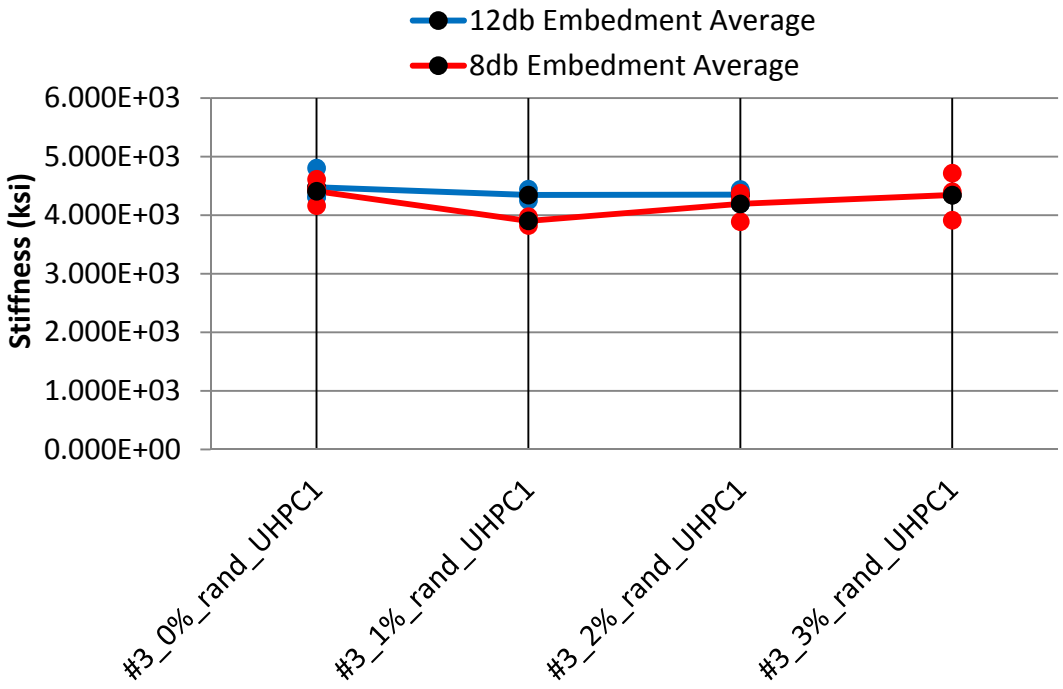

Figure 4-21: Elastic portion stiffness for #3_rand_UHPC1 specimens with varying embedment length and fiber volume fraction

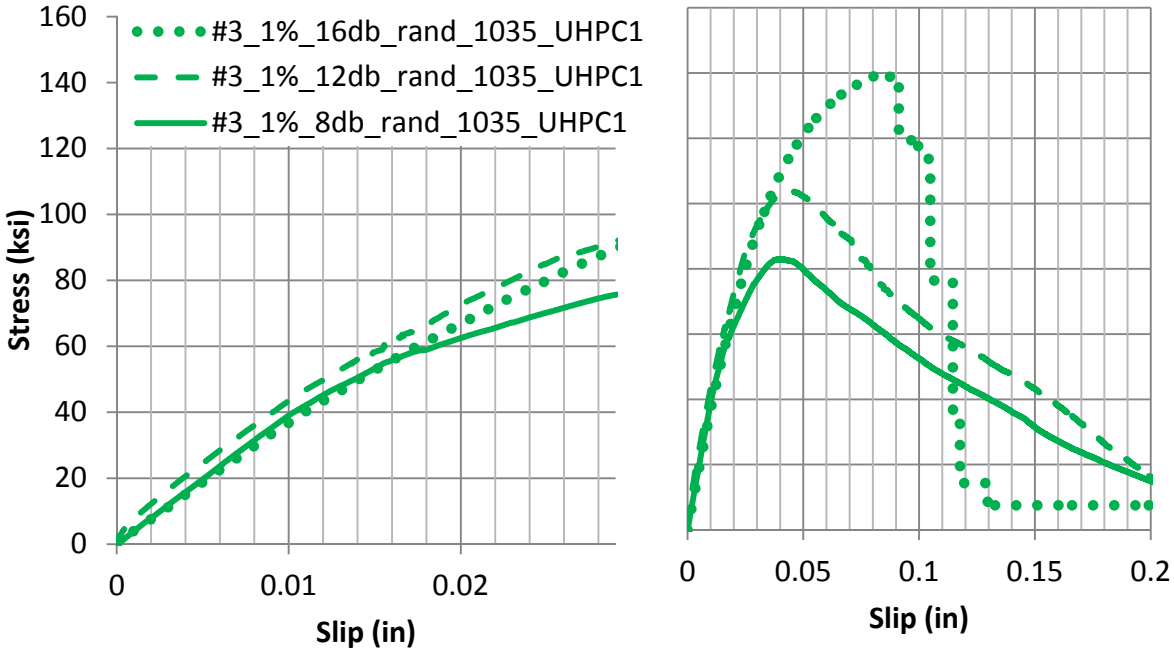

Figure 4-22: Average bar stress vs slip curves for #3 1035 bar embedded in 1% UHPC1

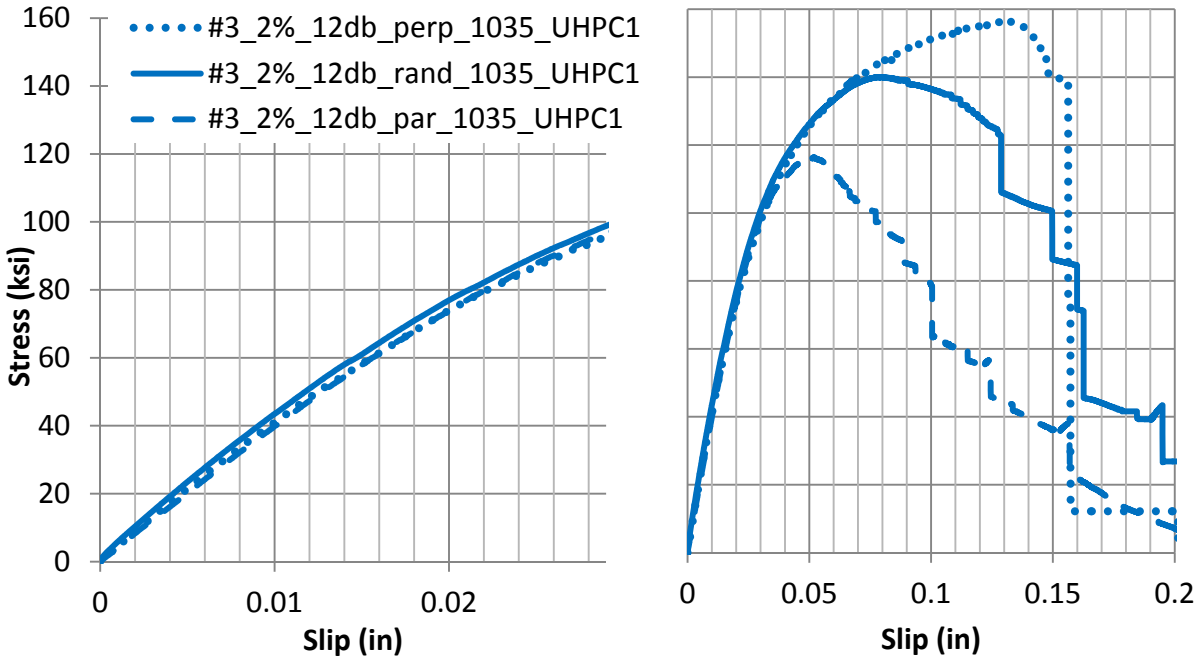

Figure 4-23: Average bar stress vs slip curves for #3 1035, 12db, UHPC1, and varying fiber orientation

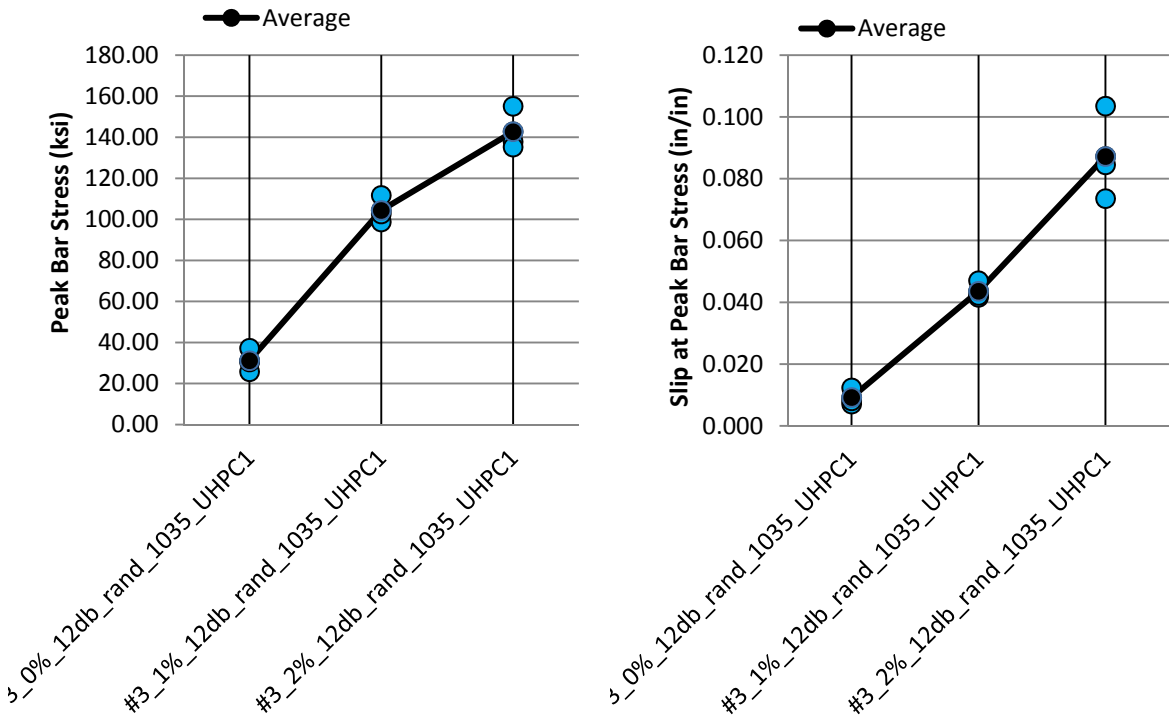

Figure 4-24: Peak bar stress and the respective slip for #3 1035, 12db, UHPC1, and varying fiber orientation

Figure 4-25: Photographs of #3_2%_12db_perp_1035_UHPC1 at different bar stresses

4.2.2 Pullout Behavior for Size #4 Bars

Table 4-7: Pullout Results for #4 bars embedded 8db

		Stiffness	F_{peak}	Θ_{peak}	S_{peak}		T_{bpeak}	
		ksi	kip	ksi	mm	x10^3in	MPa	ksi
#4_0%_8db_rand_1035_UHPC1	S1	3.17	3.77	19.23	0.17	6.65	4.1	0.601
	S2	3.63	4.72	24.04	0.20	7.78	5.2	0.751
	S3	3.66	4.73	24.07	0.19	7.68	5.2	0.752
	Avg	**3.49**	**4.41**	**22.45**	**0.19**	**7.37**	**4.8**	**0.701**
#4_1%_8db_rand_1035_UHPC1	S1	3.97	11.37	57.88	0.67	26.18	12.5	1.809
	S2	3.56	9.39	47.84	1.04	40.87	10.3	1.495
	S3	3.18	10.50	53.48	0.85	33.61	11.5	1.671
	Avg	**3.57**	**10.42**	**53.07**	0.85	33.55	11.4	**1.658**
#4_2%_8db_rand_615_UHPC1	S1	-	-	-	-	-	-	-
	S2	-	-	-	-	-	-	-
	S3	-	-	-	-	-	-	-
	Avg	-	-	-	-	-	-	-
#4_2%_8db_rand_1035_UHPC1	S1	3.53	16.11	82.05	0.90	35.30	17.7	2.564
	S2	3.63	14.88	75.77	0.90	35.35	16.3	2.368
	S3	3.74	17.38	88.51	1.01	39.92	19.1	2.766
	Avg	**3.64**	**16.12**	**82.11**	**0.94**	**36.86**	**17.7**	**2.566**
#4_3%_8db_rand_1035_UHPC1	S1	3.55	17.31	88.16	1.05	41.44	19.0	2.755
	S2	3.71	16.57	84.38	0.93	36.65	18.2	2.637
	S3	3.96	19.09	97.23	1.09	42.95	21.0	3.039
	Avg	**3.74**	**17.66**	**89.92**	**1.02**	**40.35**	**19.4**	**2.810**

Table 4-8: Pullout Results for #4 bars embedded 12db

		Stiffness	F_{peak}	Θ_{peak}	S_{peak}		T_{bpeak}	
		ksi	kip	ksi	mm	$x10^3$in	MPa	ksi
#4_1%_12db_rand_1035_UHPC1	S1	3.24	17.34	88.30	1.04	41.07	12.7	1.840
	S2	3.14	13.81	70.32	0.84	33.11	10.1	1.465
	S3	3.35	15.51	78.97	0.94	37.20	11.3	1.645
	Avg	**3.24**	**15.55**	**79.20**	**0.94**	**37.13**	**11.4**	**1.650**
#4_2%_12db_perp_1035_UHPC1	S1	3.68	22.21	113.12	1.57	61.91	16.2	2.357
	Avg*	**3.68**	**22.21**	**113.12**	**1.57**	**61.91**	**16.2**	**2.357**
#4_2%_12db_rand_1035_UHPC1	S1	3.58	19.55	99.57	1.25	49.17	14.3	2.074
	S2	3.68	20.37	103.74	1.16	45.59	14.9	2.161
	S3	3.18	22.65	115.34	1.62	63.93	16.6	2.403
	Avg	**3.48**	**20.86**	**106.22**	**1.34**	**52.90**	**15.3**	**2.213**
#4_2%_12db_par_1035_UHPC1	S1	3.43	15.36	78.23	0.84	32.91	11.2	1.630
	Avg*	**3.43**	**15.36**	**78.23**	**0.84**	**32.91**	**11.2**	**1.630**
#4_3%_12db_rand_1035_UHPC1	S1	3.85	27.03	137.67	2.14	84.42	19.8	2.868
	S2	4.06	25.85	131.65	1.82	71.54	18.9	2.743
	Avg	**3.96**	**26.44**	**134.66**	**1.98**	**77.98**	**19.3**	**2.805**

0% 1% 2% 3%

Figure 4-26: Photographs of Typical #4_8db_rand_1035_UHPC1 specimens after failure, fiber percentage varies.

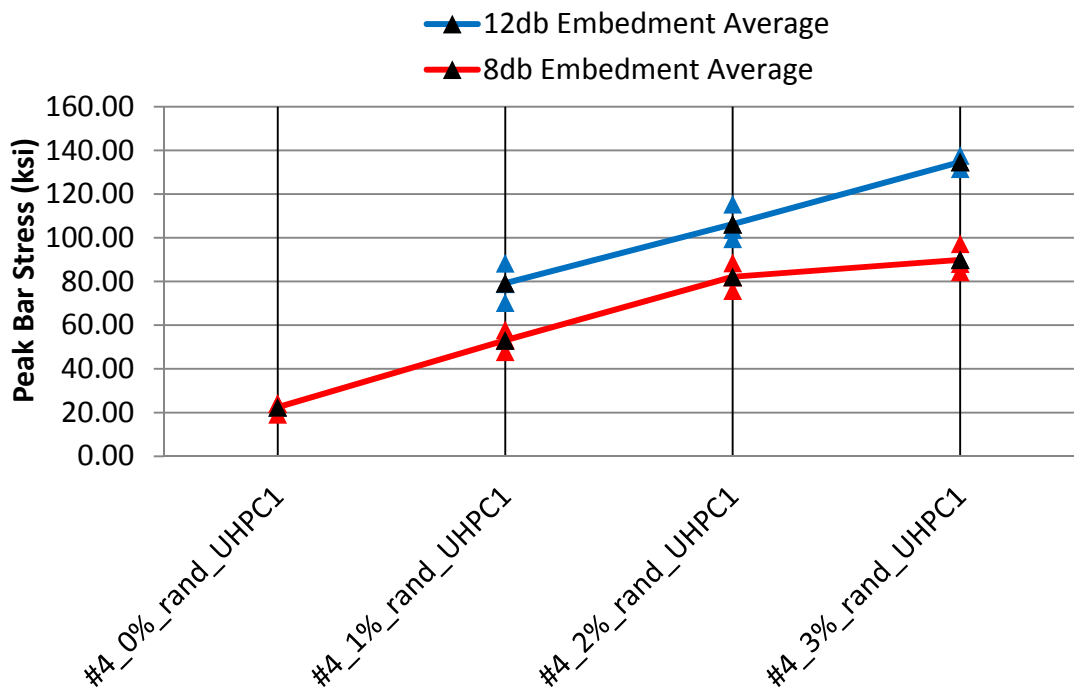

Figure 4-27: Peak bar stress for #4_rand_UHPC1 specimens with varying embedment length and fiber volume fraction

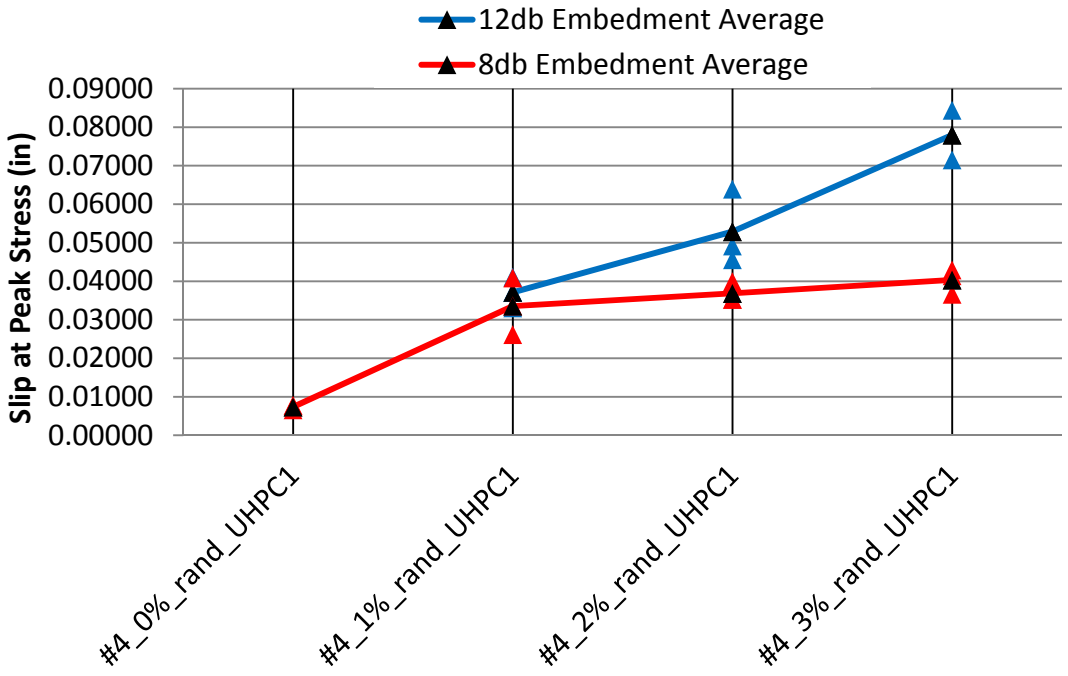

Figure 4-28: Slip at peak stress for #4_rand_UHPC1 specimens with varying embedment length and fiber volume fraction

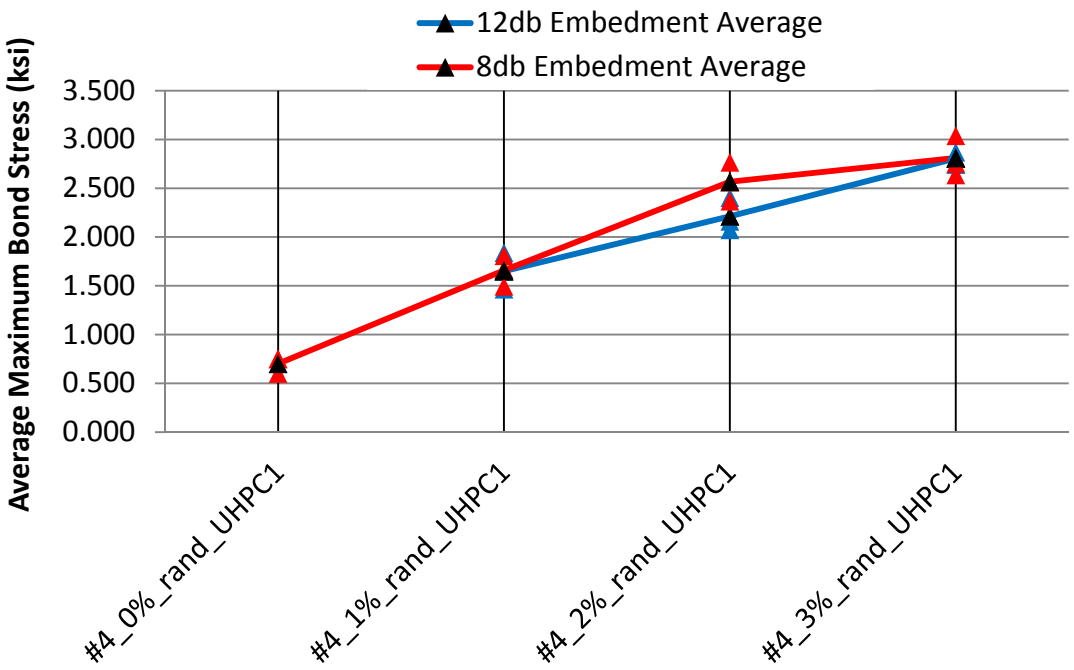

Figure 4-29: Average Maximum Bond Stress for #4_rand_UHPC1 specimens with varying embedment length and fiber volume fraction

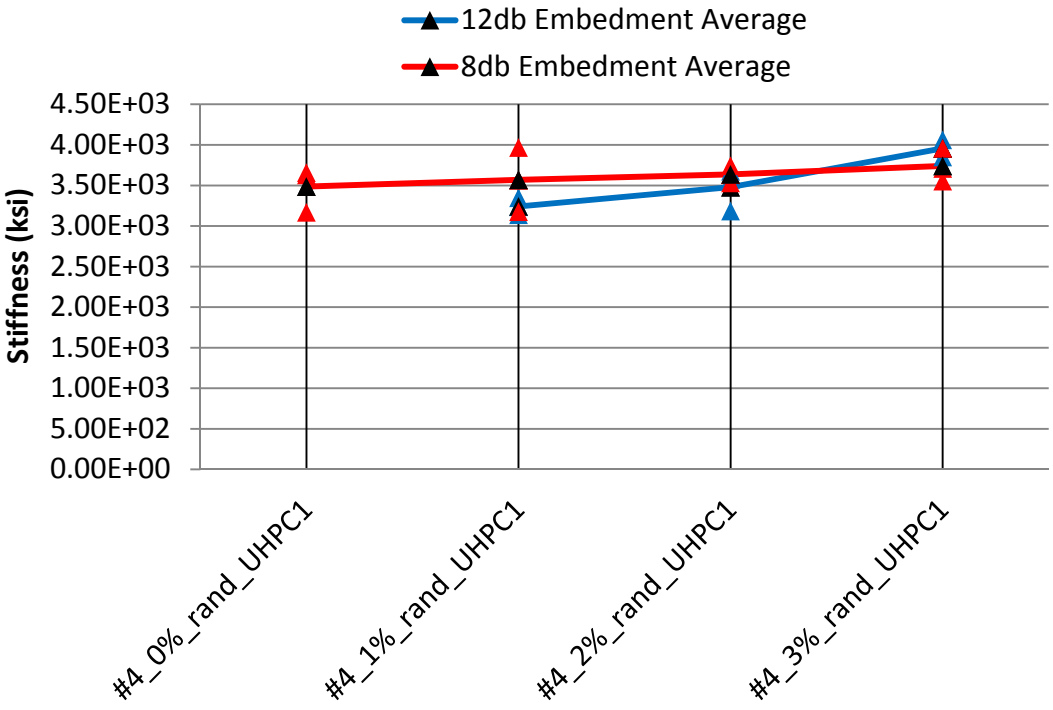

Figure 4-30: Average Maximum Bond Stress for #4_rand_UHPC1 specimens with varying embedment length and fiber volume fraction

4.2.3 Comparison of Pullout Behavior of Size #3 and #4 Bars

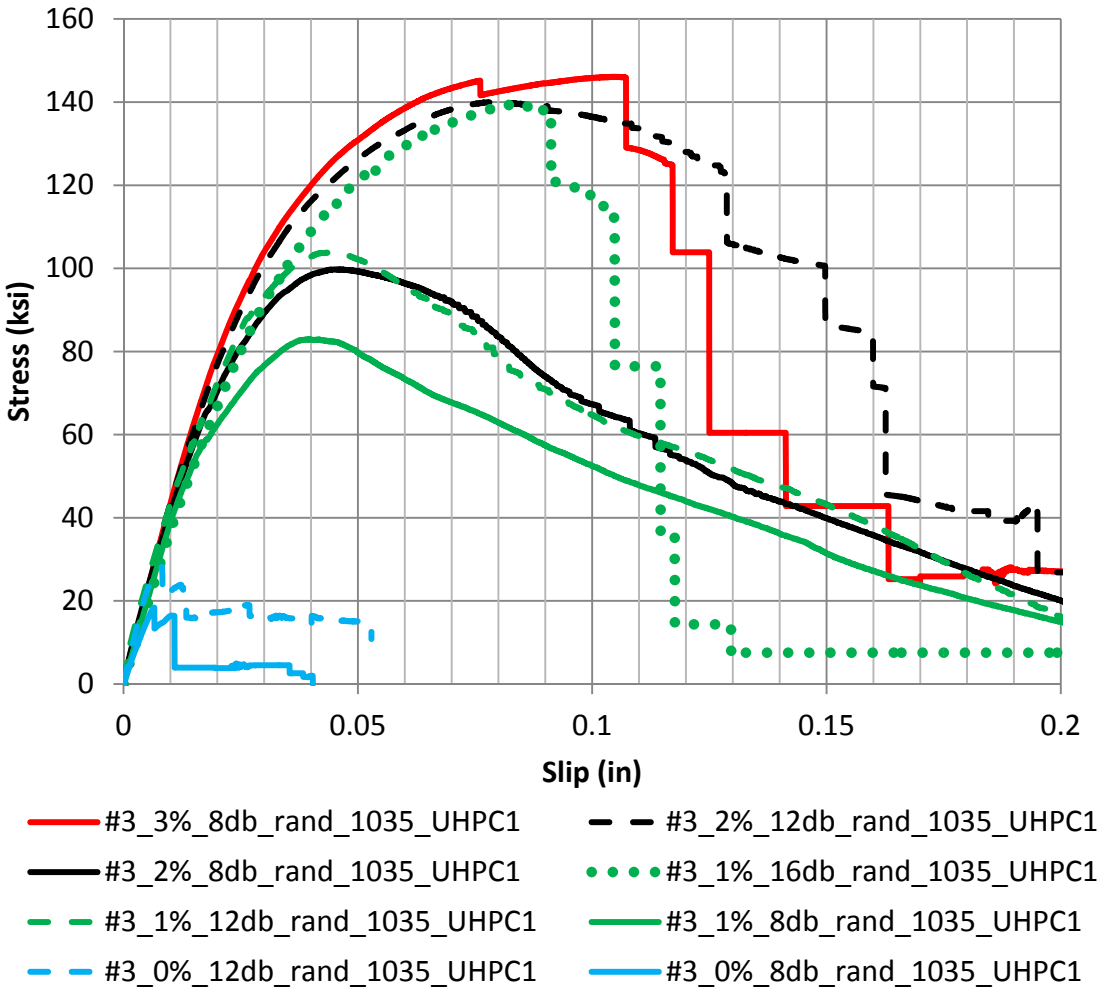

Figure 4-31: Average bar stress vs slip curves for all #3 1035 bars embedded in UHPC1

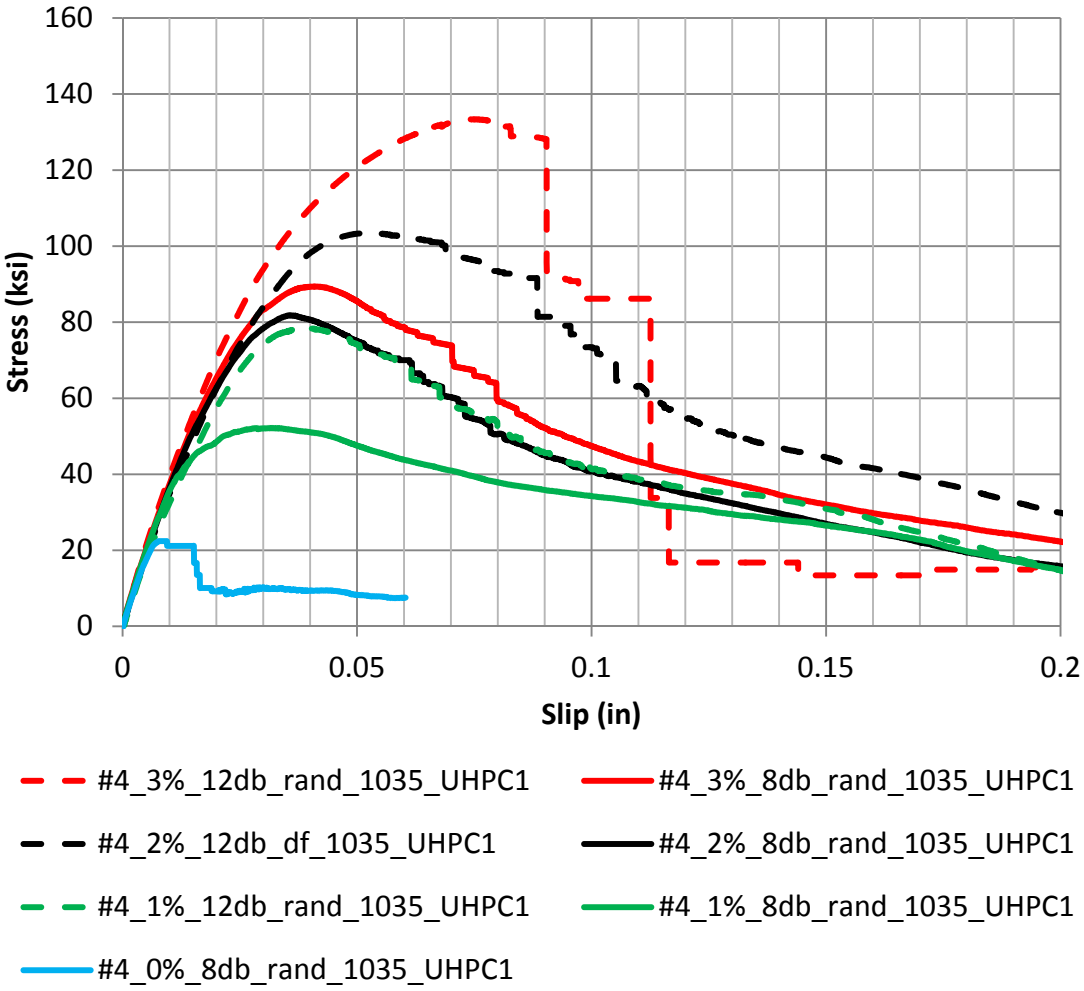

Figure 4-32: Average bar stress for all #4 1045 bars embedded in UHPC1

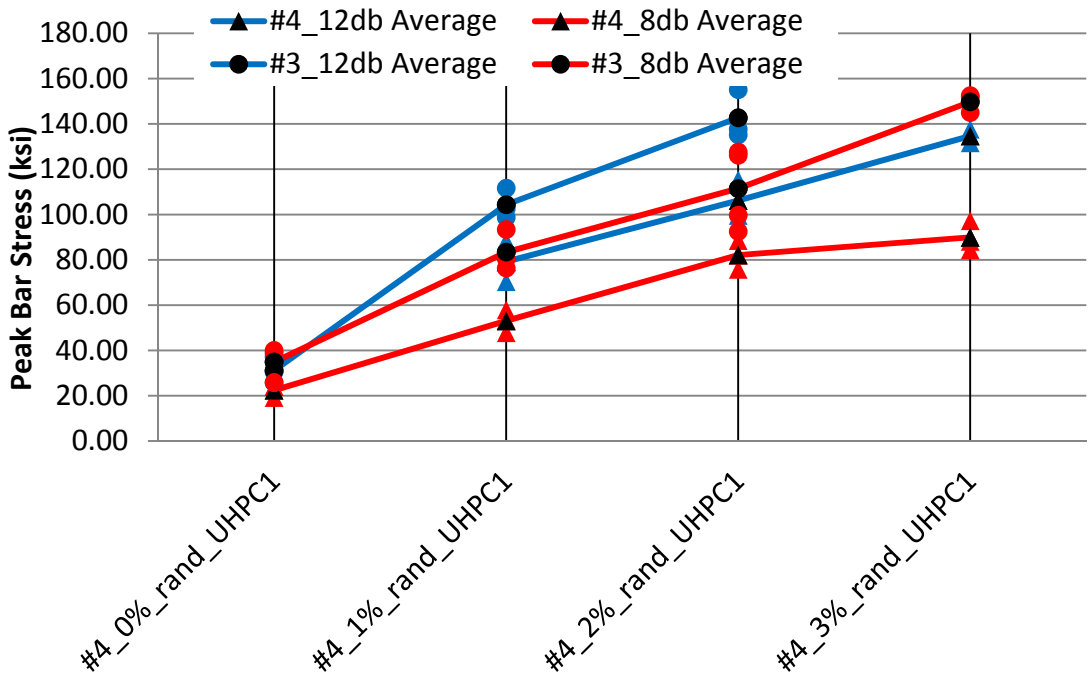

Figure 4-33: Peak Bar Stress comparison for #3 and #4 _rand_UHPC1 specimens with varying fiber percentage and embedment

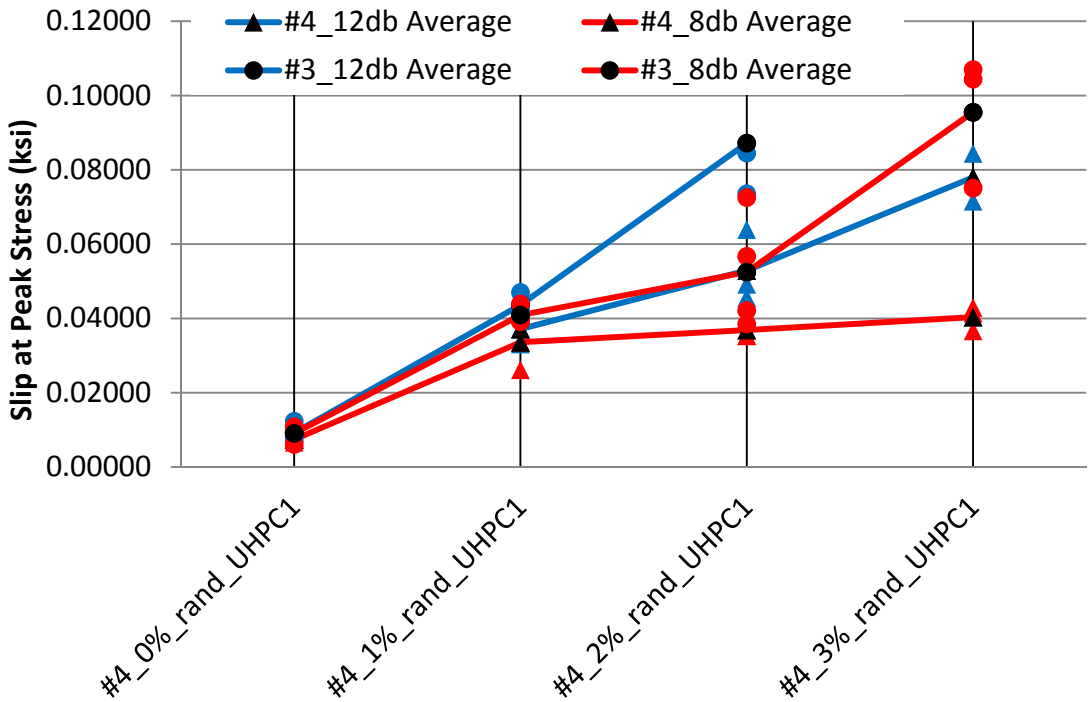

Figure 4-34: Slip at peak stress comparison for #3 and #4 _rand_UHPC1 specimens with varying fiber percentage and embedment

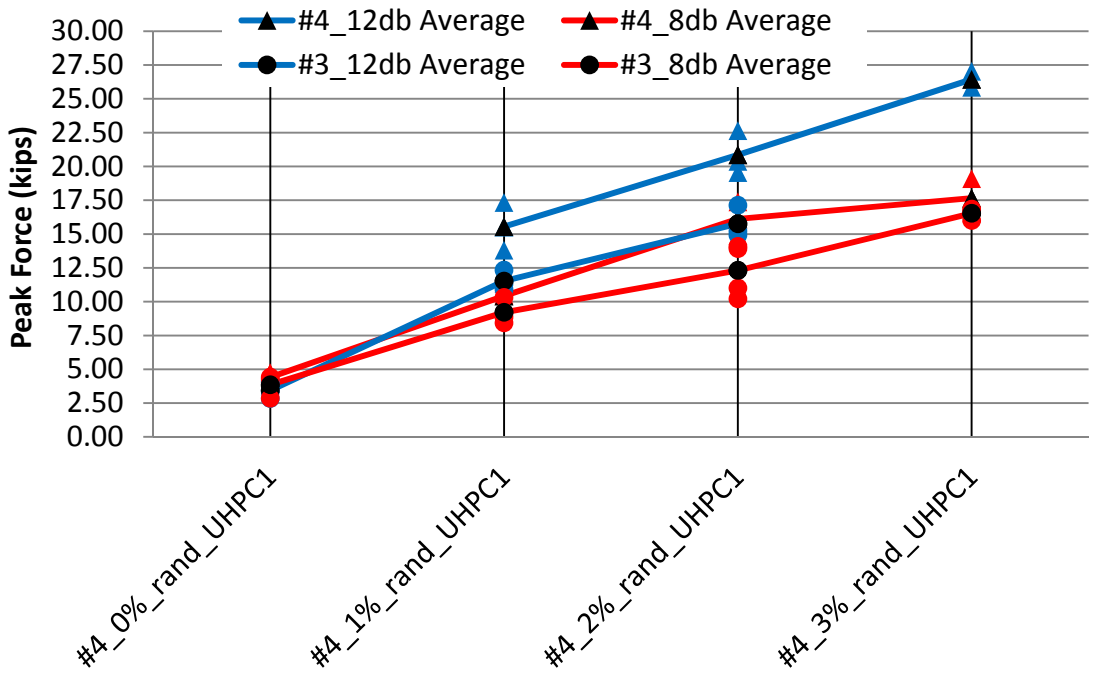

Figure 4-35: Peak Force comparison for #3 and #4 _rand_UHPC1 specimens with varying fiber percentage and embedment

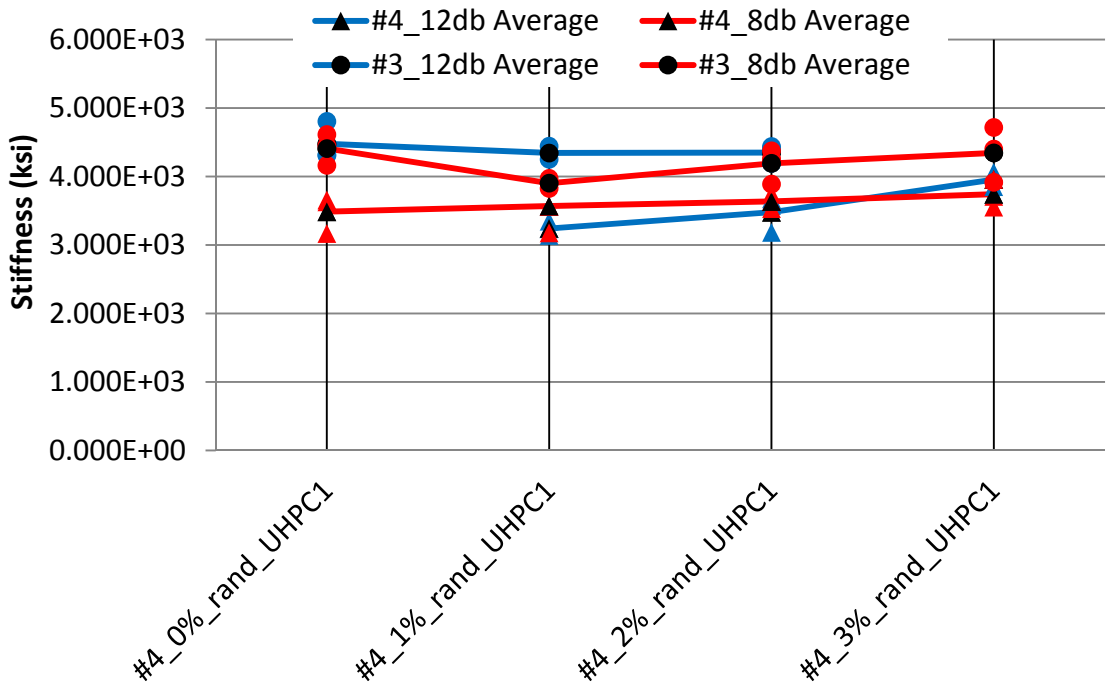

Figure 4-36: Stiffness comparison for #3 and #4 _rand_UHPC1 specimens with varying fiber percentage and embedment

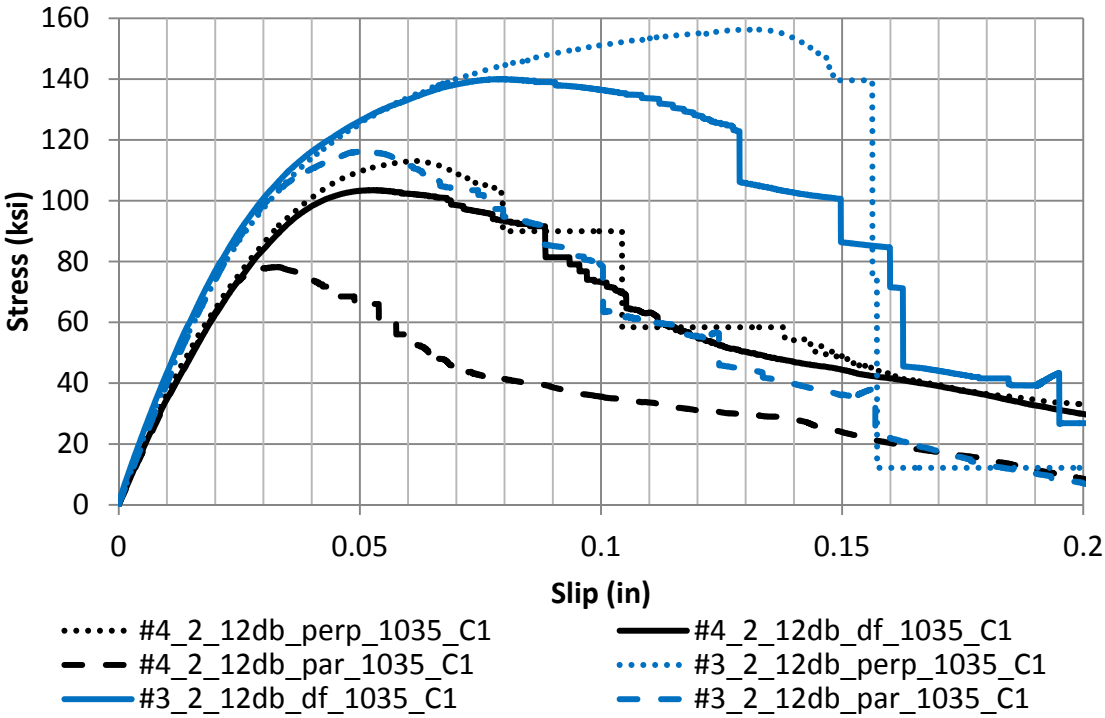

Figure 4-37: Stiffness comparison for #3 and #4 _rand_UHPC1 specimens with varying fiber percentage and embedment

4.3 Phase III: Uniaxial Tensile Behavior of Rebar Reinforced UHPFRC

4.3.1 Uniaxial Behavior of UHPFRC Reinforced with A1035 Bar

Table 4-9: Results of Reinforced UHPFRC uniaxial tension using A1035 bar

		E 10^5 ksi	Θ_{peak} ksi	F_{peak} kip	ε_{peak} in/in	ε_{ult} in/in	UHPC contribution ksi	Cr/in	$Cr_{spacing}$ in	Homogeneous Distribution? Y / N
3%_Par_1035	S1	9.26	241.8	26.71	0.0030	0.0118	3.13	4.17	0.24	Y
3%_Rand_1035	S1	9.99	219.4	24.23	0.0067	0.0159	2.27	2.08	0.48	N
2%_Par_1035	S1	9.06	241.9	26.72	0.0047	0.0144	3.13	2.92	0.34	N
2%_Rand_1035	S1	7.58	203.3	22.46	0.0071	0.0152	1.66	1.83	0.55	N
1%_Par_1035	S1	7.94	204.4	22.58	0.0070	0.0155	1.70	2.50	0.40	Y
	S2	8.87	196.5	21.70	0.0059	0.0155	1.40	1.96	0.51	Y
	Avg	8.40	200.5	22.14	0.0065	0.0155	1.55	2.23	0.46	-
1%_Rand_1035	S1	-	192.2	21.22	0.0106	0.0185	1.23	1.42	0.71	N
1%_Perp_1035	S1	-	176.4	19.48	0.0206	0.0039	0.63	0.96	1.04	Y
0.75%_Par_1035	S1	11.26	196.0	21.65	0.0114	0.0229	1.38	0.92	1.09	Y
0.5%_Par_1035	S1	-	178.1	19.67	0.0119	0.0210	0.69	1.21	0.83	Y
0.5%_Rand_1035	S1	7.84	181.6	20.05	0.0203	0.0262	0.82	1.00	1.00	Y
0%_Par_1035	S1	-	-	-	-	-	-	-	-	-
A1035Bar	Avg	0.32	160.0	17.67	3.95	9.42	-	-	-	-

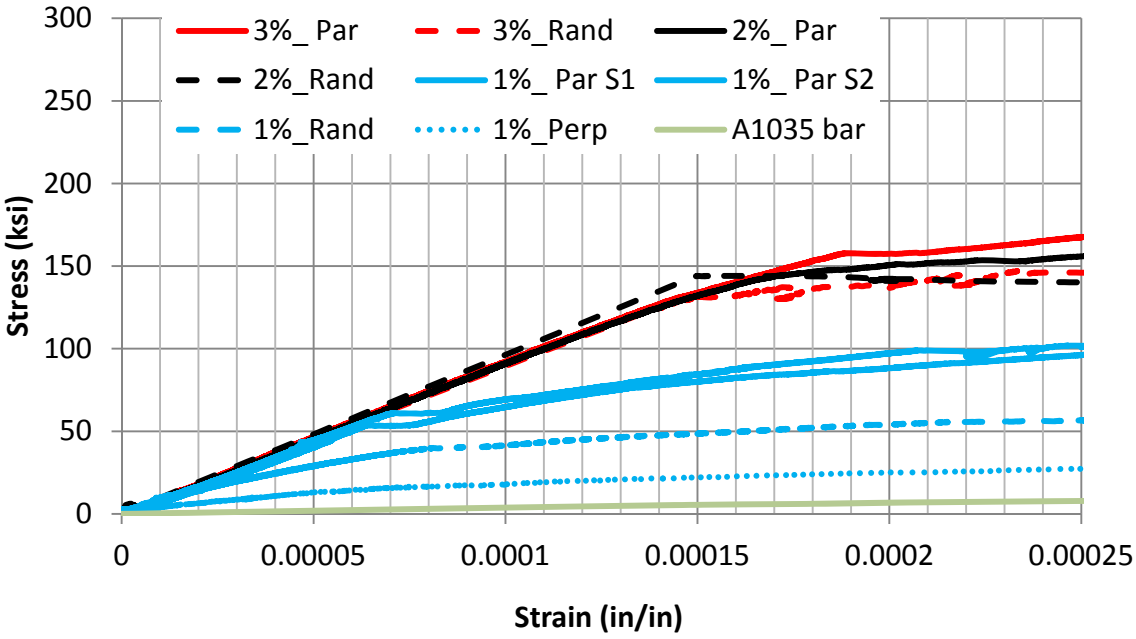

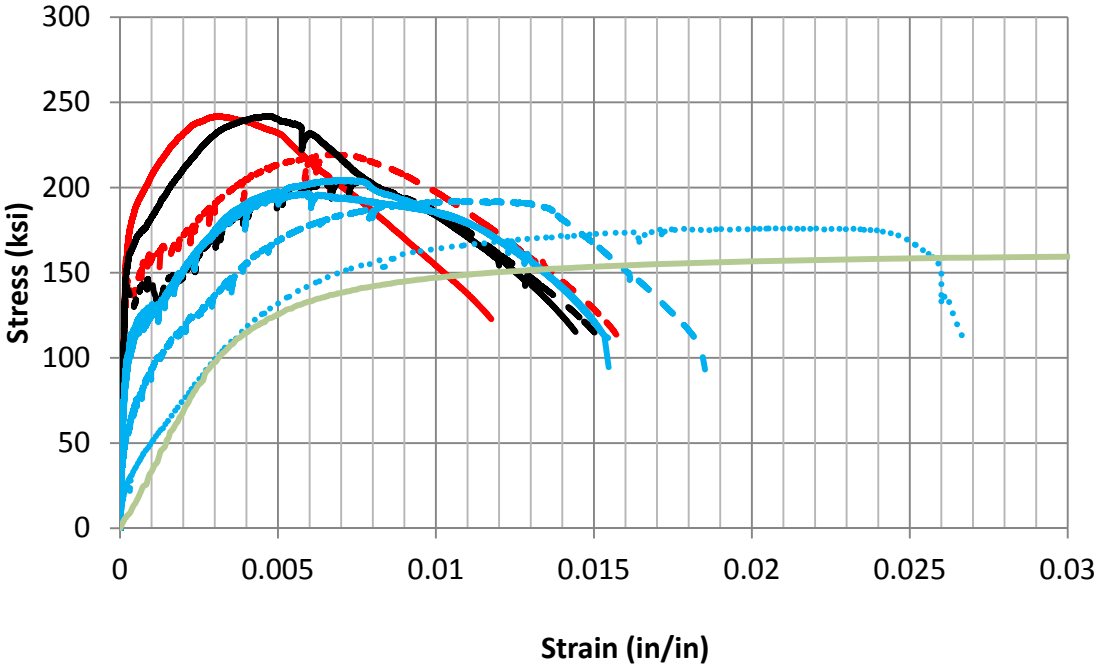

Figure 4-38: Stress vs strain curves for A1035, 1% to 3% fibers, various orientations

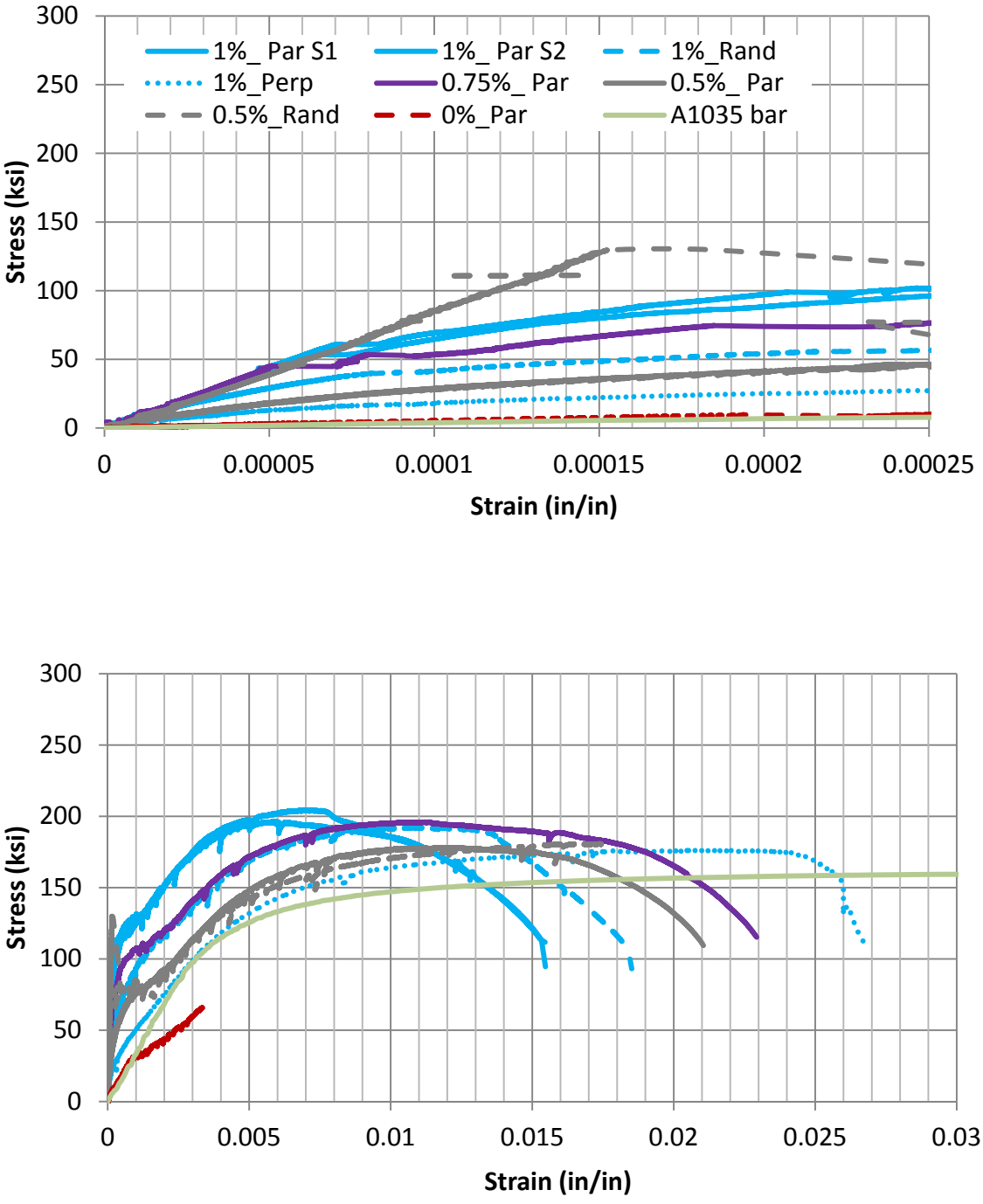

Figure 4-39: Stress vs strain curves for A1035, <=1% fibers, various orientations

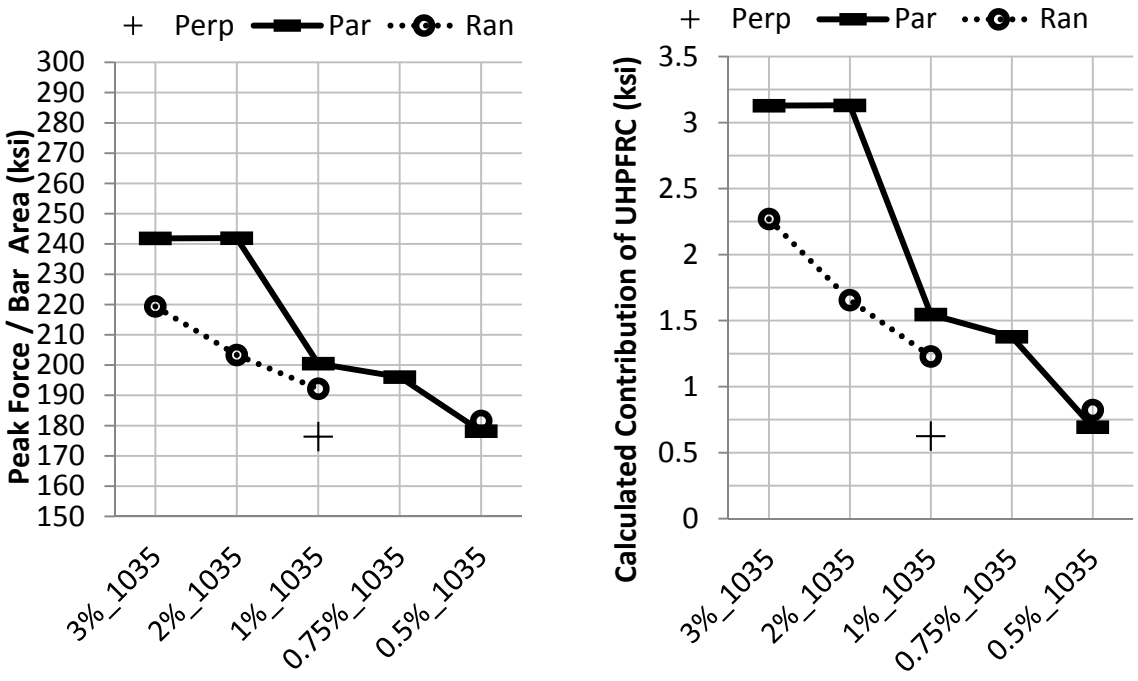

Figure 4-40: Peak bar stress and the calculated UHPFRC contribution for uniaxial tension using A1035 bar

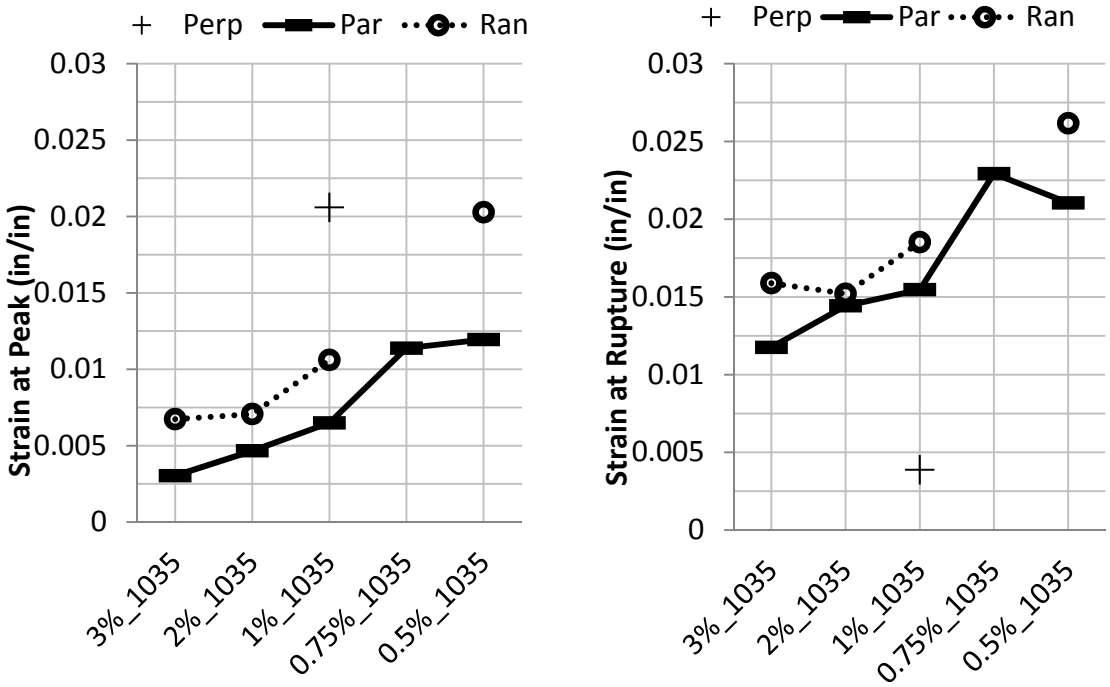

Figure 4-41: Strain at peak and strain at rupture for direct tension using A1035 bar

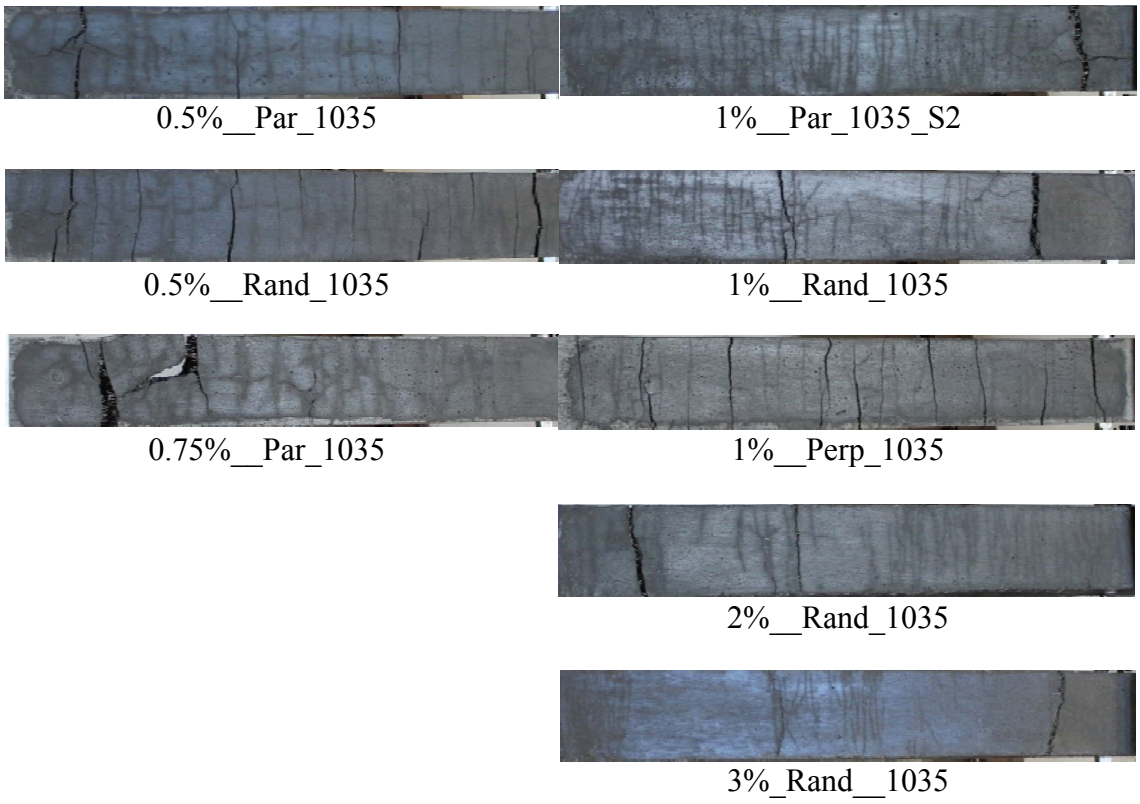

Figure 4-42: Photographs of several A1035 reinforced specimens taken as near as possible to the point of rupture

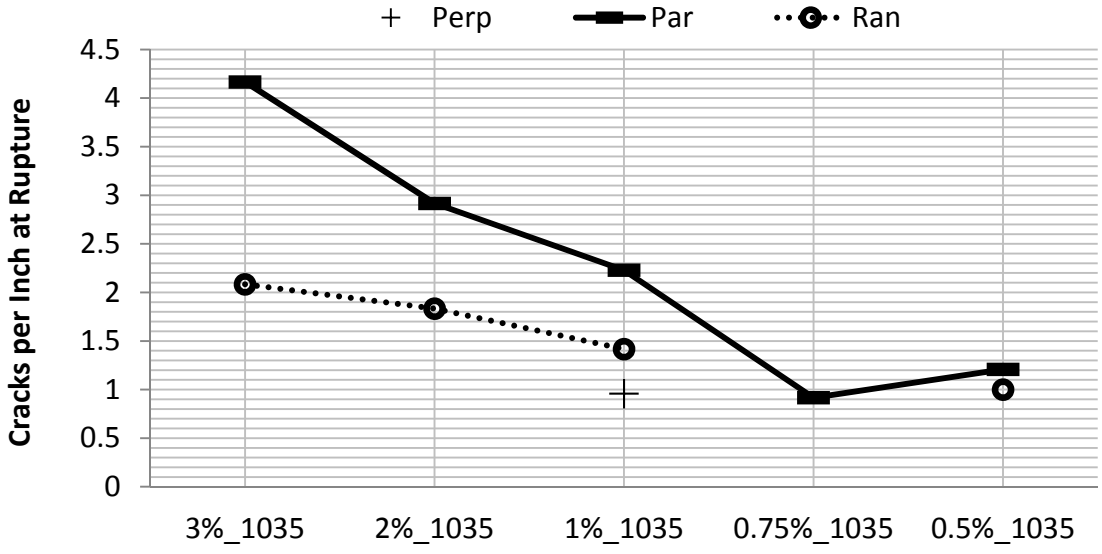

Figure 4-43: Cracks per inch at rupture for direct tension using A1035 bar

4.3.2 Uniaxial Behavior of UHPFRC Reinforced with A615 Bar

Table 4-10: Results of Reinforced UHPFRC direct tension using A615 bar

		E	Θ_{max}	F_{max}	ε_{max}	ε_{ult}	UHPC contribution	Cr/in	$Cr_{spacing}$	Homogeneous Distribution?
		10^5 ksi	ksi	kip	in/in	in/in	ksi		in	Y / N
3%_Par_615	S1	7.87	213.6	23.60	0.0017	0.0139	4.19	2.94	0.34	N
2%_Par_615	S1	8.41	212.2	23.44	0.0024	0.0159	4.14	3.00	0.33	-
	S2	9.35	238.5	26.34	0.0025	0.0150	5.14	3.38	0.30	Y
	Avg	8.88	225.3	24.89	0.0024	0.0155	4.64	3.19	0.31	-
1%_Par_615	S1	-	138.2	15.26	0.0030	0.0239	1.31	1.71	0.59	-
	S2	8.56	158.1	17.46	0.0027	0.0192	2.07	2.08	0.48	Y
	Avg	-	148.1	16.36	0.0029	0.0215	1.69	1.90	0.53	-
1%_Rand_615	S1	-	112.5	12.43	0.0075	0.0173	0.33	1.25	0.80	N
1%_Perp_615	S1	-	108.3	11.96	0.0456	0.0472	0.16	0.92	1.09	Y
0.75%_Par_615	S1	8.56	138.8	15.32	0.0034	0.0426	1.33	1.04	0.96	Y
	S2	-	125.3	13.84	0.0048	0.0188	0.81	1.17	0.86	Y
	Avg	-	132.0	14.58	0.0041	0.0307	1.07	1.10	0.91	-
0.5%_Par_615	S1	-	115.7	12.78	0.0077	0.0238	0.45	1.25	0.80	Y
0%_Par_615	S1	-	-	-	-	-	-	-	-	-
A615Bar	Avg	0.30	104.4	11.53	9.47	14.13	-	-	-	-

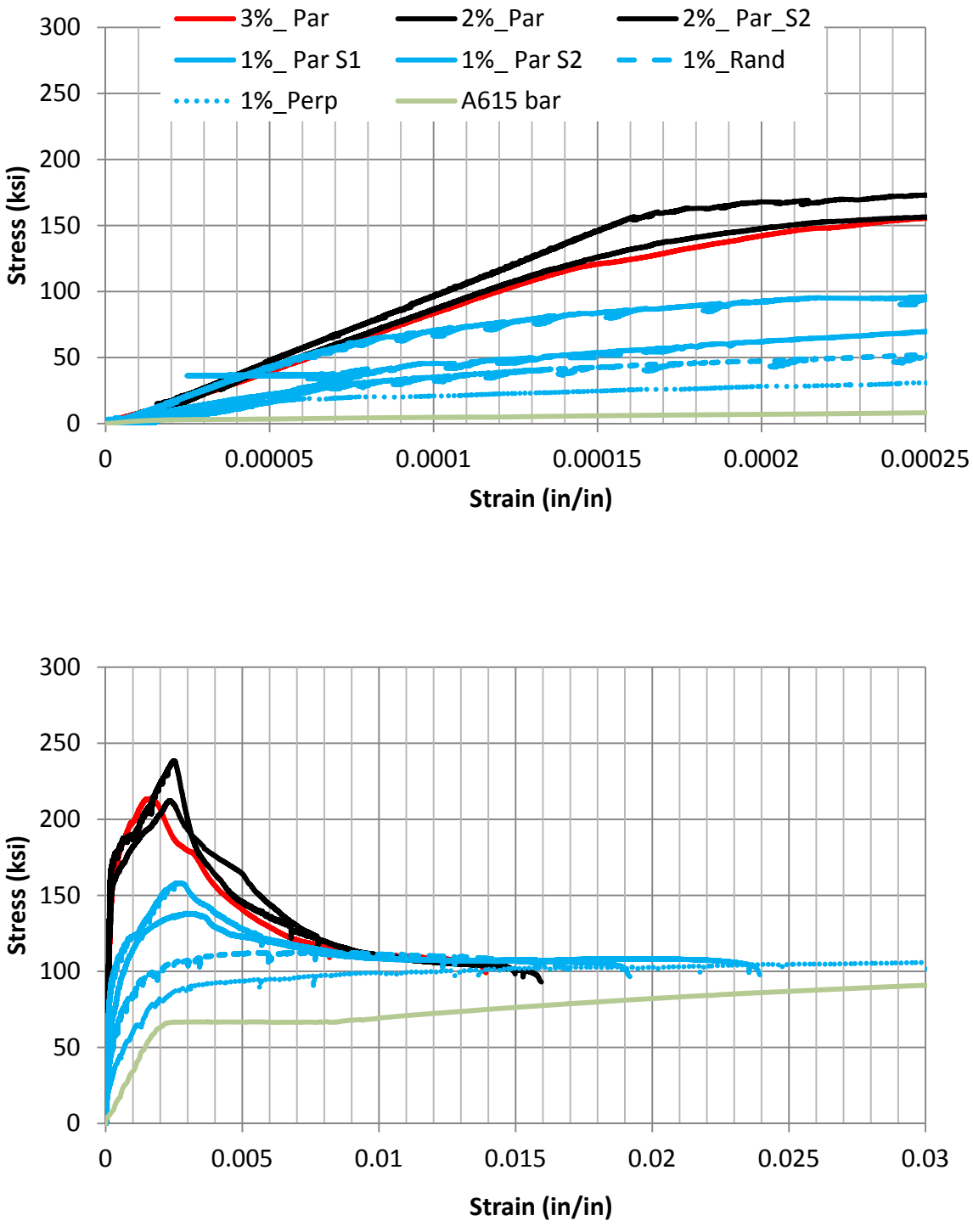

Figure 4-44: Stress vs Strain Curves for A615, 1% to 3% fibers, various orientations

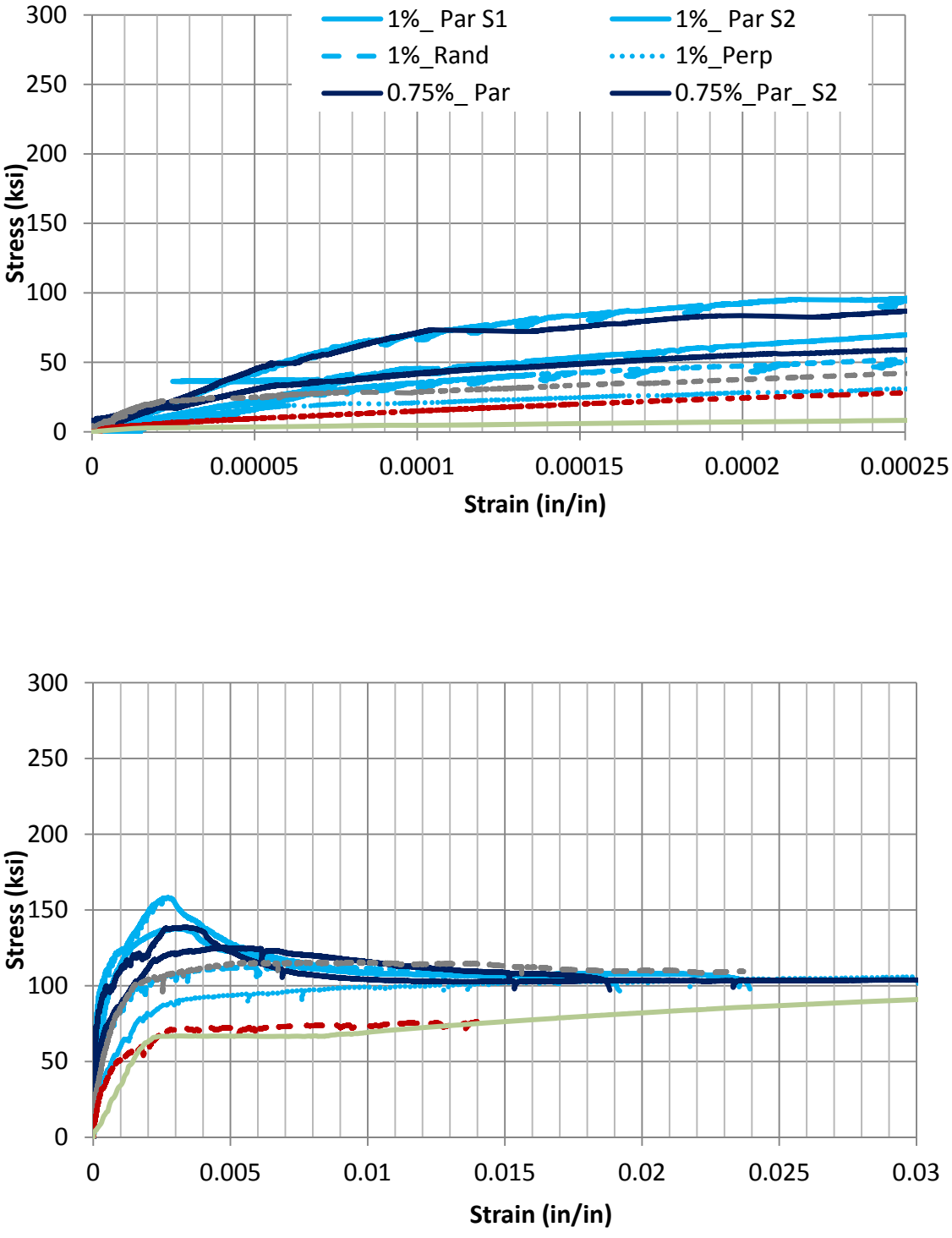

Figure 4-45: Stress vs Strain Curves for A615, <=1% fibers, various orientations

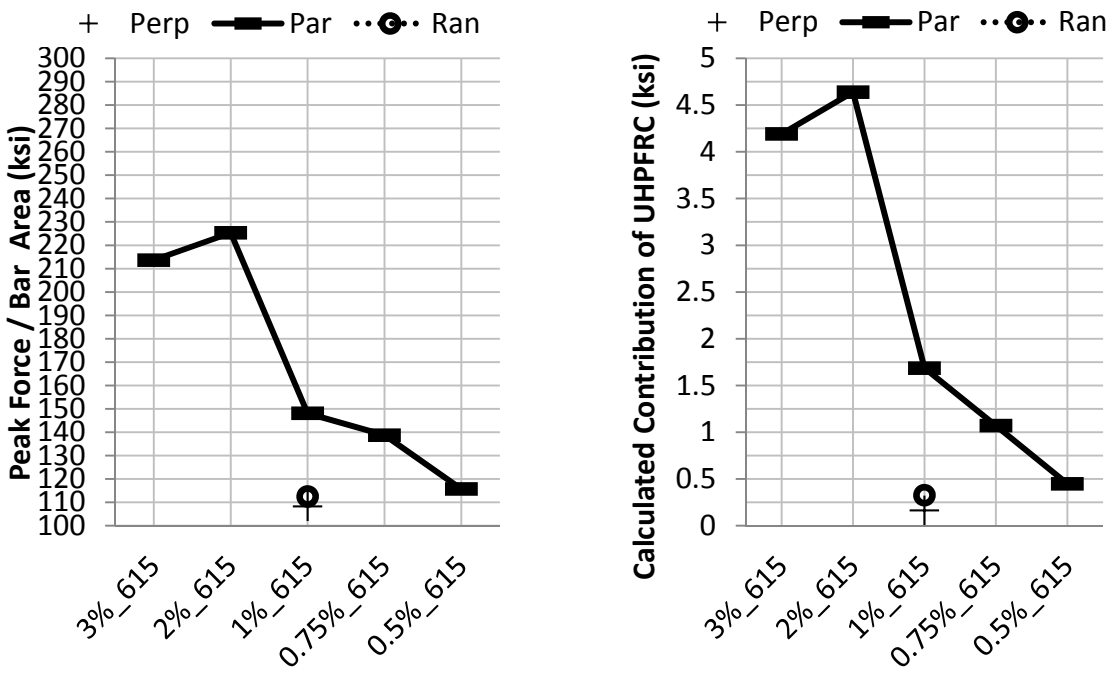

Figure 4-46: Peak bar stress and the calculated UHPFRC contribution for direct tension using A615 bar

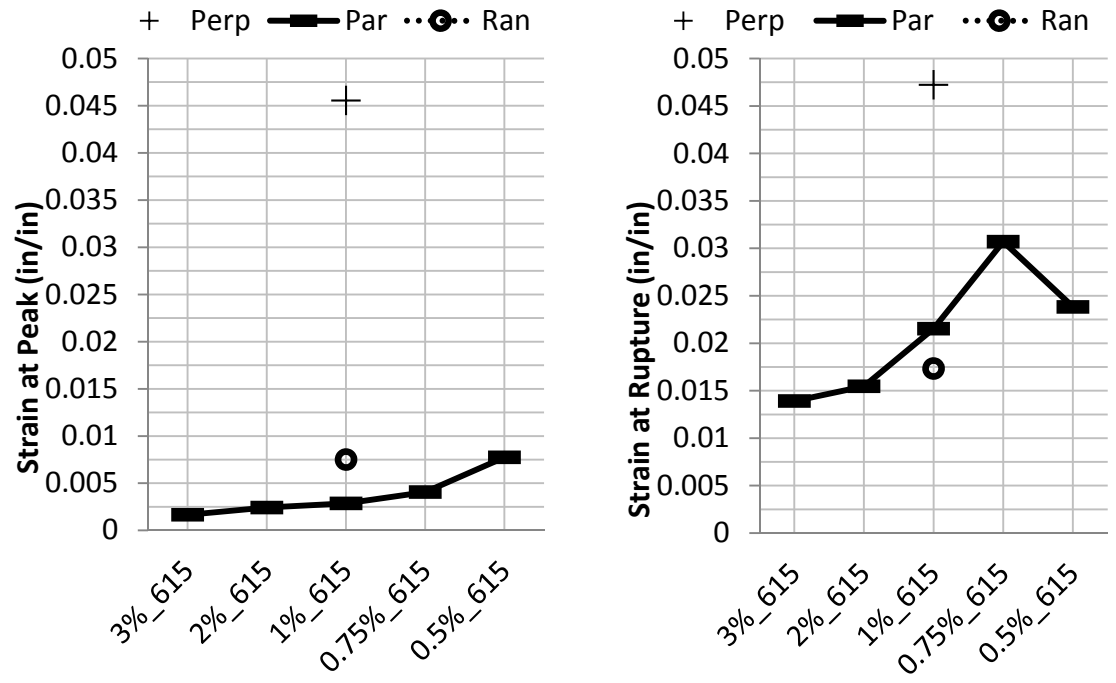

Figure 4-47: Strain at peak and strain at rupture for direct tension using A615 bar

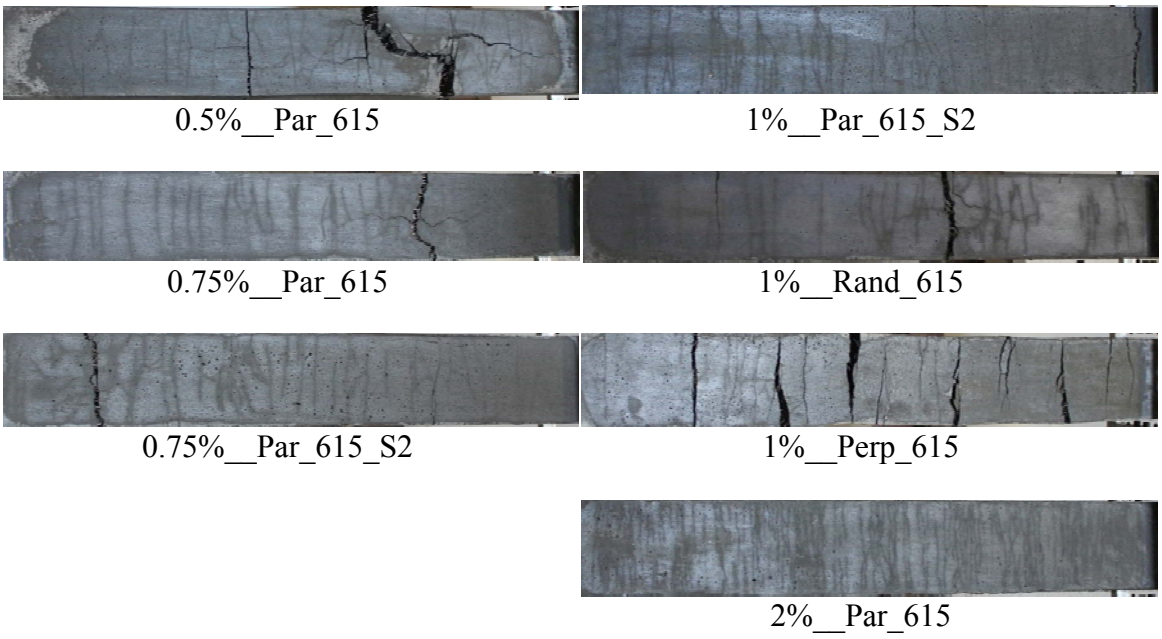

Figure 4-48: Photographs of several A615 reinforced specimens taken as near as possible to the point of rupture

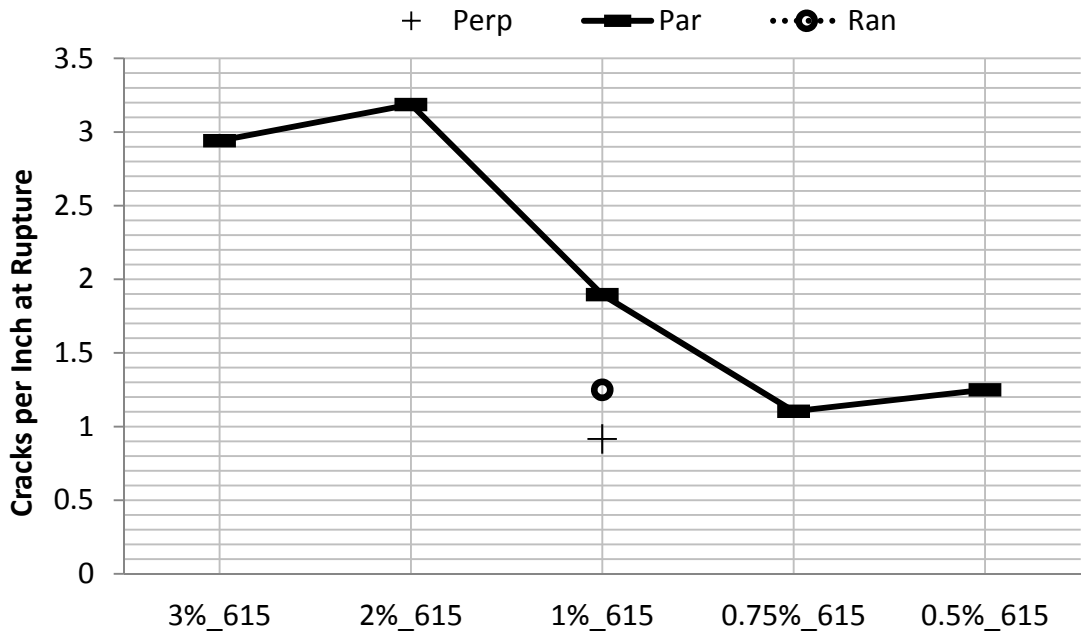

Figure 4-49: Cracks per inch at rupture for direct tension using A615 bar

5 CHAPTER FIVE - CONCLUSIONS

This three phase experiment was focused mainly on the behavior of Ductal JS1000, which in this paper is referred to as UHPC1. The three phases are: Phase I) Uniaxial tensile behavior of UHPFRC and rebar. Phase II) Bond behavior between UHPFRC and rebar embedded in UHPFRC. Phase III) Uniaxial tensile behavior of rebar reinforced UHPFRC. The specimen designs and test setup designs were either newly developed or modified in order to be used with UHPFRC and the available laboratory equipment. One overarching focus is the influence of varying fiber volume fraction between 0% and 3%. Another overarching focus is the influence of fiber orientation aligned parallel, perpendicular, and random with respect to the axis of applied load. Curing time remained constant at 14 days, room temperature.

UHPFRC1 uniaxial tension: Influence of fiber volume fraction

There is a nearly linear relationship between maximum tensile stress and fiber volume fraction for UHPFRC1 parallel aligned specimens 1%, 2%, and 3%. The number of cracks per inch, crack spacing, and strain at maximum stress have more variability and less of a linear relationship. There is a definite decrease in crack spacing as fiber volume fraction is increased up to 3%. The maximum tensile stress data agrees nicely with existing data from the literature review with similar parameters.

UHPFRC1 uniaxial tension: Influence of fiber orientation

The 2% random fiber orientation specimens have a slight decrease (roughly -17% for casting method “RandomA” and roughly -10% for casting method “RandomB”) in

maximum tensile stress compared to the 2% parallel fiber orientation specimens. At 1% fiber volume fraction this same decrease when comparing parallel to random (-1.4% for casting method "RandomA") is almost negligible. This is most likely due to 1% fiber volume fraction being too low to have a significant impact on strain hardening. Random oriented 3% specimens were not casted or tested due to a decrease in workability while casting. There is no definitive difference in regard to crack spacing and strain at peak stress when comparing random and parallel orientation UHPFRC uniaxial tension results.

UHPFRC uniaxial tension: Specimen design and test setup

The specimen cross section of 1" (25mm) x 2" (50mm) is large enough to provide a sample of how a full size specimen might behave. However, more research will need to be done using larger specimens which will allow more room in the formwork for fiber orientation to vary. The perforated aluminum grip plates epoxied to the specimen ends provide a small amount of flexibility in the wedge grip system. In many cases the initial crack occurred at stresses well below the expected cracking stress of 1.2ksi. This is perhaps indicative that, despite best efforts, there are still some bending stresses due to limited freedom of rotation.

UHPFRC compression and rebar uniaxial tension: Overall

UHPC1 surpasses the required UHPC classification lower limit of 21.7ksi (150MPa). At 14 days the average compressive strength of UHPC1 is 23.4ksi. The influence on peak compressive strength by varying fiber volume fraction from 0% to 2% is negligible. Both

the A615 rebar and A1035 rebar behave as expected in uniaxial tension and are mainly tested because they are 100% necessary to analyze the results of Phase II and Phase III.

Pullout of rebar embedded in UHPFRC: Influence of fiber volume fraction

Fiber volume fraction of 0%, 1%, 2%, 3% with random fiber orientation for both #3 and #4 bar with 8db and 12db embedment lengths are examined. There is a negligible difference in increasing fiber content on the stiffness of the ascending portion of stress slip curve. Peak bar stress increases nearly linearly with an increase in fiber content as does average maximum bond stress. Slip at peak stress increases with an increase in fiber content, although not always linearly. As with the uniaxial UHPFRC specimens, crack numbers are higher and spacing is visibly tighter for higher fiber volume fractions. A complete comparison with existing data will involve looking at many different parameters. The bond stress results compare nicely with existing bond stress results using UHPC. Bond stress is used because it allows for a relatively quick normalized comparison between test series with many differing parameters.

Pullout of rebar embedded in UHPFRC: Influence of fiber orientation

Fiber orientation has a huge influence on peak stress of pullout specimens at 2% fiber volume fraction combined with 12db embedment for both #3 and #4 bar. These parameters were the only parameters used to evaluate fiber orientation due to the labor intensive casting method involved being a limiting factor. For #3 bar the increase from random to perpendicular is 13% and the decrease from random to parallel is roughly 18%. It is expected based on the tensile results in Phase I, that at 1% fiber volume

fraction the difference in behavior due to orientation may be less due to less of an impact on strain hardening.

Pullout of rebar embedded in UHPFRC: Overall

It is important to note that A1035 bars are used because it is expected that A615pullout results are extremely similar up to the A1035 results correlating to the A615 peak stress. The difference is expected to be negligible, and therefore testing of A615 was deemed redundant. Also noteworthy, is the #3 bar pullout tests have a larger cover than the #4 bar pullout tests because the same exact formwork was used regardless. The bond stress results compare nicely to existing results and provide an additional extensive database of pullout behavior at small concrete covers. This research is the first of its kind to look at extensive variation of fiber content at low covers as well as the first to look at the influence of fiber orientation on bond between rebar and UHPFRC. The test method is repeatable, accurate, and the randomly casted specimens are relatively easy to prepare. A casting method was developed to artificially align the fibers parallel and perpendicular.

Uniaxial tension of rebar reinforced UHPFRC:

Stiffness, maximum stress (force/bar area), maximum force, strain at maximum, strain at rupture, UHPC contribution, and number of cracks are evaluated for 3"x 4" cross section UHPFRC specimens reinforced with #3 bars. Both A615 and A1035 bars are used. Fiber volume fractions range from 0%-3%. Orientations vary from parallel, perpendicular, and

random with respect to the axis of applied load. Most of the specimens were cast using parallel orientation because it was the most repeatable casting method for this type of specimen. Also, for many of the specimens, photographs were taken at various stages throughout the test and the strain and stress were recorded for each photograph. This will be important for analysis in the future.

Uniaxial tension of rebar reinforced UHPFRC: Influence of fiber volume fraction

Specimens with lower fiber volume fractions have higher strain at rupture due to a larger number of macro cracks where the rebar can strain-harden. This is of high importance with regard to design for ductility. Specimens with higher fiber volume fractions have tighter cracks and smaller crack spacing but less strain at rupture. Both A1035 and A615 specimens with 1% or less fiber volume fraction behave as expected and the contributions of UHPFRC correlates well with the tensile strengths of UHPFRC found in Phase I. Further analysis will need to be done on specimens with 2% fiber and above for both. For many of the test series, only one specimen was able to be tested due to time and material quantity limitations.

Uniaxial tension of rebar reinforced UHPFRC Influence of fiber orientation

Specimens with parallel and perpendicular fiber orientations tend to have a more homogeneous crack distribution than the specimens with random orientations. The crack per inch and crack spacing numbers are only accurate for the specimens with homogeneous crack distribution. Generally, specimens with random fiber orientations have higher strains at rupture and lower peak strength than do parallel. Generally,

perpendicular specimens have even lower peak strengths and even higher strains at rupture. They also had higher crack spacing.

This three phase experiment provides information to fill critical knowledge gaps in the behavior of UHPFRC. Specifically, the combining of reinforcement bars (rebar) with UHPFRC is important because rebar is a commonly used material in current construction practice. Fiber volume fraction and fiber orientation are two major factors which influence the behavior of UHPFRC and are therefore the focus throughout all three phases. This experiment provides a database of information regarding rebar reinforced UHPFRC and its components that can be used further to decide optimal parameters to optimize cracking, strength, ductility, and bond.

6 REFERENCES

[1] Wille, K., Naaman, A.E., Parra-Montesinos, G.J., "Ultra-High Performance Concrete with Compressive Strength Exceeding 150Mpa (22ksi): A Simpler Way," *ACI Materials Journal,* vol. 108, no. 1, 2011.

[2] Naaman, A.E., Wille, K., "The Path to Ultra-High Performance Fiber Reinforced Concrete (UHP-FRC): Five Decades of Progress," *3rd International Symposium on UHPC and Nanotechnology for High Performance Construction Materials,* pp. 3-15, 2012.

[3] Habel, K, "Structural Behavior of Elements Combining Ultra-High Performance Fibre Reinforced Concretes (UHPFRC) and Reinforced Concrete," PhD Thesis, Swiss Federal Institute of Technology in Lausanne, 2004.

[4] Lubbers, A.R., "Bond Performance Between Ultra-High Performance Concrete and Prestressing Strands," Master's Thesis, College of Engineering and Technology of Ohio University, 2003.

[5] Wille, K., Kim, D.J., Naaman, A.E., "Strain Hardening UHP-FRC with low fiber contents," *Materials and Structures,* vol. 44, pp. 583-598, 2011.

[6] Wille, K., Naaman, A.E., "Fracture Energy of UHP-FRC under Direct Tensile Loading," in *Proceedings of Fracture Mechanics of Concrete*, Korea Concrete Institure, Seoul, 2010.

[7] Ahiborn, T.M., Steinberg, E.P, "An Overview of UHPC Efforts through the North American Working Group," Proceedings of the Hipermant 2012 3rd International Symposium on UHPC and Nanotechnology for High Performance Construction Materials, Kassel, Germany, pp.43-50, 2012.

[8] Russel, H., Graybeal, B, "Publication No. FHWA-HRT-13-060: Ultra-High Performance Concrete: A State-of-the-Art Report for the Bridge Community," Federal Highway Administration, McLean, VA, 2013.

[9] Walvren, J, "On the Way to International Design Recommendations for Ultra High Performance Fibre Reinforced Concrete," Proceedings of the Hipermant 2012 3rd International Symposium on UHPC and Nanotechnology for High Performance Construction Materials, Kassel, Germany, pp.485-492, 2012.

[10] Naaman, A.E, "Toughness, Ductility, Surface Energy of Deflection-Hardening FRC Composites," Proceedings of the JCI international Workshop on Ductile Fiber Reinforced Cementitious Composites (DFRCC) - Application and Evaluation, Takayama, Japan, pp.33-57, 2002.

[11] Baby, F., Graybeal, B.A., "Development of Direct Tension Test Method for Ultra-High-Performance Fiber-Reinforced Concrete," *ACI Materials Journal,* vol. 110, no. 2, pp. 177-186, 2013.

[12] Graybeal, B., Baby, F., Merchand, P., Toutlemonde, F., "Direct and Flexural Tension Test Methods for Determination of the Tensile Stress-Strain Response of UHPFRC," International Symposium on UHPC and Nanotechnology for High Performance Construction Materials, Kassel, Germany, pp.395-402, 2012.

[13] Naaman, A.E., Reinhardt, H.W, "Proposed Classification of HPFRC composites based on their tensile response," *Materials and Structures,* vol. 39, no. DOI 10.1617/s11527-006-9103-2, pp. 547-555, 2006.

[14] Naaman, A.E., Reinhardt, H.W, "Setting the Stage: Towards Performance Based Classification of FRC Composites.," Proceedings of the 4th RILEM Symposium on High Performance Fiber Reinforced Cement Composites (HPFRCC4), pp 1-4, 2003.

[15] Wille, K., El-Tawil, S., Naaman, A.E., "Properties of Strain Hardening Ultra High Performance Fiber Reinforced Concrete (UHP-FRC) under Direct Tensile Loading," *Cement & Concrete Composites,* no. (2014), doi: http://dx.doi.org/10.1016/j.cemconcomp.2013.12.015.

[16] Fehling, E., Bunjo, K., Leutbecher, T., "Design Relevant Properties of Hardened Ultra High Performance Concrete," in *Proceedings of the International Symposium on Ultra High Performance Concrete*, Kassel, Germany, 2004.

[17] Kim, D.J., Wille, K., Naaman, A.E., El-Tawil, S. , "Strength Dependent Tensile Behavior of Strain Hardening Fiber Reinforced Concrete," *High Performance Fiber Reinforced Cement Composites 6, RILEM State of the Art Reports,* vol. 2, pp. 3-10, 2012.

[18] Wille, K., Naaman, A.E., El-Tawil, S., Parra-Montesinos, G.J., , "Ultra-High Performance Concrete and Fiber Reinforced Concrete: Achieving Strength and Ductility without Heat Curing," *Materials and Structures,* vol. 45, no. 3, pp. 309-324, 2012.

[19] Lohaus, L., Anders, S., "Effects of Polymer and Fibre Modifications on the Ductility, Fracture Properties and Micro-crack Development of Ultra-High Performance Concrete," Proceedings of the International Symposium on Ultra High Performance Concrete, Kassel, Germany, pp.625-636, 2004.

[20] Park, S.H., Kim, D.J., Ryu, G.S., Koh, K.T., "Tensile Behavior of Ultra-High Performance Hybrid Fiber Reinforced Concrete," *Cement and Concrete Composites,* vol. 34, pp. 172-184, 2012.

[21] Kim, D.J., Koh, K.T., Park, S.H., Ryu, G.S., "Comparative Flexural Behavior of Hybrid Ultra High Performance Fiber Reinforced Concrete with Different Macro Fibers," *Construction and Building Materials,* vol. 25, pp. 4144-4155, 2011.

[22] Kang, S.T., Lee, Y., Park, Y.D., Kim, J.K., "Tensile Fracture Properties of an Ultra High Performance Fiber Reinforced Concrete (UHPFRC) with Steel Fiber," *Composite Structures,* vol. 92, pp. 61-71, 2010.

[23] Wille, K., El-Tawil, S., Naaman, A.E.,, "Strain Rate Dependent Tensile Behavior or Ultra-High Performance Fiber Reinforced Concrete," *High Performance Fiber Reinforced Cement Composites 6, RILEM State of the Art Reports,* vol. 2, pp. 3-10, 2012.

[24] Tran, T.K., Kim, D.J., "High Strain Rate Effects on Direct Tensile Behavior of High Performance Fiber Reinforced Cementitious Composites," *Cement and Concrete Composites,* vol. 45, pp. 186-200, 2014.

[25] Stahli, P., Custer, R., van Mier, J.G.M., "On the Flow Properties, Fibre Distribution, Fibre Orientation, and Flexural Behavior of FRC," *Materials and Structures,* vol. 41, pp. 189-196, 2008.

[26] Fukuhara, T., Kanakubo, T., Ogawa, A., "Study on the Influence of the Fiber Orientation to the Mechanical Performance of HPFRCC," in *Proceedings of the Fourteenth World Conference on Earthquake Engineering*, Beijing, China, 2009.

[27] Ferrara, L., Ozyur, N., di Prisco, M., "High Mechanical Performance of Fibre Reinforced Cementitious Composites: The role of 'Casting-Flow Induced' Fibre Orientation," *Materials and Structures,* vol. 44, pp. 109-128, 2011.

[28] Yazici, H., Aydin, S., Yigiter, H., Yardimci, M.Y., Alptuna, G. , "Improvement on SIFCON Performance by Fiber Orientation and High-Volume Mineral Admixtures," *Journal of Materials in Civil Engineering,* vol. 22, no. 11, pp. 1093-1101, 2010.

[29] Stiel, T., Karihaloo, B.L., Fehling, E.,, "Effect of Casting Direction on the Mechanical Properties of CARDIFC," Proceedings of the International Symposium on Ultra High Performance Concrete, Kasseld, Germany, pp.481-493, 2004.

[30] Zhou, B., Uchida, Y., "Fiber Orientation in Ultra High Performance Fiber Reinforced Concrete and its Visualization," *Proceedings of Fracture Mechanics for Concrete and Concrete Structures 8 (FraMCos-8),* 2013.

[31] Osterlee, C., Denarie, E., Bruehwiler, E., "Strength and Deformability Distribution in UHPFRC Panels," *Processing Sequence in the Production of Engineered Cementitious Composites,* Vols. 1-2, no. 1, pp. 390-397, 2009.

[32] Kwon, S.H., Kang, S.T., Lee, B.Y., Kim, J.K., "The Variation of flow-dependent tensile behavior in radial flow dominant placing of Ultra High Performance Fiber Reinforced Cementitious Composites (UHPFRCC)," *Construction and Building Materials,* vol. 33, pp. 109-121, 2012.

[33] Kang, S.T., Lee, B.Y., Kim, J.K., Kim, Y.Y., "The Effect of Fibre Distribution Characterstics on the Flexural Strength of Steel Fibre Reinforced Ultra High Strength Concrete," *Construction and Building Materials,* vol. 25, pp. 2450-2457, 2011.

[34] Barnett, S.J., Lataste, J.F., Parry, T., Millard, S.G., Soutsos, M.N., "Assessment of Fiber Orientation in Ultra High Performance Fibre Reinforced Concrete and its Effect on Flexural Strength," *Materials and Structures,* vol. 43, pp. 1009-1023, 2010.

[35] Behloul, M, "Analyse et Modelisation du Compotement d-un Materiau a Matrice Cimentaire Fibree a Ultra Hautes Performances (Betons de Pudres Reactives)," Phd Thesis, L'Ecile Normale Suprieure de Cachan (Genie Civil), C.N.R.S., Universite de Paris VI, 1996.

[36] Pansuk, W., Sato, H., Sato, Y., Shionaha, R., "Tensile Behaviors and Fiber Orientation of UHPC," in *Proceedings of the International Symposium on Ultra High Performance Concrete*, Kassel, Germany, 2008.

[37] Stahli, P., van Mier, J.G.M., "Effect of Manufacturing Methods on Tensile Properties of Fibre Concrete," in *Proceedings of Fracture Mechanics for Concrete and Concrete Structures (FraMCos)6*, Catania, Italy, 2007.

[38] Van Mier, J.G.M., Nooru-Mohamed, M.B., Timmers, G., "An Experimental Study of Shear Fracture and Aggregate Interlock in Cement Composites," Heron, Vol.26, No.4, Delft University of Technology, Netherlands, 1991.

[39] Kang, S.T., Kim, J.K., "The Relation Between Fiber Orientation and Tensile Behavior in Ultra-High Performance Fiber Reinforced Cementitious Composites (UHPFRCC)," *Cement and Concrete Research,* vol. 41, pp. 1001-1014, 2011.

[40] Walravem, J.C., "High Performance Fiber Reinforced Concrete: Progress in Knowledge and Design Codes," *Materials and Structures,* vol. 42, pp. 1247-1260, 2009.

[41] Leutbecher, T., Fehling, E., "Tensile Behavior of Ultra-High-Performance Concrete Reinforced with Reniforcing Bars and Fiber: Minimizing Fiber Content," *ACI Structural Journal,* vol. 109, no. 2, p. 253, 2012.

[42] Wille, K., Parra-Montesinos, G, "Effect of Beam Size, Casting Method, and Suppport Conditions on Flexural Behavior of Ultra-High Performance Fiber-Reinforced Concrete," *ACI Materials Journal,* vol. 109, no. 3, pp. 379-388, 2012.

[43] Kang, S.T., Kim, J.K., "Numerical Simulation of the Variation of Fiber Orientation Distribution During Flow Molding of Ultra High Performance Cementitious Composites (UHPCC)," *Cement and Concrete Composites,* vol. 24, pp. 208-217, 2012.

[44] Markovic, I., "High-Performance Hybrid-Fibre Concrete- Development and Utilisation," PhD Thesis, Technical University of Delft, Netherlands, 2006.

[45] Tailhan, J.L., Rossi, P., Boulay, C., "Tensile and Bending Behavior of Strain Hardening Cement-Based Composite: Experimental and Numerical Analysis," *Cement and Concrete Composites,* vol. 34, pp. 166-171, 2012.

[46] Kang, S.T., Kim, J.K., Lee, Y., "Pullout Behavior of Inclined Steel Fiber in an Ultra-High Strength Cementitious Matrix," *Construction and Building Materials,* vol. 24, pp. 2030-2041, 2010.

[47] Krasnikovs, A., Kononova, O., "Strength Prediction of Concrete Reinforced by Different Length and Shape Short Steel Fibers," in *Publication in a Scientific Journal of the Series of Scientific Journal of Riga Technical University*, Latvia, 2010.

[48] Stahli, P, "Ultra-Fluid, Oriented Hybrid-Fibre-Concrete," PhD Thesis, ETH Zurich, Switzerland, 2008.

[49] Assication Francaise de Genie Civil (AFGC) - Service d-etudes techniques des routes et autoroutes (SETRA), "Betons fibres a ultra-hautes performances - Ultra High Performance Fibre-Reinforced Concretes, Recommendations provisoires - Interim Recommendations," p. 153, 2002.

[50] Japan Society of Civil Engineers (JSCE), "Recommendations for Design and Construction of High Performance Fiber Reinforced Cement Composites with Multiple Fine Cracks (HPFRCC)," p. 113, 2008.

[51] ASTM C1609/C1609M-10, "Standard Test Method for Flecural Performance of Fiber Reinforced Concrete (Using Beam with Third-Point Loading)," ASTM International, West Conshohocken, PA, 2010, 9pp.

[52] RILEM TC-162 TDF, "Final Recommendation of RILEM TC 162-TDF: Test and Design Methods for Steel Fiber Reinforced Concrete Sigma Expsilon-Design Method," *Materials and Structures,* vol. 36, no. 262, pp. 56-567, 2003.

[53] Lappa, E., "High Strength Fiber Reinforced Concrete: Static and Fatigue in Bending," PhD Dissertation, Delft University of Technology, Delft, Netherlands, 220pp, 2007.

[54] Wille, K., Tue, V.T., Parra-Montesinos, G.J., "Fiber Distribution and Orientation in UHP-FRC Beams and their effect on Backward Analysis," *Materials and Structures,* Vols. DOI 10.1617/s11527-013-0153-y, published online August 2013.

[55] Joint ACI-ASCE Committe 408, "ACI 408.2R-12 Report on Bond of Steel Reinforcing Bars Under Cyclic Loads," ACI, 2012.

[56] Uijl, J.A., Bigaj, A.J., "A Bond Model for Ribbed Bars Based on Concrete Confinement," *Heron,* vol. 41, no. 3, pp. 201-226, 1996.

[57] ACI Committee 408, "Bond and Development of Straight Reinforcing Bars".

[58] Tepfers, R, "A Theory of Bond Applied to Overlapped Tensile Reinforcement

Splices of Deformed Bars," Report 73-2, Chalmers University of Technology, Goteborg, 1973, 1973.

[59] Jungwirth, J., "Zum Tragverhalten von Zugbeanspruchten Bauteilen Aus Ultra-Hochleistungs-Faserbeton," Doctoral Thesis, Swiss Federal Institute of Technology in Lausanne, Switzerland, 2006.

[60] Chao, S.H., "Bond Characterization of Reinforcing Bars and Prestressing Strands in High Performance Fiber Reinforced Cementituious Composites Under Monotonic and Cyclic Loading," PhD Thesis, University of Michigan, Ann Arbor, 2005.

[61] Schumacher, P, "Rotation Capacity of Self-Compacting Steel Fiber Reinforced Concrete," PhD Thesis, Delft University of Technology, 2006.

[62] Chao, S.H., Naaman, A.E., Parra-Montesinos, G.J., "Bond Behavior of Reinforcing Bars in Tensile Strain-Hardening Fiber-Reinforced Cement Composites," *ACI Structural Journal,* vol. 106, no. 6, pp. 897-906, 2009.

[63] Holschemacher, K., Klotz, S., Weisse, D., "Bond of Reinforcement in Ultra High Strength Concrete," Seventh International Symposium on Utilization of High Strength/ High Performance Concrete, pp.513-528, 2005.

[64] Holschemacher, K., Klotz, S., Weisse, D., "Bond of Reinforcement in Ultra High Strength Concrete," Proceedings of the International Symposium on Ultra High Performance Concrete, Kassel, Germany, 2004, 2004.

[65] Jungworth, J., Muttoni, A., "Structural Behavior of Tension Memebers in UHPC," Proceedings of the International Symposium on Ultra High Performance Concrete, Kassel, Germany, 2004.

[66] Azizinamini, A., Chisala, M., Ghosh, S.K., "Tension Development Length of Reinforcing Bars Embedded in High-Strength Concrete," *Engineering Structures,* vol. 17, no. 7, pp. 512-522, 1995.

[67] RILEM, "Technical Recommendations for the Testing and Use of Construction Materials: RC 6, Bond Test for Reinforcement Steel, 2. Pull-out Test," 1970.

[68] Holschemacher, K., Weisse, D., "Bond of Reinforcement in Fibre Reinforced Concrete," Sixth RILEM Symposium on Fibre-Reinforced Concretes (FRC), Varenna, Italy, pp.349-358, 2004.

[69] Schumacher, P., Walraven, J.C., den Uijl, J.A., "Rotation Capacity of Self-Compacting Steel Fibre Reinforced Concrete Beams," in *Heron*, Vol.52, No.2/3, Delft University of Technology, Netherlands.

[70] Leutbecher, T, "Rissbildung und Zugtragverhalten von mit Stabstahl und Fasern bewehrtem Ultrahochfesten Beton (UHPC)," Doctoral Thesis, University of Kassel, 2007.

[71] Arup, B., Karlsen, J., Lindstrom, G., "Fiber Reinforced High Performance Concrete for in-situ Cast Joints," International Symposium on High Performance Concrete, Orlando, Florida, pp.379-387, 2000.

[72] Reineck, K., Greiner, S., "Tests on Ultra-High Performance Fibre Reinforced Concrete Designing Hot-Water Tanks and UHPFRC-Shells," Proceedings of the International Symposium on Ultra High Performance Concrete, Kassel, Germany, 2004.

[73] Yoo, D., Shin, H., Yang, J., Yoon, Y., "Material and Bond Properties of Ultra High Performance Fiber Reinforced Concree with Micro Steel Fibers," *Composites: Part B,* vol. 58, pp. 122-133, 2014.

[74] Bigaj-van Vliet, A.J., "Bond of Deformed Reinforcing Steel Bars Embedded in Steel Fiber Reinforced Concrete - State-of-the-art Report," Delft Cluster, 2001.

[75] Cheung, A.K.F., Leung, C.K.Y., "Effective Joining of Pre-cast Concrete Slabs with Self-compacting HSFRCC," *Journal of Advanced Concrete Technology,* vol. 9, no. 1, pp. 41-49, 2011.

[76] Fehling, E., Lorenz, P., Leutbecher, T. , "Experimental Investigations on Anchorage of Rebars in UHPC," International Symposium on UHPC and Nanotechnology for High Performance Construction Materials, Kassel, Germany, pp.533-540, 2012.

[77] Saleem, M., Mirmiran, A., Xia, J., Mackie, K, "Development Length of High-Strength Steel Rebar in Ultrahigh Performance Concrete," *Journal of Materials in Civil Engineering,* vol. 25, pp. 991-998, 2013.

[78] Sigrist, V., Rauch, M., "Deformation Behavior of Reinforced UHPFRC Elements in Tension," *Taylor Made Concrete Structures,* 2008.

[79] Redaelli, D., "Testing of Reinforced High Performance Fibre Concrete Members in Tension," in *6th International PhD Symposium in Civil Engineering*, Zurich, 2006.

[80] Redaelli, D., "Comportement et modelisation des elements de structure en Beton Fibre a Ultra-Hautes Performances avec armatures passives," PhD Thesis, Swiss Federal Institure of Technology in Laussane, 2009.

[81] Leutbecher, T., Fehling, E.,, "Crack Formation and Tensile Behaviour of UHPC Reinforced with a Combination of Rebars and Fibres," in *Proceedings of the International Symposium on Ultra High Performance Concrete*, Kassel, Germany, 2008.

[82] Kuneida, M., Hussein, M., Ueda, N., Nakamura, H., "Enhancement of Crack Distribution of UHPC-SHCC under Axial Tension Using Steel Reinforcement," *Journal of Advanced Concrete Technology,* vol. 8, pp. 49-57, 2010.

[83] Moreno, D.M., Tono, W., Jen, G., Ostertag, C., Billington, S.L., "Tension Stiffening in Reinforced High Performance Fiber Reinforced Cement-Based Composites under Direct Tension," *High Performance Fiber Reinforced Composites 6 RILEM State of the Art Reports,* vol. 2, pp. 263-270, 2012.

[84] Trono, W., Jen, G., Moreno, D., Billington, S., Ostertage, C.P., "Confinement and Tesnion Stiffening Effects in High Performance Self-Consolidated Hybrid Fiber Reinforced Concrete Composites," *High Performance Fiber Reinforced Cement Composites 6; HPFRC 6,* vol. 2, pp. 255-262, 2012.

[85] Larusson, L., Fishcer, G., Jonsson, J., "Mechanical Interaction between Concrete and Structural Reinforcement in Tension Stiffening Process," *High Performance Fiber Reinforced Cement Composites 6; HPFRCC6,* pp. 247-254, 2012.

[86] Larusson, L.H., Fishcer, G., "Bond Slip and Crack Development in FRC and Regular Concrete Specimens Longitudinally Reinfroced with FRP or Steel under Tension Loading," in *Proceedings of Bond in Concrete 2012: Bond, Anchorage,*

Detailing, Fourth International Symposium, Brescia, Italy, 2012.

[87] Deluce, J., S-C., Lee., Vecchio, F.J, "Crack Formation in FRC Structural Elements Containing Conventional Reinforcement," *High Performance Fiber Reinforced Cement Composites 6; HPFRCC 6,* pp. 271-278, 2012.

[88] Yun, H.D., Kim, S.W., Jeon, E., Park, W.S., Fukuyama, H., "Tension Stiffening and Damage Tolerance of Strain-Hardening Cement Composite (SHCC) Tension Ties Under Monotonic and Repeated Cyclic Loadings," in *The 14th World Conference on Earthquake Engineering*, Beijing, China, 2008.

[89] Leutbecher, T., Fehling, E., "Structural Behavior of UHPC under Tensile Stress and Biaxial Loading," Proceedings of the Internation Symposium on Ultra High Performance Concrete, Kassel, Germany, 2004.

[90] Sturwlad, S., Fehling, E., "Design of Reinforced UHPFRC in Flexure," Proceedings of the Hipermat 2012 3rd International Symposium on UHPC and Nanotechnology for High Performance Construction Materials, Kassel, Germany, 2012.

[91] Yuguang, Y., Walraven, J.C., den Uijl, J.A., "Combined Effect of Fibers and Steel Rebars in High Performance Concrete," in *Heron*, Vol.54,No2/3, Delf University of Technology, Netherlands, 2009.

[92] Fantilli, A.P., Mihashi, H., Vallini, P., "Strain Compatability Between HPFRCC and Steel Reinforcement," *Materials and Structures,* vol. 38, pp. 495-503, 2005.

[93] Leutbecher, T., Fehling, E., "Design for Serviceability of Ultra High Performance Concrete Structures," *High Performance Fiber Reinforced Cement Composites 6: RILEM State of the Art Reports,* vol. 2, pp. 445-452, 2012.

[94] Redaelli, D., Muttoni, A, "Tensile Behaviour of Reinforced Ultra-High Performance Fiber Reinforced Concrete Elements," in *Symposium Dubrovnik Concrete Structures: Stimulators of Development*, Dubrovnik, Croatia, 2007.

[95] Rauch, M., Sigrist, V., "Dimensioning of Structures made of UHPFRC," in *34th International Symposium on Bridge and Structural Engineering*, Venice, Italy, 2010.

[96] Fischer, G., Li, V.C., "Effect of Fiber Reinforcement on the Response of Structural Members," *Engineering Fracture Mechanics,* vol. 74, no. 1-2, pp. 258-272, January 2007.

[97] Shionaga, R, "Structural Behavior of High Performance Fiber Reinforced Concrete in Tension and Bending," in *6th International PhD Symposium in Civil Engineering*, Zurich, 2006.

[98] Otsuka, K., Mihashi, H., Kiyota, M., Mori, S., Kawamata, A., "Observation of Multiple Cracking in Hybrid FRCC at Micro and Meso Levels," *Journal of Advanced Concrete Technology,* vol. 1, pp. 291-298, 2003.

[99] ASTM A615/A615M-13, "Standard Specification for Deformed and Plain Carbon-Steel Bars for Concrete Reinforcement," *ASTM Book of Standards Volume 01.4,* ASTM International, West Conshohoken, PA, 2013.

[100] ASTM A1035/A1035M-13b, "Standard Specification for Deformed and Plain Carbon-Steel Bars for Concrete Reinforcement," *ASTM Book of Standards Volume*

01.04, ASTM International, West Conshocken, PA, 2013.

[101] Seliem, H., Hosny, A., Rizkalla, S., Zia, P., Briggs, M., Miller, S., Darwin, D., Browning, A., Glass, G., Hoyt, K., Donnelly, K., Jirsa, J, "Bond Characteristics of ASTM A1035 Steel Reinforcing Bars," *ACI Structural Journal,* vol. 106, no. 4, pp. 530-539, 2009.

[102] Way, Richard, "Material Characterization of Ultra-High Performance Fiber Reinforced Concrete at Elevated Temperatures," Master's Thesis, University of Connecticut, 2013.

[103] Graybeal, B, "Material Property Characterization of Ultra-High Performance Concrete," FHWA-HRT-06-103, 2006.

[104] ASTM A370-13, "Standard Test Methods and Definitions for Mechanical Testing of Steel Products," *ASTM Book of Standards Volume 01.03,* ASTM International, West Conshohocken, PA, 2013.

7 APPENDIX A: ADDITIONAL PHASE I FIGURES

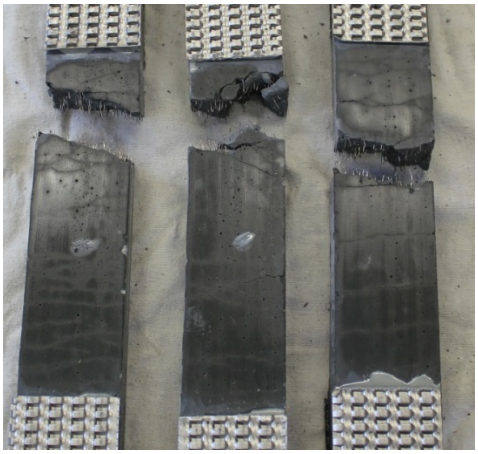

Figure 7-1: UHPC1_1%_Par (S1,S2,S3)

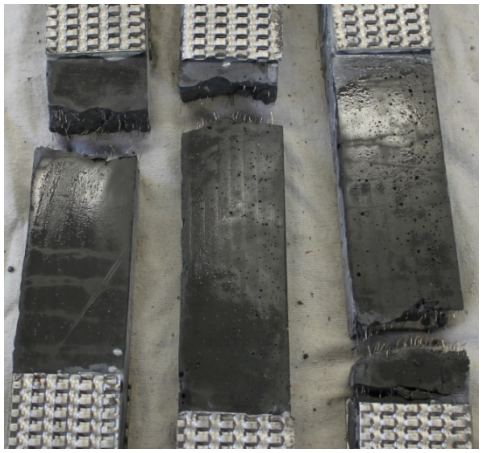

Figure 7-2: UHPC1_1%_End (S1,S2,S3)

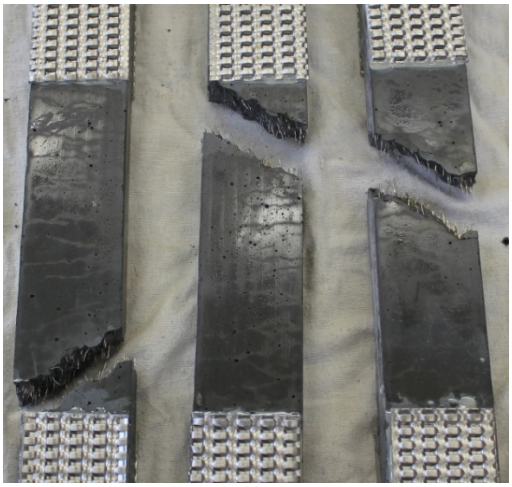

Figure 7-3: UHPC1_2%_Mid (S1,S2,S3)

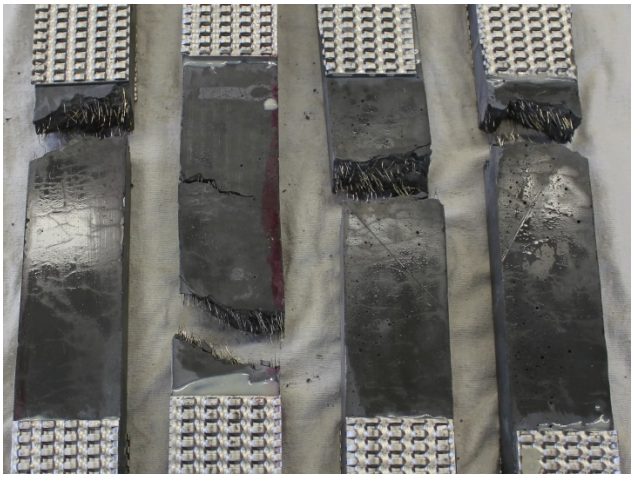

Figure 7-4: Ductal_2%_End_1_2_3

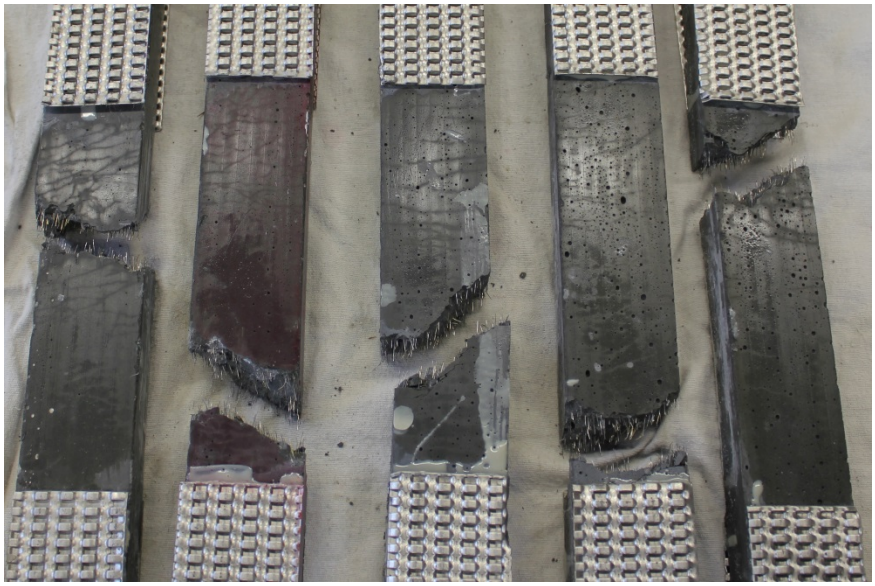

Figure 7-5: Ductal_2%_Par_1_2_4_5_6

Figure 7-6: Ductal_3%_Par_2

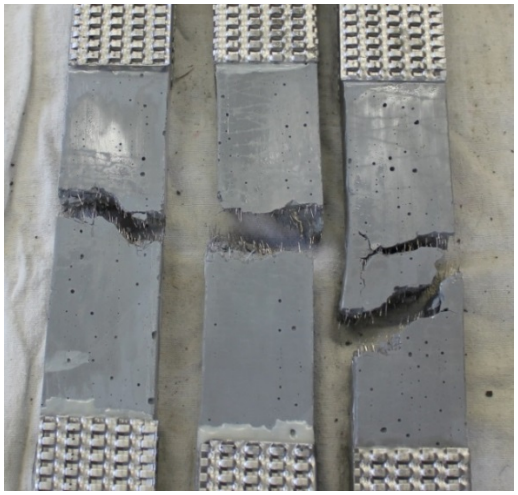

Figure 7-7: House_2%_Par_1_2_3

8 APPENDIX B: ADDITIONAL PHASE II FIGURES

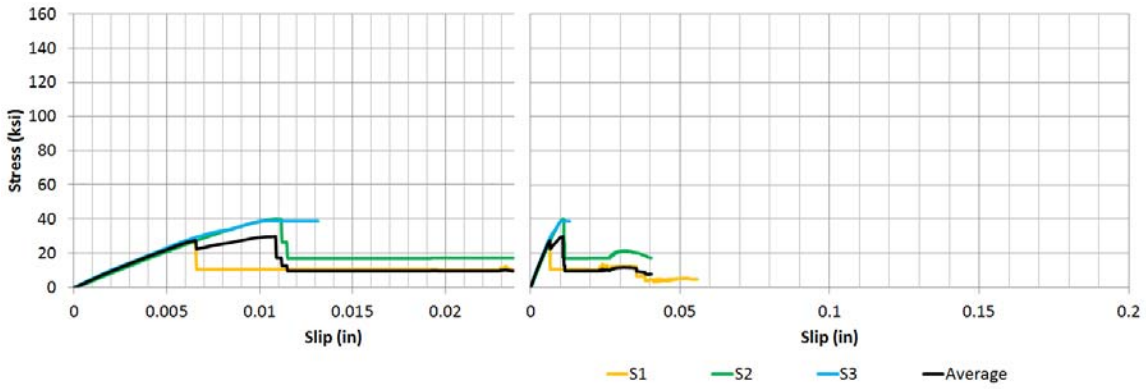

Figure 8-1: #3_0%_8db_rand_1035_UHPC1

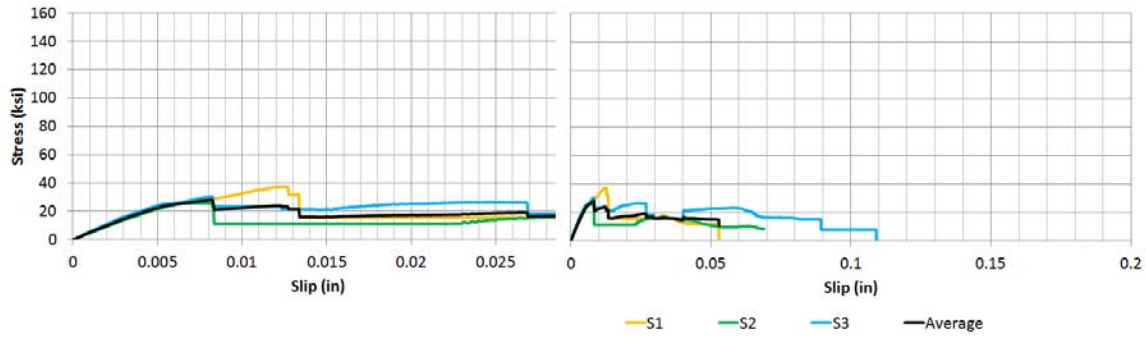

Figure 8-2: #3_0%_12db_rand_1035_UHPC1

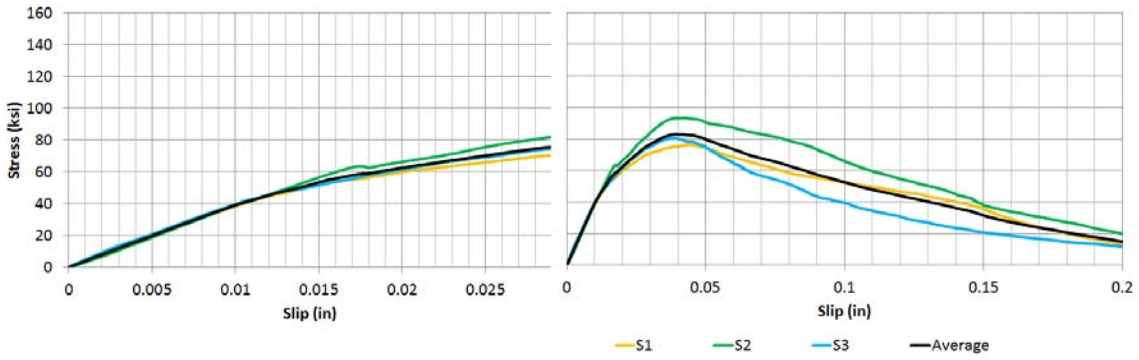

Figure 8-3: #3_1%_8db_rand_1035_UHPC1

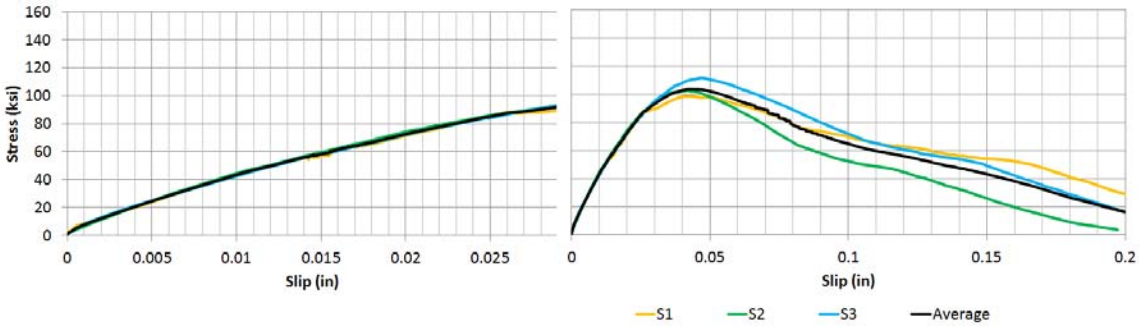

Figure 8-4: #3_1%_12db_rand_1035_UHPC1

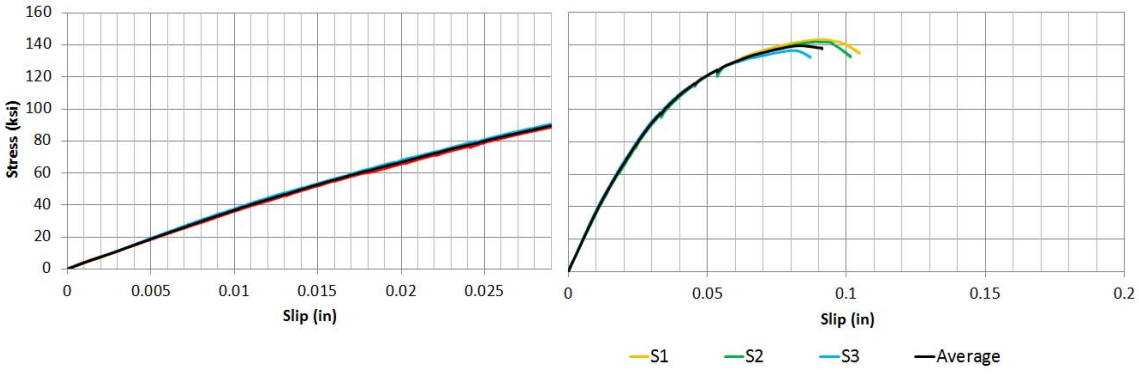

Figure 8-5: #3_1%_16db_rand_1035_UHPC1

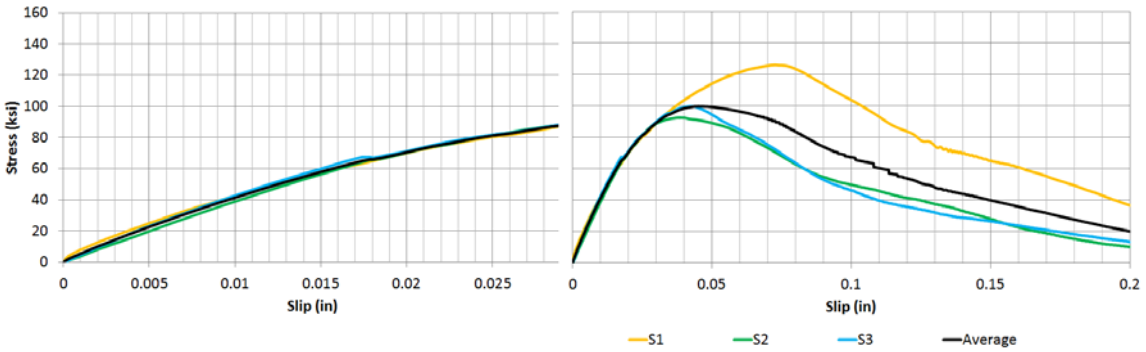

Figure 8-6: #3_2%_8db_rand_1035_UHPC1

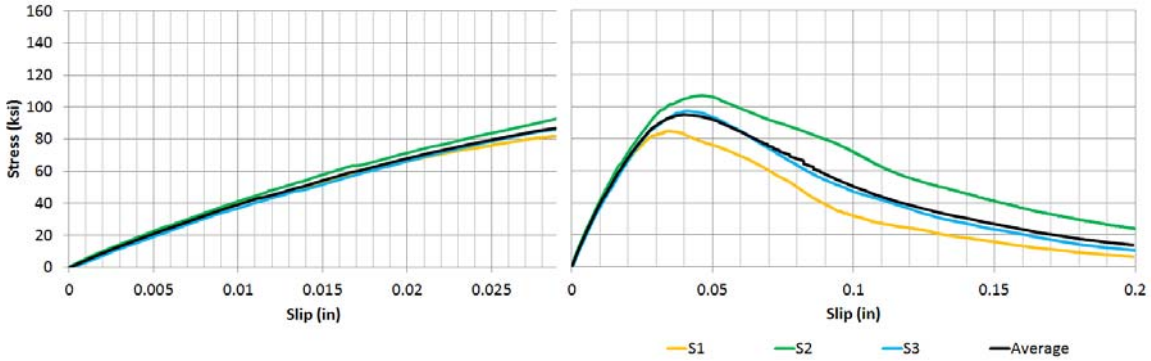

Figure 8-7: #3_2%_8db_rand_1035_UHPC2

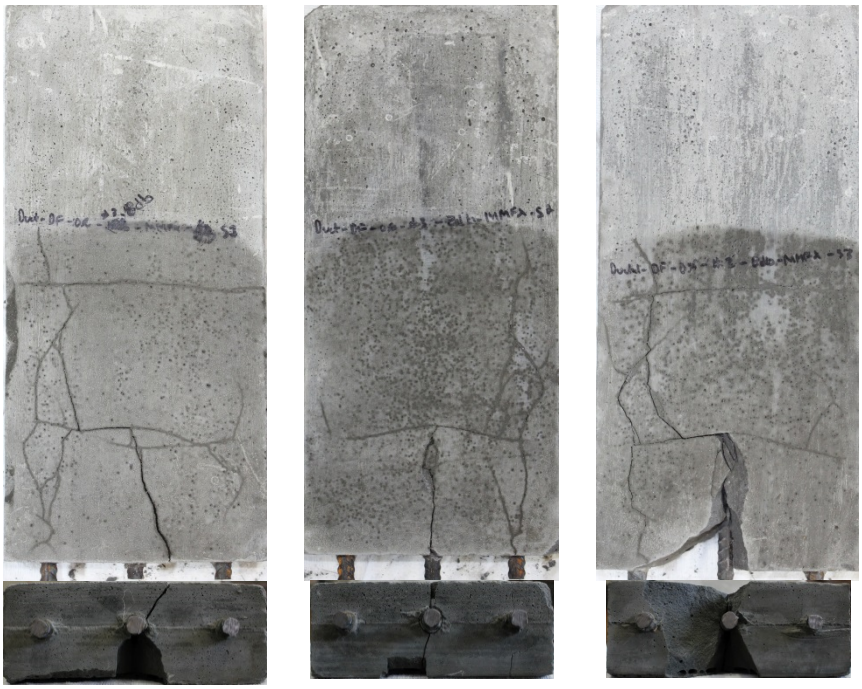

S1 S2 S3

Figure 8-8: #3_2%_8db_rand_1035_UHPC1

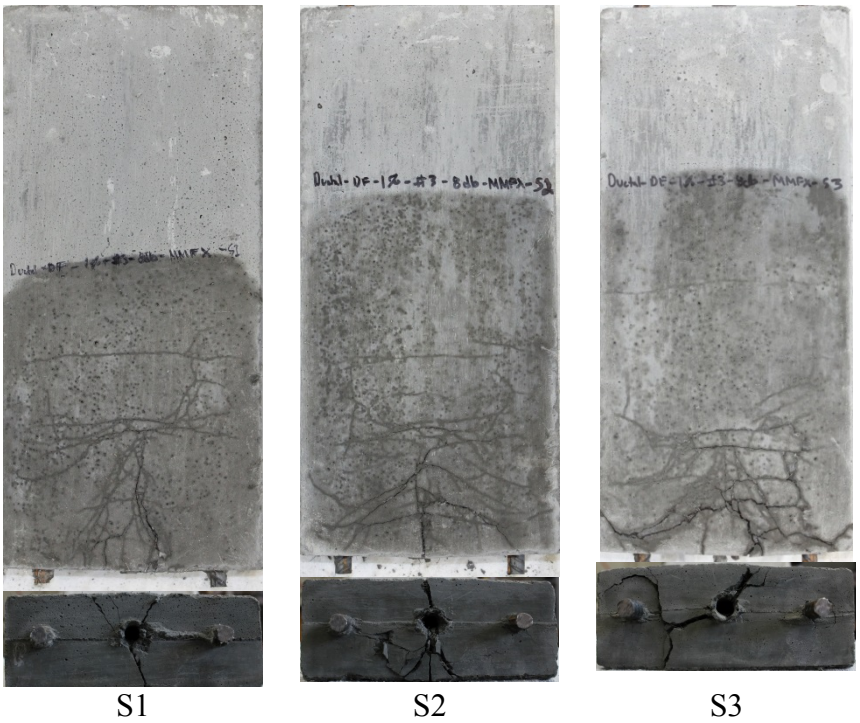

S1 S2 S3

Figure 8-9: #3_1%_8db_rand_1035_UHPC1

S1 S2 S3

Figure 8-10: #3_2%_8db_rand_1035_UHPC1

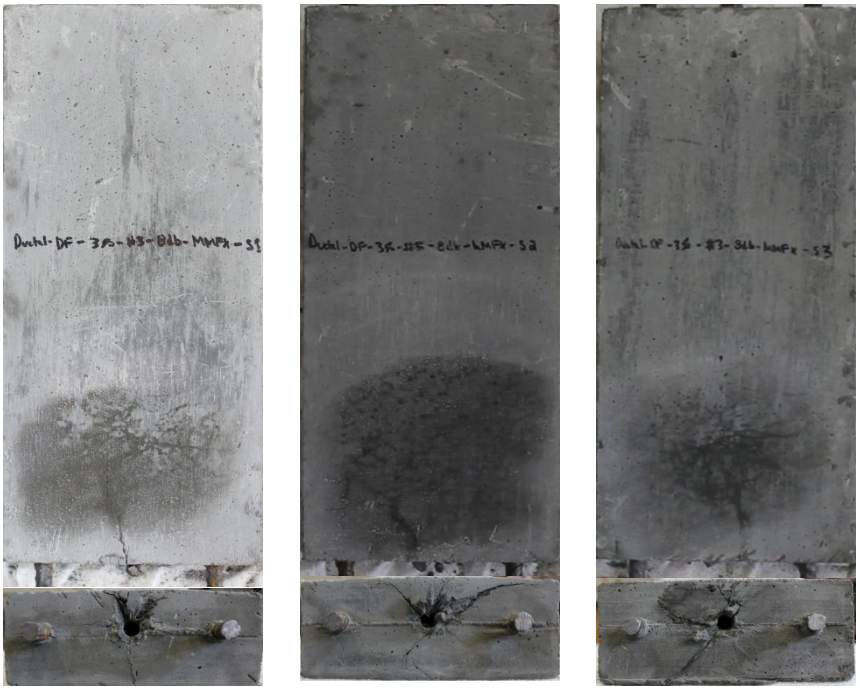

S1 S2 S3

Figure 8-11: #3_3%_8db_rand_1035_UHPC1

S1 S2 S3

Figure 8-12: #3_2%_8db_rand_1035_UHPC2

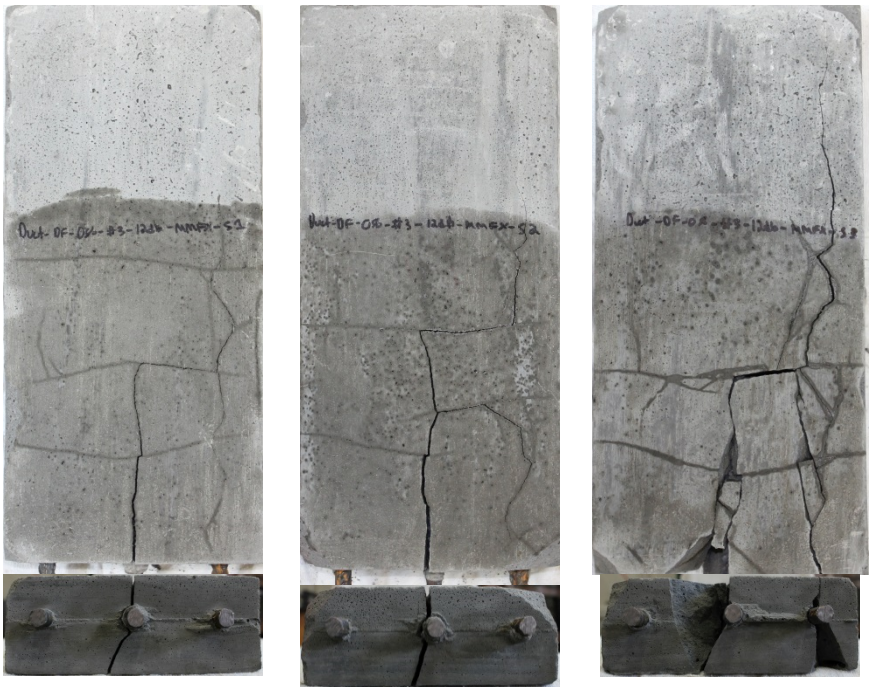

S1 S2 S3

Figure 8-13: #3_0%_12db_rand_1035_UHPC1

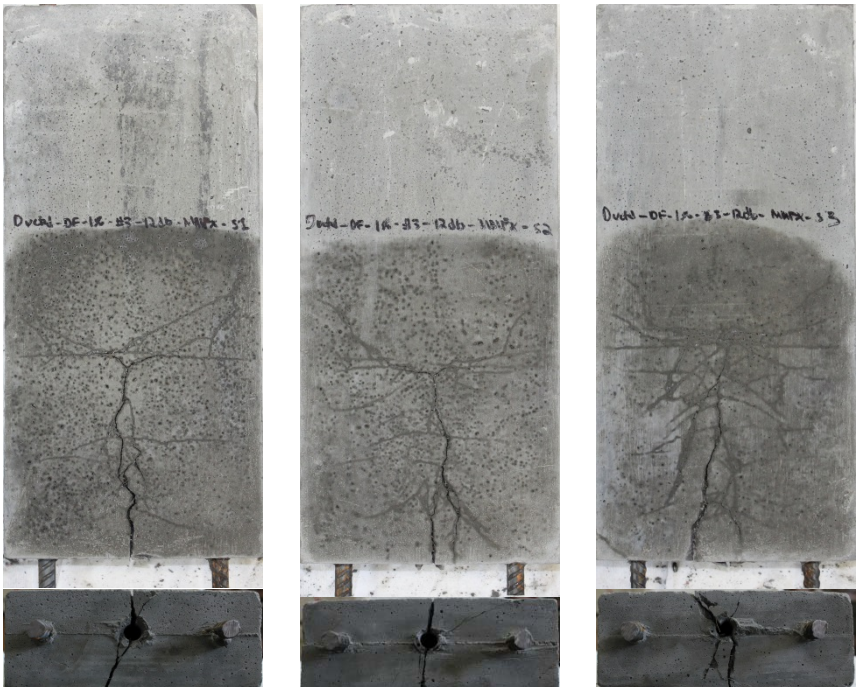

S1 S2 S3

Figure 8-14: #3_1%_12db_rand_1035_UHPC1

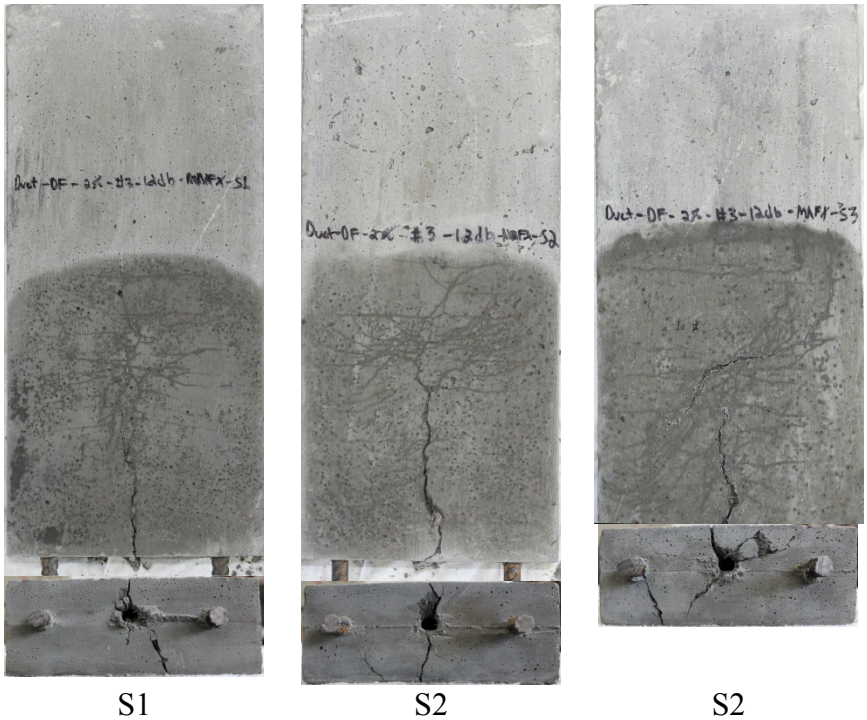

S1 S2 S2

Figure 8-15: #3_2%_12db_rand_1035_UHPC1

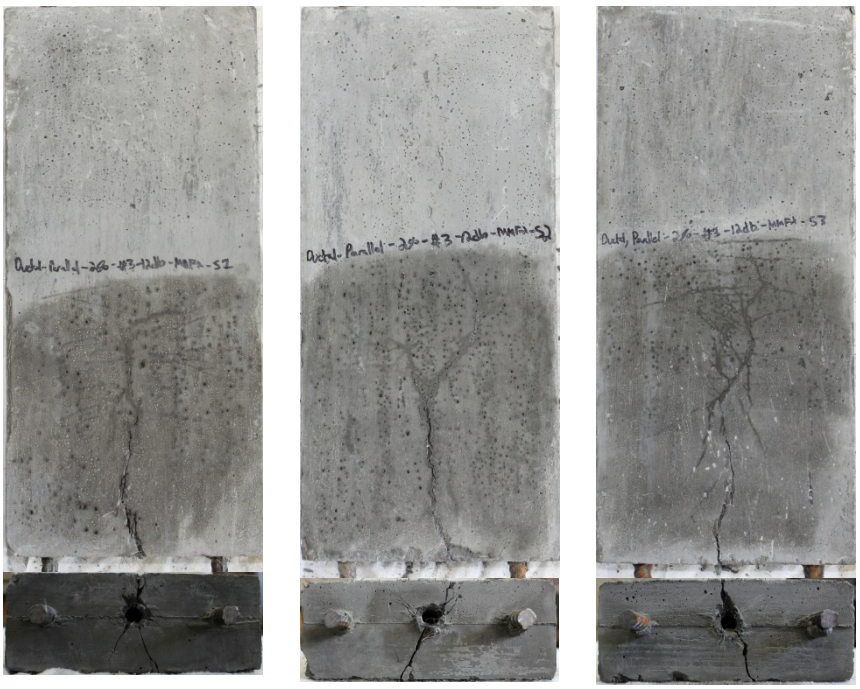

S1 S2 S3

Figure 8-16: #3_2%_12db_par_1035_UHPC1

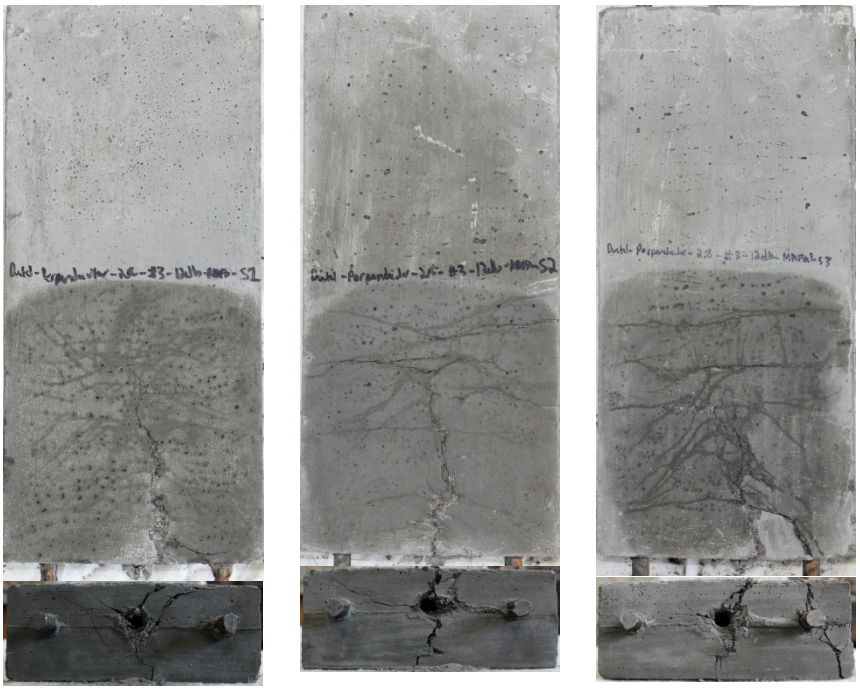

S1 S2 S3

Figure 8-17: #3_2%_12db_perp_1035_UHPC1

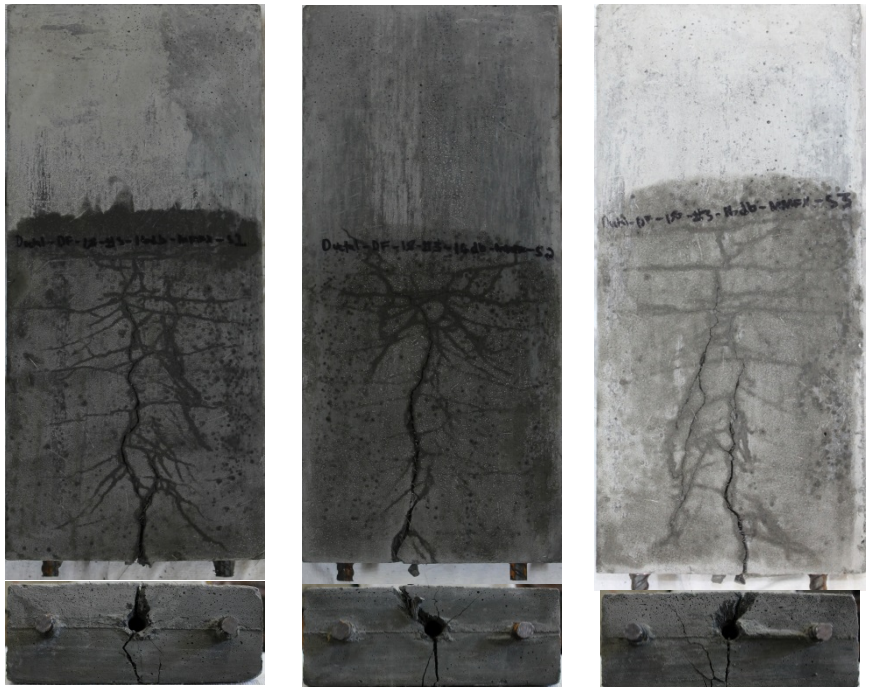

S1 S2 S3

Figure 8-18: Ductal_rand_1%_#3_16db_1035

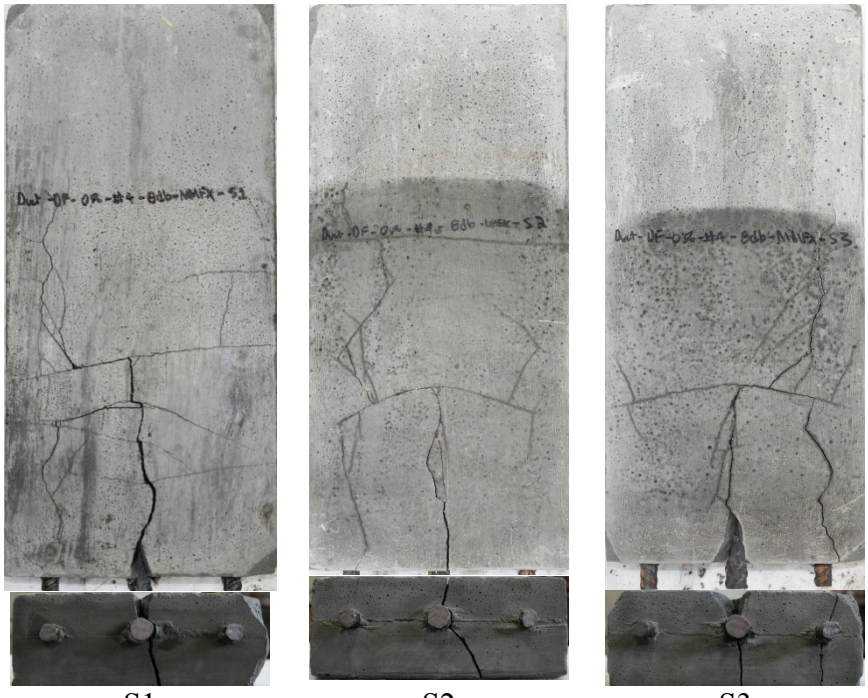

S1 S2 S3

Figure 8-19: Ductal_rand_0%_#4_8db_1035

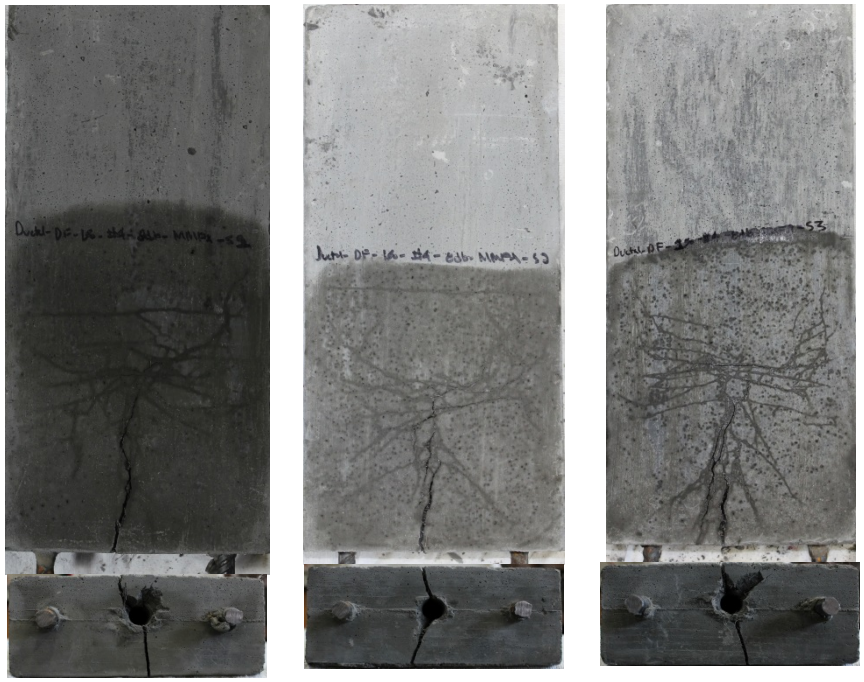

S1 S2 S3

Figure 8-20: Ductal_rand_1%_#4_8db_1035

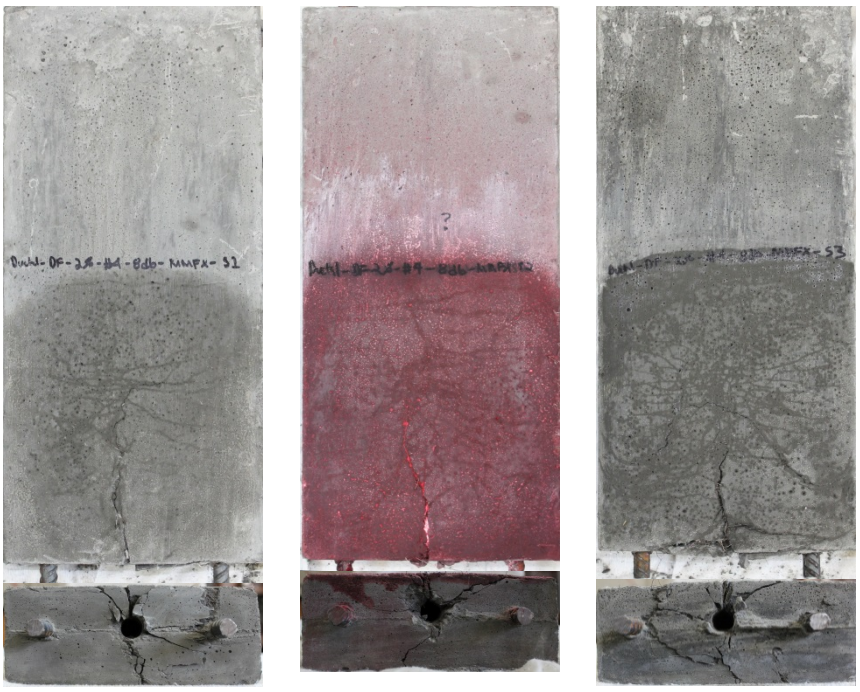

S1 S2 S3

Figure 8-21: Ductal_rand_2%_#4_8db_1035

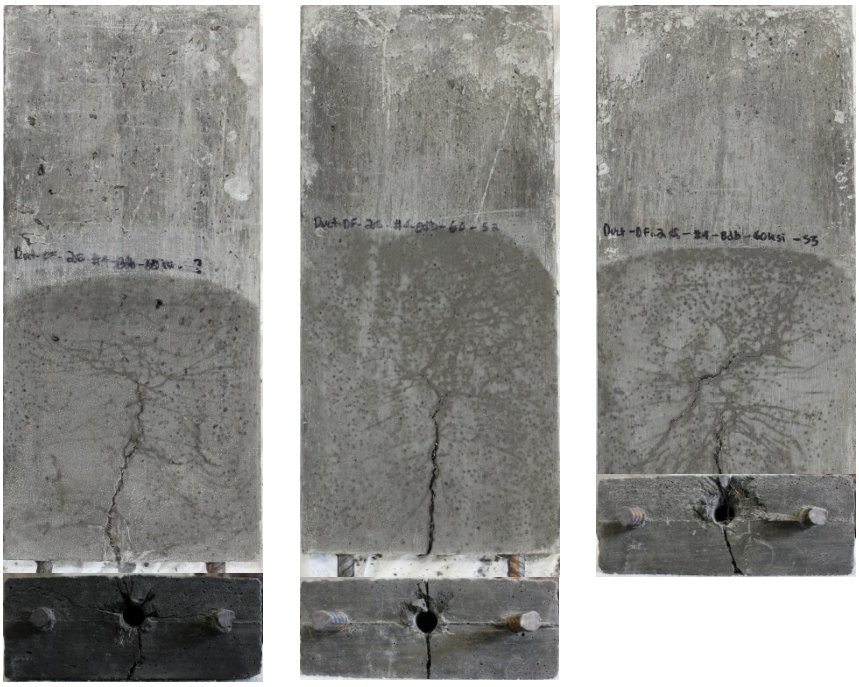

S1 S2 S3

Figure 8-22: Ductal_rand_2%_#4_8db_615

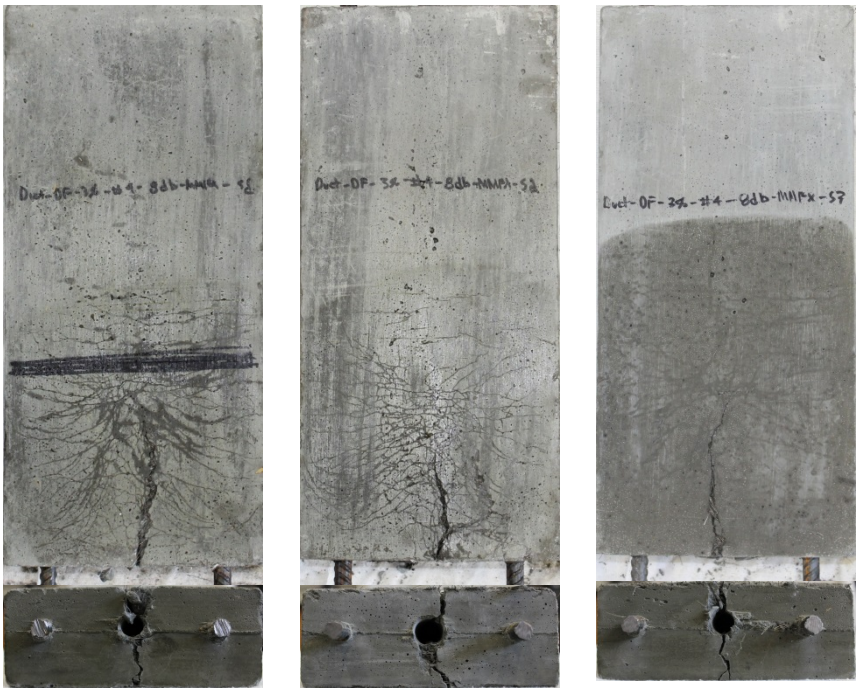

S1 S2 S3

Figure 8-23: Ductal_rand_3%_#4_8db_1035

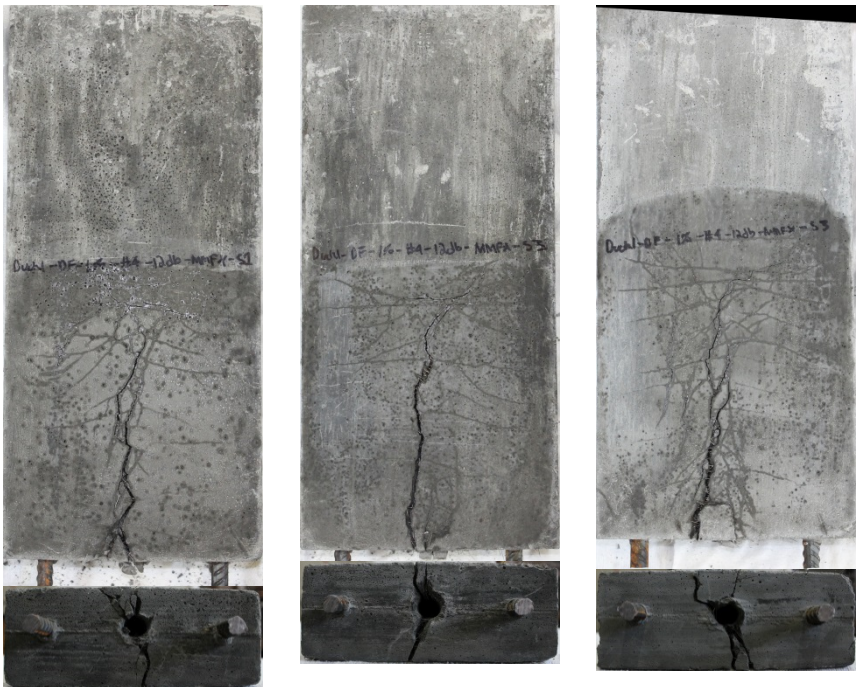

S1 S2 S3

Figure 8-24: Ductal_rand_1%_#4_12db_1035

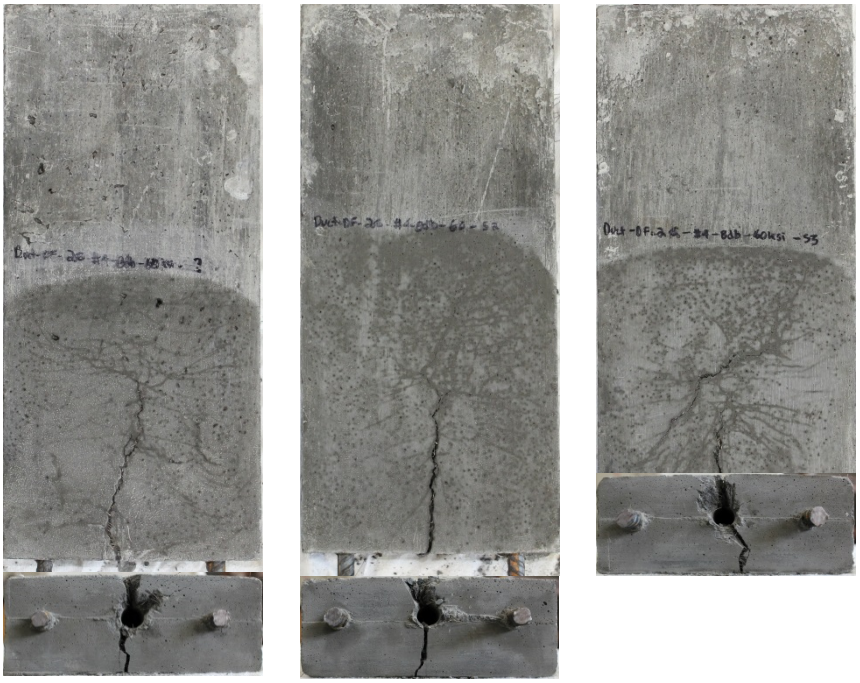

S1 S2 S3

Figure 8-25: Ductal_rand_2%_#4_12db_1035

S1

Figure 8-26: Ductal_Parallel_2%_#4_12db_1035

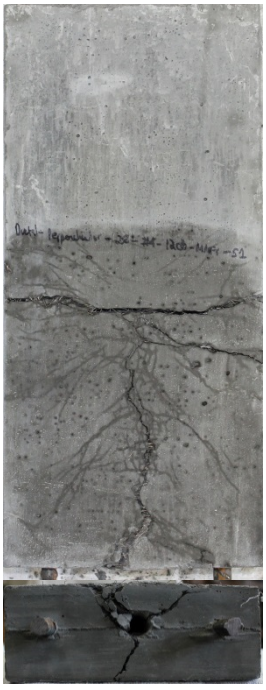

S1

Figure 8-27: Ductal_Perpendicular_2%_#4_12db_1035

S1 S2

Figure 8-28: Ductal_r and_3%_#3_12db_1035

9 APPENDIX C: ADDITIONAL PHASE III FIGURES

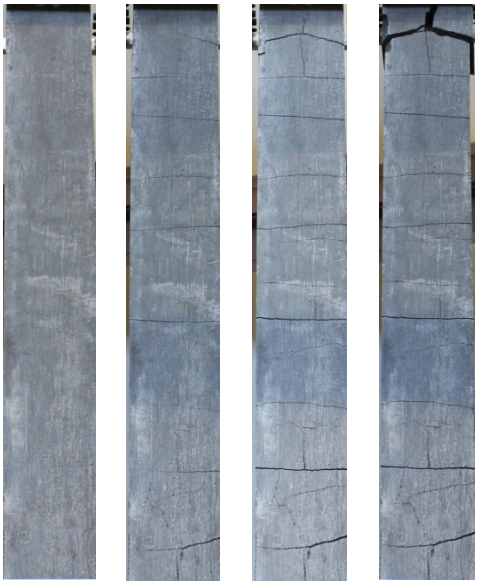

Figure 9-1: 615_0%Fiber_Parallel

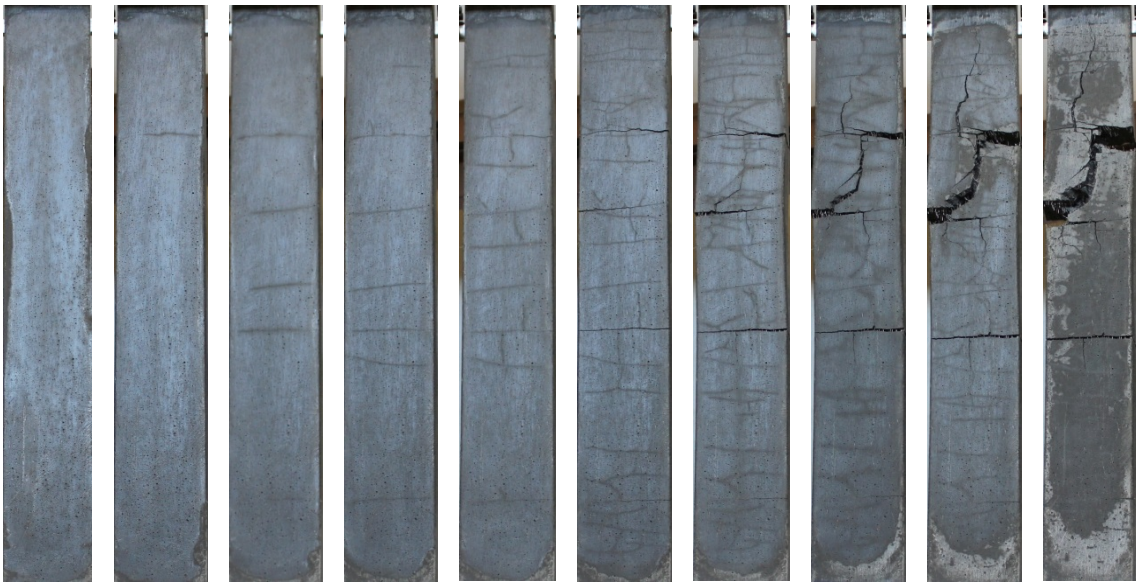

Figure 9-2: 615_0.5%Fiber_Parallel

Figure 9-3: 615_0.75%Fiber_Parallel

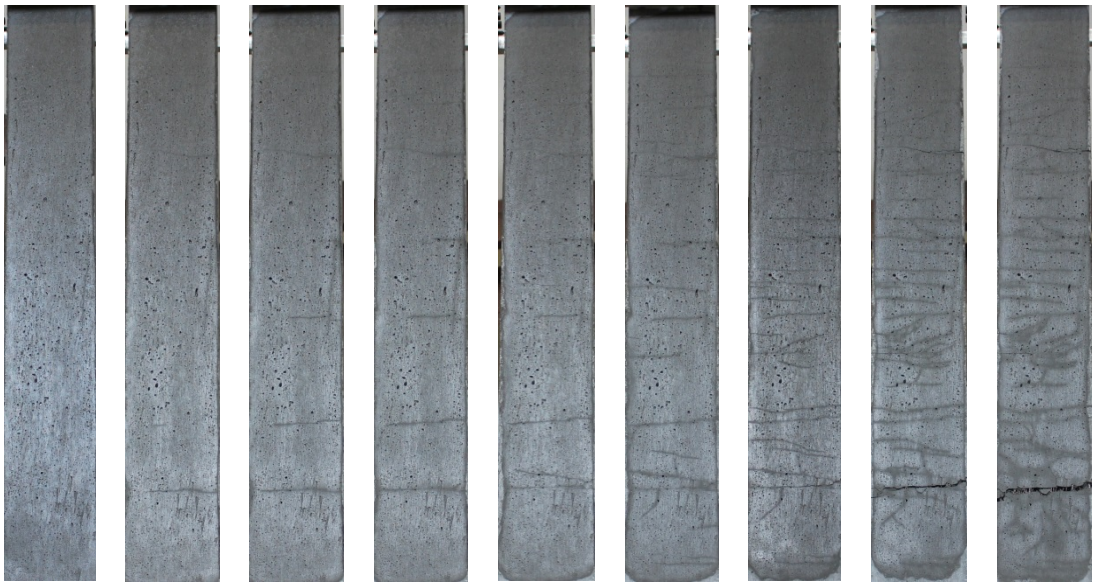

Figure 9-4: 615_0.75%Fiber_Parallel_S2

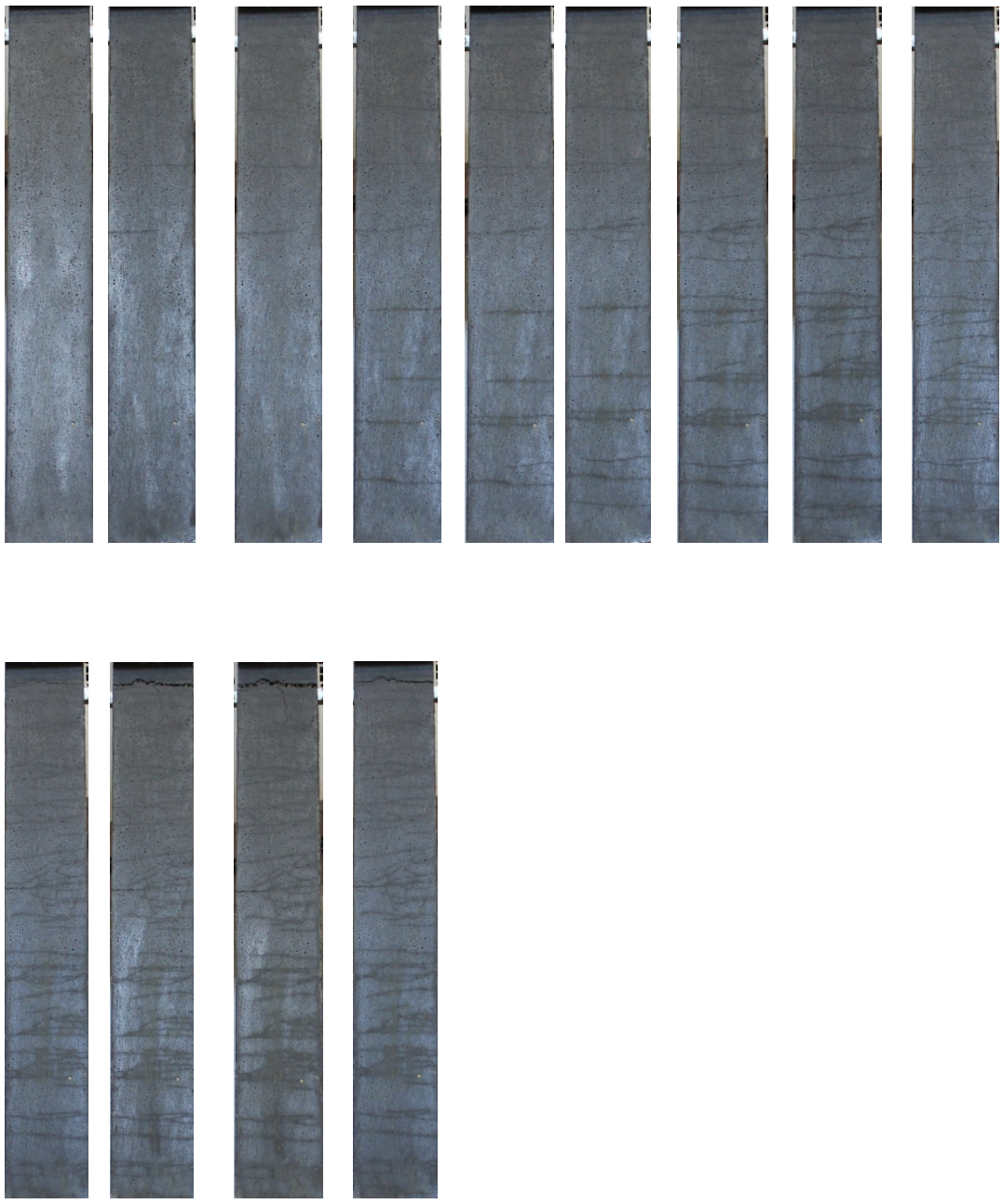

Figure 9-5: 615_1%Fiber_Parallel_S2

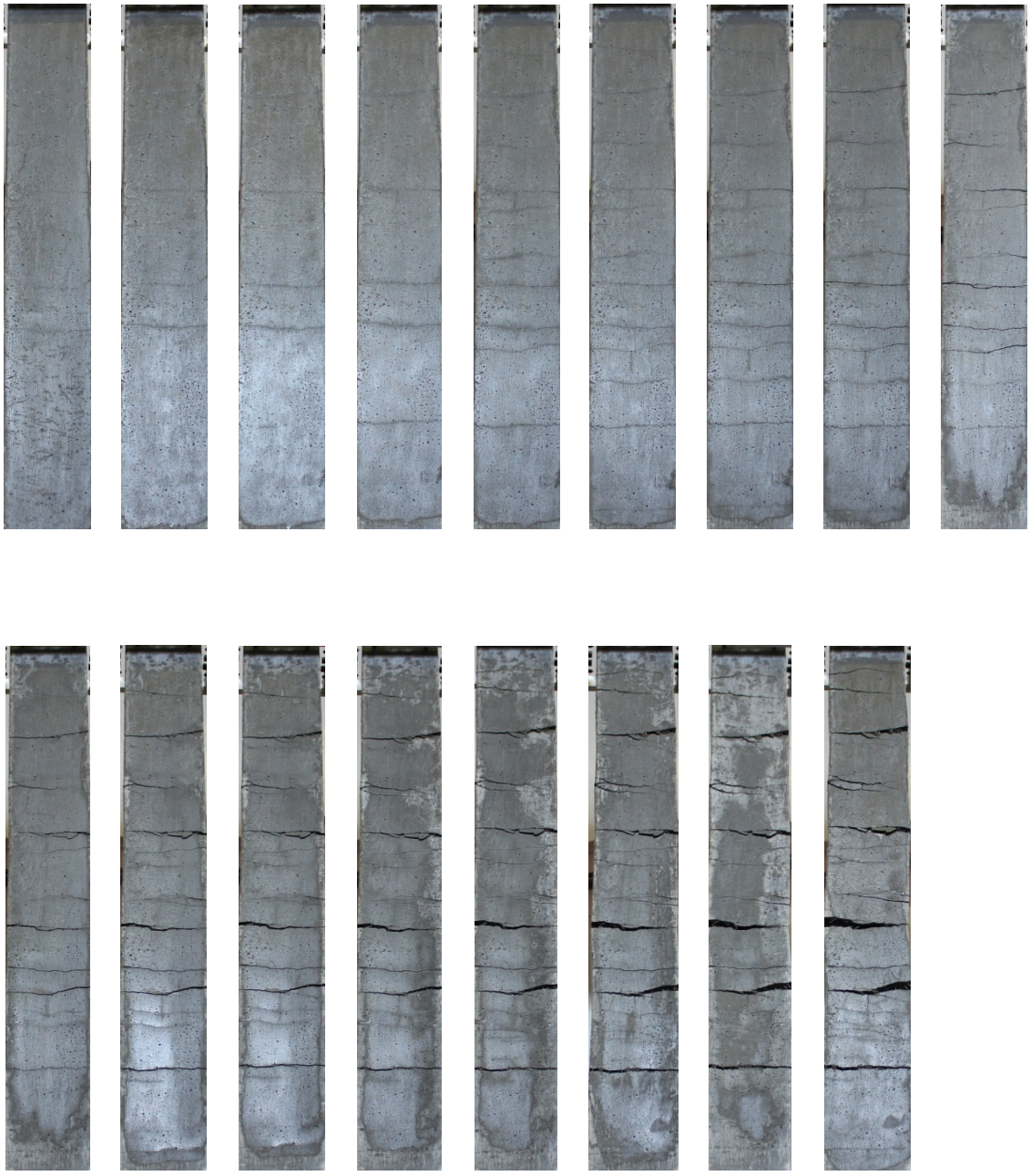

Figure 9-6: 615_1%Fiber_Perpendicular

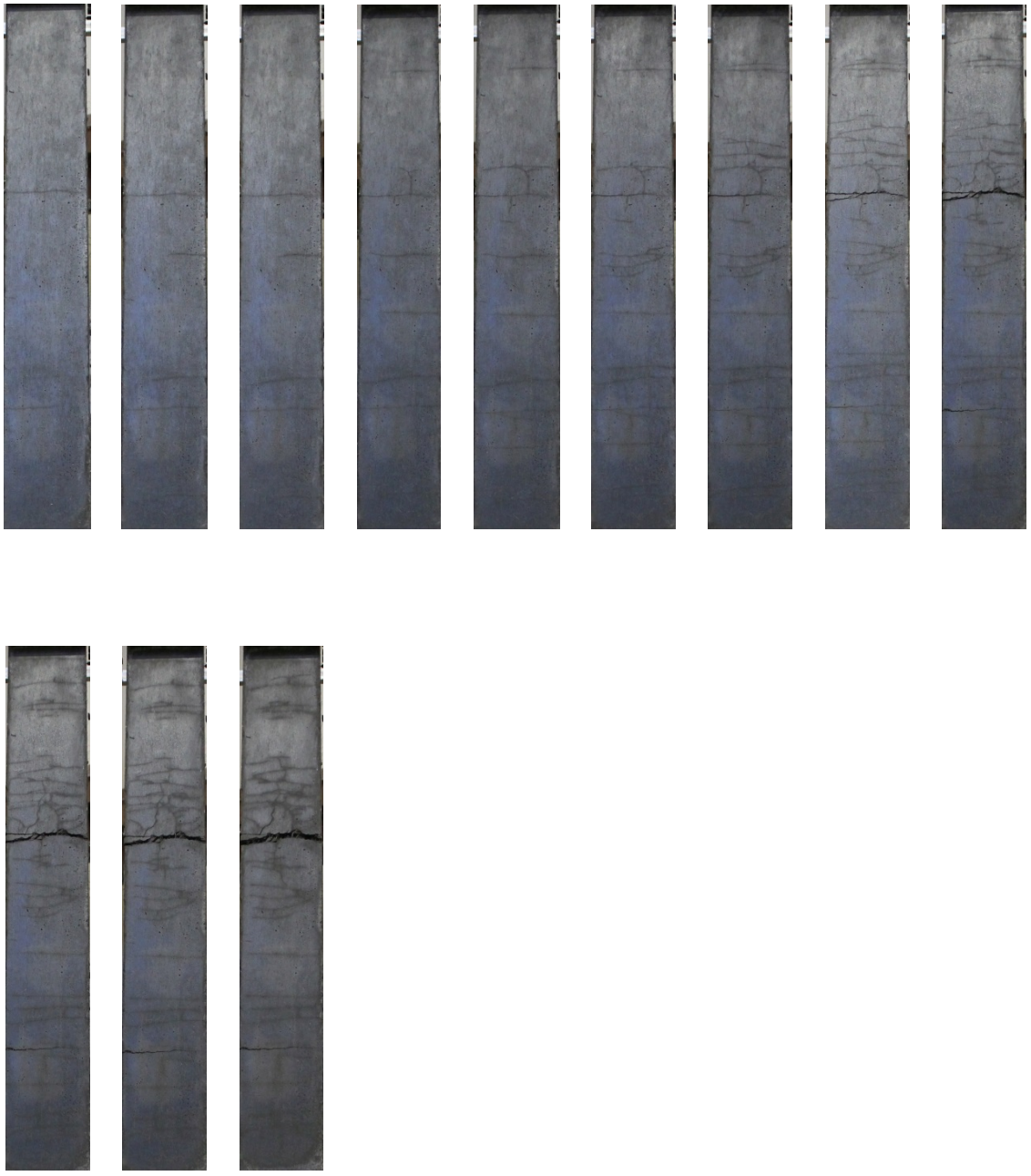

Figure 9-7: 615_1%Fiber_Random

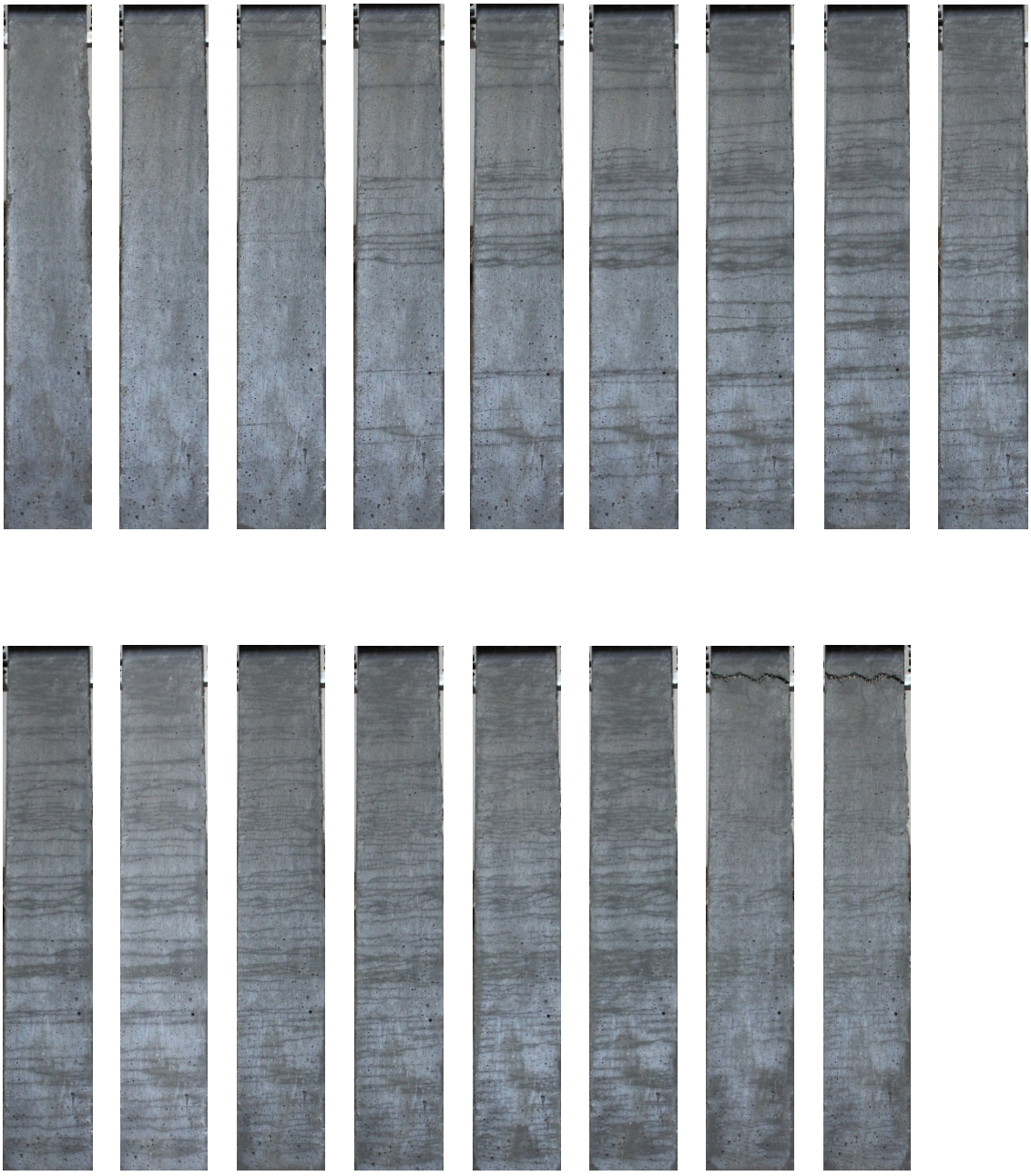

Figure 9-8: 615_2%Fiber_Parallel_S2

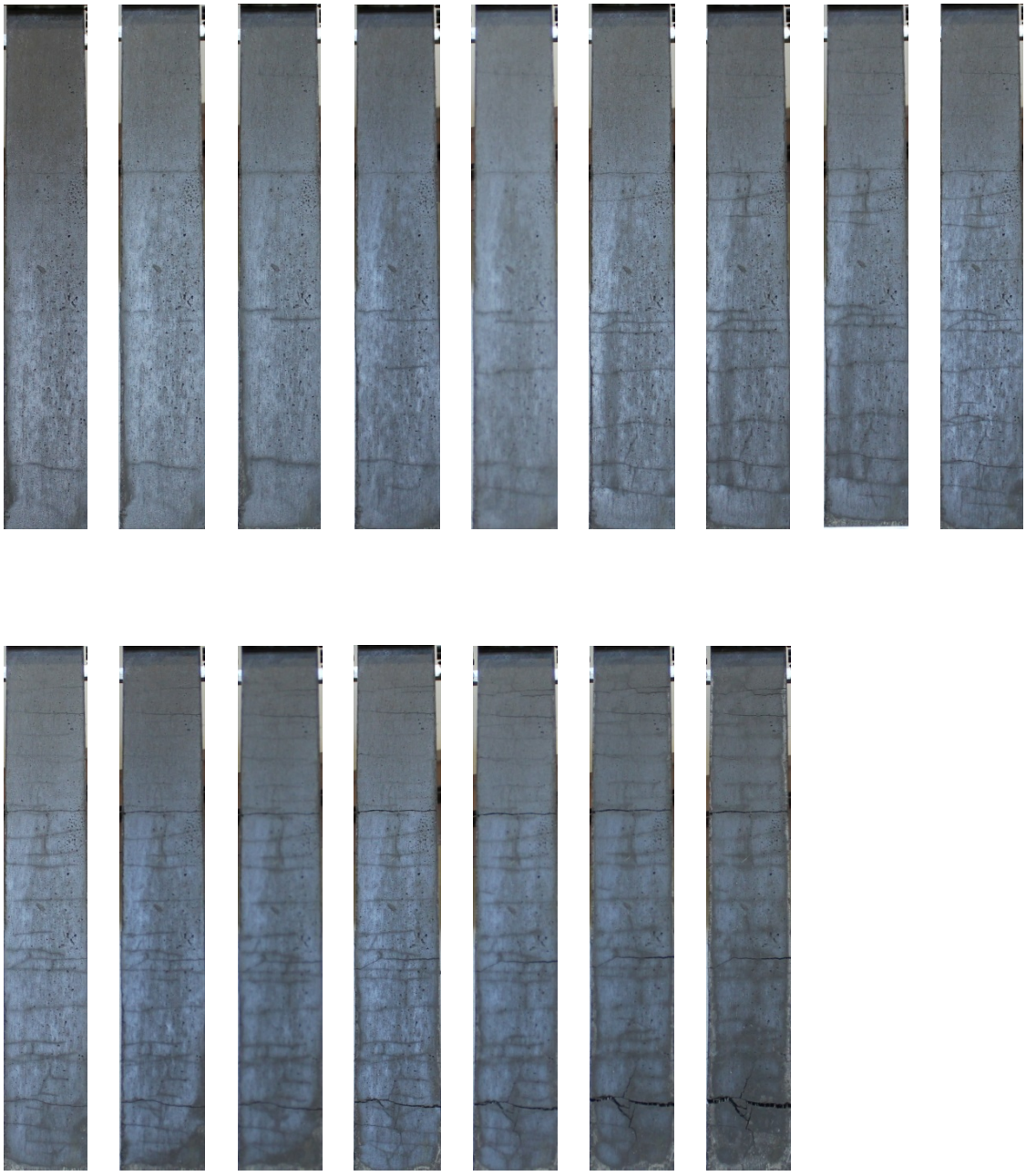

Figure 9-9: 1035_0.5%Fiber_Parallel_S2

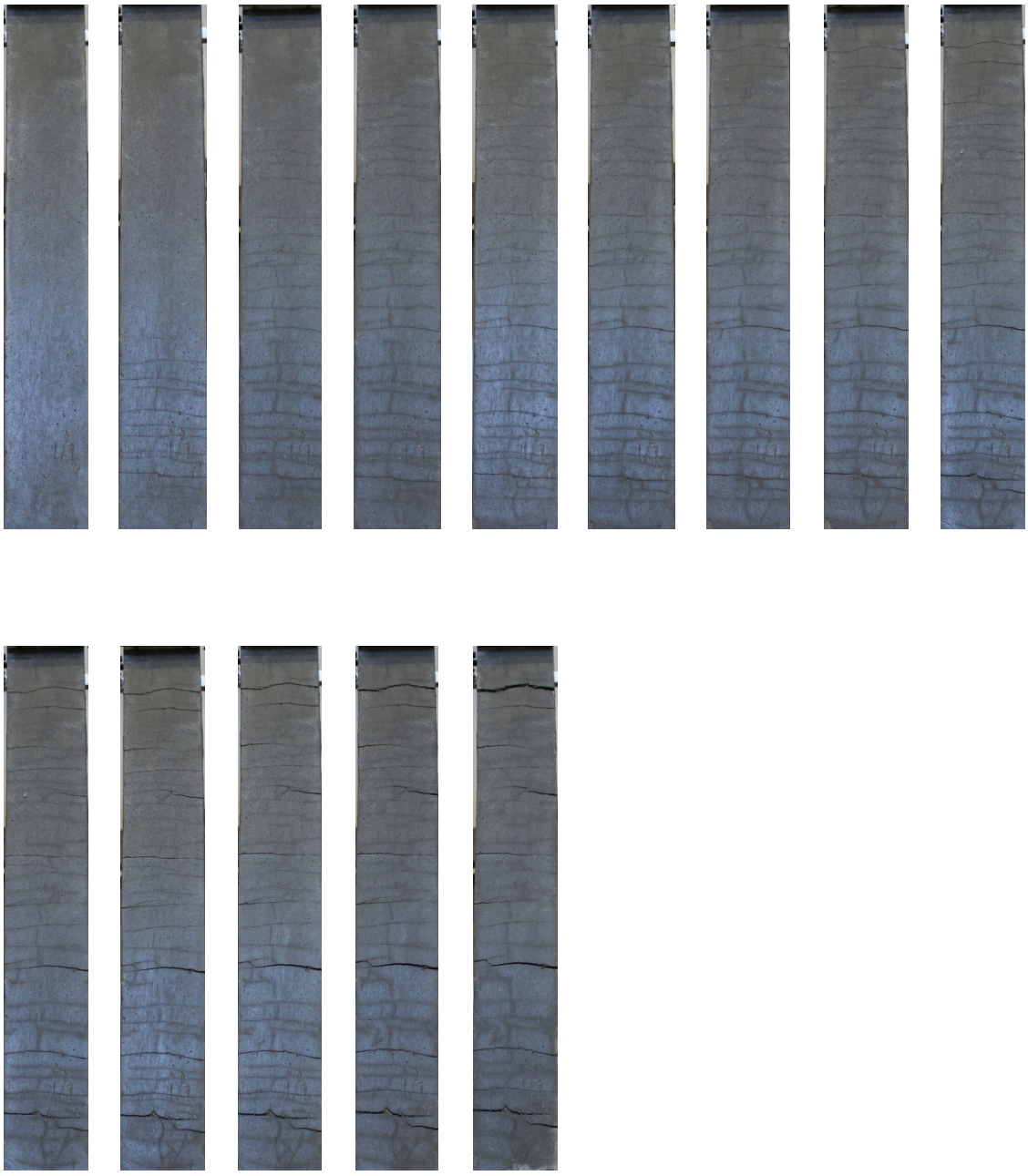

Figure 9-10: 1035_0.5%Fiber_Random

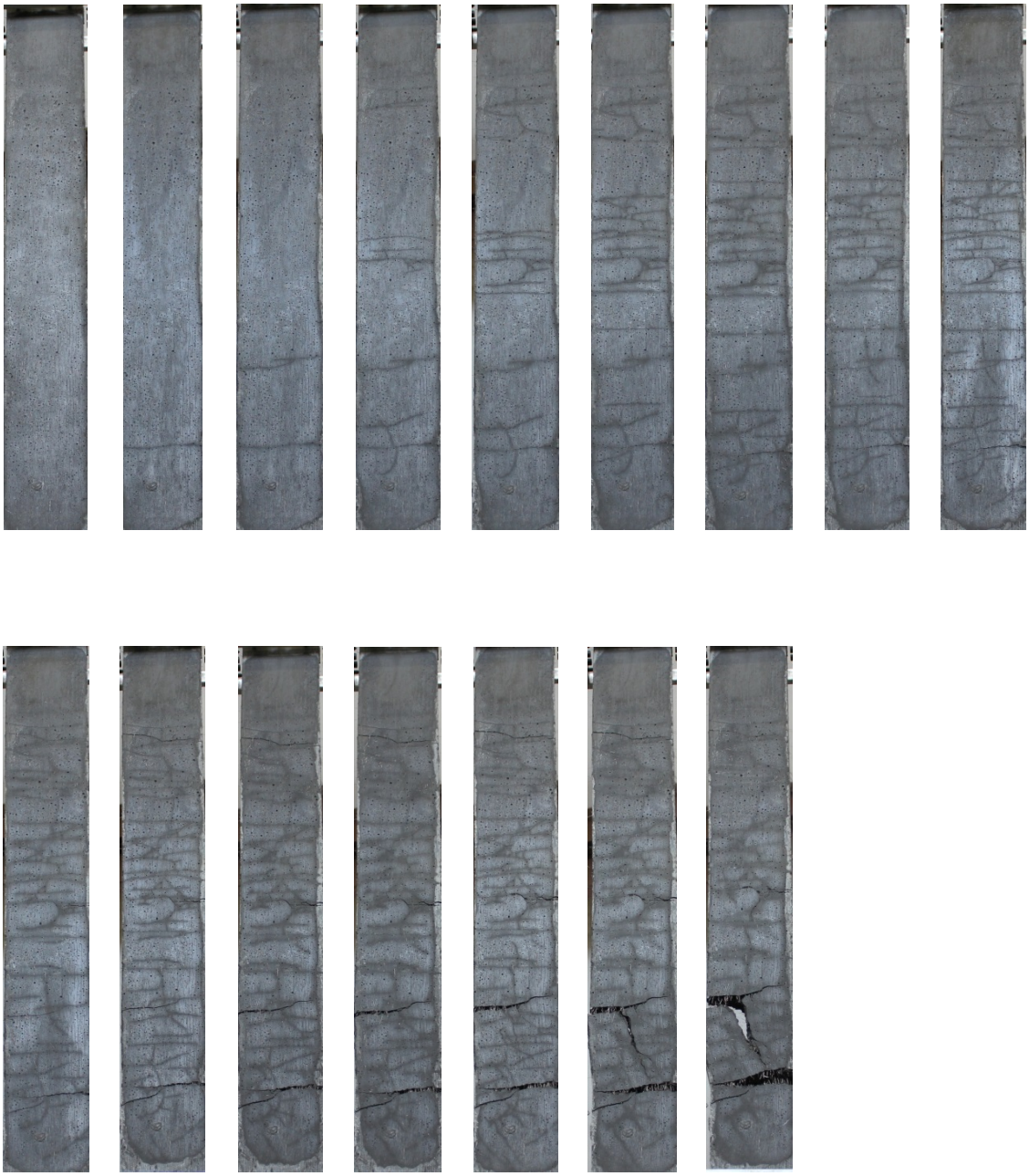

Figure 9-11: 1035_0.75%Fiber_Parallel_S2

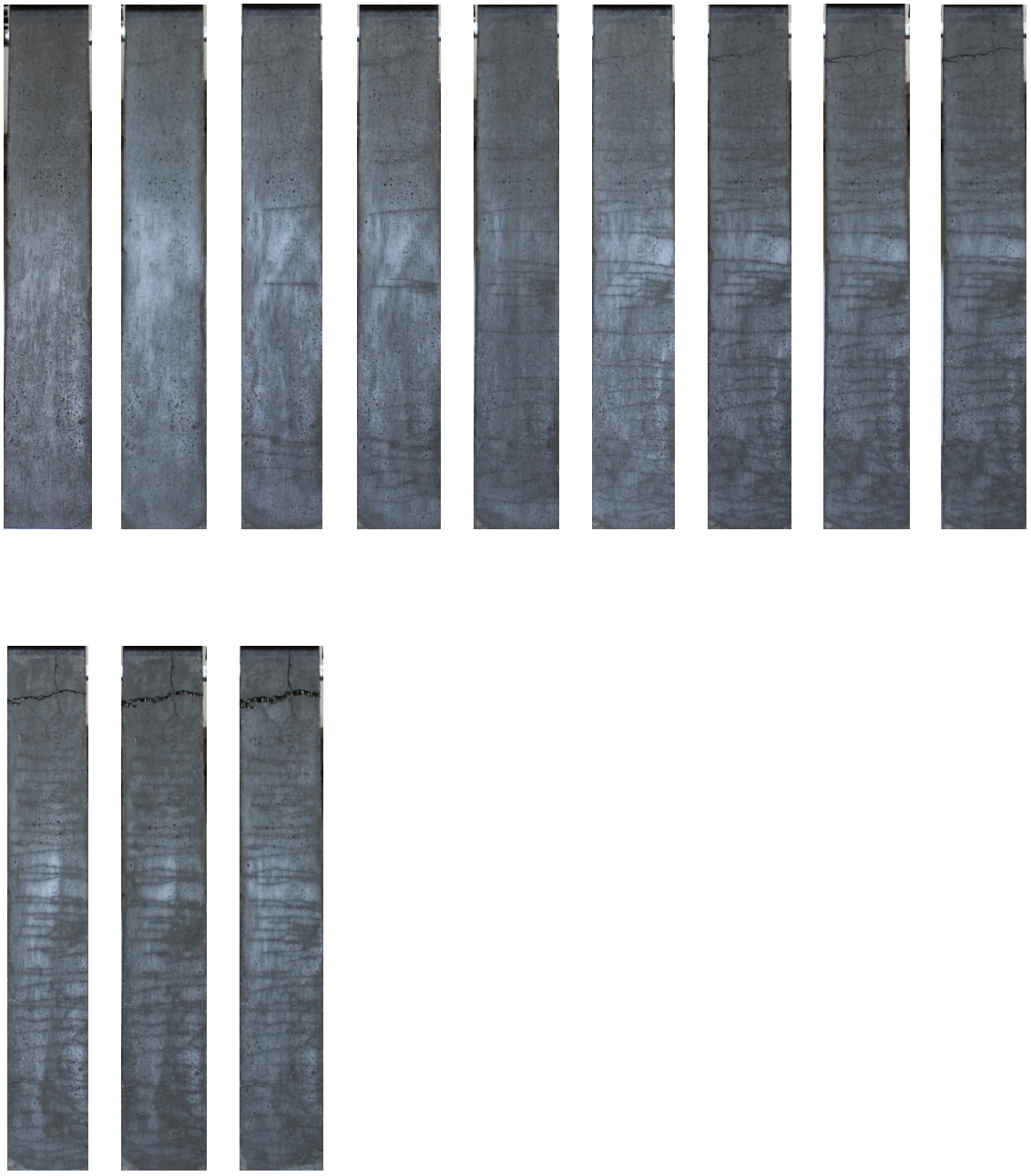

Figure 9-12: 1035_1%Fiber_Parallel_S2

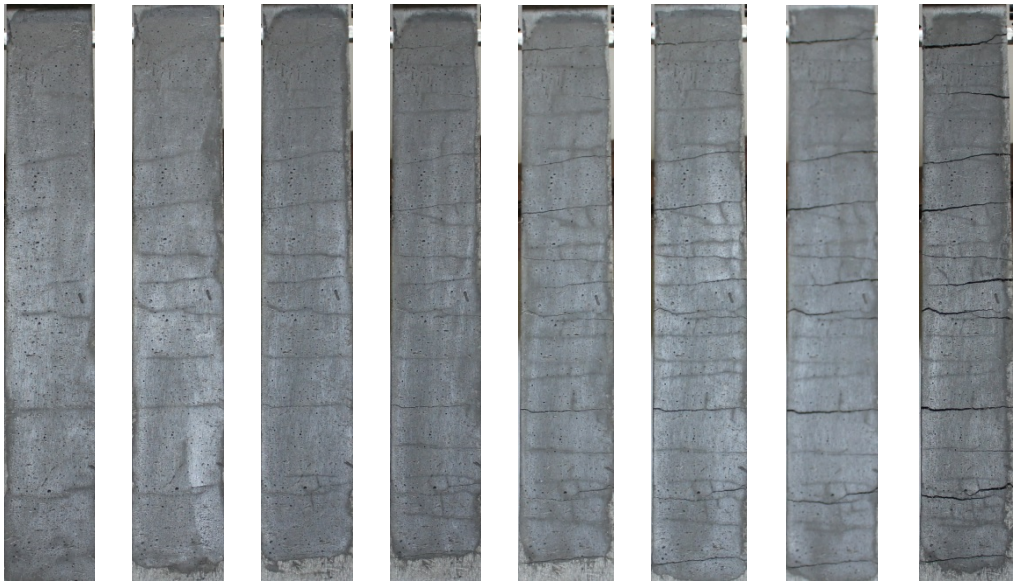

Figure 9-13: 1035_1%Fiber_Perpendicular

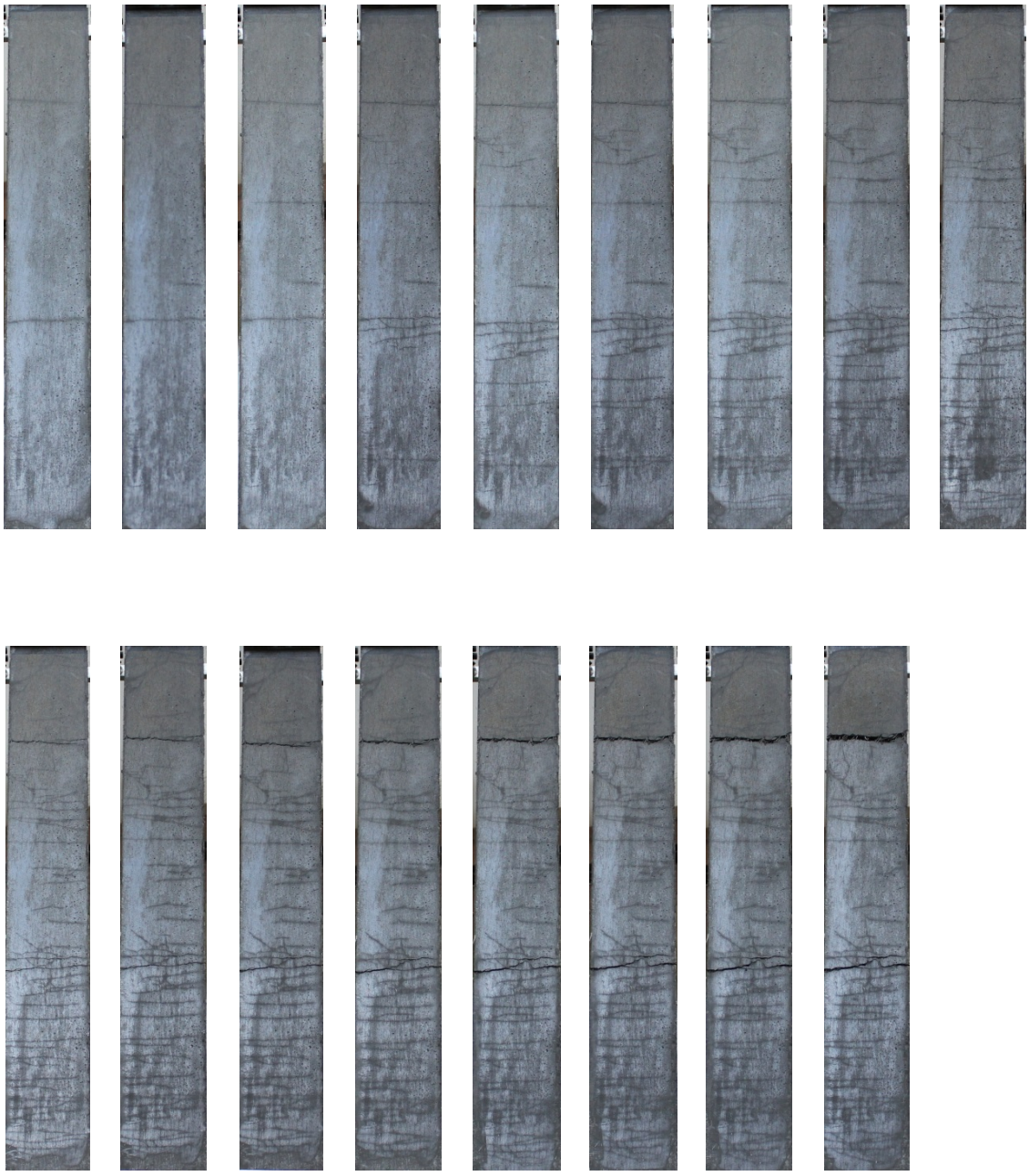

Figure 9-14: 1035_1%Fiber_Random

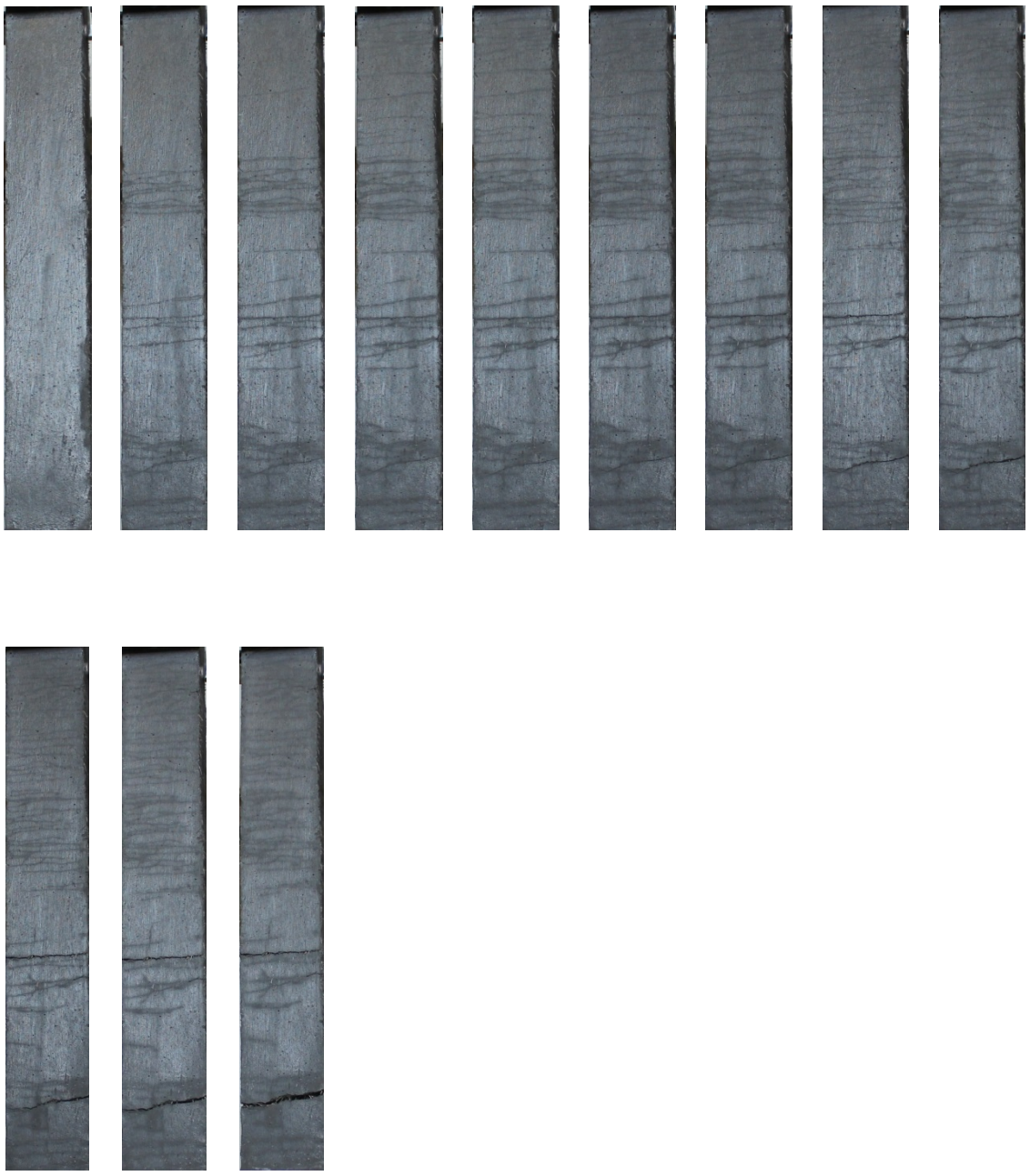

Figure 9-15: 1035_2%Fiber_Random

Figure 9-16: 1035_3%Fiber_Random